

EXPERIMENTAL INVESTIGATION OF PROPPANT TRANSPORT AND BEHAVIOR
IN HORIZONTAL WELLBORES USING LOW VISCOSITY FLUIDS

by
Faraj Ahmad

Copyright by Faraj Ahmad, 2020
All Rights Reserved

A thesis submitted to the Faculty and the Board of Trustees of the Colorado School of Mines in partial fulfillment of the requirements for the degree of Doctor of Philosophy (Petroleum Engineering).

Golden, Colorado

Date _____

Signed: _____

Faraj A. Ahmad

Signed: _____

Dr. Jennifer L. Miskimins

Thesis Advisor

Golden, Colorado

Date _____

Signed: _____

Dr. Jennifer L. Miskimins

Associate Professor and Interim Department Head

Department of Petroleum Engineering

ABSTRACT

Hydraulic fracturing has become a widely applied technology for stimulating low permeability reservoirs. The reason for stimulating tight formations is to increase recoverable reserves and to accelerate production. This can be accomplished by placing hydraulic fractures in the targeted formations to allow the flow of oil and/or gas from the reservoir to the wellbore. These fractures are created by pumping a fracturing fluid at a high flow rate and then introducing proppant with the fluid to keep the fractures open after the pumping is stopped. One of the most significant concerns in this process is the proppant transport and distribution between multiple perforation clusters. Uneven proppant distribution between multiple clusters/fractures can lead to a reduction in the fracture conductivity, which in turn impacts the viability of the entire hydraulic fracturing treatment. Even though hydraulic fracturing technology has made substantial progress over the last several years, proppant transport and distribution in multiple hydraulic fractures is not fully understood.

The objective of this experimental research is to evaluate proppant transport and behavior in horizontal wellbores using freshwater and high loading friction reducer (HLFR)-based fluids. More specifically, the focus is to experimentally investigate the parameters that have a large influence on proppant distribution between perforation clusters. These parameters include, but are not limited to, proppant concentration, injection rate, fluid viscosity, and proppant type and size.

This approach utilizes a model of a 30-foot horizontal wellbore with three perforation clusters. Four shots per foot with 90-degree phasing were designed around the pipe for each cluster. Fresh water without additives was used to simulate slickwater fluids. Tests were also run using a commercial HLFR fluid system. The elasticity and the viscosity of the HLFR fluids were measured under a variety of shear conditions across a wide range of HLFR loadings. Experiments were carried out on 20/40 and 40/70 mesh sand and ultra-light weight (ULW) ceramic across a wide range of proppant concentrations. The injection rate/slurry velocity was varied throughout the experimental tests.

The results from this work using freshwater fluids showed that 20/40 and 40/70 mesh sand at low flow rates exhibited highly uneven proppant distribution among the perforation clusters. The gravitational forces were more dominant over the momentum forces resulting in more proppant received by the first cluster. However, at higher flow rates, the amount of proppant received at the toe cluster was higher than the amount of proppant received at the other two

clusters. This occurred because the total momentum forces near the first and second clusters were relatively higher than the gravity forces. This resulted in some proppant particles not being able to make a complete turn into perforations within the clusters. On the other hand, the results from the experimental runs conducted on 20/40 ULW ceramic showed good uniform proppant distribution across each of the perforation clusters. The 40/70 ULW ceramic showed the most uniform proppant distribution between the perforation clusters. The small difference in the momentum between the proppant and the carrier fluid and also the smaller particles can cause the proppant particles to distribute more uniformly in the fluid resulting in even proppant distribution between the perforation clusters.

The results of the rheological properties measurements for HLFRR fluids showed that as the shear rate increases for these fluids, the fluid viscosity decreases. Experiments at low flow rates and low loadings of HLFRR gave results similar to freshwater fluids for both 20/40 and 40/70 mesh sand. The first cluster received more proppant than the first and the second clusters. The results demonstrate that the 20/40 mesh sand cannot be suspended efficiently in the horizontal wellbore even at relatively higher fluid viscosities (up to 17 cp in these tests). The 40/70 mesh sand showed the most uniform distribution between the perforation clusters at relatively higher fluid viscosity, where the viscous forces were very significant in the fluid flow.

The experimental results were used to develop four types of correlations for 20/40 and 40/70 mesh sand and ULW ceramic. These correlations can be used to predict the proppant distribution between the perforation clusters. The first correlation type is based on the proppant concentration, while the second type is based on the flow velocity and proppant concentration. The third correlation type includes the particle diameter as another independent variables along with the flow velocity and proppant concentration. The fourth and final developed correlation includes the proppant density along with the proppant median diameter, flow velocity and proppant concentration as its independent variables. This fourth and final correlation was verified by comparing its predicted values to the laboratory values. The results of correlation analysis on the developed correlation show that the ULW ceramic showed low error values compared to sand at low flow velocities. The low error values indicate high reliability of the developed correlation in predicting the proppant distribution between the perforation clusters.

TABLE OF CONTENTS

ABSTRACT.....	iii
LIST OF FIGURES	xi
LIST OF TABLES.....	xxi
ACKNOWLEDGEMENT	xxv
CHAPTER 1- INTRODUCTION.....	1
1.1 Problem Statement and Research Motivation	3
1.2 Objectives of the Research.....	5
CHAPTER 2 - LITERATURE REVIEW.....	7
2.1 Proppant Transport and Suspension in Horizontal Pipes	7
2.2 Proppant Settling Theories	9
2.2.1 Stokes' Law	10
2.2.2 Durand's Equation	11
2.2.3 Wasp's Modified Durand Equation	12
2.2.4 Stokes' Law (Modified).....	12
2.3 Laminar and Turbulent Flow in Horizontal Pipes.....	13
2.4 Characteristics and Behavior of Non-Newtonian Fluids.....	15
2.5 Fracturing Fluids	17
2.6 Proppants.....	23
2.6.1 Sand Proppants.....	24
2.6.2 Resin-Coated Proppants.....	24
2.6.3 Ceramic Proppants	25
2.7 Completion Methods	25
2.7.1 Plug-and-Perf Completion Method.....	26

2.7.2	Ball-Activated Completion Method.....	27
2.7.3	Coiled Tubing Activated Frac Sleeves Completion Method	27
CHAPTER 3 - EXPERIMENTAL APPARATUS AND PROCEDURES		29
3.1	Experimental Apparatus.....	29
3.1.1	Mixing Tank and Slurry Pump	30
3.1.2	Flow Meter.....	31
3.1.3	Variable Frequency Drive.....	32
3.1.4	Horizontal Wellbore.....	33
3.1.4.1	Horizontal Pipe	33
3.1.4.2	Number and Phasing of Perforations.....	34
3.1.4.3	Entrance Hole Diameter	34
3.1.4.4	Distance Between Perforation Clusters	35
3.1.4.5	Pressure Transducers	35
3.2	Laboratory Scaling.....	36
3.2.1	Reynolds Number	36
3.2.2	Entrance Length.....	37
3.2.3	Minimum Transport Velocity	38
3.2.4	Shear Rate	40
3.2.5	Perforations Alignment and Distance Between Clusters	40
3.3	Test Materials.....	42
3.3.1	Water.....	42
3.3.2	Friction Reducer.....	42
3.3.3	Proppants.....	43
3.3.3.1	20/40 Mesh White Sand	43
3.3.3.2	40/70 Mesh White Sand	46

3.3.3.3	20/40 ULW Ceramic	48
3.3.3.4	40/70 ULW Ceramic	51
3.4	Experimental Procedure	52
CHAPTER 4 - EXPERIMENTAL RESULTS USING FRESHWATER FLUIDS		54
4.1	Experimental Results.....	54
4.1.1	20/40 Mesh White Sand.....	55
4.1.1.1	Flow Velocity of 6.4 ft/s.....	55
4.1.1.2	Flow Velocity of 11.0 ft/s.....	59
4.1.1.3	Flow Velocity of 13.7 ft/s.....	61
4.1.2	40/70 Mesh White Sand.....	64
4.1.2.1	Flow Velocity of 6.4 ft/s.....	65
4.1.2.2	Flow Velocity of 11.0 ft/s.....	68
4.1.2.3	Flow Velocity of 13.7 ft/s.....	70
4.1.3	20/40 Ultra-Light Weight Ceramic.....	73
4.1.3.1	Flow Velocity of 6.4 ft/s.....	73
4.1.3.2	Flow Velocity of 11.0 ft/s.....	76
4.1.3.3	Flow Velocity of 13.7 ft/s.....	78
4.1.4	40/70 Ultra-Light Weight Ceramic.....	80
4.1.4.1	Flow Velocity of 6.4 ft/s.....	81
4.1.4.2	Flow Velocity of 11.0 ft/s.....	83
4.1.4.3	Flow Velocity of 13.7 ft/s.....	86
4.2	Proppant Settling in the Horizontal Wellbore	88
4.2.1	20/40 Mesh White Sand.....	89
4.2.2	40/70 Mesh White Sand.....	91
4.2.3	20/40 ULW Ceramic.....	93

4.2.4	40/70 ULW Ceramic.....	95
CHAPTER 5 - EXPERIMENTAL RESULTS USING FRICTION REDUCER IN WATER		98
5.1	Fluid Rheological Properties.....	98
5.2	Experimental Tests on Proppant Transport.....	102
5.2.1	20/40 Mesh White Sand.....	103
5.2.1.1	Concentration of 1 gpt of HLFR.....	103
5.2.1.2	Concentration of 2 gpt of HLFR.....	105
5.2.1.3	Concentration of 3 gpt of HLFR.....	107
5.2.1.3	Concentration of 5 gpt of HLFR.....	109
5.2.2	40/70 Mesh Sand.....	111
5.2.2.1	Concentration of 1 gpt of HLFR.....	111
5.2.2.2	Concentration of 2 gpt of HLFR.....	113
5.2.2.3	Concentration of 3 gpt of HLFR.....	115
5.2.2.4	Concentration of 5 gpt of HLFR.....	117
CHAPTER 6 - EXPERIMENTAL CORRELATIONS.....		120
6.1	20/40 Mesh White Sand.....	125
6.1.1	Proppant Distribution Determination.....	126
6.1.1.1	Flow Velocity of 6.4 ft/s.....	126
6.1.1.2	Flow Velocity of 11.0 ft/s.....	127
6.1.1.3	Flow Velocity of 13.7 ft/s.....	129
6.1.2	Correlation Development for 20/40 Mesh Sand.....	130
6.2	40/70 Mesh White Sand.....	132
6.2.1	Proppant distribution determination.....	132
6.2.1.1	Flow Velocity of 6.4 ft/s.....	133
6.2.1.2	Flow Velocity of 11.0 ft/s.....	134

6.2.1.3	Flow Velocity of 13.7 ft/s.....	135
6.2.2	Correlation Development for 40/70 Mesh Sand	137
6.3	Correlation Development for 20/40 and 40/70 Mesh Sand.....	139
6.4	20/40 Ultra-Light Weight Ceramic	140
6.4.1	Proppant Distribution Determination.....	140
6.4.1.1	Flow Velocity of 6.4 ft/s.....	140
6.4.1.2	Flow Velocity of 11.0 ft/s.....	141
6.4.1.3	Flow Velocity of 13.7 ft/s.....	143
6.4.2	Correlation Development for 20/40 ULW Ceramic	144
6.5	40/70 Ultra-Light Weight Ceramic	146
6.5.1	Proppant Distribution Determination.....	147
6.5.1.1	Flow Velocity of 6.4 ft/s.....	147
6.5.1.2	Flow Velocity of 11.0 ft/s.....	148
6.5.1.3	Flow Velocity of 13.7 ft/s.....	150
6.5.2	Correlation Development for 40/70 ULW ceramic	151
6.6	Correlation Development for 20/40 and 40/70 ULW Ceramic.....	153
6.7	Correlation Development for Sand and Ultra-light Weight Ceramic	154
6.8	Correlation Analysis.....	155
6.8.1	20/40 Mesh White Sand.....	155
6.8.2	40/70 Mesh White Sand.....	157
6.8.3	20/40 ULW Ceramic.....	158
6.8.4	40/70 ULW Ceramic.....	159
CHAPTER 7 - DISCUSSION OF THE RESULTS		161
7.1	Discussion of the Results Using Freshwater Fluids.....	161
7.2	Discussion of the Results Using Friction Reducer.....	164

7.3	Discussion of the Results for the Experimental Correlations	166
7.4	Comparison of the Experimental Results with Published Data	168
7.5	Applications to the Field	171
7.6	Experimental Limitations.....	173
CHAPTER 8 - CONCLUSIONS AND RECOMMENDATIONS.....		174
8.1	Conclusions	174
8.1.1	Proppant Transport Using Freshwater Fluids	174
8.1.2	Proppant Transport Using HLFR Fluids.....	176
8.1.3	Experimental Correlations	176
8.2	Recommendations for Future Work.....	178
NOMENCLATURE		180
ABBREVIATIONS		182
REFERENCES		183
APPENDIX A - SIEVE ANALYSIS		190

LIST OF FIGURES

Figure 1.1:	Prediction of natural gas production in the US (from US EIA 2019a).	1
Figure 1.2:	Map of U.S. shale gas and shale oil plays (from US EIA 2011).....	2
Figure 2.1:	Proppant transport modes: a) immobile proppant bed, b) initiation of grain pickup, c) bed load transport, d) heterogeneous suspension, and e) pseudo-homogeneous suspension. Brown-colored grains are stationary, and green-colored grains are in motion (from Al-Tailji et al. 2014).....	8
Figure 2.2:	Laminar/viscous sublayer over thin horizontal plane (from COMSOL 2017).	9
Figure 2.3:	Modified Froude number FL against particle diameter at various sand concentrations (adapted from Durand’s chart 1953).....	11
Figure 2.4:	The velocity profile in partially developed pipe flow (modified from Munson et al. 2012).....	13
Figure 2.5:	Turbulent and laminar velocity profiles in pipe: a) turbulent, b) laminar (modified from Munson et al. 2012).	15
Figure 2.6:	Shear stress versus rate of shearing strain for several types of fluids, including non-Newtonian fluids (from Munson et al. 2012).....	16
Figure 2.7:	Typical fracturing fluid composition (from Norton Rose Fulbright 2015).....	18
Figure 2.8:	Barnett Shale gas production after using slickwater (from King 2010).....	19
Figure 2.9:	Fracturing fluid type usages in the US in 2004 (from Schein 2005).....	20
Figure 2.10:	A chart for visual estimation of sphericity and roundness (from Miskimins 2016).....	23
Figure 2.11:	Some of the most common proppant types used in hydraulic fracturing applications (from CARBO Ceramics Inc 2017).	24
Figure 2.12:	Wellbore diagram of a plug-and-perf completion method used in hydraulic fracturing treatments (from Bagci et al. 2017).....	26
Figure 2.13:	Wellbore diagram of a ball-activated completion method used in hydraulic fracturing treatments (from Bagci et al. 2017).....	27
Figure 2.14:	Wellbore diagram of the coiled tubing-activated frac sleeves completion method used in hydraulic fracturing treatments (from Bagci et al. 2017).	28

Figure 3.1:	Schematic of the experimental apparatus used in this study.	29
Figure 3.2:	Picture of the mixing tank and the impeller.	30
Figure 3.3:	Picture of the rubber vibration reducer.....	31
Figure 3.4:	Picture of the self-priming centrifugal pump and the rubber vibration reducer.....	31
Figure 3.5:	Flow meter used to measure the slurry flow.	32
Figure 3.6:	Variable frequency drive (VFD) used in the experimental apparatus.....	32
Figure 3.7:	The horizontal wellbore apparatus used in this study.	33
Figure 3.8:	Perforation shot density: example of four shots/foot and 90° phasing.	34
Figure 3.9:	Schematic of the horizontal wellbore.....	35
Figure 3.10:	Picture of one of the pressure transducers used in the experimental apparatus.	35
Figure 3.11:	Minimum/critical transport velocity for different types of proppant at various particle concentrations using Wasp’s Modified Durand Equation (Equation 2.3).....	39
Figure 3.12:	Water distribution through three perforation clusters at three different flow velocities (all three perforation clusters are open).	41
Figure 3.13:	Water distribution through two perforation clusters at three different flow velocities (middle perforation cluster is intentionally plugged).....	42
Figure 3.14:	Picture of 20/40 white sand used in the experimental tests.....	43
Figure 3.15:	Picture of the sieve shaker used to perform the sieve analysis.	44
Figure 3.16:	Proppant particle distribution for the 20/40 mesh white sand.....	45
Figure 3.17:	Cumulative weight percent for the 20/40 mesh white sand.	46
Figure 3.18:	Picture of 40/70 white sand used in the experimental study.	47
Figure 3.19:	Proppant particle distribution for the 40/70 mesh white sand.....	48
Figure 3.20:	Cumulative weight percent for the 40/70 mesh white sand.	48
Figure 3.21:	Picture of the 20/40 ULW ceramic used in the experimental study.....	49

Figure 3.22: Proppant particle distribution for the 20/40 ULW ceramic.....	50
Figure 3.23: Cumulative weight percent for 20/40 ULW ceramic.	50
Figure 3.24: Picture of the 40/70 ULW ceramic used in the experimental study.....	51
Figure 3.25: Proppant particle distribution for the 40/70 ULW ceramic.....	52
Figure 3.26: Cumulative weight percent for the 40/70 ULW ceramic.	52
Figure 4.1: Proppant and slurry distribution between the perforation clusters at a slurry velocity of 6.4 ft/s and an injected proppant concentration of 0.12 ppg.	56
Figure 4.2: Proppant behavior of 20/40 mesh sand at a slurry velocity of 6.4 ft/s.	57
Figure 4.3: Proppant and slurry distribution between the perforation clusters at a slurry velocity of 6.4 ft/s and an injected proppant concentration of 0.21 ppg.	57
Figure 4.4: Proppant and slurry distribution between the perforation clusters at a slurry velocity of 6.4 ft/s and an injected proppant concentration of 0.31 ppg.	57
Figure 4.5: Particle distribution between the perforation clusters at a slurry velocity of 6.4 ft/s.....	58
Figure 4.6: Proppant and slurry distribution between the perforation clusters at a slurry velocity of 11.0 ft/s and an injected proppant concentration of 0.10 ppg.	60
Figure 4.7: Proppant behavior of 20/40 mesh sand at a slurry velocity of 11.0 ft/s (example of heterogeneous suspension).....	60
Figure 4.8: Proppant and slurry distribution between the perforation clusters at a slurry velocity of 11.0 ft/s and an injected proppant concentration of 0.23 ppg.	60
Figure 4.9: Proppant and slurry distribution between the perforation clusters at a slurry velocity of 11.0 ft/s and an injected proppant concentration of 0.36 ppg.	61
Figure 4.10: Proppant and slurry distribution between the perforation clusters at a slurry velocity of 13.7 ft/s and an injected proppant concentration of 0.13 ppg.	62
Figure 4.11: Proppant behavior of 20/40 mesh sand at a slurry velocity of 13.7 ft/s (example of heterogenous suspension).	62
Figure 4.12: Proppant and slurry distribution between the perforation clusters at a slurry velocity of 13.7 ft/s and an injected proppant concentration of 0.31 ppg.	63
Figure 4.13: Particle distribution between the perforation clusters at a slurry velocity of 13.7 ft/s.....	64

Figure 4.14: Proppant and slurry distribution between the perforation clusters at a slurry velocity of 6.4 ft/s and an injected proppant concentration of 0.3 ppg.	65
Figure 4.15: Proppant behavior and distribution for 40/70 mesh sand at a slurry velocity of 6.4 ft/s.....	66
Figure 4.16: Proppant and slurry distribution between the perforation clusters at a slurry velocity of 6.4 ft/s and an injected proppant concentration of 0.93 ppg.	66
Figure 4.17: Proppant and slurry distribution between the perforation clusters at a slurry velocity of 6.4 ft/s and an injected proppant concentration of 1.10 ppg.	67
Figure 4.18: Particle distribution between the perforation clusters at a slurry velocity of 6.4 ft/s.....	68
Figure 4.19: Proppant and slurry distribution between the perforation clusters at a slurry velocity of 11.0 ft/s and an injected proppant concentration of 0.3 ppg.	69
Figure 4.20: Proppant and slurry distribution between the perforation clusters at a slurry velocity of 11.0 ft/s and an injected proppant concentration of 0.9 ppg.	69
Figure 4.21: Proppant and slurry distribution between the perforation clusters at a slurry velocity of 11.0 ft/s and an injected proppant concentration of 1.2 ppg.	70
Figure 4.22: Proppant and slurry distribution between the perforation clusters at a slurry velocity of 11.0 ft/s and an injected proppant concentration of 0.20 ppg.	70
Figure 4.23: Proppant behavior and distribution for 40/70 mesh sand at a slurry velocity of 13.7 ft/s (example of heterogenous suspension).	71
Figure 4.24: Proppant and slurry distribution between the perforation clusters at a slurry velocity of 13.7 ft/s and an injected proppant concentration of 0.8 ppg.	71
Figure 4.25: Proppant and slurry distribution between the perforation clusters at a slurry velocity of 13.7 ft/s and an injected proppant concentration of 1.17 ppg.	72
Figure 4.26: Particle distribution between the perforation clusters for the 40/70 mesh white sand at a slurry velocity of 13.7 ft/s.	73
Figure 4.27: Proppant and slurry distribution between the perforation clusters at a slurry velocity of 6.4 ft/s and an injected proppant concentration of 0.3 ppg.	74
Figure 4.28: Proppant and slurry distribution between the perforation clusters at a slurry velocity of 6.4 ft/s and an injected proppant concentration of 0.72 ppg.	74
Figure 4.29: Proppant behavior and distribution of 20/40 ULW ceramic at a slurry velocity of 6.4 ft/s.	75

Figure 4.30: Proppant and slurry distribution between the perforation clusters at a slurry velocity of 6.4 ft/s and an injected proppant concentration of 1.14 ppg.	75
Figure 4.31: Proppant and slurry distribution between the perforation clusters at a slurry velocity of 6.4 ft/s and an injected proppant concentration of 1.8 ppg.	76
Figure 4.32: Proppant and slurry distribution between the perforation clusters at a slurry velocity of 11.0 ft/s and an injected proppant concentration of 0.7 ppg.	77
Figure 4.33: Proppant and slurry distribution between the perforation clusters at a slurry velocity of 11.0 ft/s and an injected proppant concentration of 0.94 ppg.	77
Figure 4.34: Proppant and slurry distribution between the perforation clusters at a slurry velocity of 11.0 ft/s and an injected proppant concentration of 1.3 ppg.	78
Figure 4.35: Proppant behavior and distribution of 20/40 ULW ceramic at a slurry velocity of 11.0 ft/s.	78
Figure 4.36: Proppant and slurry distribution between the perforation clusters at a slurry velocity of 13.7 ft/s and an injected proppant concentration of 0.21 ppg.	79
Figure 4.37: Proppant and slurry distribution between the perforation clusters at a slurry velocity of 13.7 ft/s and an injected proppant concentration of 0.55 ppg.	79
Figure 4.38: Proppant and slurry distribution between the perforation clusters at a slurry velocity of 13.7 ft/s and an injected proppant concentration of 0.85 ppg.	80
Figure 4.39: Proppant and slurry distribution between the perforation clusters at a slurry velocity of 13.7 ft/s and an injected proppant concentration of 1.10 ppg.	80
Figure 4.40: Proppant and slurry distribution between the perforation clusters at a slurry velocity of 6.4 ft/s and an injected proppant concentration of 0.46 ppg.	82
Figure 4.41: Proppant and slurry distribution between the perforation clusters at a slurry velocity of 6.4 ft/s and an injected proppant concentration of 1.08 ppg.	82
Figure 4.42: Proppant and slurry distribution between the perforation clusters at a slurry velocity of 6.4 ft/s and an injected proppant concentration of 1.64 ppg.	83
Figure 4.43: Proppant and slurry distribution between the perforation clusters at a slurry velocity of 6.4 ft/s and an injected proppant concentration of 2.2 ppg.	83
Figure 4.44: Proppant and slurry distribution between the perforation clusters at a slurry velocity of 11.0 ft/s and an injected proppant concentration of 0.39 ppg.	84
Figure 4.45: Proppant and slurry distribution between the perforation clusters at a slurry velocity of 11.0 ft/s and an injected proppant concentration of 0.94 ppg.	85

Figure 4.46: Proppant and slurry distribution between the perforation clusters at a slurry velocity of 11.0 ft/s and at an injected proppant concentration of 1.25 ppg.	85
Figure 4.47: Proppant distribution of 40/70 ULW ceramic at a slurry velocity of 11.0 ft/s.....	85
Figure 4.48: Proppant and slurry distribution between the perforation clusters at a slurry velocity of 11.0 ft/s and an injected proppant concentration of 2.1 ppg.	86
Figure 4.49: Proppant and slurry distribution between the perforation clusters at a slurry velocity of 13.7 ft/s and an injected proppant concentration of 0.45 ppg.	87
Figure 4.50: Proppant and slurry distribution between the perforation clusters at a slurry velocity of 13.7 ft/s and an injected proppant concentration of 1.02 ppg.	87
Figure 4.51: Proppant and slurry distribution between the perforation clusters at a slurry velocity of 13.7 ft/s and an injected proppant concentration of 1.2 ppg.	88
Figure 4.52: Proppant and slurry distribution between the perforation clusters at a slurry velocity of 13.7 ft/s and an injected proppant concentration of 1.79 ppg.	88
Figure 4.53: Picture of proppant settling in the horizontal wellbore for 20/40 mesh sand at a flow velocity of 6.4 ft/s and at an injected proppant concentration of 0.31 ppg.	89
Figure 4.54: Amount of settled proppant in the horizontal wellbore for 20/40 mesh sand at a flow velocity of 6.4 ft/s and at different injected proppant concentrations.	90
Figure 4.55: Amount of settled proppant in the horizontal wellbore for 20/40 mesh sand at a flow velocity of 11.0 ft/s and at different injected proppant concentrations.	90
Figure 4.56: Amount of settled proppant in the horizontal wellbore for 20/40 mesh sand at a flow velocity of 13.7 ft/s and at different injected proppant concentrations.	91
Figure 4.57: Amount of settled proppant in the horizontal wellbore for 40/70 mesh sand at a flow velocity of 6.4 ft/s and at different injected proppant concentrations.	92
Figure 4.58: Amount of settled proppant in the horizontal wellbore for 40/70 mesh sand at a flow velocity of 11.0 ft/s and at different injected proppant concentrations.	92
Figure 4.59: Amount of settled proppant in the horizontal wellbore for 40/70 mesh sand at a flow velocity of 13.7 ft/s and at different injected proppant concentrations.	93
Figure 4.60: Amount of settled proppant in the horizontal wellbore for 20/40 ULW ceramic at a flow velocity of 6.4 ft/s and at different injected proppant concentrations.	94

Figure 4.61: Amount of settled proppant in the horizontal wellbore for 20/40 ULW ceramic at a flow velocity of 11.0 ft/s and at different injected proppant concentrations.....	94
Figure 4.62: Amount of settled proppant in the horizontal wellbore for 20/40 ULW ceramic at a flow velocity of 11.0 ft/s and at different injected proppant concentrations.....	95
Figure 4.63: Picture of proppant settling in the horizontal wellbore for 40/70 ULW ceramic at a flow velocity of 6.4 ft/s and at an injected proppant concentration of 2.2 ppg.....	96
Figure 4.64: Amount of settled proppant in the horizontal wellbore for 40/70 ULW ceramic at a flow velocity of 6.4 ft/s and at different injected proppant concentrations.....	96
Figure 4.65: Amount of settled proppant in the horizontal wellbore for 40/70 ULW ceramic at a flow velocity of 11.0 ft/s and at different injected proppant concentrations.....	97
Figure 4.66: Amount of settled proppant in the horizontal wellbore for 40/70 ULW ceramic at a flow velocity of 13.7 ft/s and at different injected proppant concentrations.....	97
Figure 5.1: Picture of a M3600 Fann Viscometer used to measure the rheological properties of fracturing fluid.	99
Figure 5.2: Shear stress versus shear rate for different concentrations of HLFRR.	100
Figure 5.3: Shear stress versus shear rate at different concentrations of HLFRR on logarithmic coordinates showing Power Law behavior.	101
Figure 5.4: Proppant and slurry distribution between the perforation clusters at a flow velocity of 4.5 ft/s and an injected proppant concentration of 1.0 ppg.	104
Figure 5.5: Proppant and slurry distribution between the perforation clusters at a flow velocity of 8.2 ft/s and an injected proppant concentration of 1.0 ppg.	104
Figure 5.6: Proppant and slurry distribution between the perforation clusters at a flow velocity of 11.0 ft/s and an injected proppant concentration of 1.0 ppg.	105
Figure 5.7: Proppant and slurry distribution between the perforation clusters at a flow velocity of 4.5 ft/s and an injected proppant concentration of 0.5 ppg.	106
Figure 5.8: Proppant and slurry distribution between the perforation clusters at a flow velocity of 8.2 ft/s and an injected proppant concentration of 1.0 ppg.	106

Figure 5.9:	Proppant and slurry distribution between the perforation clusters at a flow velocity of 11.0 ft/s and an injected proppant concentration of 1.25 ppg.	107
Figure 5.10:	Proppant and slurry distribution between the perforation clusters at a flow velocity of 4.5 ft/s and an injected proppant concentration of 0.75 ppg.	108
Figure 5.11:	Proppant and slurry distribution between the perforation clusters at a flow velocity of 8.2 ft/s and an injected proppant concentration of 0.9 ppg.	108
Figure 5.12:	Proppant and slurry distribution between the perforation clusters at a flow velocity of 11.0 ft/s and an injected proppant concentration of 1.0 ppg.	109
Figure 5.13:	Proppant and slurry distribution between the perforation clusters at a flow velocity of 4.5 ft/s and an injected proppant concentration of 1.0 ppg.	110
Figure 5.14:	Proppant and slurry distribution between the perforation clusters at a flow velocity of 8.2 ft/s and an injected proppant concentration of 1.25 ppg.	110
Figure 5.15:	Proppant and slurry distribution between the perforation clusters at a flow velocity of 11.0 ft/s and an injected proppant concentration of 1.5 ppg.	111
Figure 5.16:	Proppant and slurry distribution between the perforation clusters at a flow velocity of 4.5 ft/s and an injected proppant concentration of 0.75 ppg.	112
Figure 5.17:	Proppant and slurry distribution between the perforation clusters at a flow velocity of 8.2 ft/s and an injected proppant concentration of 1.0 ppg.	112
Figure 5.18:	Proppant and slurry distribution between the perforation clusters at a flow velocity of 11.0 ft/s and an injected proppant concentration of 0.9 ppg.	113
Figure 5.19:	Proppant and slurry distribution between the perforation clusters at a flow velocity of 4.5 ft/s and an injected proppant concentration of 0.75 ppg.	114
Figure 5.20:	Proppant and slurry distribution between the perforation clusters at a flow velocity of 8.2 ft/s and an injected proppant concentration of 1.0 ppg.	114
Figure 5.21:	Proppant and slurry distribution between the perforation clusters at a flow velocity of 11.0 ft/s and an injected proppant concentration of 1.15 ppg.	115
Figure 5.22:	Proppant and slurry distribution between the perforation clusters at a flow velocity of 4.5 ft/s and an injected proppant concentration of 1.0 ppg.	116
Figure 5.23:	Proppant and slurry distribution between the perforation clusters at a flow velocity of 8.2 ft/s and an injected proppant concentration of 1.25 ppg.	116
Figure 5.24:	Proppant and slurry distribution between the perforation clusters at a flow velocity of 11.0 ft/s and an injected proppant concentration of 1.3 ppg.	117

Figure 5.25: Proppant and slurry distribution between the perforation clusters at a flow velocity of 4.5 ft/s and an injected proppant concentration of 1.0 ppg.	118
Figure 5.26: Proppant and slurry distribution between the perforation clusters at a flow velocity of 8.2 ft/s and an injected proppant concentration of 1.0 ppg.	118
Figure 5.27: Proppant and slurry distribution between the perforation clusters at a flow velocity of 11.0 ft/s and an injected proppant concentration of 1.1 ppg.	119
Figure 6.1: Proppant distribution between the perforation clusters for 20/40 mesh sand at a slurry velocity of 6.4 ft/s and injected proppant concentrations of 0.12, 0.13, 0.21 and 0.31 ppg.	126
Figure 6.2: Proppant distribution between the perforation clusters for 20/40 mesh sand at a slurry velocity of 11.0 ft/s and injected proppant concentrations of 0.1, 0.12, 0.23 and 0.36 ppg.	128
Figure 6.3: Proppant distribution between the perforation clusters for 20/40 mesh sand at a slurry velocity of 13.7 ft/s and injected proppant concentrations of 0.07, 0.1, 0.13 and 0.3 ppg.	129
Figure 6.4: Proppant distribution as function of proppant concentration to fluid density ratio for slurry velocities of 6.4, 11.0 and 13.7ft/s.	131
Figure 6.5: Proppant distribution between the perforation clusters for 40/70 mesh sand at a slurry velocity of 6.4 ft/s and injected proppant concentrations of 0.3, 0.37, 0.93 and 1.1 ppg.	133
Figure 6.6: Proppant distribution between the perforation clusters for 40/70 mesh sand at a slurry velocity of 11.0 ft/s and injected proppant concentrations of 0.26, 0.3, 0.9 and 1.2 ppg.	135
Figure 6.7: Proppant distribution between the perforation clusters for 40/70 mesh sand at a slurry velocity of 13.7 ft/s and injected proppant concentrations of 0.2, 0.23, 0.8 and 1.17 ppg.	136
Figure 6.8: Proppant distribution as function of proppant concentration to fluid density ratio for slurry velocities of 6.4, 11.0 and 13.7ft/s.	138
Figure 6.9: The predicted and the measured PD for 20/40 and 40/70 mesh white sand.	139
Figure 6.10: Proppant distribution between the perforation clusters for 20/40 ULW ceramic at slurry velocity of 6.4 ft/s and injected proppant concentrations of 0.3, 0.72, 1.14 and 1.80 ppg.	141
Figure 6.11: Proppant distribution between the perforation clusters for 20/40 ULW ceramic sand at a slurry velocity of 11.0 ft/s and proppant concentrations of 0.21, 0.7, 0.94 and 1.3 ppg.	142

Figure 6.12: Proppant distribution between the perforation clusters for 20/40 ULW ceramic at a slurry velocity of 13.7 ft/s and injected proppant concentrations of 0.21, 0.55, 0.85 and 1.1 ppg.....	143
Figure 6.13: Proppant distribution as function of proppant concentration to fluid density ratio for 20/40 ULW ceramic at flow velocities of 6.4, 11.0 and 13.7 ft/s.	145
Figure 6.14: Proppant distribution between the perforation clusters for 40/70 ULW ceramic at a slurry velocity of 6.4 ft/s and injected proppant concentrations of 0.46, 1.08, 1.64 and 2.2 ppg.	147
Figure 6.15: Proppant distribution between the perforation clusters for 40/70 ULW ceramic at a slurry velocity of 11.0 ft/s and injected proppant concentrations of 0.39, 0.94, 1.25 and 2.1 ppg.....	149
Figure 6.16: Proppant distribution between the perforation clusters for 40/70 ULW ceramic at a slurry velocity of 13.7 ft/s and injected proppant concentrations of 0.45, 1.02, 1.2 and 1.8 ppg.....	150
Figure 6.17: Proppant distribution as function of proppant concentration to fluid density ratio for 40/70 ULW ceramic at flow velocities of 6.4, 11.0 and 13.7 ft/s.	152
Figure 6.18: The predicted and the measured PD for 20/40 and 40/70 ULW ceramic.	154
Figure 6.19: The predicted PD from the developed correlation and the measured PD for 20/40 mesh white sand.	156
Figure 6.20: The predicted PD from the developed correlation and the actual PD for 40/70 mesh white sand.	158
Figure 6.21: The predicted PD from the developed correlation and the measured PD for 20/40 ULW ceramic.	159
Figure 6.22: The predicted PD from the correlation and the measured PD for 40/70 ULW ceramic.	160
Figure 7.1: Proppant distribution in four perforation clusters within one fracturing stage (from Yu et al. 2015).....	169
Figure 7.2: Comparison of cumulative gas production in a 30-year period between three scenarios (from Yu et al. 2015).....	169
Figure 7.3: Proppant distribution between four perforation clusters in one fracturing stage (from Daneshy 2011).	170

LIST OF TABLES

Table 2.1:	Terminal settling velocity rate for different proppant sizes and types (from Schein 2005).....	12
Table 2.2:	Fracturing fluid types and conditions for their use (from PetroWiki 2016).....	21
Table 2.3:	List of fracturing fluid additives and their purpose and common uses (from U.S. Department of Energy Office of Fossil Energy and National Energy Technology Laboratory 2009).....	22
Table 3.1:	The Reynolds number calculations for a 1.5-inch pipe (Laboratory Data)	36
Table 3.2:	The Reynolds number calculations for a 5.5-inch casing (Field Data)	37
Table 3.3:	Entrance length and Reynolds number for the selected pipe (1.5-inch pipe).....	38
Table 3.4:	Specifications of proppants used in the study.....	39
Table 3.5:	Laboratory flow rates for a 1.5-inch pipe matched with field rates for a 4.778-inch casing	40
Table 3.6:	Results of the sieve analysis for 20/40 mesh white sand.....	45
Table 3.7:	Results of a sieve analysis test for 20/40 mesh white sand	47
Table 3.8:	Results of sieve analysis test for 20/40 ULW ceramic	49
Table 3.9:	Results of sieve analysis test for 40/70 ULW ceramic	51
Table 4.1:	Reynolds number for 20/40 mesh white sand at slurry velocities of 6.4, 11.0 and 13.7 ft/s	55
Table 4.2:	Reynolds number for 40/70 mesh white sand at slurry velocities of 6.4, 11.0 and 13.7 ft/s	64
Table 4.3:	Reynolds number for 20/40 ULW ceramic at flow velocities of 6.4, 11.0 and 13.7 ft/s.....	73
Table 4.4:	Reynolds number for 40/70 ULW ceramic at flow velocities of 6.4, 11.0 and 13.7 ft/s.....	81
Table 5.1:	The rheological properties of fracturing fluid at concentrations of 1, 2, 3, and 5 gpt of HLFRR	99
Table 5.2:	The flow behavior index (n) and the consistency index (K) and the associated viscosity at different loading of HLFRR.....	101

Table 5.3: Flow regimes for HLFBR concentrations at flow velocities of 4.5, 8.2 and 11.0 ft/s	102
Table 6.1: Proppant distribution status for each value of percentage increase/decrease	121
Table 6.2: Basic dimensions for all the variables involved in the experimental tests	122
Table 6.3: Fluid and the proppant properties for 20/40 mesh white sand at slurry velocities of 6.4, 11.0 and 13.7 ft/s.....	125
Table 6.4: Proppant distribution and the percentage increase/decrease for 20/40 mesh sand at a slurry velocity of 6.4 ft/s and injected proppant concentrations of 0.12, 0.13, 0.21 and 0.31 ppg	127
Table 6.5: Proppant distribution and the percentage increase/decrease for 20/40 mesh sand at a slurry velocity of 11.0 ft/s and injected proppant concentrations of 0.1, 0.12, 0.23 and 0.36 ppg	128
Table 6.6: Proppant distribution and the percentage increase/decrease for 20/40 mesh sand at a slurry velocity of 13.7 ft/s and injected proppant concentrations of 0.07, 0.1, 0.13 and 0.31 ppg	129
Table 6.7: Proppant distribution and the associated dimensionless terms for each test for 20/40 mesh white sand	130
Table 6.8: Power law equations and R^2 values for different slurry velocities for 20/40 mesh sand	131
Table 6.9: Fluid and the proppant properties for 40/70 mesh white sand at slurry velocities of 6.4, 11.0 and 13.7 ft/s.....	132
Table 6.10: Proppant distribution and the percentage increase/decrease for 40/70 mesh sand at a slurry velocity of 6.4 ft/s and injected proppant concentrations of 0.3, 0.37, 0.93 and 0.31 ppg	134
Table 6.11: Proppant distribution and the percentage increase/decrease for 40/70 mesh sand at slurry velocity of 11.0 ft/s and injected proppant concentrations of 0.26, 0.3, 0.89 and 1.2 ppg	135
Table 6.12: Proppant distribution and the percentage increase/decrease for 40/70 mesh sand at a slurry velocity of 13.7 ft/s and injected proppant concentrations of 0.21, 0.23, 0.8 and 1.17 ppg	136
Table 6.13: Proppant distribution and the associated dimensionless terms for each test for 40/70 mesh white sand	137
Table 6.14: Power law equations and R^2 values for different slurry velocities for 40/70 mesh white sand	138

Table 6.15: Fluid and the proppant properties for 20/40 ULW ceramic at slurry velocities of 6.4, 11.0 and 13.7 ft/s.....	140
Table 6.16: Proppant distribution and the percentage increase/decrease for 20/40 ULW ceramic at a slurry velocity of 6.4 ft/s and injected proppant concentrations of 0.3, 0.72, 1.14 and 1.8 ppg	141
Table 6.17: Proppant distribution and the percentage increase/decrease for 20/40 ULW ceramic at slurry velocity of 11.0 ft/s and injected proppant concentrations of 0.21, 0.7, 0.94 and 1.3 ppg	143
Table 6.18: Proppant distribution and the percentage increase/decrease for 20/40 ULW ceramic at a slurry velocity of 11 ft/s and proppant concentrations of 0.21, 0.55, 0.85 and 1.1 ppg	144
Table 6.19: Proppant distribution and the associated dimensionless terms for each test for 20/40 ULW ceramic	144
Table 6.20: Power law equations and R^2 values at different slurry velocities for 20/40 ULW ceramic	146
Table 6.21: Fluid and the proppant properties for 40/70 ULW ceramic at slurry velocities of 6.4, 11.0 and 13.7 ft/s.....	146
Table 6.22: Proppant distribution and the percentage increase/decrease for 40/70 ULW ceramic at a slurry velocity of 6.4 ft/s and injected proppant concentrations of 0.46, 1.08, 1.64 and 2.2 ppg	148
Table 6.23: Proppant distribution and the percentage increase/decrease for 40/70 ULW ceramic at a slurry velocity of 11.0 ft/s and injected proppant concentrations of 0.39, 0.94, 1.25 and 2.1 ppg	149
Table 6.24: Proppant distribution and percentages increase/decrease for 40/70 ULW ceramic at a slurry velocity of 13.7 ft/s and injected proppant concentrations of 0.45, 1.02, 1.2 and 1.80 ppg	151
Table 6.25: Proppant distribution and the associated dimensionless terms for each test for 40/70 ULW ceramic	151
Table 6.26: Power law equations and R^2 values for different slurry velocities for 40/70 ULW ceramic	152
Table 6.27: The predicted PD values and their calculated error values for 20/40 mesh white sand.....	156
Table 6.28: The predicted PD values and their calculated error values for 40/70 mesh white sand.....	157

Table 6.29: The predicted PD values and their calculated error values for 20/40 ULW ceramic	159
Table 6.30: The predicted PD values and their calculated error values for 40/70 ULW ceramic	160

ACKNOWLEDGEMENT

Foremost, I would like to express my sincere appreciation and thankful to my advisor, Dr. Jennifer Miskimins for the nonstop support of my PhD study and research, for her patience, motivation, enthusiasm, and enormous knowledge. Her guidance helped me in research and writing the PhD thesis. I could not have imagined having a better advisor and mentor for my PhD study.

My sincere thanks must also go to the committee members, the late Dr. Azra Tutuncu, Dr. Nicole Smith, Dr. Stephen Sonnenberg, Dr. Luis Zerpa, and Dr. Yilin Fan for serving as my committee members and their support in this research project.

I am also very thankful to the consortium members of the Fracturing, Acidizing, Stimulation Technology (FAST) at the Colorado School of Mines for providing support and valuable feedback for this study.

I would like to thank all the faculty members and the staff in the Petroleum Engineering Department at Colorado School of Mines. Also, I would like to express my sincere thanks to Denise Winn-Bower for her support, and Joe Chen for providing technical suggestions in the experimental setup. My thank must also go to Arlybek Altazhanov for his extremely hard, excellent, and outstanding work in helping to conduct the first phase of the experiments.

I would also like to say a heartfelt thank you to my parents, my father Ashor Milood Ahmad Al-Ferjani, and my mother Jazia Khalifa Al-Saih, for their support and encouragement to achieve the PhD degree. Without their prayers and support, I would never be where I am today. Also, my deep sincere thanks to my wife Katwer Mahfoid for her support and understanding during my PhD study that made the completion of the degree possible.

CHAPTER 1

INTRODUCTION

Hydraulic fracturing has become a widely applied technology for stimulating low-permeability oil and gas reservoirs to increase recoverable reserves and to accelerate production. Stimulation of oil and gas reservoirs can be accomplished by creating hydraulic fractures in the formation to allow the flow of oil and/or gas from the reservoir to the wellbore. More precisely, the objective of hydraulic fracturing is to create new fractures in the rock to provide conductive paths for the fluid to flow from the reservoir to the wellbore. These conductive paths are created by pumping a large amount of fracturing fluid under high pressure into the formation. This process involves drilling a vertical well to the chosen depth and then horizontal drilling is utilized, where more access to the formation can be achieved.

During the past three decades, the number of oil and gas wells that have been stimulated by hydraulic fracturing has increased dramatically in the United States and in the world. Most of these wells would never be produced commercially without hydraulic fracturing applications (Fisher 2012). The cutting-edge technology in hydraulic fracturing in conjunction with horizontal drilling technology made the U.S. the world's largest oil and gas producer (US EIA 2018). The Energy Information Administration (US EIA 2019a) expects U.S. natural gas production to continue to increase, driven almost entirely by hydraulic fracturing in shale gas formations as shown in Figure 1.1.

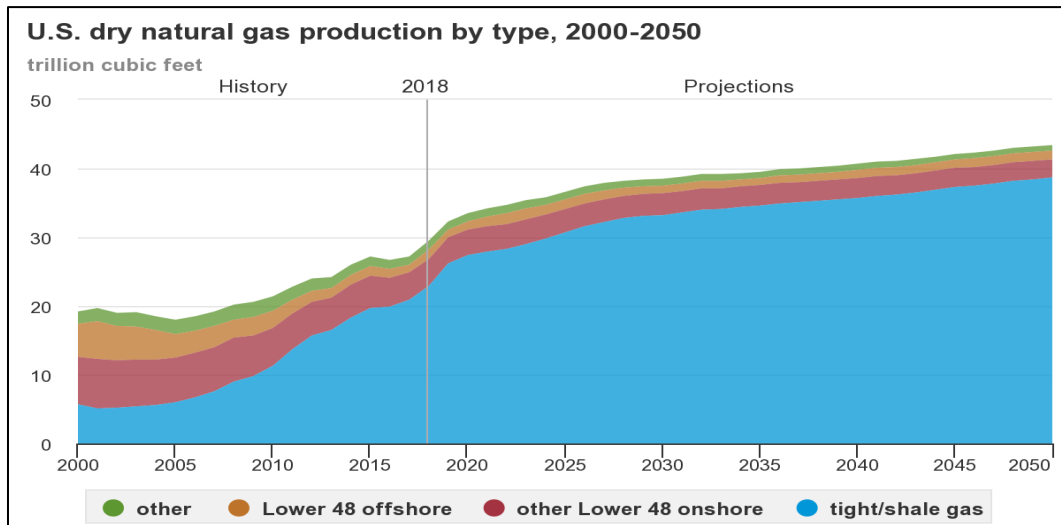


Figure 1.1: Prediction of natural gas production in the US (from US EIA 2019a).

The first successful hydraulic fracturing treatment on a commercial scale was conducted in 1949 (Speight 2016), and it was implemented to increase oil production by improving reservoir drainage area. At that time, the primary objective of hydraulic fracturing was to bypass the formation damage in the near wellbore area and/or to enhance the formation of interest (Coulter et al. 1976).

In 1949, there were about 332 wells fractured which led to an increase in the oil production by 75% (Montgomery and Smith 2010). After 1949, the applications of hydraulic fracturing treatments increased rapidly across the world to both enhance production and increase the oil recovery. By the mid-1960's, hydraulic fracturing was the primary method of well stimulation and is applicable to all types of formation mineralogy (Miskimins 2016).

The first potential hydraulic fracturing treatment on unconventional gas shales was conducted in 1981 by Mitchell Energy in Barnett Shale formation (Parshall 2008). Since then, hydraulic fracturing has been used intensively to extract oil and gas that is trapped in low permeability formations which are technically and economically difficult to produce. Also, the advances in multistage hydraulic fracturing combined with directional drilling and new completion methods allowed development of many shale plays in North America and the world. Figure 1.2 shows the major and minor oil and gas shale plays in the U.S. as of May 2011.

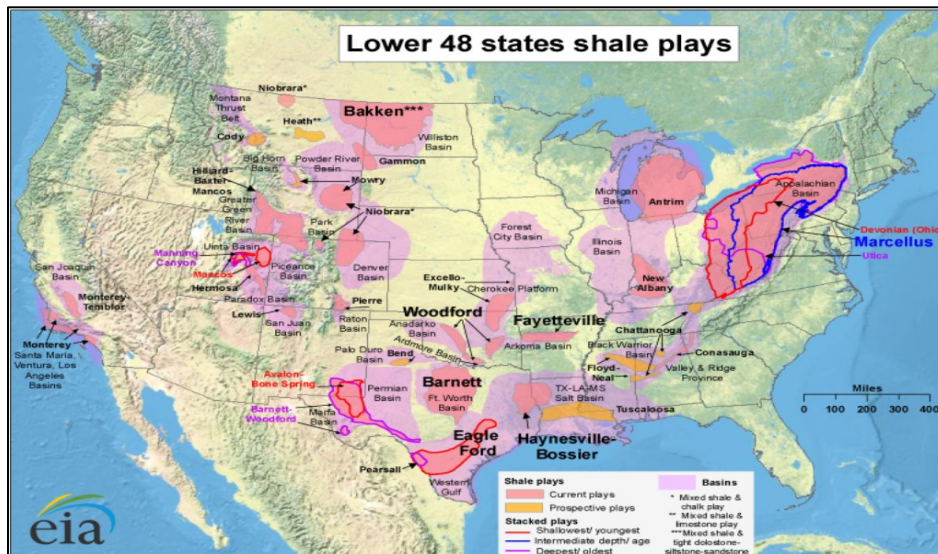


Figure 1.2: Map of U.S. shale gas and shale oil plays (from US EIA 2011).

Currently, hydraulic fracturing technology is a critical part of petroleum and natural gas production. There are about 2.5 million hydraulic fracture treatments that have been conducted

worldwide, and some estimate that around 60% of the wells that are drilled and completed today are hydraulically fractured (Montgomery and Smith 2010).

According to the EIA and Advanced Resources International (ARI), the United States is the world's largest producer of commercially viable natural gas from shale formations, where the average daily production of natural gas is averaged around 92.8 Bcf/d in August 2019. The biggest portion of gas production comes from the Appalachian region which includes the Marcellus and Utica shale plays with an average daily production of 28.5 Bcf/d (US EIA 2019b). The increase in natural gas production and crude oil from these shale plays has played an important role in lowering and stabilizing the crude oil and natural gas prices (Fisher 2012).

There are some important factors that should be considered in any hydraulic fracturing treatment. These factors include prediction of the well productivity, selection/transport of the proppant, fracture geometry requirements, and treatment cost (Hareland et al. 1993). Numerous studies have been conducted on understanding these factors in order to optimize hydraulic fracturing treatments. However, in terms of proppant transport, the industry has extensively evaluated the proppant transport in fractures via slot flow tests, yet little work has been accomplished in horizontal wellbores that are common in the development of shale plays.

The purpose of this PhD research is to conduct experimental tests to evaluate proppant transport in a horizontal wellbore apparatus in a low pressure and temperature laboratory setting. This chapter discusses the following topics: the problem statement, research motivation, and objectives of the research. Chapter 2 provides a comprehensive literature review on proppant transport and suspension in horizontal wellbores. Chapter 3 discusses the experimental setup along with the lab procedure that is implemented in this study. Chapters 4 and 5 summarize the results of the laboratory experiments. Development of experimental correlations to predict the proppant distribution between the perforation clusters is discussed in Chapter 6. Chapter 7 discusses the experimental results relative to previous experimental work and hydraulic fracturing of shale formations in general. Conclusions are provided in Chapter 8, along with future work and recommendations on proppant transport.

1.1 Problem Statement and Research Motivation

Transport of the proppant by fracturing fluids in horizontal wellbores and fractures is still a challenge in designing hydraulic fracturing treatments. There are several parameters that have

an impact on proppant transport including injection rate and associated velocity, proppant size, concentration, specific gravity, and carrier-fluid rheology (Harris et al. 2005).

Proppant transport in horizontal wellbores is not well understood, and in years past, it was frequently assumed that all the proppant that is injected into a wellbore is distributed evenly between the perforation clusters. In hydraulic fracturing applications, most of the experimental studies on proppant transport and behaviors have been focusing on proppant transport into the fractures. Only a few studies have been conducted on proppant transport in horizontal wellbores and most of these studies are simulation work in which Computational Fluid Dynamics (CFD) is used.

Over the last three decades, only three experimental studies are found in the literature describing proppant transport in horizontal wellbores. The first experimental study was conducted by Shah and Lord (1990) to evaluate transport properties of different hydraulic fracturing slurries in three horizontal pipes with different diameters. Their results indicate that particle deposition and suspension are greatly dependent on the particle density, where higher denser proppant requires higher critical velocities. Also, the critical deposition and resuspension velocities are independent of proppant concentration for more viscous fluids. However, their work was limited to pipes without perforations which are required to mimic flow behavior under field conditions. Another study was conducted by Crespo et al. (2013) on large scale tests to investigate the proppant distribution using a 63-foot stage and three 0.42-inch simulated perforations with zero phasing. Their work demonstrates that proppant does not distribute evenly, but the work was also limited to a single perforation scheme.

The most recent study was conducted by Ngameni et al. (2017), where they utilized a 2.5-inch horizontal wellbore with three perforation clusters at 6 SPF at a 90-degree phasing using fresh water. Their conclusions were that uneven distribution of proppant was observed between each of the clusters when using 100, 40/70, and 20/40 mesh sand sizes. However, even proppant distribution was observed using ultra-light weight (ULW) proppants. But their work was limited to one fluid type (fresh water) and a specific gravity of 2.65, as the ULW proppant has a specific gravity of 1.0 which indicates that the momentum difference between the fluid and the proppant is negligible.

There are other theoretical studies in the literature, among them a study conducted by Warpinski et al. (2009). These studies indicate that proppant distribution between the perforation

clusters in tight shale reservoirs is very critical, and low propped fracture areas lead to a reduction in the oil and gas recoveries. If the proppant is not evenly distributed between the perforation clusters, it follows that not all the perforated intervals will be adequately stimulated. In the study conducted by Miller et al. (2011), they indicate that 70% of the production in tight gas formations is contributed by only 30% of the perforated intervals. In other words, two-thirds of the perforation intervals do not contribute much to production. In addition, there appears to be no published studies on correlations for proppant distribution prediction between perforation clusters.

Therefore, it is crucial to ensure that proppant is sufficiently transported both in the wellbore and into the induced fractures. This PhD research presents the results obtained from experimental tests conducted on different types of proppant using fresh water and high loading friction reduced fluids (HLFR). The project investigates parameters that have a large influence on the proppant settling in the wellbore and the distribution of the proppant between perforation clusters. These parameters include, but are not limited to, proppant concentration, injection rate, fluid viscosity, and proppant types and sizes.

In addition, the project aims to develop experimental correlations that can be the first of their kind to be based on experimental data obtained by utilizing a horizontal wellbore apparatus. The distribution of proppant in multiple perforation clusters after hydraulic fracturing must be fully understood in order to achieve a uniform proppant distribution during fracturing operations. If performed correctly, the production from unconventional shale gas and oil reservoirs will be optimized.

1.2 Objectives of the Research

One aim of multistage hydraulic fracturing treatments is to place equal amounts of proppant into various fractures, since the production from these fractures is dependent on the amount of proppant and associated conductivity placed inside each fracture. Prediction of proppant transport in horizontal wellbores and in complex fracture networks is vital to achieving better conductivity and is useful for designing the overall hydraulic fracture treatment. Therefore, the ultimate goal of this PhD research project is to conduct an experimental study for investigating the effects of injection rate, fracturing fluid viscosity, and proppant concentration on proppant transport and distribution in the horizontal wellbore and also out of the perforation clusters. The main objectives of the experimental research are summarized in the following steps:

1. To develop and build an experimental apparatus with a series of perforation clusters to study the proppant behavior in horizontal wellbores using fresh water and high loading friction reduced (HLFR) fluids;
2. To investigate the parameters that have a significant impact on proppant transport through the horizontal wellbore and the perforation clusters. These parameters include injection rate, proppant concentration, fluid viscosity, and proppant types and sizes;
3. To vary the parameters that can have a significant impact on proppant distribution such as fluid viscosity, proppant concentration, proppant size, proppant density, and flow rate;
4. To evaluate proppant that settled/left in the horizontal wellbore after the pumping is stopped for each test;
5. To develop experimental correlations to predict the proppant distribution between the perforation clusters using the data acquired. This takes into consideration such parameters as flow rate, proppant concentration, proppant density, and proppant median diameter;
6. To provide recommendations to improve proppant transport in horizontal wellbores and through perforation clusters; and,
7. Finally, to deepen theoretical knowledge of proppant transport mechanisms in the horizontal wellbore as well as between the perforation clusters. Having understood this phenomena, hydraulic fracturing treatment designs can be improved.

CHAPTER 2

LITERATURE REVIEW

As it was mentioned in Chapter 1, the main goal of this study is to investigate the effects of the fracturing fluid viscosity, flow rate, proppant concentration, and proppant size and type on the proppant behavior and distribution between perforation clusters in horizontal wellbores. Therefore, the literature review and background material in Chapter 2 highlight the following areas (1) proppant transport and suspension in horizontal pipes, (2) proppant settling theories, (3) laminar and turbulent flow in horizontal wellbores, (4) characteristics and behavior of Newtonian and non-Newtonian fluids, (5) proppants and fracturing fluids, and (6) completion methods.

2.1 Proppant Transport and Suspension in Horizontal Pipes

The particle transport process is extensively encountered in several applications such as sewer water and pipeline operations, chemical and nuclear industries, and mining and factory applications. In the oil and gas industry, most recent studies and research into particle transport have been focused on sand production, and more recently on proppant transport and proppant flowback in hydraulic fracturing treatments.

Due to the uncertainties associated with the prediction of slurry flow in pipes, several studies have been conducted to quantify the effect of particle concentrations, pipe orientations, and flow conditions on slurry flow. The initial classification of slurry flow regimes was developed by Durand and Condolios in 1952. Other investigators such as Zandi (1971) have explained that different flow patterns can be created by different slurry concentrations and compositions.

In any typical fracturing treatment, proppants with fracturing fluids are pumped from the surface into the wellbore and finally into the induced fractures and the natural fracture networks. Therefore, proppant suspension in the fracturing fluid is very important to deliver proppant, and it can be as complex as viscous fluids or as simple as water. Low viscosity fluids such as slickwater can be pumped in laminar or turbulent flow. However, when the fluid moves in the wellbore and enters the perforations, the remaining fluid velocity continually decreases, and as a result, turbulent flow may not continue away from the perforations into the induced fractures (Daneshy 2011).

Another study was conducted by Biot and Medlin in 1985 to quantify the parameters that have a significant impact on particle suspension in horizontal wellbores. According to their study,

three conditions in which the proppant transport behavior can be determined are suspension transport, critical pickup, and bed load transport. They found that the ratio of particle settling velocity (V_t) to horizontal fluid flow velocity (u), i.e. V_t/u , can be utilized as a simple method for predicting the mechanism of suspension that proppant will encounter at different fluid velocities. If the ratio of V_t/u is less than 0.1, the particles are completely in suspension; if the ratio is between 0.9 and 0.1, bed load transport is taking place; but if this ratio is equal to around 0.9, then critical pickup starts to occur. Figure 2.1 shows the different types of proppant transport mechanisms that can be encountered during slurry transport in a horizontal pipe.

During particle transport in horizontal pipes, when the fluid velocity drops below the critical flow velocity, solid particles in the carrier fluid come out of suspension and form a bed on the bottom of the pipe. This bed can be designated as mobile or immobile bed load transport. If the fluid velocity is further decreased below the critical settling velocity, the immobile bed load transport occurs as shown in Figure 2.1a. Mobile bed load transport occurs if the particle layer loses adhesive friction and begins to flow above a stationary bed as can be seen in Figure 2.1c. But the velocity of this bed load is always less than the fluid stream velocity that is above it.

Regarding the particle suspension, if the horizontal slurry velocity of proppant is equal to the carrier fluid velocity, the proppant grains will be fully suspended in the flow stream. According to Biot and Medlin, the suspension transport mechanisms can be divided into heterogeneous suspension as shown in Figure 2.1d or pseudohomogeneous suspension as shown in Figure 2.1e. As can be noted, the heterogeneous suspension occurs when the concentration of the sediment increases from the top to the bottom of the fluid column, whereas the pseudohomogeneous suspension occurs when there is uniform distribution of the particles in the fluid column.

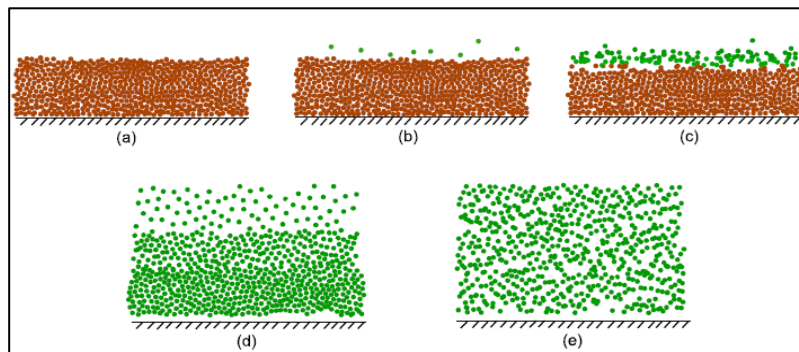


Figure 2.1: Proppant transport modes: a) immobile proppant bed, b) initiation of grain pickup, c) bed load transport, d) heterogeneous suspension, and e) pseudo-homogeneous suspension. Brown-colored grains are stationary, and green-colored grains are in motion (from Al-Tailji et al. 2014).

If fluid flows in a horizontal pipe, a viscous or laminar sublayer, which is typically a very thin layer, occurs adjacent to the pipe wall as shown in Figure 2.2. For example, if water flows with an average fluid velocity of 10 ft/sec in a 3-inch diameter pipe, the viscous/laminar sublayer is approximately a 0.002-inch thickness (Munson et al. 2012). The fluid velocity in this sublayer is critical for the reason that the turbulent flow properties in this thin layer are dependent mostly on the pipe wall roughness, unlike laminar flow which is independent of pipe roughness.

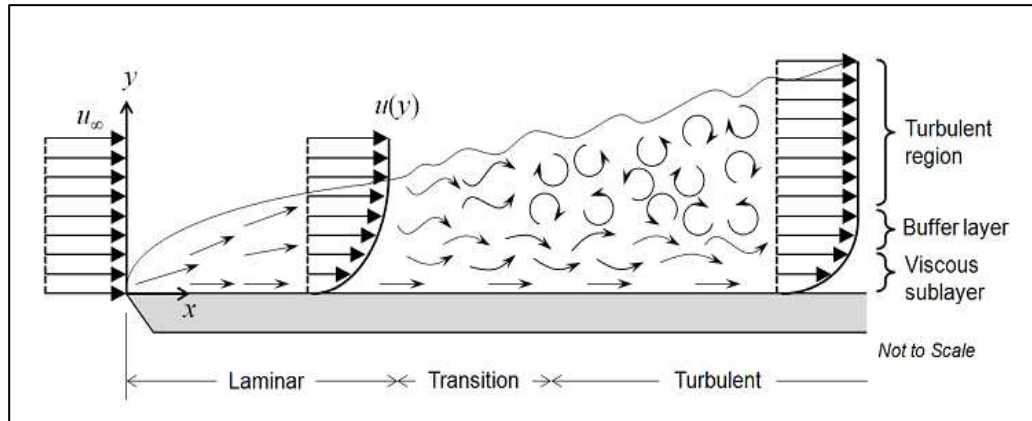


Figure 2.2: Laminar/viscous sublayer over thin horizontal plane (from COMSOL 2017).

Some papers in the literature demonstrate that higher viscosity fluids are assumed to be very significant at suspending proppant in horizontal wellbores since higher viscosity fluids have higher drag. This can be explained because viscous sublayers that exist adjacent to the pipe wall may hinder the viscosified fluid's ability to transport proppant particles that are deposited on the bottom of the pipe. In this case, thinner fluids such as slickwater at higher Reynolds numbers can transport proppant that is deposited in the viscous sublayer because the diffusive forces on proppant particles will have a more significant effect on re-suspending the proppant than drag only.

2.2 Proppant Settling Theories

Knowing the particle settling velocity before a hydraulic fracturing treatment is critical for predicting the final proppant distribution in the wellbore and between the perforation clusters. When slurry flows through a horizontal pipe and particles of the slurry settle down by their gravity through the fluid column without being affected by the existence of other adjacent particles or by any outside forces, the process is described as "free settling." In contrast, if the proppant particles

in the fluid column are affected by other nearby particles, then movement of these particles is also hindered by other adjacent particles, and this process is referred to as "hindered settling."

As mentioned in Section 2.1, there are some parameters that have a significant effect on particle transport settling in horizontal wellbores. These factors include, but are not limited to, flow rate, fluid viscosity, proppant concentration, the difference in density between the fluid and the proppant, and proppant median diameter. In the literature, there are several correlations for determination of particle settling velocity. In this section, correlations that have been considered by some authors to be helpful for estimating the settling velocity of the particles are addressed.

2.2.1 Stokes' Law

The first equation used to determine the vertical settling velocity for a single particle was derived by Stokes as presented in Equation 2.1. The Stokes' Law equation states that the settling velocity is directly proportional to the difference between particle and fluid densities and is inversely proportional to the viscosity of the fluid.

This equation has been used for a while, but it is only valid for a single particle and static fluid conditions. The terminal particle settling velocity can be expressed by:

$$V_t = \frac{dp^2(\rho_p - \rho_f)g}{18\mu_f} \quad (2.1)$$

Where,

V_t = Terminal settling velocity, m/s

dp = Average particle diameter, m

g = Gravitational velocity, m/s²

ρ_f = Density of the fluid carrier, g/cm³

ρ_p = Density of the particle, g/cm³

μ_f = Fluid dynamic viscosity, Pa-s

Several experimental and numerical simulation studies for single particle settling in hydraulic fracturing fluids indicate that Stokes' Law is insufficient to predict particle settling in flowing fluid, and it is only valid for a Reynolds number of about 0.1 (Roodhart 1985; Daneshy 1978; Goel and Shah 2001; Cleary and Fonseca 1992).

2.2.2 Durand's Equation

Since Stokes' Law equation is not valid for dynamic fluid conditions, Durand in 1953 conducted experimental tests on sand-water and gravel-water flow at different pipe and particle sizes to determine behaviors under these conditions. He derived a new empirical correlation for predicting particle transport velocities in pipes as shown in Equation 2.2.

$$V_c = F_L [2g(s - 1)D]^{1/2} \quad (2.2)$$

Where,

V_c = Minimum/critical transport velocity, m/s

D = Pipe inner diameter, m

F_L = Modified Froude number, dimensionless

s = Ratio of particle and fluid densities, (unitless)

The Modified Froude number can vary based on the particle concentration as well as on the particle diameter. In order to determine the Modified Froude number, Durand provided a graph where particle diameter and concentration could be used to determine F_L . A graph of quartz sand concentrations adapted from Durand's chart is displayed in Figure 2.3.

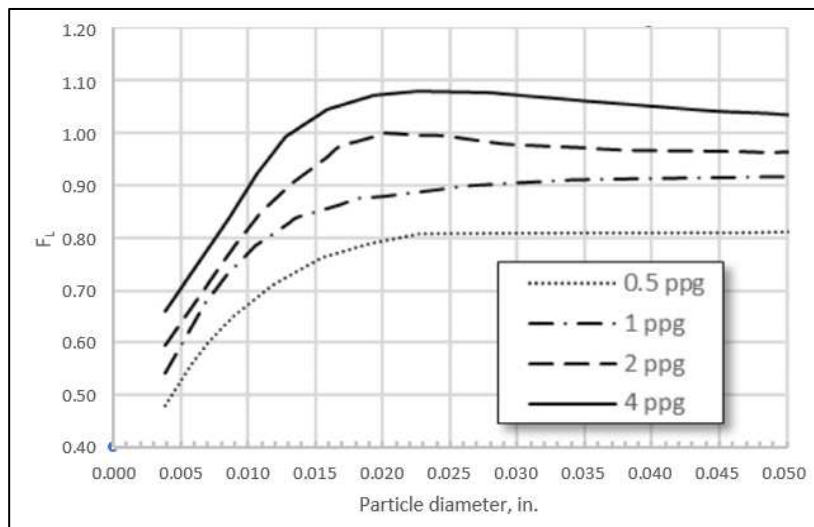


Figure 2.3: Modified Froude number F_L against particle diameter at various sand concentrations (adapted from Durand's chart 1953).

2.2.3 Wasp’s Modified Durand Equation

Wasp et al. (1970) added a modification to the Durand equation (Equation 2.2) to account for the effect of particle size distribution as shown in Equation 2.3. This technique is the most widely used technique for applications of slurry transport to determine the minimum critical velocity (Mali et al. 2014). This correlation is also considered to be optimistic in accounting for small particle diameter, and it requires looking up the F_L from the Durand’s chart.

$$V_c = F_L [2g(s - 1)D]^{1/2} \left(\frac{d_p}{D}\right)^{1/6} \quad (2.3)$$

2.2.4 Stokes’ Law (Modified)

In 2005, Schein presented a correlation for determining the terminal settling velocities as described in Equation 2.4. This equation accounts for the particle diameter, and it has been validated for different proppant types and sizes.

$$V_t = 1.15 \times 10^3 (dp^2/\mu_f)(SG_p - SG_f) \quad (2.4)$$

Where,

SG_f = Fluid specific gravity, dimensionless

SG_p = Particle specific gravity, dimensionless

In addition, Schein determined the terminal settling velocity for different types of proppant across a wide range of specific gravities. Table 2.1 shows a comparison of settling velocities for two proppant sizes, 20/40 and 40/70, at different specific gravities using Equation 2.4.

Table 2.1: Terminal settling velocity rate for different proppant sizes and types (from Schein 2005)

20/40 Proppant	Specific Gravity	Settling Velocity ft/minute
Bauxite	3.65	23.2
White Sand	2.65	16.6
Resin Coated Sand	2.55	15.9
ULW-125	1.25	4.3
40/70 Proppant	Specific Gravity	Settling Velocity ft/minute
Bauxite	3.65	6.0
White Sand	2.65	4.4
Resin Coated Sand	2.55	4.2
45/65 ULW-125	1.25	1.2

It can be noted from Table 2.1 that the terminal settling velocities for bauxite with a specific gravity of 3.65 at proppant sizes of 20/40 and 40/70 are 23.2 ft/minute and 6.0 ft/minute, respectively. This indicates that proppant size has a significant impact on the settling velocity: as proppant size increases, the settling velocity increases and vice versa. Also, as can be seen from the table, the terminal settling velocity for ULW-125 with a specific gravity of 1.25 and proppant size of 20/40 is 4.3 ft/minute. This is quite low, if compared with the settling velocity of sand with a specific gravity of 2.65 and 20/40 mesh size. This demonstrates that the specific gravity of the proppant also has a significant effect on the settling velocity, which needs to be considered during hydraulic fracturing treatments.

A study was conducted by Shah and Lord (1990) to quantify transport properties of different hydraulic fracturing slurries in three horizontal wellbores with different diameters. The study suggest that particle deposition and suspension are greatly dependent on the particle density, where higher density proppant requires higher critical velocities.

2.3 Laminar and Turbulent Flow in Horizontal Pipes

A velocity profile is developed when fluid flows in a horizontal pipe. Many fluid mechanics textbooks, such as Munson et al. (2012), divide the velocity profile into three sections: a turbulent layer, a buffer layer, and a viscous sublayer as shown in Figure 2.4. Starting with the viscous sublayer, which is always thin as discussed in Section 2.1, the flow in this region is identified as streamlined. The velocity is extremely low because of the no-slip condition that exists at the pipe wall where the fluid velocity is zero. In this region, the dominance of the viscous forces over the momentum lead to a decrease in the turbulent forces until they become laminar; hence, the viscous sublayer is also known as the laminar sublayer.

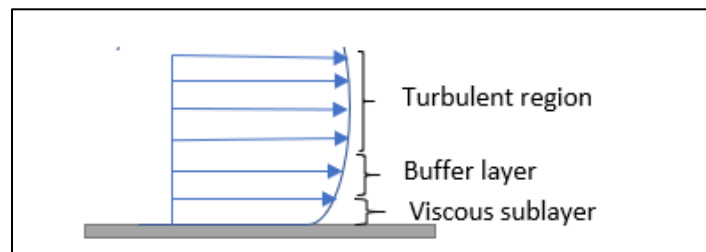


Figure 2.4: The velocity profile in partially developed pipe flow (modified from Munson et al. 2012).

The second velocity profile region is the buffer layer, which is next to the viscous sublayer. In this region, the fluid velocity increases significantly from the pipe wall and the laminar flow starts to have a vertical segment. This layer acts as a cushion between the viscous sublayer and the main flow (turbulent layer) where turbulence is fully developed. Next to the buffer layer is the turbulent layer through which the turbulent flow is fully active in the pipe. In this section, the turbulent forces are dominant over the viscous, and the fluid velocity reaches a maximum value.

To determine the velocity profile from the pipe wall to the center of the pipe, the shear velocity must be determined first as shown in Equation 2.5.

$$u_s = \sqrt{\frac{\tau_w}{\rho_f}} \quad (2.5)$$

Where,

u_s = Shear velocity at pipe wall, ft/s

τ_w = Wall shear stress, psi

The wall shear stress τ_w is determined by calculating the pressure drop in a pipe and can be determined from the Darcy Weisbach Equation as follows:

$$\tau_w = \frac{D}{4} \left(\frac{Lp}{l} \right) \quad (2.6)$$

Where,

$\frac{Lp}{l}$ = Pressure drop gradient in a pipe, psi/in.

The velocity profile for fully developed turbulent flow in a horizontal pipe tends to be flatter at the center with a vertical drop near the wall of the pipe as shown in Figure 2.5a. In contrast, for fully developed laminar flow, the velocity profile has a parabolic velocity distribution. The layers of the fluid flow slide along each other, and the vertical velocity is zero as shown in Figure 2.5b. The fluid velocity for both regimes increases from a zero value at the pipe wall and reaches a maximum value at the center. For hydraulic fracturing fluids, it is important to work with an average fluid velocity, which stays constant as the pipe diameter remains constant (Munson et al. 2012).

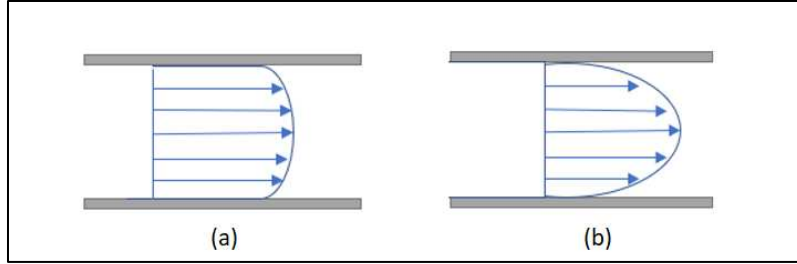


Figure 2.5: Turbulent and laminar velocity profiles in pipe: a) turbulent, b) laminar (modified from Munson et al. 2012).

Typically, there are three flow regimes for fluid flow in a pipe: laminar, transitional, and turbulent flow regimes. In order to determine the flow regimes for fluid flow in a pipe, the Reynolds number needs to be determined for that fluid. In 1883, Reynolds developed an expression called Reynolds number (dimensionless quantity), which can be defined as the ratio of inertial forces to viscous forces. The Reynolds number has a formula of $Re = uD/v$, where u is the average fluid velocity, D is the pipe inner diameter, and v is the kinematic viscosity of the fluid, where the Reynolds number is dimensionless. However, Reynolds number is only valid for Newtonian fluids where the relationship between the shear rate and shear stress is constant. In other words, the fluid viscosity remains constant as shear rate increases. Therefore, in this study, fresh water (Newtonian fluid) was used to evaluate transport proppant in a horizontal wellbore, where the fluid viscosity remains constant over the entire period of any experimental test.

2.4 Characteristics and Behavior of Non-Newtonian Fluids

Non-Newtonian fluids are encountered in many applications such as industrial, chemical, and mining engineering, and more recently in hydraulic fracturing applications. Most of the fluids used in hydraulic fracturing applications follow non-Newtonian fluid behavior where the fluid viscosity varies with the wide variations in the shear rate (Roodhart 1985). Different from Newtonian fluids, the viscosity characteristic for non-Newtonian fluids is more complex, and the viscosity of these fluids decreases as shear rate increases and vice versa. Metzner and Reed (1955) derived a formula to identify the non-Newtonian fluid flow regimes. This formula is called the generalized Reynolds number, Re_{gen} . It results from its relationship to the Darcy friction factor, f_{Darcy} , and is defined by the expression presented in Equation 2.7.

$$Re_{gen} = \frac{\rho D^n u^{2-n}}{K ((3n+1)/(4n))^n 8^{n-1}} \quad (2.7)$$

Where,

Re_{gen} = Generalized Reynolds number, dimensionless

K = Consistency index, $Pa \times s^n$

n = Flow behavior index, dimensionless

In hydraulic fracturing treatments, the geometry and extension of the fracture network depends somewhat on rheological properties of the fluids. A study conducted by Shah (1993) indicates that fluid rheology can have a significant effect on the proppant distribution in the induced fractures. Another experimental study conducted by Ibrahim et al. 2018 using friction reducer in slickwater fracturing treatments. Their work demonstrated that friction reducer has lower energy loss and better proppant transport capacity with no damage to reservoir formations compared to the conventional fracturing fluids.

In this research, high loading friction reducer (HLFR) was used at different concentrations to increase the fluid viscosity. These fluids are characterized by having high molecular weight. They are added to water at low concentrations to reduce the frictional energy that dissipates in turbulent flow. These fluids are also considered as shear thinning fluids where the viscosity behaves significantly different than Newtonian liquids as shown in Figure 2.6. As can be noted from the graph, the viscosity of these fluid decreases as the shear rate increases.

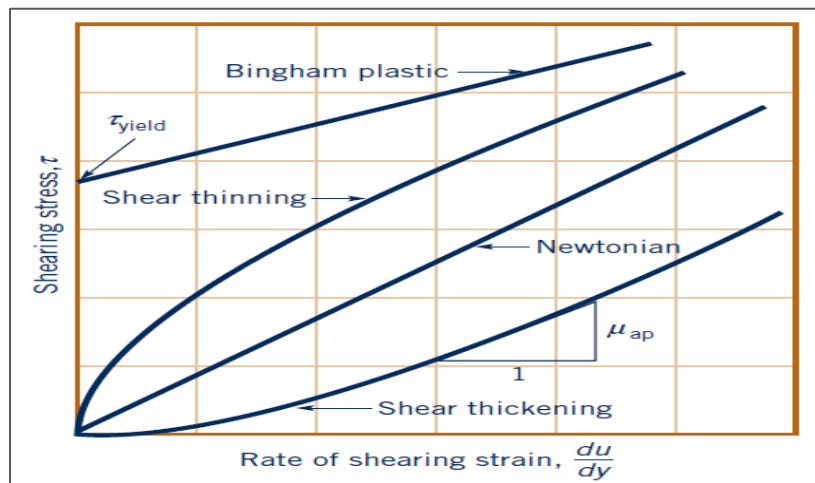


Figure 2.6: Shear stress versus rate of shearing strain for several types of fluids, including non-Newtonian fluids (from Munson et al. 2012).

When the HLFR fluid is at static fluid conditions, the viscosity is high, because there are no shear forces applied. In hydraulic fracturing treatments, the fracturing fluid is pumped from the

tank through the pumping unit, and then through the wellbore and finally out of the perforations. The fluid viscosity is reduced because of high shear forces applied to the fluid. Some of the most common non-Newtonian fluids are the pseudoplastic fluids which have large apparent viscosities. The viscosity of these fluids is dependent on the shear rate. Therefore, laminar flow conditions are encountered more frequently at low flow velocities but can also occur at relatively high flow velocities (Chhabra and Richardson 2008).

There are various mathematical models used to describe the behavior of these fluids. Among them is the Power Law Model as shown in Equation 2.8. This model has been widely used to describe the behavior of fracturing fluids in hydraulic fracturing treatments.

$$\tau = K\gamma^n \quad (2.8)$$

Where,

τ = Shear stress, Pa

γ = Shear rate, s^{-1}

The Power Law model has two parameters, the flow behavior index, n , and the flow consistency index, K . For $n > 1$, the fluid shows shear-thickening behavior where the viscosity increases with the increase of the shear rate. For $n = 1$, the fluid exhibits Newtonian properties where the relationship between the shear rate and shear stress is constant, and the viscosity also remains constant. However, for $n < 1$, the fluid shows shear-thinning behaviors in which the viscosity decreases with the increase of the shear rate as shown in Figure 2.6. Therefore, in this study, the rheological properties of the fracturing fluid were determined at different concentrations of HLFRR and across a wide range of shear conditions. All the results are presented and discussed in more detail in Chapter 5.

2.5 Fracturing Fluids

One of the most important properties of fracturing fluid is viscosity. It is generally assumed that higher viscosities do a better job of transporting proppant as well as generating a given fracture geometry. Much study and efforts go into the development of fracturing fluids. These fluids are designed to withstand the high temperatures encountered during hydraulic fracturing treatments. A typical hydraulic fracturing fluid is composed of around 99.5% water and sand and less than 1%

of additives, depending on the characteristics of the formation (Anadarko 2015). Figure 2.7 shows a typical fracturing fluid composition for hydraulic fracturing treatments.

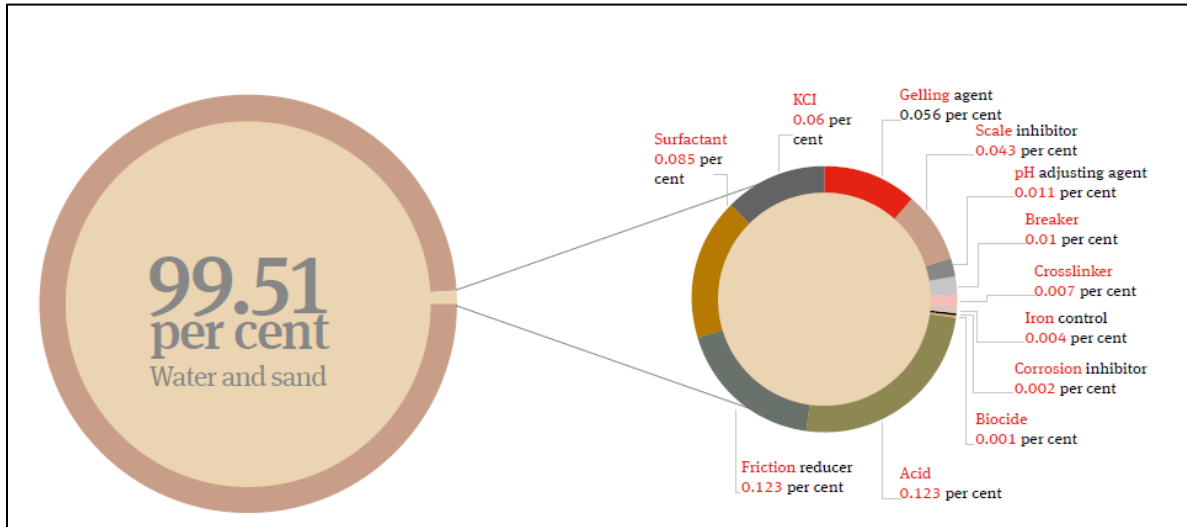


Figure 2.7: Typical fracturing fluid composition (from Norton Rose Fulbright 2015).

There are some important parameters or properties that should be considered when designing or selecting fracturing fluid in hydraulic fracturing treatments. These include:

- The fluid must provide sufficient fracture width to ensure proppants can enter the fracture (Penny et al. 2012);
- The fluid must create a desired net pressure to create some desired height growth or prevent breaking out into some unwanted zone;
- The fluid should have enough viscosity to transport proppant from the wellbore to the fracture tip (Ibrahim et al. 2018);
- The fluid should be safe to avoid on-site danger for personnel (Miskimins 2016);
- The fluid must not cause negative environmental impacts. In other words, the composition of the fluid should be as “green” as possible (Nixon et al. 2014);
- The fluid should break down easily to low viscosity to have easy flowback (Montgomery 2013);
- The fluid should be cost effective;
- The fluid must not interact and cause damage to the formation mineralogy and formation fluids (Montgomery 2013);

- The fluid should not change the relative permeability of the formation or create damage to the fracture conductivity (Murtaza et al. 2013).
- The fluid must mix easily even under threatening weather conditions (Montgomery 2013); and,
- The fluid needs to have less friction pressure loss in order to avoid generating high pressure at the surface (Montgomery 2013).

The most prevalent fracturing fluids currently used in hydraulic fracturing treatments are slickwater fluids. These fluids are preferred due to their low cost and their tendency to create more fracture networks in the shale formations. During the last three decades, slickwater fluids have achieved great success for increasing the stimulated reservoir volume (SRV) by increasing the induced fractures compared to conventional fracturing fluid (Kostenuk and Browne 2010). A field case study was conducted by King (2010). His results reveal that slickwater fluid has a significant effect on SRV for the Barnett shale, as can be shown in Figure 2.8. The figure shows that the production was tripled when the cross-linked fracturing fluid was replaced by slickwater fluid. Another advantage of using slickwater fluids is that they have a much lower chemical loading. This generally allows for inexpensive, faster, and easier well cleanup, and overall leads to less formation damage (Palisch et al. 2010).

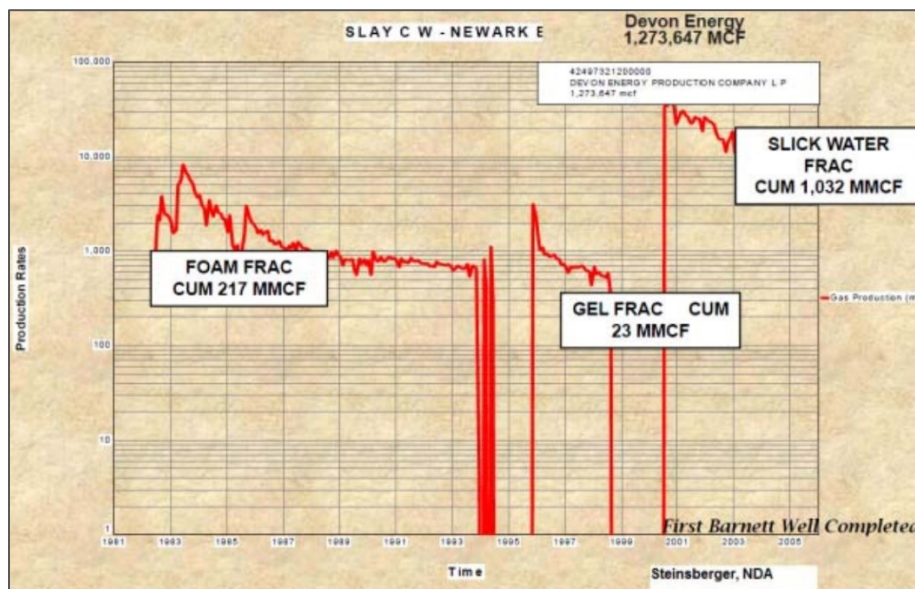


Figure 2.8: Barnett Shale gas production after using slickwater (from King 2010).

In 2005, Schein investigated the usage of different fracturing fluid types in the U.S. in 2004. Figure 2.9 represents the percentage of total jobs performed for each type of fluid.

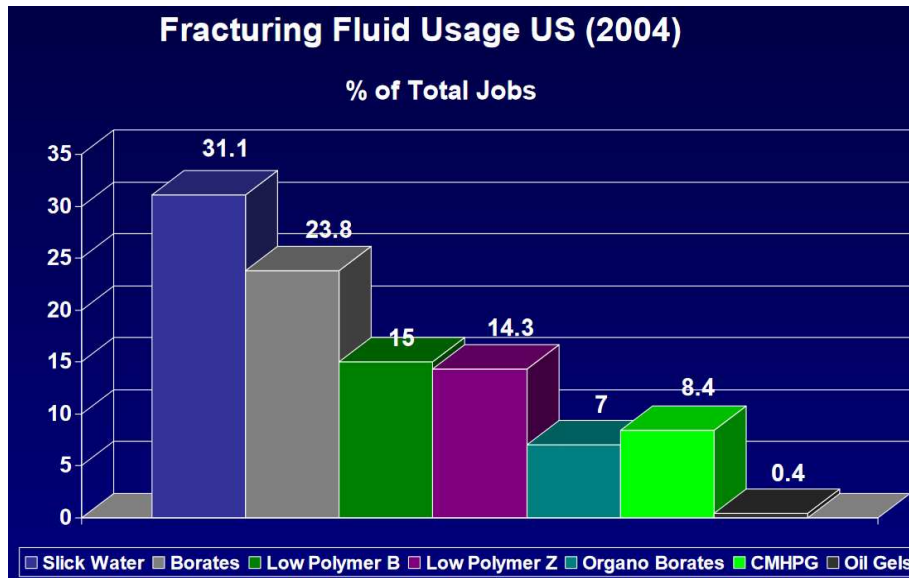


Figure 2.9: Fracturing fluid type usages in the US in 2004 (from Schein 2005).

However, there are some challenges associated with slickwater fluids. One of the key challenges is the ability to transport proppant. The low viscosity associated with these fluids can lead to poor proppant transport as proppant is deposited before reaching the tip of the fractures. Therefore, a significant reduction in the propped fracture half-length and height will occur; hence, the productivity can be low.

Also, because of the low viscosity of the slickwater fluids, the injection rate at the surface increases to achieve effective proppant transportation. Therefore, pressure loss due to the friction inside the tubulars will increase rapidly, and as result, more hydraulic horsepower is required to redeem this energy loss (Ibrahim et al. 2018). A successful fracturing stimulation treatment utilizing slickwater fluids can be achieved after overcoming the incapability of these fluids to transport proppant efficiently (Palisch et al 2010).

Beside water-based fluids, there are other classifications of fracturing fluids such as, oil-based fluids, alcohol-based fluids, emulsion fluids, and foam-based fluids. Linear gel fluids are formed from a wide selection of different polymers in an aqueous base. The polymers that are most commonly used to formulate these linear gels are hydroxypropyl guar (HPG), carboxymethyl HPG (CMHPG), and hydroxyethyl cellulose (HEC). These polymers come in dry powders that hydrate

or swell when blended with water and form a viscous fluid (Montgomery 2013). Table 2.2 represents the most common types of fracturing fluids and conditions for their use.

Table 2.2: Fracturing fluid types and conditions for their use (from PetroWiki 2016)

Base Fluid	Fluid Type	Main Composition	Used For
Water	Linear	Guar, HPG, HEC, CMHPG	Short fractures, low temperature
	Crosslinked	Crosslinker + Guar, HPG, CMHPG or CMHEC	Long fractures, high temperature
	Micellar	Electrolite + Surfactant	Moderate length fractures, moderate temperature
Foam	Water based	Foamer + N ₂ or CO ₂	Low-pressure formations
	Acid based	Foamer + N ₂	Low-pressure, carbonate formations
	Alcohol based	Methonal + Foamer + N ₂	Low-pressure, water-sensitive formations
Oil	Linear	Gelling agent	Short fractures, water-sensitive formations
	Crosslinked	Gelling agent + Crosslinker	Long fractures, water-sensitive formations
	Water emulsion	Water + Oil + Emulsifier	Moderate length fractures, good fluid loss control
Acid	Linear	Guar or HPG	Short fractures, carbonate formations
	Crosslinked	Crosslinker + Guar or HPG	Longer, wider fractures, carbonate formations
	Oil emulsion	Acid + Oil + Emulsifier	Moderate length fractures, carbonate formations

The additives that are added to the fracturing fluid varies from one shale basin or formation to another. These additives are chemicals commonly used in daily life and are safe when properly handled and used correctly, but if not used appropriately it may have a significant effect on human health and the environment. Table 2.3 shows a list of potential additives that used in hydraulic fracturing treatments.

Table 2.3: List of fracturing fluid additives and their purpose and common uses (from U.S. Department of Energy Office of Fossil Energy and National Energy Technology Laboratory 2009)

Additive Type	Main Compound(s)	Purpose	Common Use of Main Compound
Diluted Acid (15%)	Hydrochloric acid or muriatic acid	Help dissolve minerals and initiate cracks in the rock	Swimming pool chemical and cleaner
Biocide	Glutaraldehyde	Eliminates bacteria in the water that produce corrosive byproducts	Disinfectant; sterilize medical and dental equipment
Breaker	Ammonium persulfate	Allows a delayed break down of the gel polymer chains	Bleaching agent in detergent and hair cosmetics, manufacture of household plastics
Corrosion Inhibitor	N,n-dimethyl formamide	Prevents the corrosion of the pipe	Used in pharmaceuticals, acrylic fibers, plastics
Crosslinker	Borate salts	Maintains fluid viscosity as temperature increases	Laundry detergents, hand soaps, and cosmetics
Friction Reducer	Polyacrylamide	Minimizes friction between the fluid and the pipe	Water treatment, soil conditioner
	Mineral oil		Make-up remover, laxatives, and candy
Gel	Guar gum or hydroxyethyl cellulose	Thickens the water in order to suspend the sand	Cosmetics, toothpaste, sauces, baked goods, ice cream
Iron Control	Citric acid	Prevents precipitation of metal oxides	Food additive, flavoring in food and beverages; Lemon Juice ~7% Citric Acid
KCl	Potassium chloride	Creates a brine carrier fluid	Low sodium table salt substitute
Oxygen Scavenger	Ammonium bisulfite	Removes oxygen from the water to protect the pipe from corrosion	Cosmetics, food and beverage processing, water treatment
pH Adjusting Agent	Sodium or potassium carbonate	Maintains the effectiveness of other components, such as crosslinkers	Washing soda, detergents, soap, water softener, glass and ceramics
Proppant	Silica, quartz sand	Allows the fractures to remain open so the gas can escape	Drinking water filtration, play sand, concrete, brick mortar
Scale Inhibitor	Ethylene glycol	Prevents scale deposits in the pipe	Automotive antifreeze, household cleansers, and de-icing agent
Surfactant	Isopropanol	Used to increase the viscosity of the fracture fluid	Glass cleaner, antiperspirant, and hair color

2.6 Proppants

Proppants are solid materials with uniformly sized particles, treated sand or man-made ceramic materials. They are designed to keep the induced fractures in the productive formation open after pumping is stopped. Proppants should withstand closure stress under downhole conditions (Clark 2006) and should be carefully sorted for size and sphericity to provide an effective conduit for fluid to flow from the reservoir to the wellbore (Liang et al. 2016).

In addition, the optimum proppant shape should be spherical or approximately spherical and non-angular since such that shape keeps the proppant particles packed together in such a way to maximize permeability. A typical proppant shape is either spherical or near spherical. ISO 13503-2:2006 provides standard testing measurements for evaluating proppants used in hydraulic fracturing treatments. Figure 2.10 shows the standard reference scale that has been used for rating proppant shapes. For example, an average of 0.7 or greater (sphericity and roundness) is required for ceramic and resin coated proppants, and an average of 0.6 or greater (sphericity and roundness) is required for other types of proppant to reach the ISO requirements.

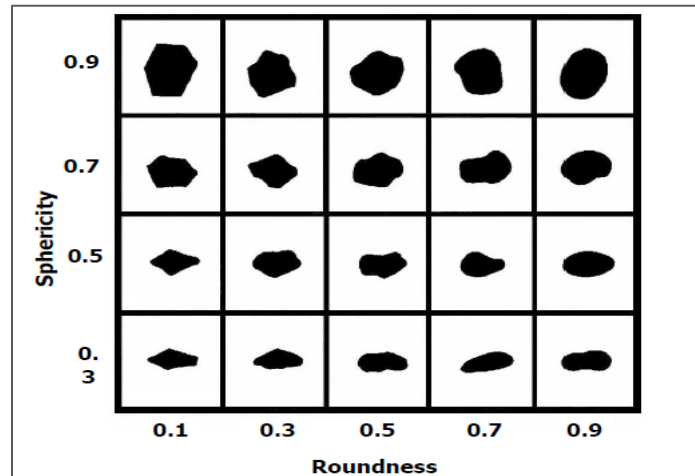


Figure 2.10: A chart for visual estimation of sphericity and roundness (from Miskimins 2016).

Many different proppants have been developed in the oil and gas industry with several types, sizes, shapes, and applications. Most proppants are simply made of silica or ceramics. However, there are some advanced proppants like ultra-light weight proppant which decreases proppant settling when using low viscosity fluids for proppant transportation (Palisch et al. 2014). Figure 2.11 shows some of the most common proppant types that are used in the oil and gas industry.

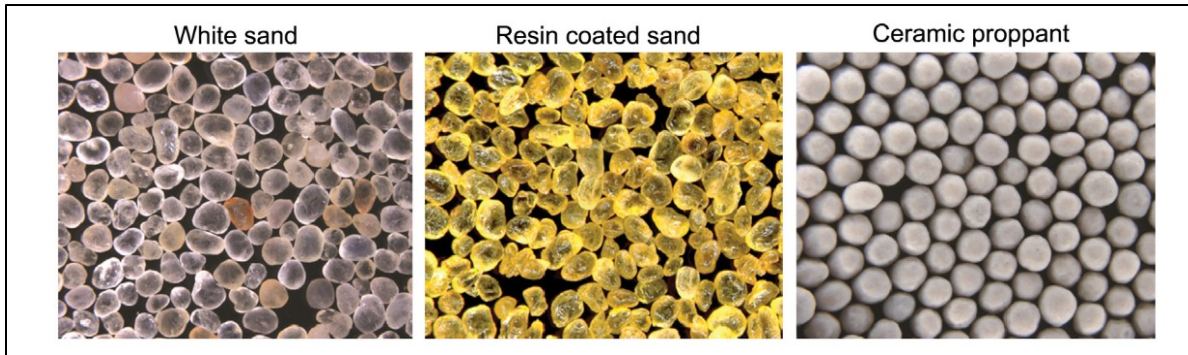


Figure 2.11: Some of the most common proppant types used in hydraulic fracturing applications (from CARBO Ceramics Inc 2017).

2.6.1 Sand Proppants

Since the first use of sand in hydraulic fracturing applications from the Arkansas River in 1947 by Stanolind Oil, proppant sand is still the most commonly natural mineral proppant used in hydraulic fracturing treatments (Liang et al. 2016). Quality products have round angles and a narrower particle-size distribution. The quality of the sand proppants is dependent on density, roundness, sphericity, and size (Liang et al. 2016). As an example, the 40/70 grade is frequently used in unconventional horizontal gas wells such as those in the Barnett, Fayetteville, Haynesville and Marcellus shales (Almond et al. 1995)

There are mainly two types of proppant sand, white sand and brown sand. White sand has few impurities (light color) and is rich in silicon dioxide compared with brown sand. It is generally mined from the Midwest region of the United States (Stephenson et al. 2003). In contrast, brown sand has a smaller amount of silicon dioxide, and it is not as strong as white sand; hence, the cost is lower (Liang et al. 2016). In this study, white sand with mesh sizes of 20/40 and 40/70 was used to evaluate their transport and behavior in various fluid viscosities.

2.6.2 Resin-Coated Proppants

Resin coated sand was developed when white and brown sand was crushed at high closure stress (Liang et al. 2016). The first use was to improve the conductivity of fracturing sand. Proppants are either coated with resins at the well location, where the hydraulic fracturing treatment is pumped, or coated at the production facility (Underdown et al. 1980). There are some advantages of using resin-coated proppant over sand proppant including:

- It is more uniform and can have a high significant strength by distributing the pressure load more uniformly (Sinclair et al. 1983);

- It can trap pieces of proppant (“fines”) and prevent them from entering the borehole (Liang et al. 2016); and,
- It combines particles together at high pressure and temperature to minimize proppant flowback (Sinclair et al. 1983).

2.6.3 Ceramic Proppants

Ceramic proppants are manufactured to have higher crush resistance and relatively high roundness and sphericity compared with white and brown sand; hence, the fracture conductivity is very high (Vincent 2002). They are manufactured from different minerals such as bauxite, magnesium silicate, kaolin, or mixtures of bauxite and kaolin. Some types of ceramic, such as high-density ceramic with a specific gravity of 3.6, can withstand stresses up to 18,000 psi (Liang et al. 2016).

Properties such as strength, shape, uniform size, and thermal stability that are associated with ceramic proppants can provide high performance in hydraulic fracturing treatments. A study conducted by Vincent (2002) shows that the combination of ceramic proppant properties such as strength, uniform shape and size has provided higher production performance than other types of proppant.

Ceramic proppants can be classified into three types based on their density: ultra-lightweight ceramics (ULWC), intermediate density ceramics (IDC) and high-density ceramics (HDC). In this research, ULW ceramic with proppant sizes of 20/40 and 40/70 were used to evaluate their transport in horizontal wellbores using low viscosity fluids. All the obtained results are presented and discussed in Chapter 4.

2.7 Completion Methods

Three types of completion methods have proved to be very successful in the stimulation of low-permeability reservoirs in the North America shale plays. These methods are plug-and-perf methods, ball-activated methods, and coiled tubing-activated frac sleeve methods. Sections 2.7.1-2.7.3 present these three methods of completion techniques.

2.7.1 Plug-and-Perf Completion Method

The plug-and-perf (PnP) completion method is indubitably the most common type of multistage completion methods used today. Around 85% of the wells that have been stimulated in shale formations in the United States used a plug-and-perf technique in a cemented casing (Algadi et al. 2015). This method is employed in wells with a cemented casing or liner. It involves pumping down a composite plug on a wireline-deployed string with perforating guns. The purpose of using a plug is to isolate a section of the wellbore from the previously fractured stages, so that fracturing fluid can be diverted out of the perforations. Each section of the stimulated wellbore is called a stage and each stage is perforated in several locations called clusters. Once the fracturing job is completed, the plugs are milled out to place the well on production. Figure 2.12 shows a wellbore diagram of a plug-and-perf completion method used in hydraulic fracturing treatments.

From the operational standpoint, this method is simple to implement, but the dynamics of operation should be fully understood. Since this method involves stimulating multiple clusters at the same time, operators are allowed to pump the fracturing fluid at relatively high flow rates. Also, screen out might not be a major issue. However, fracturing time could increase to uneconomic levels due to the number of trips and time required to perforate and isolate each individual stage.

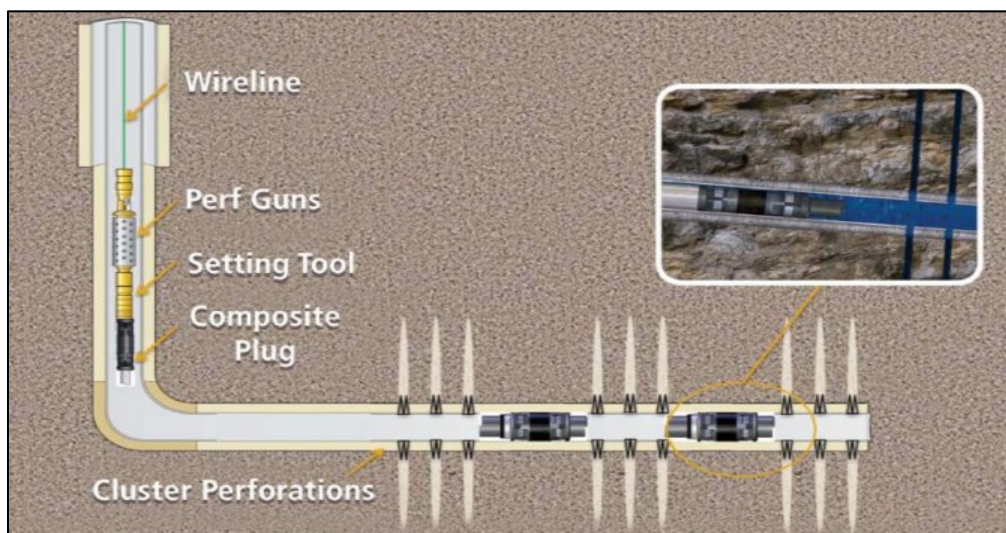


Figure 2.12: Wellbore diagram of a plug-and-perf completion method used in hydraulic fracturing treatments (from Bagci et al. 2017).

2.7.2 Ball-Activated Completion Method

This method of completion utilizes ball-activated fracturing sleeves to achieve multistage hydraulic fracturing. It has two main components; open-hole packers, which provide isolation, and ball-activated frac sleeves to divert fracturing fluid to each individual section/stage. The latter contains a ball seat that corresponds to a fracturing ball. Each of these sleeves is designed to facilitate a different size ball seat so that every sleeve can be selectively open. These sleeves are activated by dropping various sized frac balls from the surface. In most cases, these balls can dissolve within days or weeks after the stimulation treatment. After, the fracturing treatment is completed, the stimulated well can be put on production immediately. Figure 2.13 shows a wellbore diagram of a ball-activated completion method used in hydraulic fracturing treatments.

One of the advantages of this method is that it does not require to drill out any plugs. This results in a reduction of the post fracturing time. At the same time, the ball seats in the system will create restrictions inside the wellbore. Also, the number of the stages is highly dependent on the internal diameter of the wellbore, as a result, the number of stages per well will be limited.

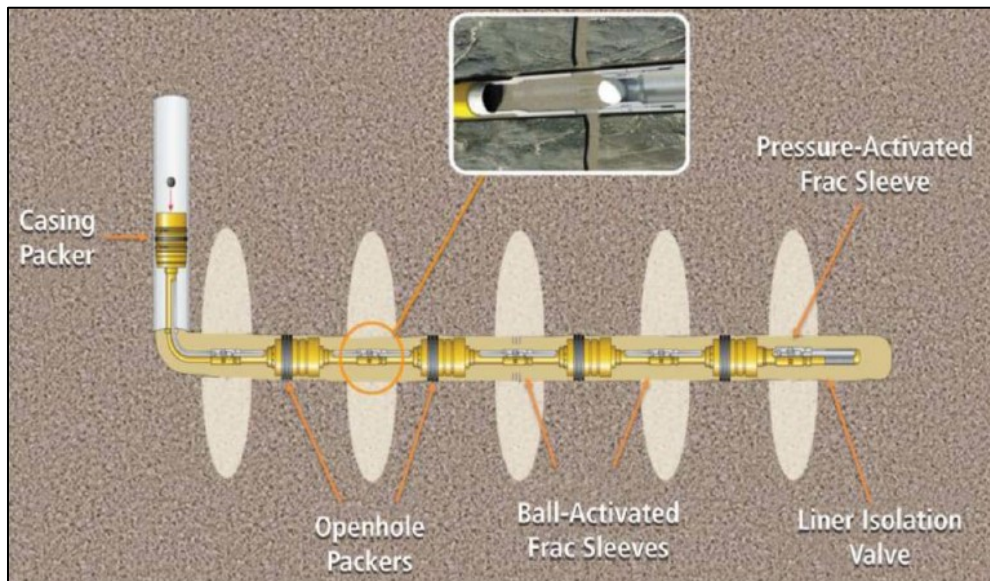


Figure 2.13: Wellbore diagram of a ball-activated completion method used in hydraulic fracturing treatments (from Bagci et al. 2017).

2.7.3 Coiled Tubing Activated Frac Sleeves Completion Method

This method of completion systems uses a coiled tubing (CT) with resettable packers. The packers are designed for openhole and cased-hole applications to isolate individual stages.

Fracturing sleeves are incorporated in the system to provide a path for the fracturing fluid to enter the selected interval of the formation. The locations and number of the sleeves should be determined when the casing or liner is run into the lateral section. Each sleeve has two internal pressure ports, one at the top and the other one at the bottom. In order to open the fracturing sleeves individually, a CT packer is used to create a pressure difference across the ports. When a specific stage is completed, the pumping is stopped. Then tension is applied to the packer to release it, and the assembly is relocated to the next sleeve. This process will be repeated until the completion of all stages. Figure 2.14 shows a wellbore diagram of the coiled tubing-activated frac sleeves completion method.

The advantage of CT is that time between frac stages is reduced due to no need for the abrasive perforating. Also, the post frac time is reduced due to not having to mill out any plugs. The average hydraulic horsepower (HHP) required for the operation is relatively low if compared with plug-and-perf completion method. This leads to a reduction in the footprint on site as less pumping equipment needed. The challenges include the potential for screen out, the failure in opening of the sliding sleeves, and limited treatment pump rates.

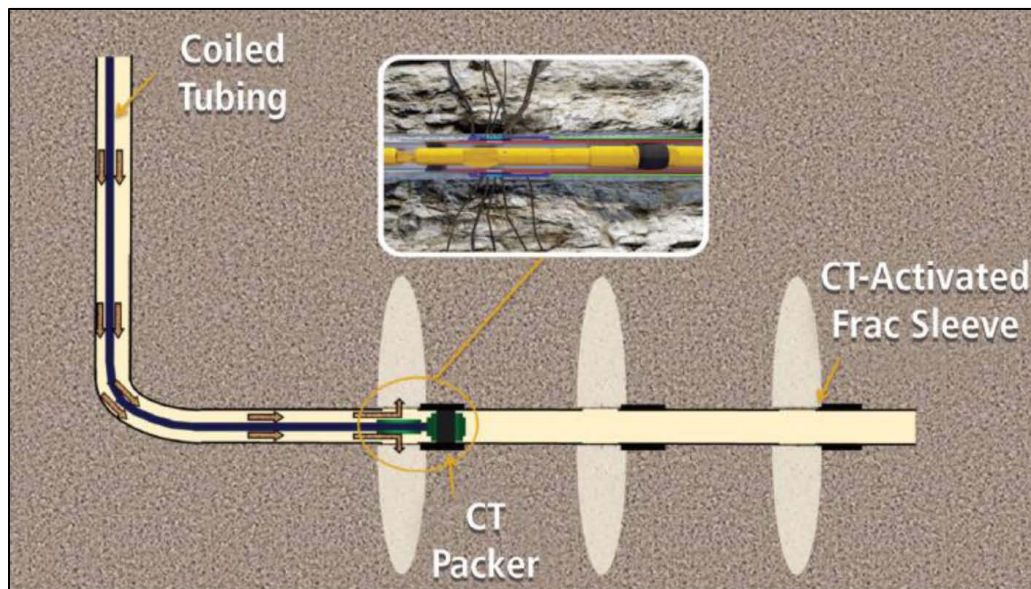


Figure 2.14: Wellbore diagram of the coiled tubing-activated frac sleeves completion method used in hydraulic fracturing treatments (from Bagci et al. 2017).

CHAPTER 3

EXPERIMENTAL APPARATUS AND PROCEDURES

Experimental tests were conducted on proppant transport in a horizontal wellbore apparatus. The apparatus was designed and developed in the Alderson Hall High-Bay Lab at the Colorado School of Mines to simulate proppant transport in horizontal wellbores. This chapter describes the experimental apparatus, laboratory scaling, experimental procedure, test materials, and proppant sieve analysis that were used in this study.

3.1 Experimental Apparatus

The schematic of the experimental setup used in this study is shown in Figure 3.1. The proppant and fracturing fluid were prepared in a 200-gallon-mixing tank connected to a 30-foot horizontal wellbore system. During each experimental test, the slurry was transported through the system by a single 270 gpm centrifugal pump. The main section of the horizontal wellbore consisted of a 30-foot horizontal pipe with a series of three perforation clusters. Four shots per foot (4 SPF) at 90-degree phasing were placed all around the pipe for each cluster. A variable frequency drive (VFD) and flow meter were also incorporated into the system. Three pressure transducers were installed on the top of the pipe immediately before each of the perforation clusters. A video camera was installed to capture the behavior and distribution of the proppant at different flow rates in the horizontal pipe. Tap water was used as a base fluid at temperature ranges between 20 and 23 °C. The following sections discuss the components of the experimental apparatus in more detail.

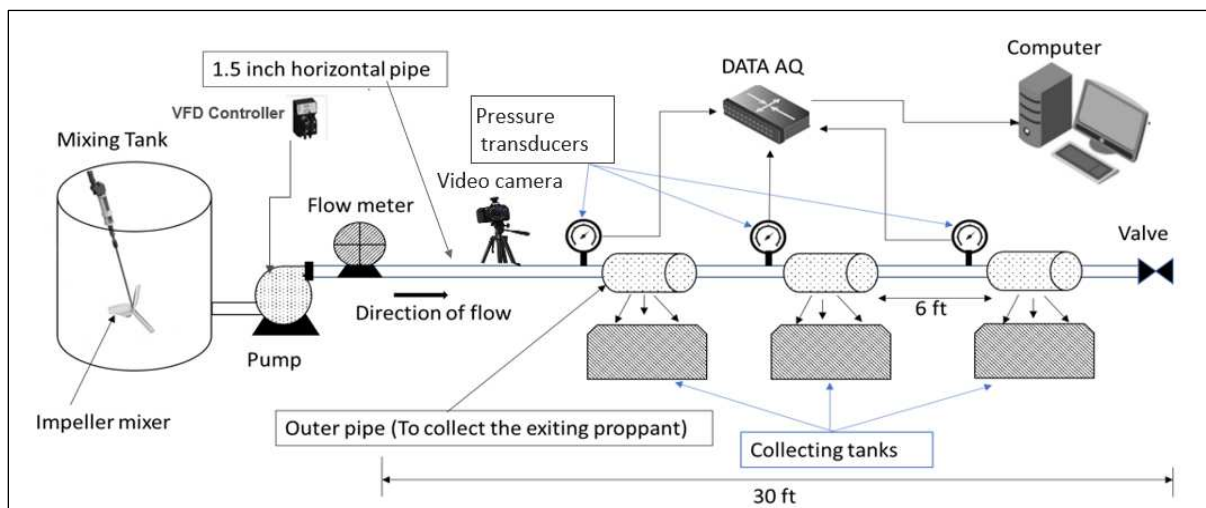


Figure 3.1: Schematic of the experimental apparatus used in this study.

3.1.1 Mixing Tank and Slurry Pump

The experimental apparatus started with a 200-gallon tank with a diameter of 3 ft. The mixing tank had a 3-inch hole where the suction occurred via a pipe to the pump located approximately 8 inches above the base. The slurry for each test was mixed in the tank using a mixer with three blade propellers, each with a 14-inch diameter, all connected to a 50-inch long shaft as shown in Figure 3.2. A digital speed controller was used to control the rpms of the mixer. For all the tests, the speed controller was set at a maximum speed of 60 HZ and 3600 rpm.

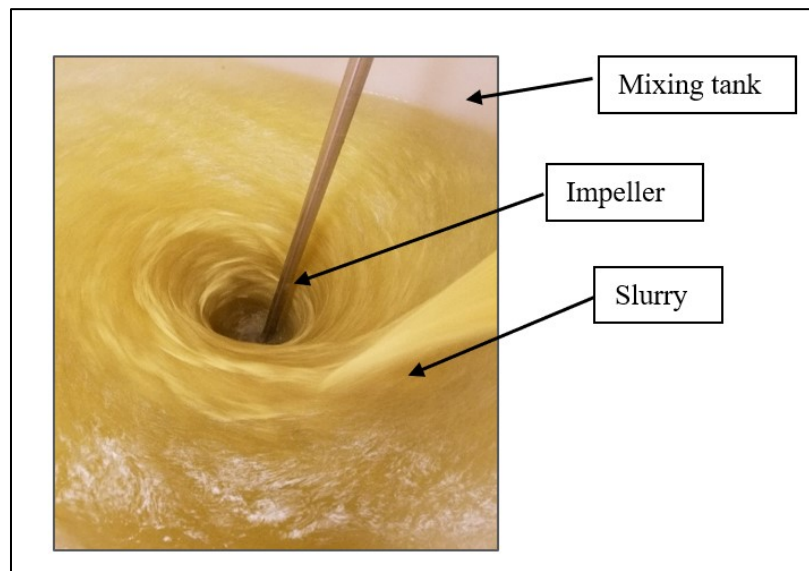


Figure 3.2: Picture of the mixing tank and the impeller.

Once the slurry is mixed, it is pumped through a 3” rubber vibration reducer that connects the bottom of the mixing tank to the pump as shown in Figure 3.3. The purpose of using the rubber vibration reducer was to reduce the effect of the mixer’s vibration on the pump in order to maintain a constant flow rate. The pump unit is a 3” self-priming centrifugal pump as shown in Figure 3.4. It is designed for a wide range of applications such as dewatering, liquid transfer, and slurry transport. The pump was designed to handle solids of a 3/8” maximum size and a maximum flow rate of 375 GPM. It can handle a maximum working pressure of 125 psi and a maximum head of 110 feet. A 10-inch rubber vibration reducer was also used from the discharge port of the pump to the elbow as shown in Figure 3.4.

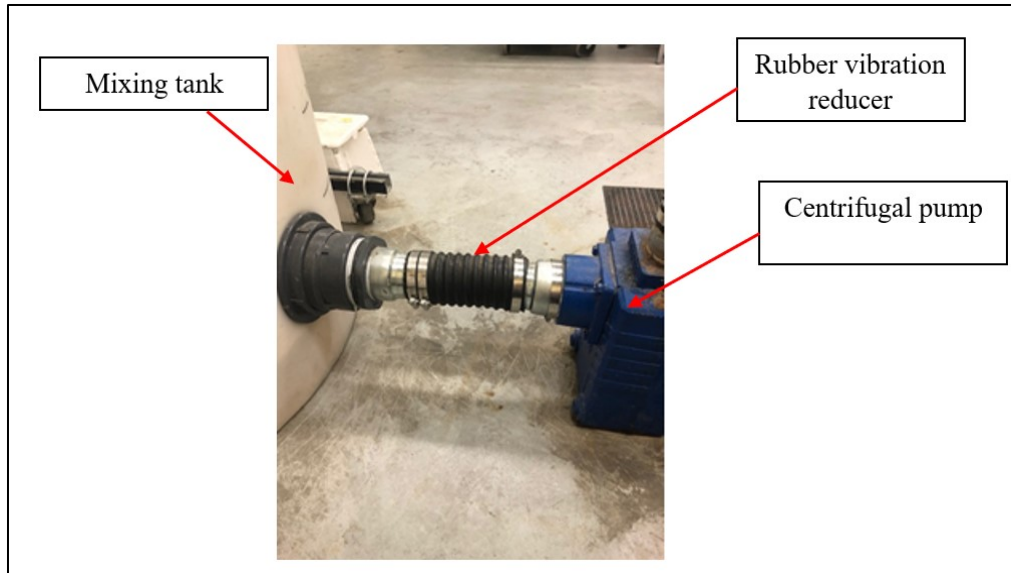


Figure 3.3: Picture of the rubber vibration reducer.

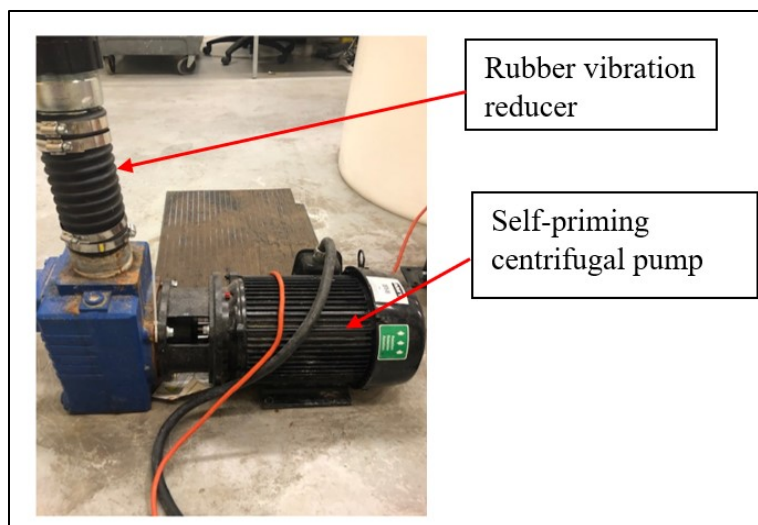


Figure 3.4: Picture of the self-priming centrifugal pump and the rubber vibration reducer.

3.1.2 Flow Meter

The flow meter is electromagnetic with a plus or minus 0.25 percent accuracy. This electromagnetic flow meter has no moving parts and is suitable for measuring flow rate in a wide range of applications, among them the slurry flow. The flow meter is independent of fluid density, viscosity, and temperature. It works with the passing fluid being measured by the voltage created across the slurry by its movement through a magnetic field. Then the measured voltage is converted

to a fluid velocity based on the pipe diameter by which the flow rate is determined. Figure 3.5 shows the flow meter that is used to measure the flow rate for the experimental tests.



Figure 3.5: Flow meter used to measure the slurry flow.

3.1.3 Variable Frequency Drive

A variable frequency drive (VFD) is a type of motor regulator that drives an electric motor by changing the voltage and frequency of its power supply. The VFD is able to adjust the flow rate based on the flow meter output reading. As the flow meter output signal is received by the VFD, the VFD reads that signal and based on its value, the pump RPMs either increase or decrease to achieve the required flow rate. Figure 3.6 shows the VFD that is used in the experimental apparatus to maintain a constant flow rate.



Figure 3.6: Variable frequency drive (VFD) used in the experimental apparatus.

3.1.4 Horizontal Wellbore

The horizontal wellbore is composed of a 30-foot-long PVC pipe with three perforation clusters as shown in Figure 3.7. A perforation density of 4 SPF and a perforation phasing of 90 degrees were placed around the pipe for each one of the three clusters. Pressure transducers were installed at each perforation cluster to measure the pressure drop across the perforations. Sections 3.1.4.1-3.1.4.5 discuss the components of the horizontal wellbore.

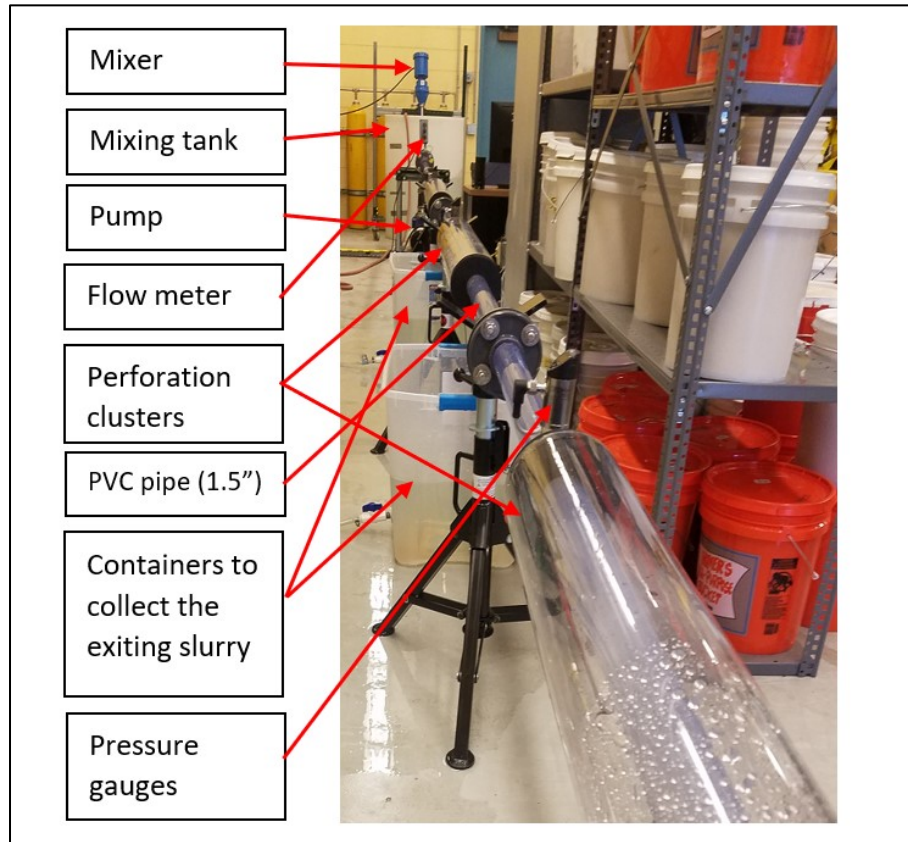


Figure 3.7: The horizontal wellbore apparatus used in this study.

3.1.4.1 Horizontal Pipe

A 30-foot-long PVC pipe with a wall thickness of 0.25 inch was used in the experimental apparatus. The PVC pipes came in 10 ft sections; therefore, flanges were used to connect these sections to meet the required length of the horizontal wellbore. These connections were also designed to allow access for dismantling the PVC pipe during cleaning. The pipe has a smooth interior surface with a roughness value of 0.0015 mm, which leads to a small pressure drop due to pipe friction. The pipe was also chosen for its clarity. A video camera was installed to observe and

capture the flow behavior inside the horizontal pipe. The selected pipe was able to withstand an interior pressure up to 150 psi and fluid temperature ranges between 33°F to 140°F.

3.1.4.2 Number and Phasing of Perforations

The number of clusters and number of perforations in each cluster were determined based on the planned injection rate. It is generally accepted as an industry practice to have between 1.5 and 2.0 bbl/min of flow through each perforation. Shot densities of 4 SPF with 90-degree phasing and with 0.5-inch radius holes usually are appropriate to ensure the equivalent of open hole productivity (Wutherich and Walker 2012). However, to improve the productivity under certain conditions, such as in very high flow rate wells or in gravel-packed wells, shot densities greater than four can be used. Therefore, four shots per foot (4 SPF) at 90-degree phasing, as shown in Figure 3.8, were placed around the horizontal pipe for each one of the three clusters to simulate the slurry flow in horizontal wellbores. This made for a total of twelve perforations in the pipe through three clusters, four shots each cluster.

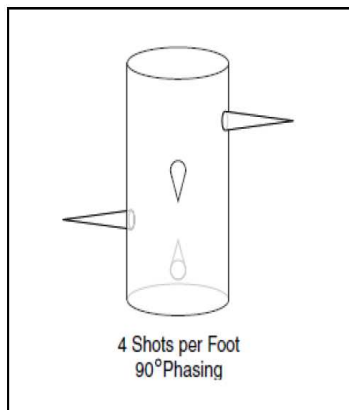


Figure 3.8: Perforation shot density: example of four shots/foot and 90° phasing.

3.1.4.3 Entrance Hole Diameter

According to experimental tests conducted by Gruesbeck and Collins (1982) to prevent bridging of proppant in the near wellbore, the perforation diameter should be eight to ten times larger than the median proppant diameter. Since the median diameter for the 20/40 mesh sand that was used in this research is 0.025 inch, the perforation holes were designed to be 0.25-inch in diameter.

3.1.4.4 Distance Between Perforation Clusters

Regarding spacing between perforation clusters, there are a number of different scenarios. For instance, in the Barnett shale, microseismic studies have shown an optimal spacing of 1.5 times the fracture height, while in the Eagle Ford formation, the optimal spacing between perforation clusters is between 35 and 40 feet (Fisher et al. 2004). Based on these values, scaled to the laboratory scale, and the available laboratory space for this study, spacing between the perforation clusters was chosen to be six feet as shown in Figure 3.9.

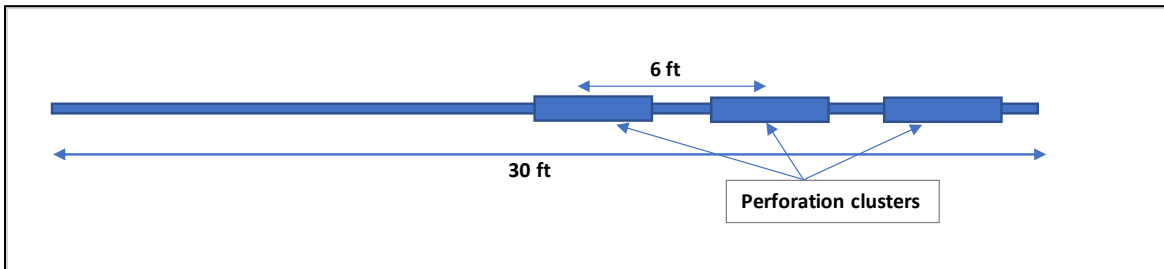


Figure 3.9: Schematic of the horizontal wellbore.

3.1.4.5 Pressure Transducers

Pressure transducers were installed on the top of the pipe immediately before each of the perforation clusters as shown in Figure 3.10. The pressure drop through each perforation cluster was measured with a differential pressure transducer over a pipe length of 6 ft. The pressure transducers used in the experimental apparatus read pressure values up to 150 psi.



Figure 3.10: Picture of one of the pressure transducers used in the experimental apparatus.

3.2 Laboratory Scaling

Laboratory scaling was conducted in order to determine what would best represent field conditions. Scaling parameters such as Reynolds number, suspension effect, velocity diameter ratio, and distance between perforation clusters were considered for operation of the experimental tests. Sections 3.2.1-3.2.5 discuss scaling parameters in more detail.

3.2.1 Reynolds Number

Calculation of the Reynolds number (Re) is the first fluid mechanics investigation for determining if fluid flow in a particular pipe is turbulent or laminar. The selection of the pipe diameter in the laboratory was based on the Reynolds number calculations for field and laboratory conditions. The calculations of the Reynolds number were determined by using the following Equation 3.1:

$$Re = \frac{\rho_f D u}{\mu_f} \quad (3.1)$$

Equation 3.1 was used to compute the Reynolds number for laboratory and field conditions. The results of the Reynolds number calculations for a 1.5-inch pipe (laboratory condition) and a 4.778-inch casing (field condition) are presented in Tables 3.1 and 3.2, respectively. Based on the results of the Reynolds number calculations for various flow conditions, the 1.5” internal diameter pipe was selected. Results showed that using a 1.5-inch pipe diameter with a flow rate above 0.25 bbl/min using fresh water will keep the flow turbulent.

Table 3.1: The Reynolds number calculations for a 1.5-inch pipe (Laboratory Data)

Laboratory Data				
Inner Pipe Diameter, in.	1.5			
Inner Pipe Diameter, m	0.038			
Area, m ²	0.001			
Fluid Viscosity, kg/m/s	0.001			
Fluid Density, kg/m ³	1000			
Flow Rate, bpm	Flow Rate, m ³ /s	Velocity, m/s	Velocity, ft/s	Re
2.00	0.005	4.651	15.254	177188
1.75	0.005	4.069	13.347	155039
1.50	0.004	3.488	11.440	132891
1.25	0.003	2.907	9.534	110742
1.00	0.003	2.325	7.627	88594
0.75	0.002	1.744	5.720	66445
0.50	0.001	1.163	3.813	44297
0.25	0.001	0.581	1.907	22148

Table 3.2: The Reynolds number calculations for a 4.778-inch casing (Field Data)

Field Data				
Inner Pipe Diameter, in.	4.778			
Inner Pipe Diameter, m	0.121			
Area, m ²	0.012			
Fluid viscosity, kg/m/s	0.001			
Fluid density, kg/m ³	1000			
Flow rate, bpm	Flow rate, m ³ /s	Velocity, m/s	Velocity, ft/s	Re
80	0.212	18.334	60.136	2225043
75	0.199	17.188	56.377	2085978
70	0.185	16.042	52.619	1946913
65	0.172	14.896	48.860	1807848
60	0.159	13.751	45.102	1668782
55	0.146	12.605	41.343	1529717
50	0.132	11.459	37.585	1390652

3.2.2 Entrance Length

The entrance length is the minimum length that fluid moves in a pipe before the flow becomes fully developed or uniform. This aspect might have an effect on proppant suspension in the horizontal wellbore. The typical entrance length for laminar and turbulent flow rates can be determined using Equations 3.2 and 3.3, respectively, as described by Munson et al. (2012).

$$\frac{l_e}{D} = 0.06Re \quad \text{for laminar flow} \quad (3.2)$$

$$\frac{l_e}{D} = 4.4(Re)^{1/6} \quad \text{for turbulent flow} \quad (3.3)$$

Where,

l_e = Entrance length, m

Re = Reynolds number, dimensionless

Based on the values of Reynolds number, Equation 3.3 was used to determine the entrance length for a 1.5-inch pipe. Table 3.3 shows the results of the entrance length for a 1.5-inch pipe at different flow rates using freshwater fluid.

Table 3.3: Entrance length and Reynolds number for the selected pipe (1.5-inch pipe)

Pipe Diameter, in.	1.500				
Pipe Diameter, m	0.038				
Area, m ²	0.001				
Fluid Viscosity, kg/m/s	0.001				
Fluid Density, kg/m ³	1000.0				
Flow Rate, bpm	Flow Rate, m ³ /s	Velocity, m/s	Velocity, ft/s	Reynolds Number, unitless	Entrance Length, m
3.00	0.008	6.976	22.881	265781	1.344
2.75	0.007	6.395	20.974	243633	1.325
2.50	0.007	5.813	19.067	221485	1.304
2.25	0.006	5.232	17.161	199336	1.281
2.00	0.005	4.651	15.254	177188	1.256
1.75	0.005	4.069	13.347	155039	1.229
1.50	0.004	3.488	11.440	132891	1.198
1.25	0.003	2.907	9.534	110742	1.162
1.00	0.003	2.325	7.627	88594	1.119
0.75	0.002	1.744	5.720	66445	1.067
0.50	0.001	1.163	3.813	44297	0.997
0.25	0.001	0.581	1.907	22148	0.888

As can be noted from the Table 3.3, the entrance length can be quite short for very low Reynolds numbers, whereas it may take a distance equal to many pipe diameters for large Reynolds numbers. For the subject experimental tests, the steady state condition was reached by obtaining a fully developed velocity profile in the horizontal wellbore before the fluid reaches the perforation clusters. Since the distance between the perforation clusters is 6 ft (1.83 m), fluid velocities which have entrance length above 1.83 m were excluded from the experimental tests.

3.2.3 Minimum Transport Velocity

To avoid settling of proppant in horizontal wellbores, the slurry velocity must be higher than the critical transport velocity of the particles. As discussed in Chapter 2, there are several equations that are used to compute the settling velocity of slurry particles that flow in a pipe. The proppants that were used in the study have a range of particle sizes within the proppant. For instance, the typical proppant size for 20/40 is between 20 and 40 ASTM mesh (420 μm - 840 μm). Therefore, the correlation that was used to determine the critical velocity for these experiments is Wasp's Modified Durand Equation (Equation 2.3) by Wasp et al. (1970) as described in Chapter 2. The properties of two types of proppant, sand and ultra-light weight ceramic, with 20/40 and 40/70 mesh sizes are listed in Table 3.4.

Table 3.4: Specifications of proppants used in the study

Proppant Type	Mesh Size	Median Diameter		Specific Gravity		Bulk Density	
		(in.)	(μm)	(g/cm^3)	(lb/ft^3)	(g/cm^3)	(lb/ft^3)
White Sand	40/70	0.0142	360	2.65	165.43	1.51	94.30
White Sand	20/40	0.0265	675	2.65	165.43	1.52	94.89
ULW Ceramic	40/70	0.0138	350	2.00	124.86	1.21	75.53
ULW Ceramic	20/40	0.0256	650	2.00	124.86	1.23	76.68

The minimum/critical transport velocities for the proppants listed in Table 3.4 were calculated at various proppant concentrations. The results are shown in Figure 3.11.

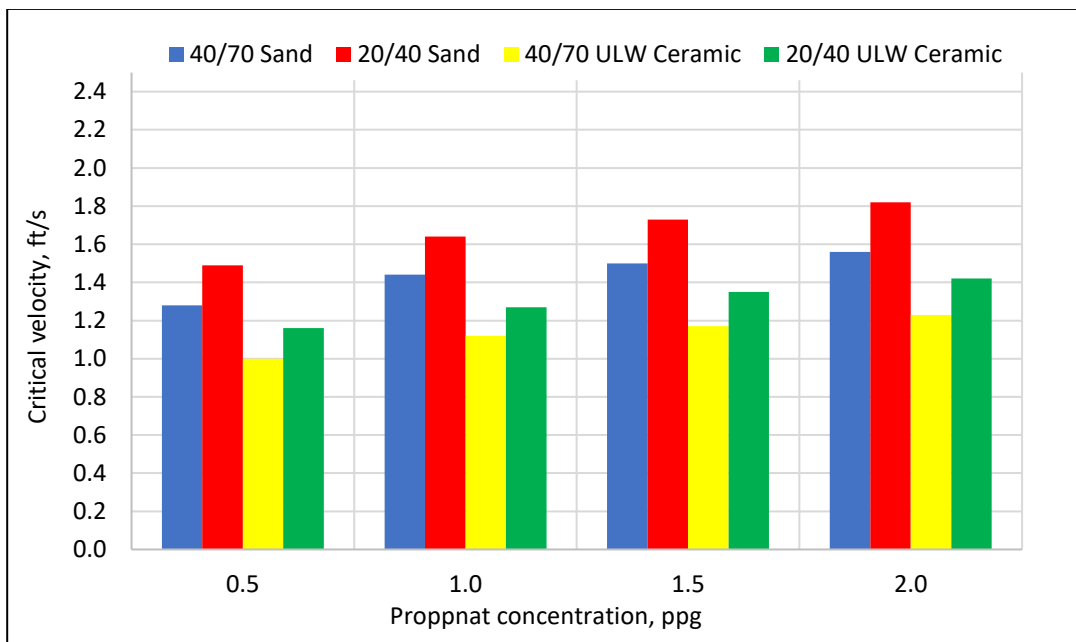


Figure 3.11: Minimum/critical transport velocity for different types of proppant at various particle concentrations.

From Figure 3.11, it should be noted that the minimum transport velocity for all proppants listed in the table is increasing as there is an increase in the proppant concentration. The minimum transport velocity for 20/40 mesh sand at a proppant concentration of 2.0 ppg is 1.82 ft/s, whereas at a proppant concentration of 0.5 ppg is 1.28 ft/s. However, when there is a decrease in the particle size, there is also a significant decrease in the minimum settling velocity. For example, the minimum transport velocity of 40/70 ULW ceramic is 1.0 ft/sec at 0.5 ppg, which is less than the velocity of 20/40 ULW ceramic (1.16 ft/sec) at the same proppant concentration. Also, the results in Figure 3.11 illustrate that the specific gravity of proppant can play a significant role in the settling of the particles in horizontal wellbores. If the specific gravity of the proppant is high, the

minimum/critical velocity is high and vice versa. These findings indicate that proppant size, proppant concentration, and the specific gravity of proppant have a significant effect on the distribution of proppant in horizontal wellbores. In the experimental tests, to ensure that proppant particles do not settle down by weight, the injected fluid velocity in the horizontal pipe was chosen to be greater than the critical transport velocity.

3.2.4 Shear Rate

Another important aspect of laboratory scaling is the shear rate. Scaling of the laboratory data is required to mimic flow behavior under field conditions. Therefore, the shear rate was determined for both laboratory and field flow rates. Then the flow rates that were used in the experiments were matched with the flow rates for a 4.778-inch casing (field conditions) as shown in Table 3.5.

Table 3.5: Laboratory flow rates for a 1.5-inch pipe matched with field rates for a 4.778-inch casing

Laboratory Data		Field Data	
Pipe Diameter (ID), in.	1.5	Pipe Diameter (ID), in.	4.778
Pipe Diameter, m	0.03810	Pipe Diameter, m	0.12136
Area, m ²	0.00114	Area, m ²	0.01157
Flow Rate, gpm	Shear rate, s ⁻¹	Flow Rate, bpm	Shear rate, s ⁻¹
25	287	19	287
35	408	27	408
45	528	35	528
60	695	46	695
75	876	58	876

As shown in Table 3.5, the flow rates of 25, 35, 45, 60, and 75 gpm utilized in this study, combined with a horizontal pipe of 1.5 inches, can mimic the field conditions for flow rates of 19, 27, 35, 46, and 58 bpm, respectively, with a 4.778-inch casing

3.2.5 Perforations Alignment and Distance Between Clusters

Tests were carried out with fresh water for 60 seconds to ensure that the perforations alignment and the distance between the perforation clusters do not have an effect on the proppant distribution. The experimental tests started with a flow velocity of 6.4 ft/s ($Re = 75,304$), then

increased to 8.3 ft/s ($Re = 93,023$) and finally increased to 14.6 ft/s ($Re = 168,328$). Figure 3.12 shows the water distribution between the three perforation clusters at the three flow velocities.

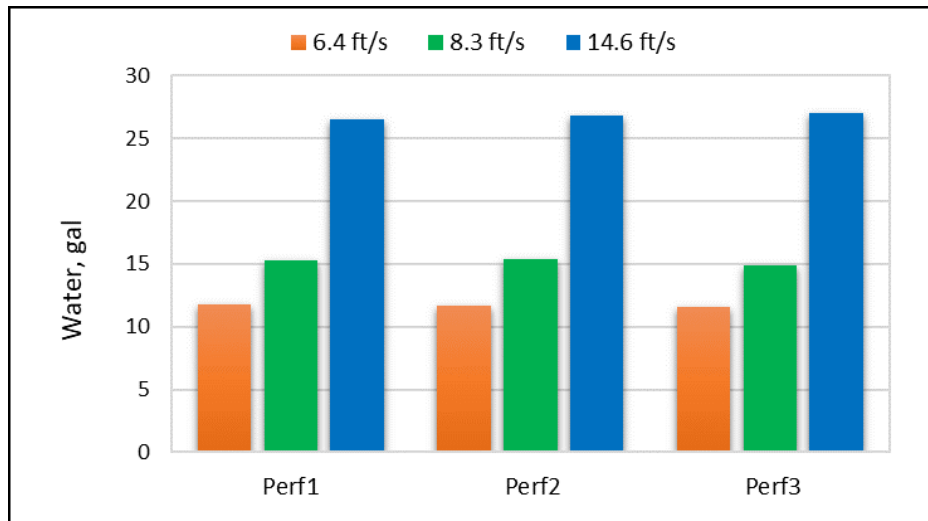


Figure 3.12: Water distribution through three perforation clusters at three different flow velocities (all three perforation clusters are open).

As can be seen in the graph, the quantities of water received at the three perforation clusters are equal at the three tested flow velocities. This implies that the perforation alignment in the three clusters is consistent and does not have a significant impact on the flow distribution.

In contrast, when there was a plug on the middle cluster perforations, as shown in Figure 3.13, the amount of water received through perforation clusters one and two is the same for flow velocities of 6.4 and 8.3 ft/s. However, at a flow velocity of 14.6 ft/s, the amount of water that was received at the two perforation clusters is different. This indicates that the distance between perforation clusters at higher fluid velocities may have an impact on the water distribution and could impact the transport results. As a result, flow velocities which have a Reynolds number above 168,328 were not included in the experimental tests.

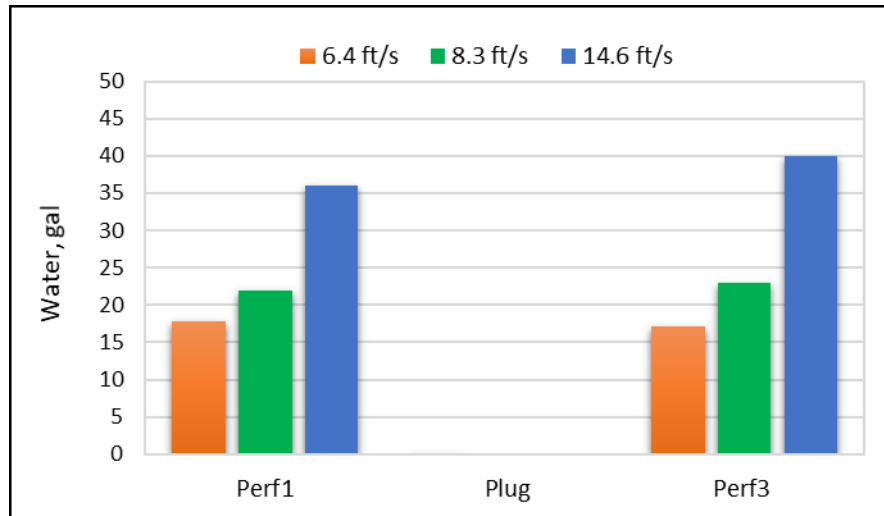


Figure 3.13: Water distribution through two perforation clusters at three different flow velocities (middle perforation cluster is intentionally plugged).

3.3 Test Materials

The materials utilized to run the tests consisted of three main items, tap water, high loading friction reducer (HLFR) and proppant. Sections 3.3.1-3.3.3 discuss the three main materials in more detail.

3.3.1 Water

For this study, tap water was used as a carrying fluid in two ways. The first use is to simulate slickwater fluid with no chemical additives. In this case, the mixing tank was filled with only tap water to a required volume then proppant was added at different concentrations to the tank. The second use for water was with HLFR, where HLFR was added to water at a wide range of concentrations to increase the fluid viscosity as discussed in Chapter 5. The temperature of tap water for both systems ranged between 20 and 23 °C.

3.3.2 Friction Reducer

The reason for using friction reducer in these tests is to evaluate and determine how different types of proppant are transported along the wellbore in HLFR, also known as high viscosity friction reducer (HVFR). The use of HVFR as a fracturing fluid in hydraulic fracturing treatments has been tested in many shales plays in North America, such as the Eagle Ford and Bakken shale (Van Domelen et al. 2017). The rheological properties for the friction reducer fluids

were determined and are presented in Chapter 5. The physical and chemical properties of HLFRR are listed as follows:

1. Appearance: Milky viscous liquid
2. Color: White
3. Physical State: Liquid
4. pH (5 g/L): 5 to 9
5. Boiling Point: > 100 °C (212 °F)
6. Flash Point: Does not flash
7. Relative Density: 1.0 to 1.1 (Water = 1)
8. Solubilities: Completely miscible in water
9. Kinematic viscosity: > 20.5 m²/s at 40 °C (104 °F)

3.3.3 Proppants

Four types of proppant were used in this study: white sand with a specific gravity of 2.65 (20/40 and 40/70) and ultra-light-weight ceramic with a specific gravity of 2.0 (20/40 and 40/70). White sand was selected because it is currently the most widely used proppant in the oil and gas industry (Vincent 2011). The ultra-light weight (ULW) ceramic was chosen because it is lighter with more uniform shape than sand.

3.3.3.1 20/40 Mesh White Sand

Sets of tests were conducted on 20/40 mesh white sand with a median diameter of 0.645 mm and a specific gravity of 2.65 g/cm³ as shown in Figure 3.14. A wide range of fluid velocities were used to evaluate the effect of velocity on proppant distribution between the perforation clusters.



Figure 3.14: Picture of 20/40 white sand used in the experimental tests.

Before conducting the experimental tests, the sieve analysis for the 20/40 mesh white sand was performed in order to determine the particle size distribution. According to the API RP-19C (API 2006) specifications, at least 90% of the tested proppant must fall between the specified sieve sizes with no more than 0.1% of the tested sample be retained in the first sieve, and no more than 1.0% of the proppant be received at the pan.

Five tests were performed for the sieve analysis. The proppant samples for the sieve analysis were collected randomly from different buckets for the same proppant type. For the 20/40 mesh sand, seven sieves plus the collecting pan were selected to do the sieve analysis where the smallest sieve was 50 and the largest sieve was 16. For one of the tests, a sample weight of 1327.59 g was placed in the first sieve 16 mesh and then the whole stack was placed on a Ro-Tap machine as shown in Figure 3.15. The duration for each test was set to 10 minutes in the sieve shaker. The proppant weight retained in each sieve and in the pan was recorded and as shown in Table 3.7.



Figure 3.15: Picture of the sieve shaker used to perform the sieve analysis.

As mentioned above, per API requirement at least 90% of the tested proppant should be retained between the 20 and 40 mesh sieves. The results of the tests show proppant retained between 20 and 40 mesh was 97.087%. Also, the weight percent at the first sieve 16 was 0.0135% which is less than 0.1%. The weight percent of the proppant in the pan was 0.5137% which is also less than 1%. Therefore, the results of the sieve analysis test successfully met the API requirements. The weight percent was plotted for the same Table 3.6 is shown in Figure 3.16. From the graph, around 40% and 35% of proppant was retained in sieves of 25 and 30, respectively.

Table 3.6: Results of the sieve analysis for 20/40 mesh white sand

Sieve Size, mesh	Sieve Weight, g	Sieve Opening, mm	Full Sieve Weight, g	Net Weight, g	Weight Percent, %	Cumulative Weight Percent, %
16	413.12	1.190	413.30	0.18	0.014	0.014
20	387.32	0.841	443.83	56.51	4.257	4.270
25	385.17	0.707	930.17	545.00	41.052	45.322
30	373.28	0.595	847.58	474.30	35.726	81.048
35	353.20	0.500	488.51	135.31	10.192	91.241
40	357.60	0.420	435.40	77.80	5.860	97.101
50	348.22	0.297	379.89	31.67	2.386	99.486
Pan	369.40	-	376.22	6.82	0.514	100.000

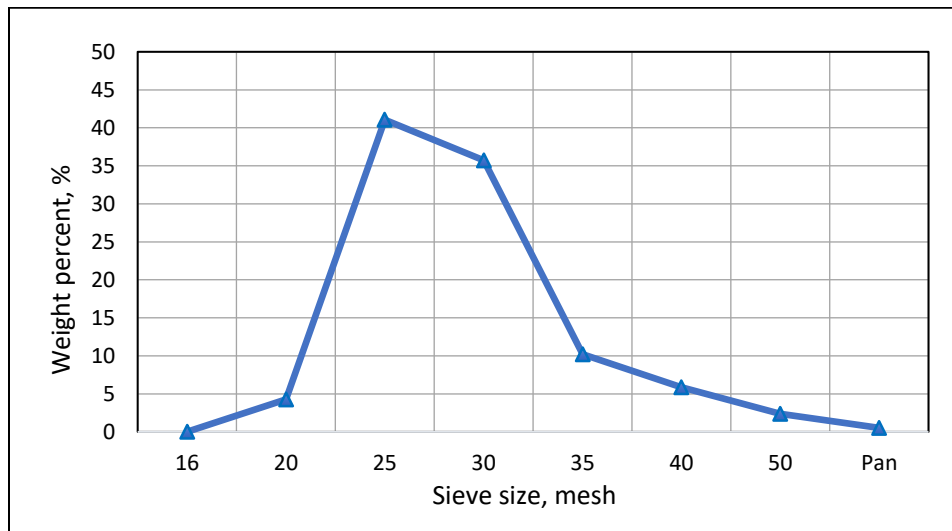


Figure 3.16: Proppant particle distribution for the 20/40 mesh white sand.

The median diameter, which represents the particle size at which 50% of the grains are smaller and 50% are larger, can be determined from the grain size distribution. In order to determine the median diameter, there are several formulas that are used. The most comprehensive graphical method is that given by Folk and Ward (1957) as described in the following equation:

$$d_p = \frac{\Phi_{16} + \Phi_{50} + \Phi_{84}}{3} \quad (3.4)$$

Where,

d_p = Median particle diameter, mm

Φ_{16} = Sieve size at 16% of the sample weight, mm

Φ_{50} = Sieve size at 50% of the sample weight, mm

Φ_{84} = Sieve size at 84% of the sample weight, mm

The cumulative weight percent was plotted against the sieve size as shown in Figure 3.17. The values of the Φ_{16} , Φ_{50} , and Φ_{84} were determined from the graph. Then median diameter was then calculated from Equation 3.4 to be 0.675 mm. The other four sieve analysis tests for 20/40 mesh white sand can be found in Appendix A.

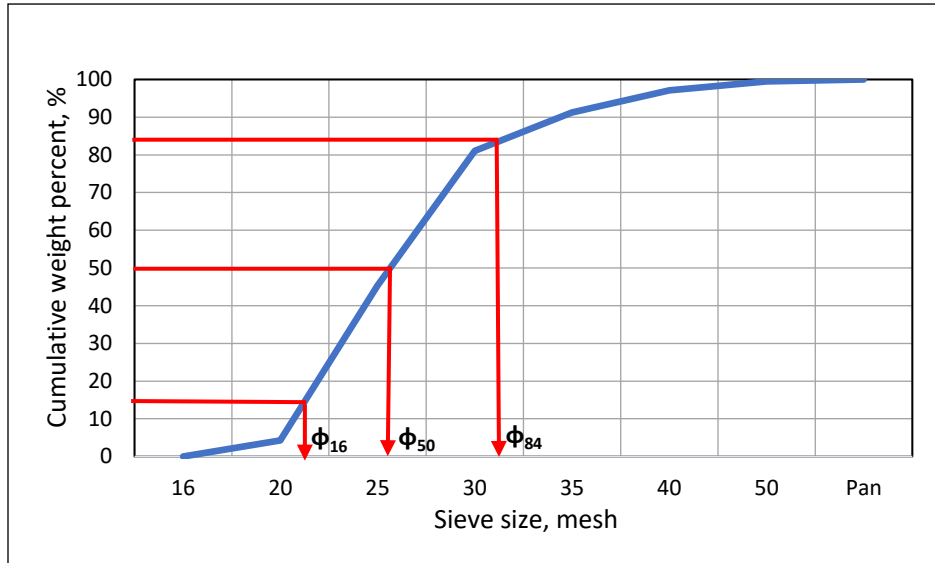


Figure 3.17. Cumulative weight percent for the 20/40 mesh white sand.

3.3.3.2 40/70 Mesh White Sand

A number of experimental tests were also conducted using 40/70 mesh white sand with a specific gravity of 2.65 and a median diameter of 0.360 mm as shown in Figure 3.18. The median diameter of the 40/70 mesh white sand is 45% smaller than the median diameter of 20/40 mesh white sand.



Figure 3.18: Picture of 40/70 white sand used in the experimental study.

Similar to the tests performed on 20/40 mesh white sand; five proppant sieve distribution tests were performed on 40/70 mesh white sand. Table 3.7 shows the results of one of the sieve distribution tests for a sample of 1233.56 g of the 40/70 mesh white sand.

Table 3.7: Results of a sieve analysis test for 20/40 mesh white sand

Sieve Size, mesh	Sieve Weight, g	Sieve Opening, mm	Full Sieve Weight, g	Net Weight, g	Weight Percent, %	Cumulative Weight Percent, %
30	373.29	0.595	373.36	0.07	0.006	0.006
40	357.63	0.420	459.53	101.90	8.261	8.266
50	348.23	0.297	1072.97	724.74	58.752	67.018
60	341.38	0.250	558.16	216.78	17.574	84.592
70	332.3	0.210	500.27	167.97	13.617	98.208
100	334.22	0.149	352.97	18.75	1.520	99.728
Pan	369.36	-	372.71	3.35	0.272	100.000

As can be observed from the Table 3.7, the proppant that was retained between 40 and 70 meshes is 98.203%, which is higher than 90% (API requirement). The weight percent at the first sieve 30 mesh was 0.006%, which is less than 0.1%. The weight percent of the proppant received at the pan was 0.271%, which is also less than 1.0%. Therefore, the results of the sieve analysis test successfully met the API requirements.

The weight percent for the sample in Table 3.7 was plotted as shown in Figure 3.19. From the graph, around 57% of the proppant was retained in the 50-mesh sieve. The median diameter was computed by determining the values of Φ_{16} , Φ_{50} , and Φ_{84} , and the cumulative weight percent for the tested sample was plotted as shown in Figure 3.20. The median diameter was calculated using Equation 3.4 and determined to be 0.354 mm. The average medium diameter based on five

tests for 40/70 mesh white sand was 0.360 mm. The other four sieve analysis tests for the 40/70 mesh white sand are presented in Appendix A.

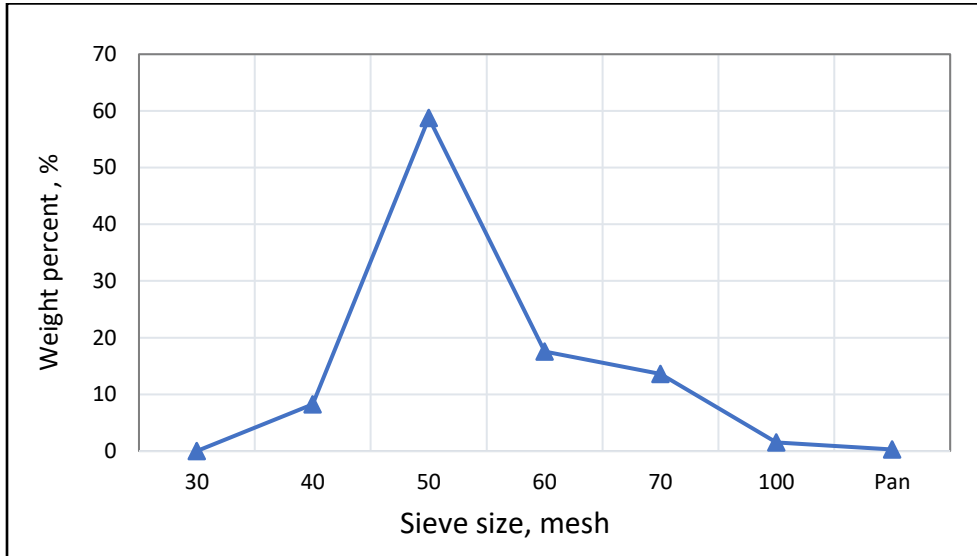


Figure 3.19: Proppant particle distribution for the 40/70 mesh white sand.

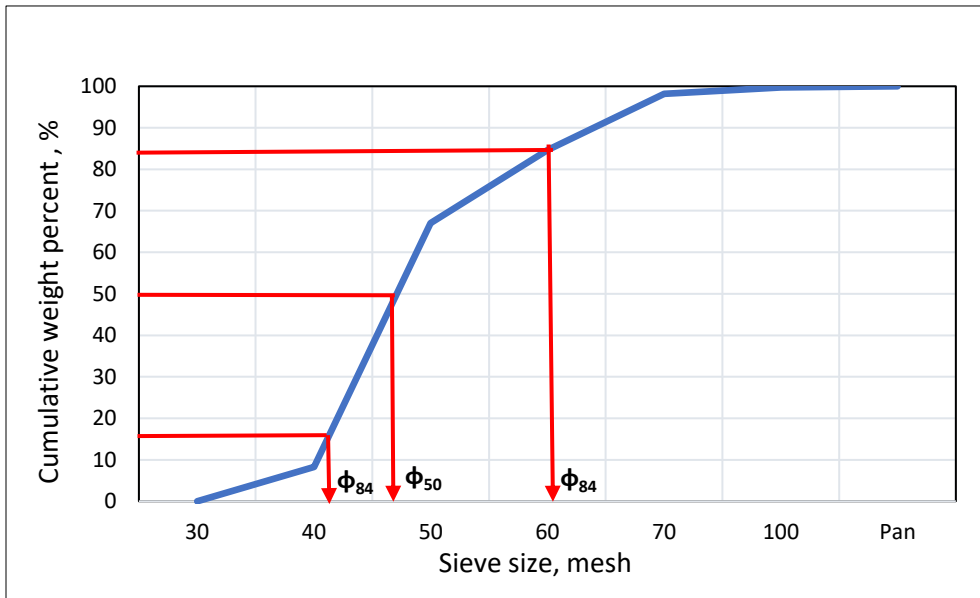


Figure 3.20: Cumulative weight percent for the 40/70 mesh white sand.

3.3.3.3 20/40 ULW Ceramic

A number of experimental tests were also conducted on 20/40 ultra-light weight (ULW) ceramic, which is shown in Figure 3.21. The specific gravity of the 20/40 ULW ceramic is 2.0, which is 24.53% less than the specific gravity of the sand at 2.65. The ULW ceramic has a higher

conductivity along with 30% to 40% slower settling rates in the wellbore compared to sand and resin-coated sand (CARBO Ceramics Inc 2017).



Figure 3.21: Picture of the 20/40 ULW ceramic used in the experimental study.

Three sieve analysis tests were also conducted on 20/40 ULW ceramic to determine the median diameter of the proppant particles, and to ensure that the used proppant meets the API requirements. As an example, proppant sample of 1050.32 g was placed in the first sieve 16 mesh, and then the whole stack was placed in the sieve shaker for 10 minutes. The proppant weight that was retained in each sieve and in the pan was recorded as illustrated in Table 3.8. The weight percent was also plotted for the same tested sample as shown in Figure 3.22. As can be noted from the graph, around 52% and 36% of proppant was retained in the sieves of 35 and 30 mesh, respectively.

Table 3.8: Results of sieve analysis test for 20/40 ULW ceramic

Sieve Size, mesh	Sieve Weight, g	Sieve Opening, mm	Full Sieve Weight, g	Net Weight, g	Weight Percent, %	Cumulative Weight Percent, %
16	413.12	1.190	413.1200	0.00	0.000	0.000
20	387.32	0.841	387.3200	0.00	0.000	0.000
25	385.17	0.707	403.0254	17.86	1.700	1.700
30	373.28	0.595	755.5965	382.32	36.400	38.100
35	353.20	0.500	905.6683	552.47	52.600	90.700
40	357.60	0.420	455.2798	97.68	9.300	100.000
50	348.22	0.297	348.2200	0.00	0.000	100.000
Pan	369.40	-	369.4000	0.00	0.000	100.000

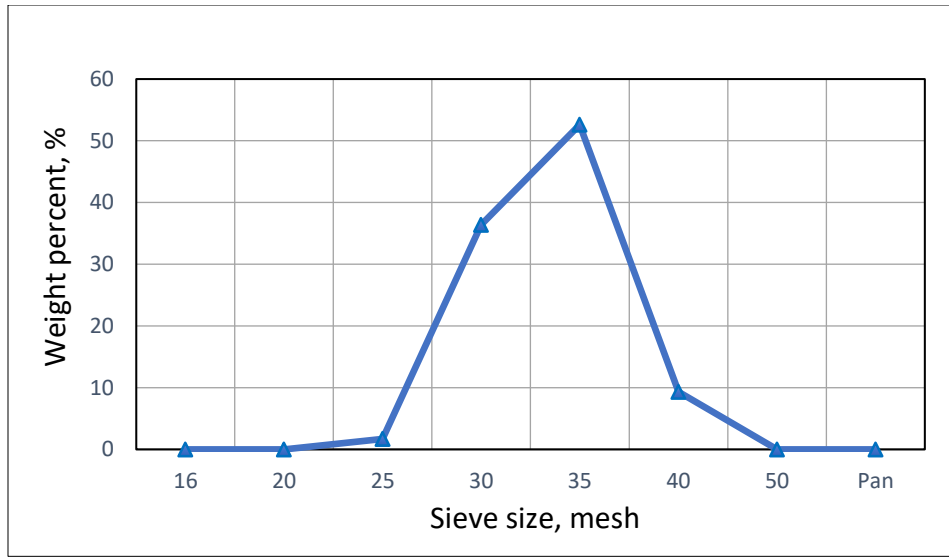


Figure 3.22: Proppant particle distribution for the 20/40 ULW ceramic.

As mentioned previously, the median diameter was computed by determining the values of Φ_{16} , Φ_{50} , and Φ_{84} , which requires plotting the cumulative weight percent for the tested sample as shown in Figure 3.23. Then, the median diameter was computed from Equation 3.4 to be 0.65 mm. The other two sieve analysis tests for the 20/40 ULW ceramic can be found in Appendix A.

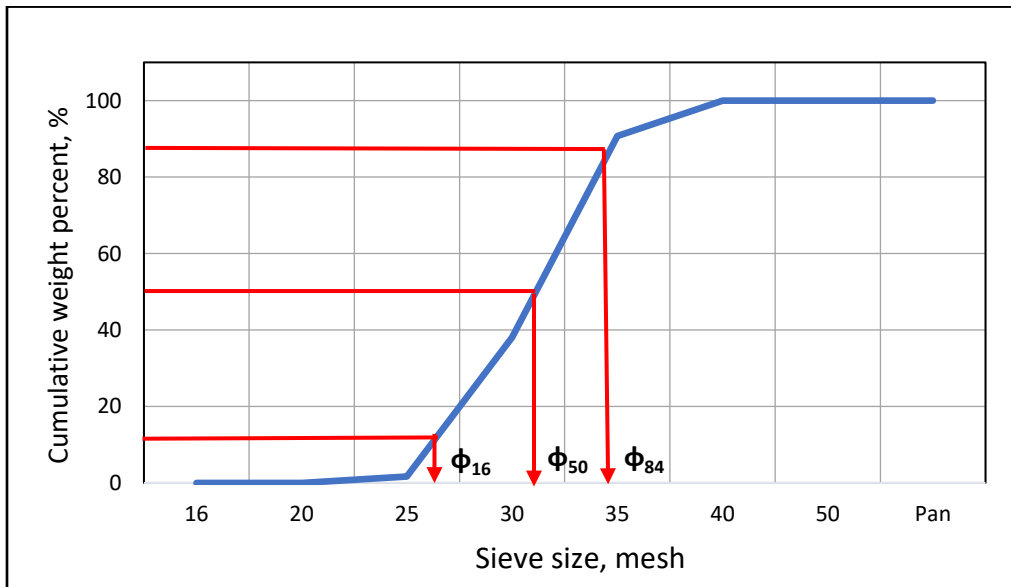


Figure 3.23: Cumulative weight percent for 20/40 ULW ceramic.

3.3.3.4 40/70 ULW Ceramic

Sets of experimental runs were also conducted using 40/70 ultra-light weight (ULW) ceramic. The specific gravity of the 40/70 ULW ceramic is 2.0. The median diameter of the 40/70 mesh is 40% smaller than the median diameter of the 20/40 mesh. A picture of the ULW ceramic that is used in the study is shown in Figure 3.24. This type of proppant has a much rounder and more uniform shape and size which can potentially provide better proppant transport performance than sand.



Figure 3.24: Picture of the 40/70 ULW ceramic used in the experimental study.

Similar sieve tests were also conducted on 40/70 ULW ceramic. Table 3.9 shows the results for sieve distribution for a sample of 1037.5 g of 40/70 ULW ceramic. The resulting trend for proppant particle distribution is illustrated in Figure 3.25. As can be observed from the graph, the highest weight percent (88.22%) was recorded at a sieve size of 50 mesh. As can be observed, the particle size distribution is totally different than the 40/70 mesh white sand, both of which meet the API requirement for the specified mesh distribution.

Table 3.9: Results of sieve analysis test for 40/70 ULW ceramic

Sieve Size, mesh	Sieve Weight, g	Sieve Opening, mm	Full Sieve Weight, g	Net Weight, g	Weight Percent, %	Cumulative Weight Percent, %
30	358.48	0.595	358.55	0.07	0.007	0.007
40	349.85	0.420	356.43	6.58	0.634	0.641
50	346.07	0.297	1261.25	915.18	88.210	88.851
60	337.21	0.250	408.91	71.70	6.911	95.762
70	325.85	0.210	354.88	29.03	2.798	98.560
100	319.14	0.149	333.51	14.37	1.385	99.945
Pan	357.76	-	358.33	0.57	0.055	100.000

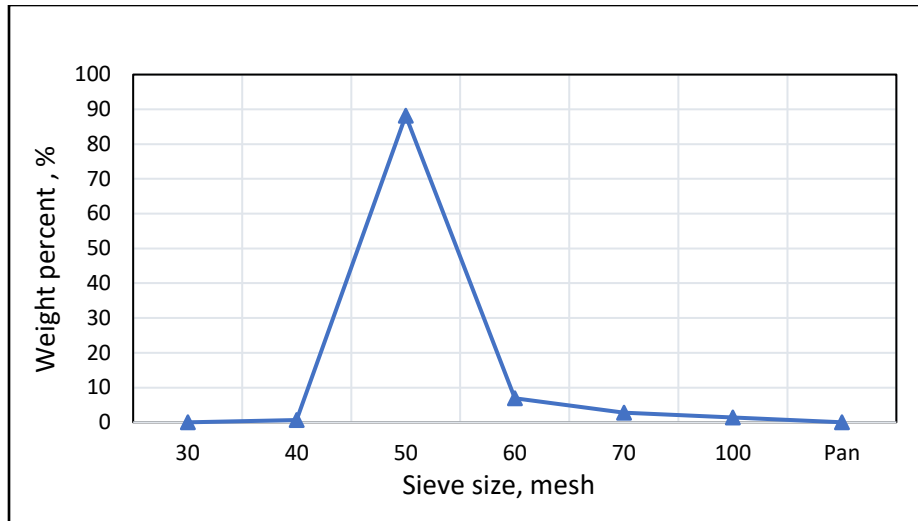


Figure 3.25: Proppant particle distribution for the 40/70 ULW ceramic.

The median diameter was also computed by determining the values of Φ_{16} , Φ_{50} , and Φ_{84} . The cumulative weight percent for the tested sample was plotted as shown in Figure 3.26. Then, the median diameter was also determined from Equation 3.4 to be 0.35 mm. The other two sieve analysis tests for the 40/70 ULW ceramic are provided in Appendix A.

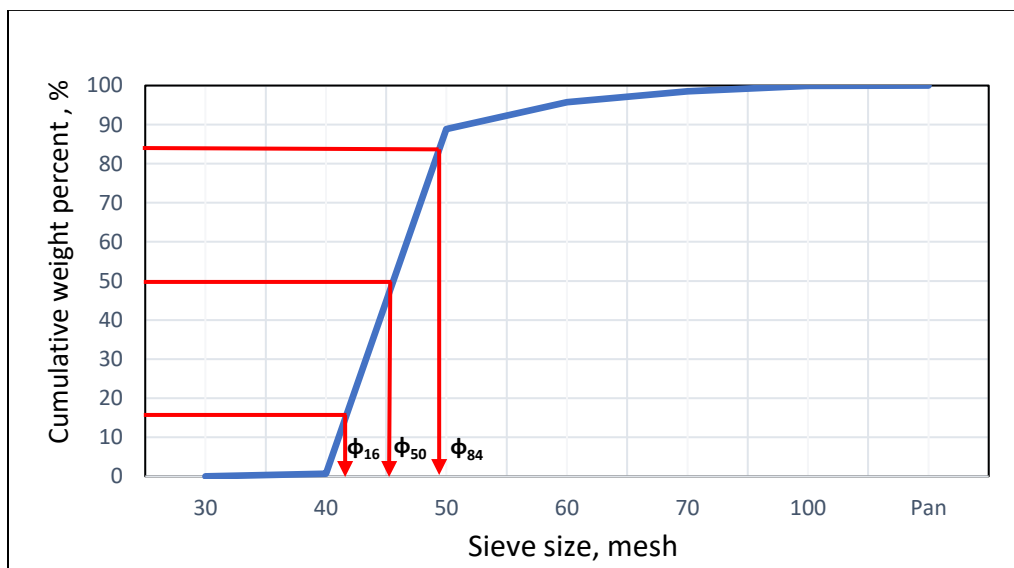


Figure 3.26: Cumulative weight percent for the 40/70 ULW ceramic.

3.4 Experimental Procedure

Before conducting the experimental tests, tap water without proppant was pumped through the apparatus for two main reasons. The first reason was to ensure that the perforation alignment was consistent (Section 3.2.5), and the second to ensure there were no leaks through the system.

The reason for having the perforation alignment consistent was to avoid any different flow patterns that could occur in the system as well as to mimic the flow behavior under field conditions. As discussed in the previous sections, sieve analysis was performed on proppant before each test to ensure the tested proppants have met the API specifications.

The typical procedure for each test that was conducted on proppant transport is summarized as follows:

1. Fill the tank with tap water.
2. Weigh the proppant to obtain the desired proppant concentration.
3. Turn on pump, flow meter, and VFD.
4. Place the video camera 6 feet after the flow meter to record and capture the slurry flow in the horizontal section.
5. Load the appropriate proppant size and type in the tank.
6. Set the mixer at 60 HZ (3600 RPM) to uniformly mix the proppant and water before pumping.
7. Add HLFR at a desired concentration for tests performed with HLFR fluids.
8. Mix the slurry for 5 minutes to ensure a proper mix of the water and the proppant.
9. Adjust the VFD to the desired value.
10. Pump the slurry through the horizontal wellbore; based on the tank size, injection should last 60 seconds for tests with high flow rates and 120 seconds for tests with low flow rates.
11. Record any observations of proppant transport in the wellbore and exiting the perforations.
12. Record the pressure from the gauges that are placed before each of the perforation clusters.
13. Stop pumping when the time for the test is elapsed.
14. Wait until the fluid is entirely drained out of the horizontal wellbore.
15. Record the volume of the exiting slurry in the collecting tanks.
16. Drain out the fluid from the collecting tanks.
17. Measure and record the proppant that has settled in the horizontal wellbore.
18. Dry the proppant in the oven at 120 °C for quantification.
19. Clean the apparatus by pumping water to be ready for the next test.
20. Repeat Steps 1 to 19 as needed for the next experimental test.

CHAPTER 4

EXPERIMENTAL RESULTS USING FRESHWATER FLUIDS

This chapter presents the results of the laboratory tests that were conducted on proppant transport in horizontal wellbores using freshwater fluids. Fresh water without additives was used as a carrier fluid to simulate slickwater fluids. There are two main sections in this chapter: the first section (Section 4.1) consists of the experimental results conducted on two types of proppants with two different sizes utilizing fresh water, while the second section (Section 4.2) presents the proppant settling in the horizontal wellbore. A total of 48 tests were carried out to investigate the effect of the slurry velocity and the proppant concentration on the distribution of the proppant between the perforation clusters. Furthermore, the effect of the proppant size and density was also investigated for various fluid velocities.

4.1 Experimental Results

Experiments were carried out on sand and ultra-light weight (ULW) ceramic across a wide range of proppant concentrations to quantify the proppant distribution and particle concentrations in the wellbore and through each of the perforation clusters. For all the tests that were conducted using fresh water as a fracturing fluid, the valve which was placed at end of the horizontal wellbore was one quarter open. The reason for keeping the valve a little open was to achieve high flow rates through the apparatus. Previously it had been closed, and due to the back pressure acting upon the pump, which was greater than the maximum operating pressure for the pump, the pump turned off automatically. The pressure that was measured inside the horizontal wellbore for the experimental tests ranged from 16.7 to 24.7 psi, but pressure drop due to the perforations was between 1.5 and 2.0 psi.

The parameters which were varied during the experimental tests included slurry velocity, proppant size, proppant density and proppant concentration. The slurry behavior in the wellbore was also observed and analyzed at different flow rates to understand how different types of proppant could be transported in the horizontal wellbore. Finally, the even and uneven proppant distributions' phenomena between the perforation clusters were analyzed.

4.1.1 20/40 Mesh White Sand

Several experimental tests were conducted on 20/40 mesh white sand with a median diameter of 0.675 mm and a specific gravity of 2.65 g/cm³. Three flow velocities were utilized to investigate the effect of slurry velocity on proppant distribution between the perforation clusters as illustrated in Table 4.1. As can be seen in the table, the three flow velocities achieved Reynolds numbers above 4000. In other words, turbulent flow was observed for all the tests at different proppant concentrations.

One thing that should be noted is that particles of 20/40 mesh sand associated with the high specific gravity 2.65 led to high proppant settling in the mixing tank. Therefore, particle settling of the 20/40 mesh sand on the bottom of the mixing tank was observed for all the tests even at high RPM of the mixer. As a result, the maximum injection concentration that was achieved for 20/40 mesh white sand was 0.36 ppg at a flow velocity of 11.0 ft/s.

Sections 4.1.1.1- 4.1.1.3 discuss the effect of the slurry velocity and injected proppant concentrations on the distribution of 20/40 mesh white sand in the horizontal wellbore and between the perforation clusters.

Table 4.1: Reynolds number for 20/40 mesh white sand at slurry velocities of 6.4, 11.0 and 13.7 ft/s

Velocity, ft/s	Velocity, m/s	Fluid Density, kg/m ³	Fluid Viscosity, kg/m/s	Proppant Density, kg/m ³	Proppant Size, mm	Pipe Diameter, m	Re, unitless
6.4	1.948	1000	0.001	2650	0.675	0.038	74,016
11.0	3.339	1000	0.001	2650	0.675	0.038	126,886
13.7	4.174	1000	0.001	2650	0.675	0.038	158,607

4.1.1.1 Flow Velocity of 6.4 ft/s

Four experiments were conducted at a flow velocity of 6.4 ft/s at injected proppant concentrations of 0.12, 0.13, 0.20 and 0.31 ppg. The flow regime for this slurry velocity was turbulent, where the Reynolds number was 74,016.

Figure 4.1 shows the proppant and slurry distribution between the perforation clusters at an injected proppant concentration of 0.12 ppg. The 20/40 mesh sand showed highly uneven distribution with higher concentrations towards the first perforation cluster. A proppant concentration of 0.3 ppg was measured at the first cluster, which was three times greater than the injected proppant concentration, although the amount of the slurry received at each perforation

cluster was almost equal as shown in Figure 4.1. However, the proppant concentration that was received at the last perforation cluster was 0.05 ppg which is six times less than the proppant that was received at the first cluster. Due to the gravity forces (particle weight) acting on the carrying fluid, the particles of the 20/40 mesh sand settled down in the fluid column and form a high concentration gradient in the lower section of the pipe as shown in Figure 4.2. However, at an injected proppant concentration of 0.13 ppg, the results were nearly identical to those at a concentration of 0.12 ppg.

The next test was conducted using the same fluid velocity of 6.4 ft/s, but at an injected proppant concentration of 0.21 ppg. Figure 4.3 shows the proppant and slurry distribution between the perforation clusters at the injected proppant concentration of 0.21 ppg. A similar trend was observed at this injected concentration, where more proppant concentration was received at the first cluster and less concentration was received at the third cluster. Figure 4.4 shows the proppant and the slurry distribution between the perforation clusters at the injected proppant concentration of 0.31 ppg. The highest proppant concentration was received at the first cluster followed by a less proppant concentration at the second cluster. Therefore, a highly uneven proppant distribution was observed between the perforation clusters at the injected proppant concentration of 0.31 ppg.

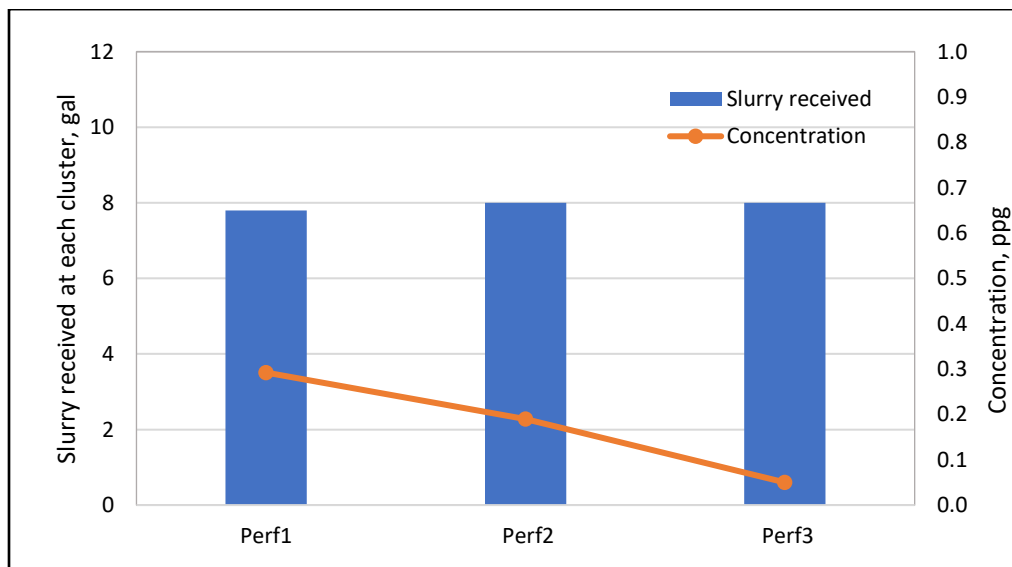


Figure 4.1: Proppant and slurry distribution between the perforation clusters at a slurry velocity of 6.4 ft/s and an injected proppant concentration of 0.12 ppg.

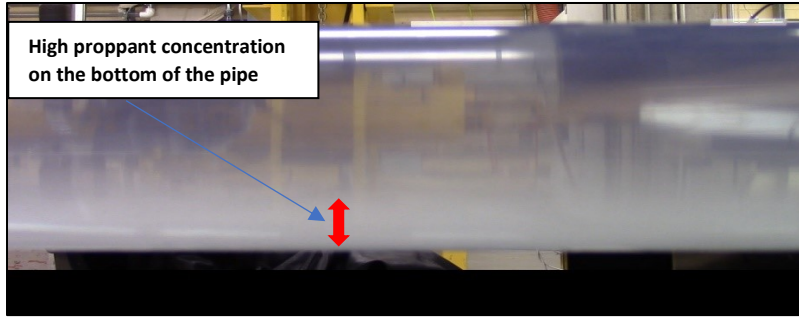


Figure 4.2: Proppant behavior of 20/40 mesh sand at a slurry velocity of 6.4 ft/s.

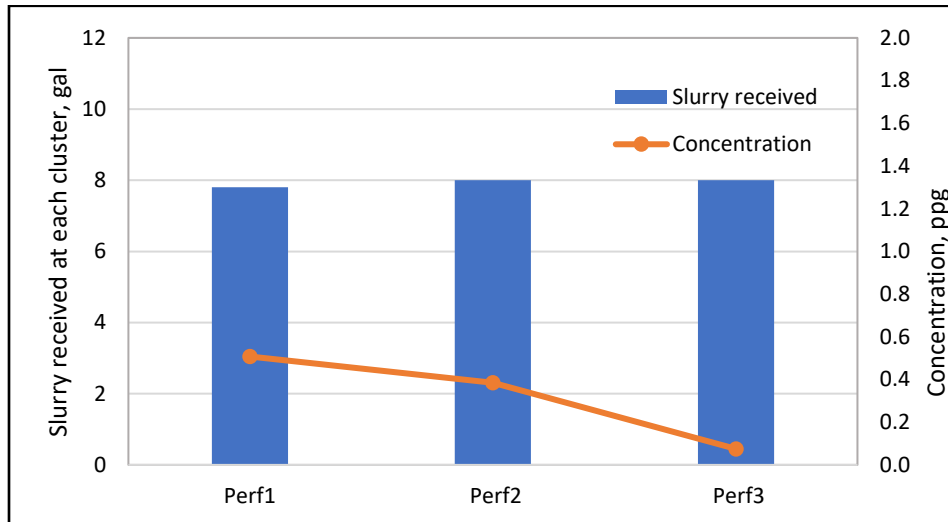


Figure 4.3: Proppant and slurry distribution between the perforation clusters at a slurry velocity of 6.4 ft/s and an injected proppant concentration of 0.21 ppg.

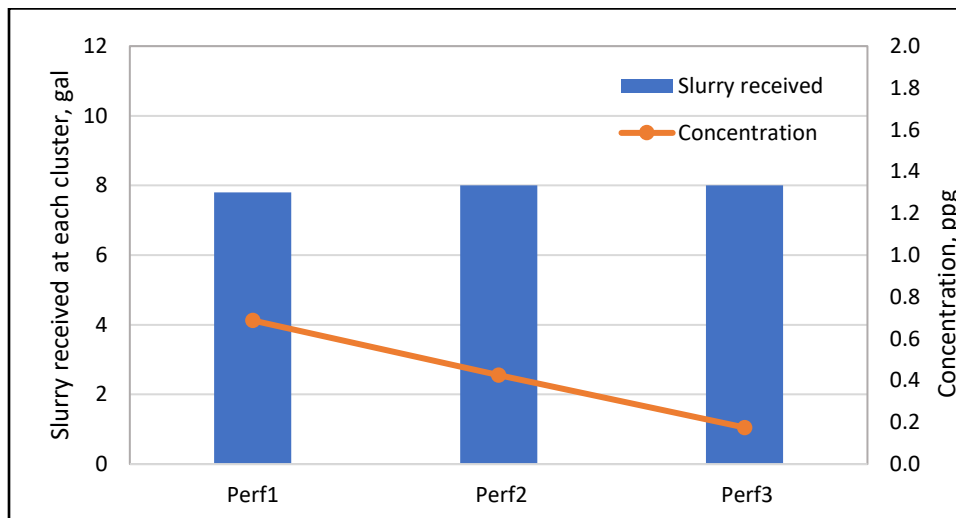


Figure 4.4: Proppant and slurry distribution between the perforation clusters at a slurry velocity of 6.4 ft/s and an injected proppant concentration of 0.31 ppg.

The sieve analysis for the three perforation clusters at a flow velocity of 6.4 ft/s showed little variation in the particle distribution observed between the three clusters, as can be seen in Figure 4.5. A median diameter of 0.679 mm was measured at the first cluster, whereas median diameters of 0.676 and 0.673 mm were measured at the second and the third perforation clusters, respectively. The larger particles interacted with the wall sides of the pipe and dropped to the bottom of the horizontal pipe, whereas the smaller and intermediate particles travelled with the fluid. The small variation in the particle distribution between the perforation clusters was due to the turbulence energies that existed close to the pipe wall. These turbulence energies were able to create eddy currents in the viscous sublayers and were considered as the main reason to transport the proppant particles. Also, these turbulence energies may cause the proppant particles to distribute uniformly in the lower section of the horizontal wellbore.

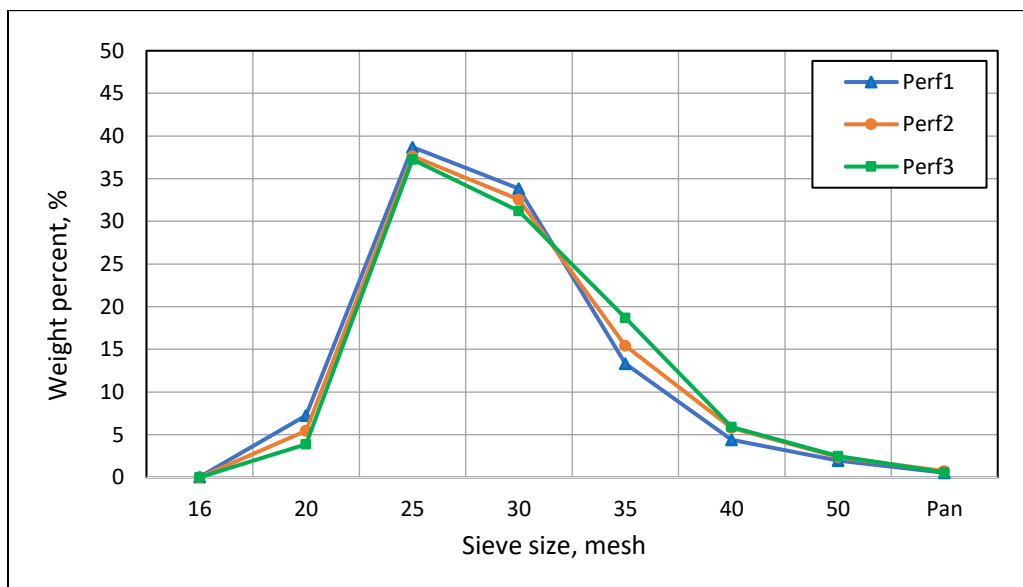


Figure 4.5: Particle distribution between the perforation clusters at a slurry velocity of 6.4 ft/s.

The interpretation of the results that were obtained from the four tests at the low slurry velocity of 6.4 ft/s suggests proppant particles tend to settle down due to their weight and lead to having high proppant concentration on the bottom of the pipe. As the perforation density is 4 SPF at 90-degree phasing, one of the four perforations placed at the bottom of the pipe. Hence, the bottom perforation in the first perforation cluster received more particle concentration than the other three perforations within the cluster, spaced around the pipe. As fluid traveling in the pipe passed the first cluster, and arrived at the second cluster, the proppant concentration became less;

hence, the second perforation cluster received less proppant concentration than the first cluster, and the same is true for the third cluster.

4.1.1.2 Flow Velocity of 11.0 ft/s

A total of four tests were conducted on 20/40 mesh sand at a slurry velocity of 11.0 ft/s and injected proppant concentrations of 0.1, 0.12, 0.23 and 0.36. In this section, the fluid velocity was increased to 11.0 ft/s, at which the flow regime in the horizontal wellbore was turbulent ($Re = 126,886$). Figure 4.6 shows the proppant and slurry distribution between the perforation clusters at an injected proppant concentration of 0.1 ppg. As can be observed from the plot, the 20/40 mesh sand showed uneven distribution with higher concentrations towards the middle cluster followed by a lesser amount of proppant at the third cluster. The particle distribution in the horizontal wellbore was heterogenous where the proppant concentration decreased upward in the fluid column as illustrated in Figure 4.7. The results for the injected proppant concentration of 0.12 ppg, were nearly identical to those at an injected concentration of 0.1 ppg.

At the injected proppant concentration of 0.21 ppg as shown in Figure 4.8, the same behavior was observed where more proppant concentration was measured at the second cluster followed by a less amount measured at the third cluster, and even less proppant concentration was measured at the first cluster. For an injected proppant concentration of 0.36 ppg, as shown in Figure 4.9, there was a nearly even proppant distribution between the perforation clusters. However, the proppant amount that was received at the second cluster was higher than the proppant at the first and the second clusters. For all the tests, the amount of fluid that was received at each cluster was mostly equal.

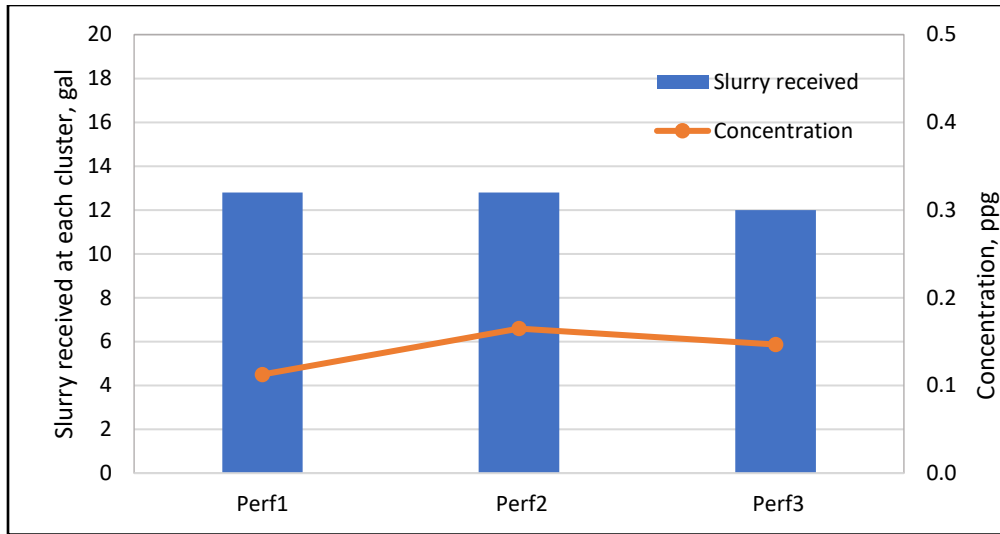


Figure 4.6: Proppant and slurry distribution between the perforation clusters at a slurry velocity of 11.0 ft/s and an injected proppant concentration of 0.10 ppg.

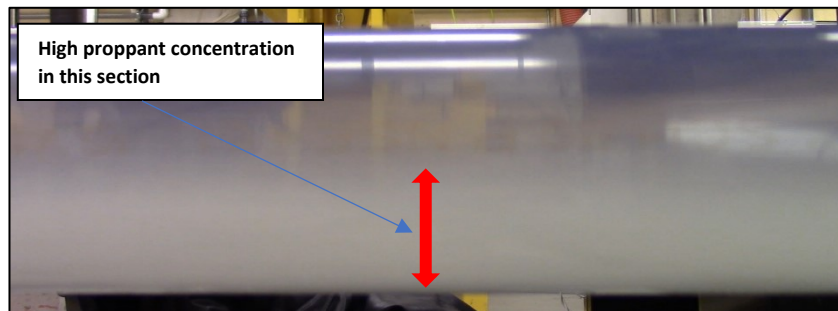


Figure 4.7: Proppant behavior of 20/40 mesh sand at a slurry velocity of 11.0 ft/s (example of heterogeneous suspension).

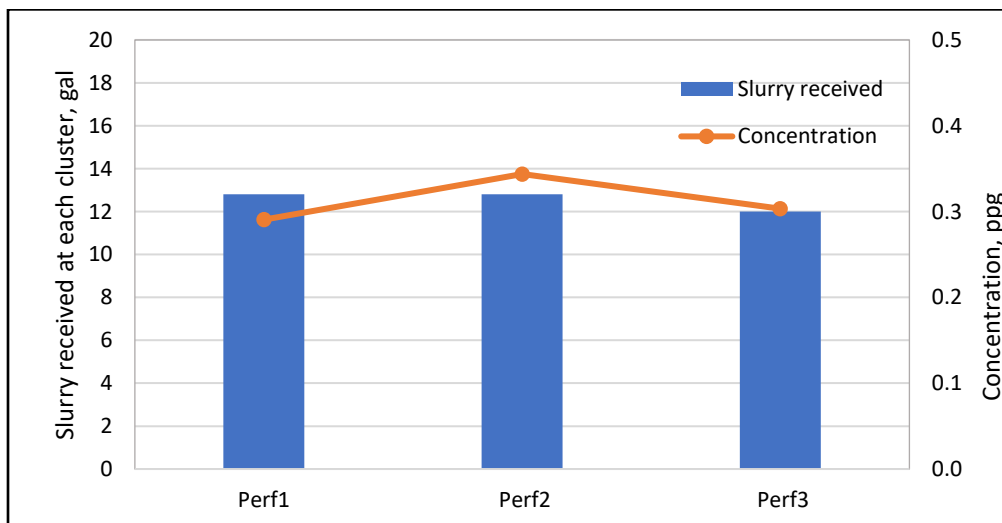


Figure 4.8: Proppant and slurry distribution between the perforation clusters at a slurry velocity of 11.0 ft/s and an injected proppant concentration of 0.23 ppg.

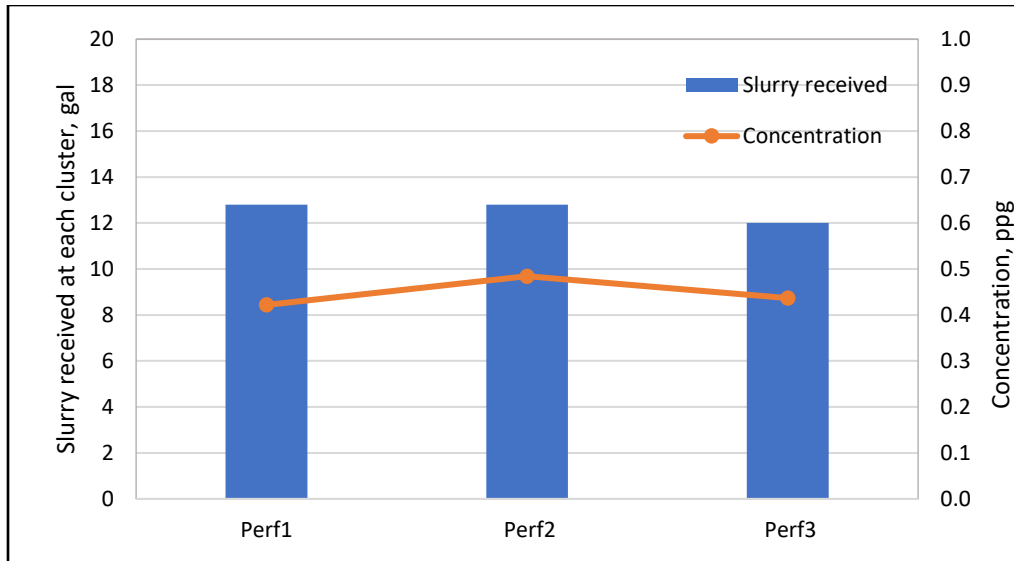


Figure 4.9: Proppant and slurry distribution between the perforation clusters at a slurry velocity of 11.0 ft/s and an injected proppant concentration of 0.36 ppg.

The interpretation of the results obtained from the tests that were conducted at a flow velocity of 11.0 ft/s show that the momentum forces near the first perforation cluster were significant and prevented the proppant from turning into the perforations within the first cluster. As fluid traveled in the wellbore and reached the second cluster, the slurry velocity dropped. The reduction in the slurry velocity near the second cluster led to an increase in the gravity forces by which the larger particles tended to concentrate on the bottom of the pipe. Therefore, particles of proppant were able to turn into the perforation tunnels within the second cluster. As a result, a high proppant concentration was received at the second perforation cluster. After the second cluster, the slurry traveled down the wellbore with less proppant concentration; hence, the proppant concentration at the third cluster was less than the proppant concentration at the second cluster.

4.1.1.3 Flow Velocity of 13.7 ft/s

In this phase of the experiments, the fluid velocity was increased to 13.7 ft/s. A total of two tests were conducted on 20/40 mesh white sand at two different injected proppant concentrations of 0.13 and 0.31 ppg at this velocity.

Figure 4.10 shows the proppant and slurry distribution between the perforation clusters at a slurry velocity of 13.6 ft/s and at an injected proppant concentration of 0.13 ppg. As can be observed from the graph, uneven proppant distribution occurred between the perforation clusters. The proppant concentration at the third cluster was higher than the concentration at the first and

the second clusters. According to Biot and Medlin (1985), the suspension transport mechanisms here can be described as heterogenous, where more proppant concentration occurred in the lower section of the fluid column as illustrated in Figure 4.11.

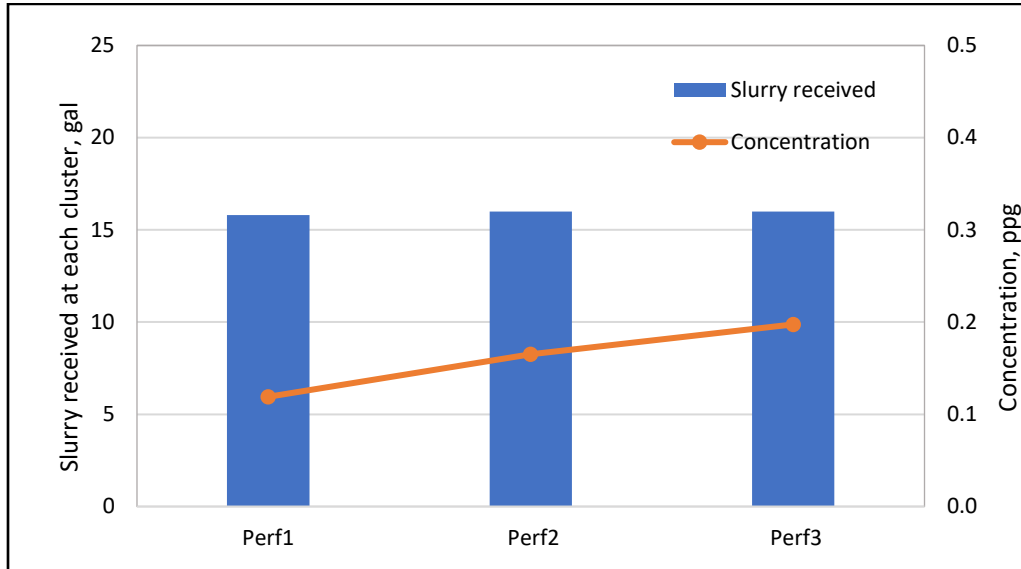


Figure 4.10: Proppant and slurry distribution between the perforation clusters at a slurry velocity of 13.7 ft/s and an injected proppant concentration of 0.13 ppg.

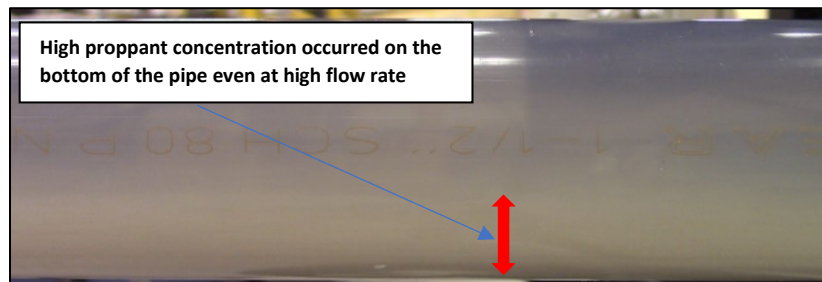


Figure 4.11: Proppant behavior of 20/40 mesh sand at a slurry velocity of 13.7 ft/s (example of heterogenous suspension).

When the proppant concentration was increased to 0.31 ppg, a similar trend was also observed at this injected concentration. More proppant concentration was received at the third cluster and less concentration was received at the first cluster, even though the amount of the slurry received at each perforation cluster was almost the same as shown in Figure 4.12. One of the reasons attributed for uneven proppant distribution between the perforation clusters is that the total momentum near the first and second perforation clusters was fairly high. This was the main reason

that the proppant particles were prevented from turning into the perforations within the first and the second clusters.

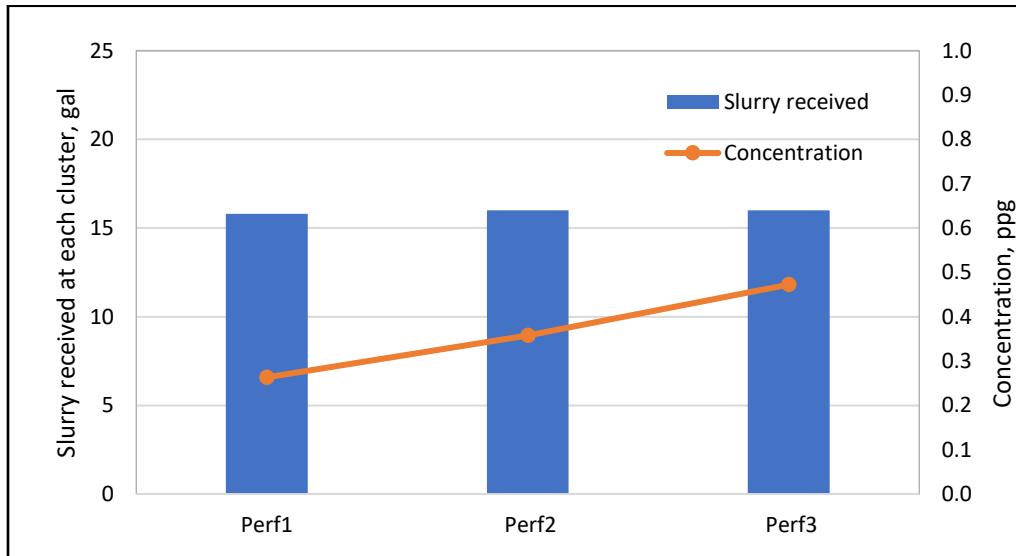


Figure 4.12: Proppant and slurry distribution between the perforation clusters at a slurry velocity of 13.7 ft/s and an injected proppant concentration of 0.31 ppg.

The particle distribution between the three perforation clusters at a flow velocity of 13.7 ft/s is shown in Figure 4.13. The median diameter that was measured at the first cluster was 0.665 mm, whereas the median diameters that were measured at the second and the third perforation clusters were of 0.670 and 0.682, respectively. As can be noted that the median diameter that was measured at the toe perforation cluster was higher than the median diameter that was measured at the first and second clusters. This can be explained that at high flow rates, the larger mass particles were not able to make a complete turn at the first and the second clusters. According to the Newton's second law of motion, it is difficult to deviate larger mass particles from their preferred path of the motion in a straight line than smaller mass particles. Therefore, larger particle proppant such as 20/40 mesh could have a significant effect on the proppant distribution between the perforation clusters and must be considered when designing a horizontal well fracturing treatment.

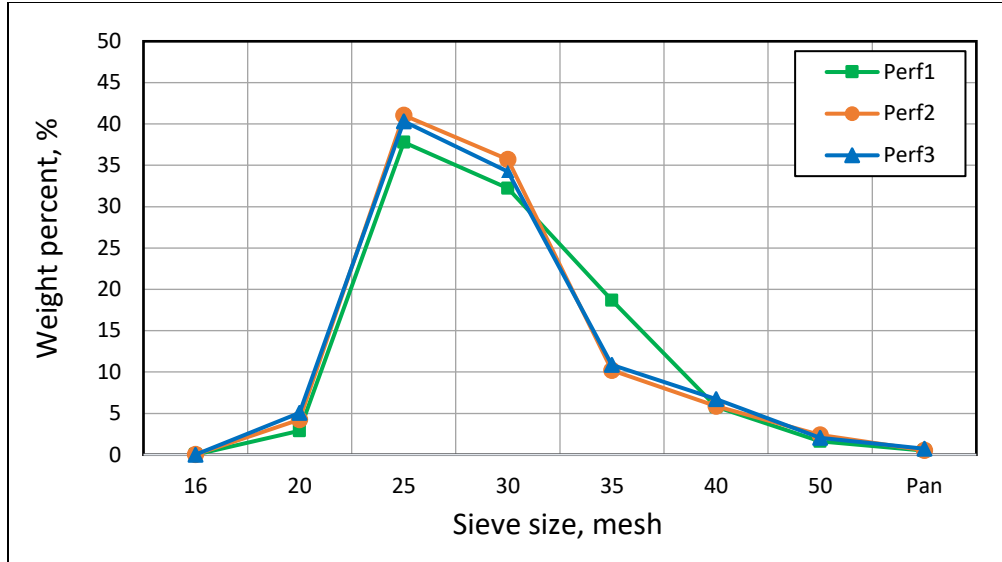


Figure 4.13: Particle distribution between the perforation clusters at a slurry velocity of 13.7 ft/s.

4.1.2 40/70 Mesh White Sand

A number of experimental tests were also conducted on 40/70 mesh white sand with a median diameter of 0.360 mm. The median diameter of the 40/70 is about 45% smaller than the median diameter of 20/40 mesh white sand at 0.675 mm. Three flow velocities were used to study the effect of slurry velocity on proppant distribution between the perforation clusters as shown in Table 4.2. The values of Reynolds number for the three flow velocities were all above 4000 which indicates the flow is highly turbulent as illustrated in Table 4.2.

Table 4.2: Reynolds number for 40/70 mesh white sand at slurry velocities of 6.4, 11.0 and 13.7 ft/s

Velocity, ft/s	Velocity, m/s	Fluid Density, kg/m ³	Fluid Viscosity, kg/m/s	Proppant Density, kg/m ³	Proppant Size, mm	Pipe Diameter, m	Re, unitless
6.4	1.948	1000	0.001	2650	0.360	0.038	74,017
11.0	3.339	1000	0.001	2650	0.360	0.038	126,886
13.7	4.174	1000	0.001	2650	0.360	0.038	158,608

Sections 4.1.2.1 through 4.1.2.3 discuss the effect of the slurry velocity and proppant concentration on the distribution of 40/70 mesh white sand in the horizontal wellbore.

4.1.2.1 Flow Velocity of 6.4 ft/s

Four experiments were carried out on 40/70 mesh white sand at a flow velocity of 6.4 ft/s. The proppant concentration at each cluster was measured across a range of injected proppant concentrations of 0.3, 0.37, 0.93 and 1.1 ppg. At the injected proppant concentration of 0.3 ppg, the proppant concentration that was received at the first cluster was a little higher than the concentration that was received at the second cluster, as shown in Figure 4.14. Whereas, the proppant that was received at the third cluster was much less than the proppant that was received at the first and the second clusters. As stated previously, gravity forces were dominant over viscous and momentum forces in this situation. In this case, particles of the proppant settled on the bottom of the pipe. As a result, more proppant concentration was received at the perforation within the first cluster which has a downward orientation in the first cluster.

The particle distribution in the horizontal wellbore was heterogenous where more proppant concentration occurred in the lower section of the fluid column as illustrated in Figure 4.15. The results for the injected proppant concentration of 0.37 ppg were nearly identical to those at an injected concentration of 0.3 ppg.

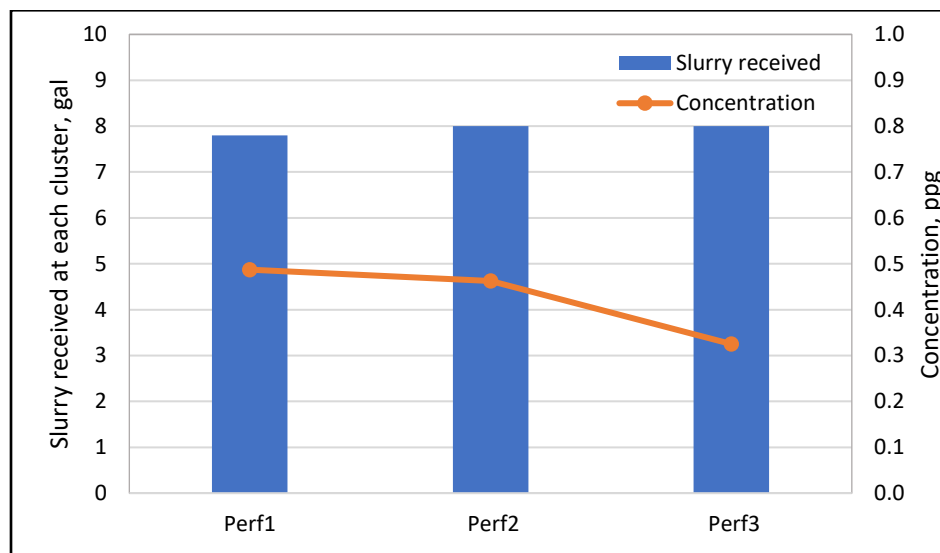


Figure 4.14: Proppant and slurry distribution between the perforation clusters at a slurry velocity of 6.4 ft/s and an injected proppant concentration of 0.3 ppg.

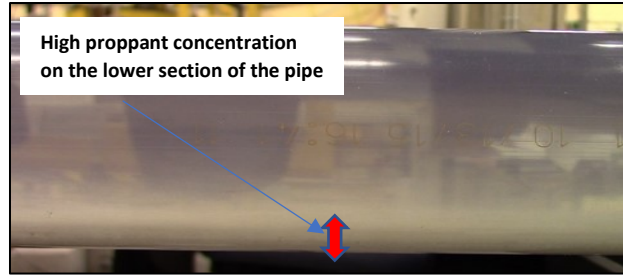


Figure 4.15: Proppant behavior and distribution for 40/70 mesh sand at a slurry velocity of 6.4 ft/s.

When the injected proppant concentration was increased to 0.93 ppg as shown in Figure 4.16, more proppant concentration was received at the first cluster and less concentration was received at the third cluster. However, there was a mostly even proppant distribution between the first and the second clusters, which was a noticeably different condition than for the 20/40 mesh white sand. As proppant particles became smaller, i.e. 40/70 mesh, fluid was able to transport and carry proppant particles further in the wellbore. However, when the slurry arrived at the third cluster, the particle concentration was less; hence, the third perforation cluster received less proppant concentration than the first and the second clusters.

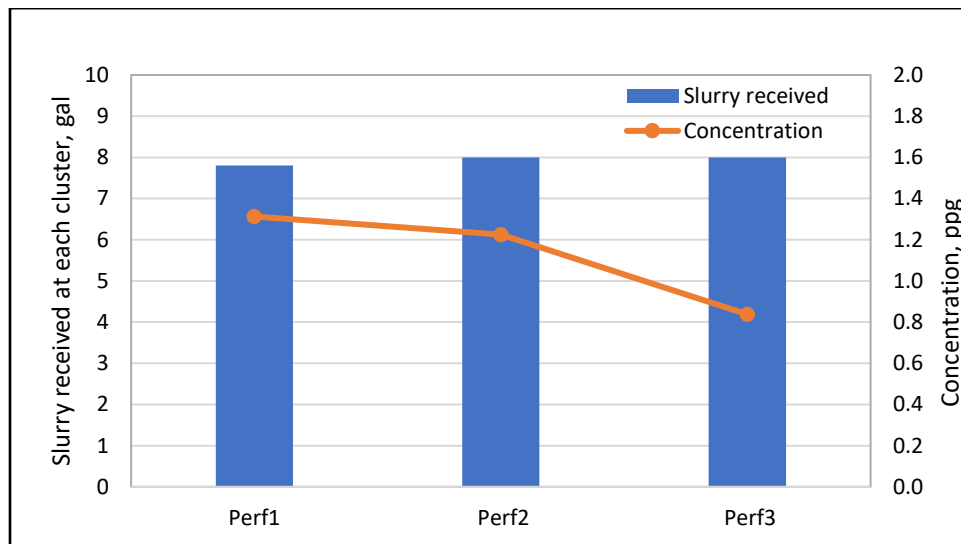


Figure 4.16: Proppant and slurry distribution between the perforation clusters at a slurry velocity of 6.4 ft/s and an injected proppant concentration of 0.93 ppg.

The next test was with an injection concentration of 1.1 ppg as shown in Figure 4.17. As can be seen from the graph, there was an increase in the proppant concentration at the third cluster. Also, the proppant distribution between the three clusters was high, in other words, mostly even distribution was observed. There are some reasons that might explain this phenomenon. The first

reason could be the interaction between the particles by which larger grains of the proppant will tend to settle down and exit the perforation holes that are placed on the bottom of the pipe. The second reason could be the interaction between the particles and the pipe wall. This interaction can occur from the high turbulent velocity which can force the particles to move away from the centerline of the pipe. This results in more friction loss and leads the particles to settle in the low velocity region near the pipe wall.

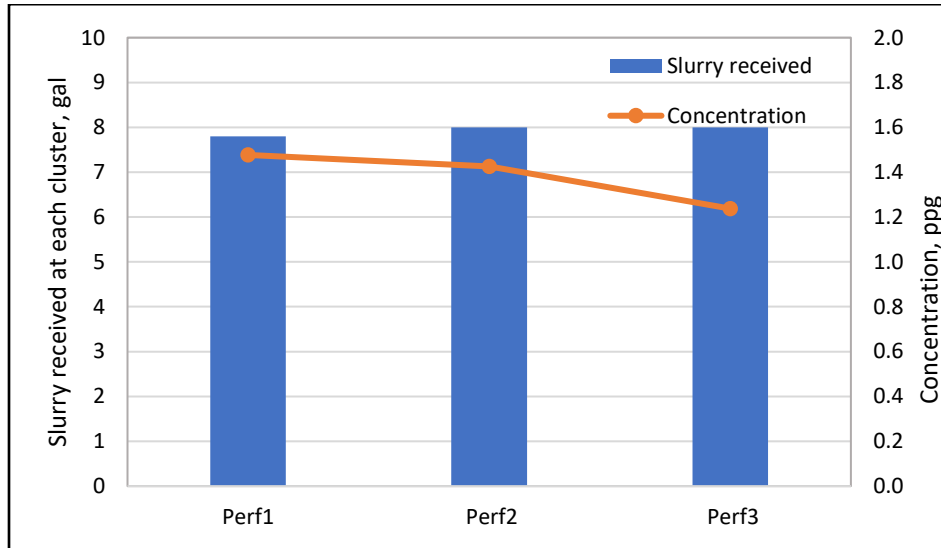


Figure 4.17: Proppant and slurry distribution between the perforation clusters at a slurry velocity of 6.4 ft/s and an injected proppant concentration of 1.10 ppg.

The change in the particle distribution between the perforation clusters at a flow velocity of 6.4 ft/s for 40/70 mesh white sand was small if compared with the 20/40 mesh sand at the same flow velocity. Figure 4.18 shows the particle distribution between the three perforation clusters at a slurry velocity of 6.4 ft/s. A median diameter of 0.362 mm was measured at the first cluster, whereas median diameters of 0.359 and 0.356 mm were measured at the second and the third perforation clusters, respectively.

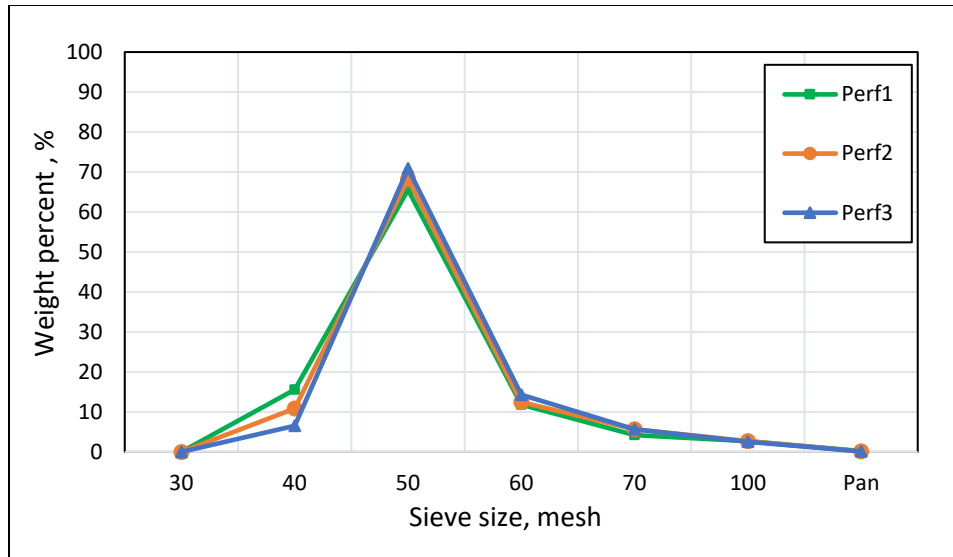


Figure 4.18: Particle distribution between the perforation clusters at a slurry velocity of 6.4 ft/s.

4.1.2.2 Flow Velocity of 11.0 ft/s

Three experiments were conducted with 40/70 mesh white sand at a slurry velocity of 11.0 ft/s. At a velocity of 11.0 ft/s, the Reynolds number was calculated to be 126,886 which indicates the flow is highly turbulent. The proppant concentration at each cluster was measured across a range of injected proppant concentrations of 0.3, 0.9 and 1.2 ppg. Figure 4.19 shows the proppant and slurry distribution between the perforation clusters at an injected proppant concentration of 0.3 ppg. As can be observed from the graph, the 40/70 mesh sand showed slightly uneven proppant distribution with higher concentrations towards the third cluster.

The same trend was also observed at injection proppant concentrations of 0.9 and 1.2 ppg as illustrated in Figures 4.20 and 4.21, respectively, even though the amount of the slurry received at each perforation cluster was almost the same. As stated previously, the reason attributed for the uneven proppant distribution between the three clusters is that the total momentum near the first and the second perforation clusters being fairly high. This was the main reason for preventing the proppant particles from turning into the perforations within these two clusters.

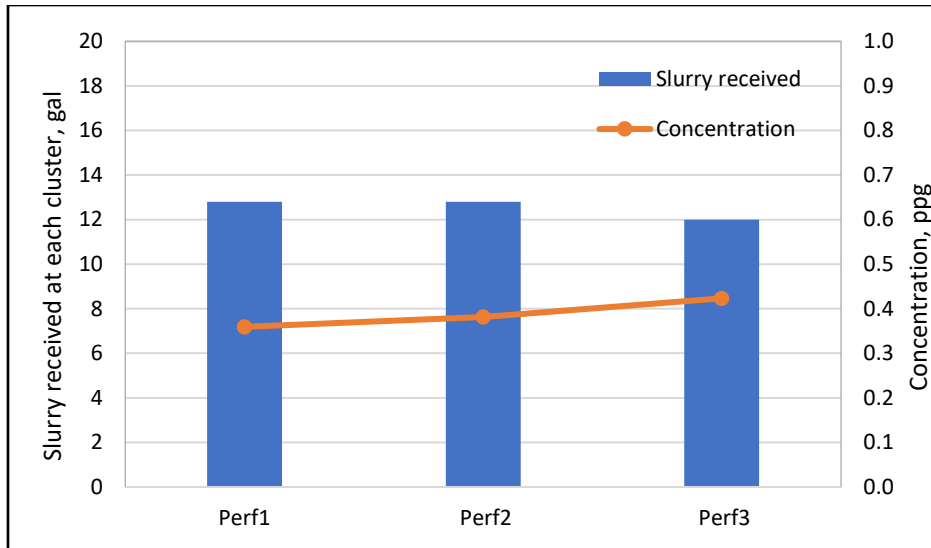


Figure 4.19: Proppant and slurry distribution between the perforation clusters at a slurry velocity of 11.0 ft/s and an injected proppant concentration of 0.3 ppg.

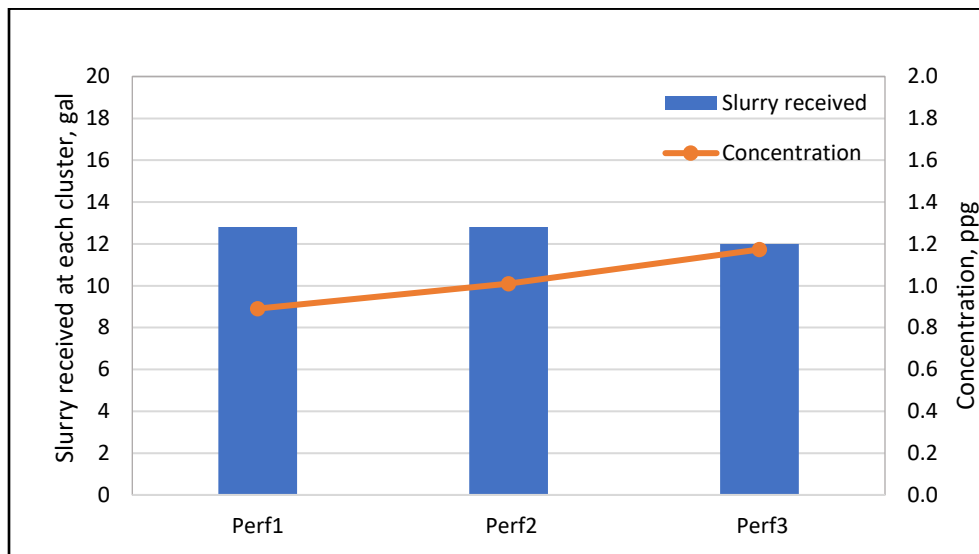


Figure 4.20: Proppant and slurry distribution between the perforation clusters at a slurry velocity of 11.0 ft/s and an injected proppant concentration of 0.9 ppg.

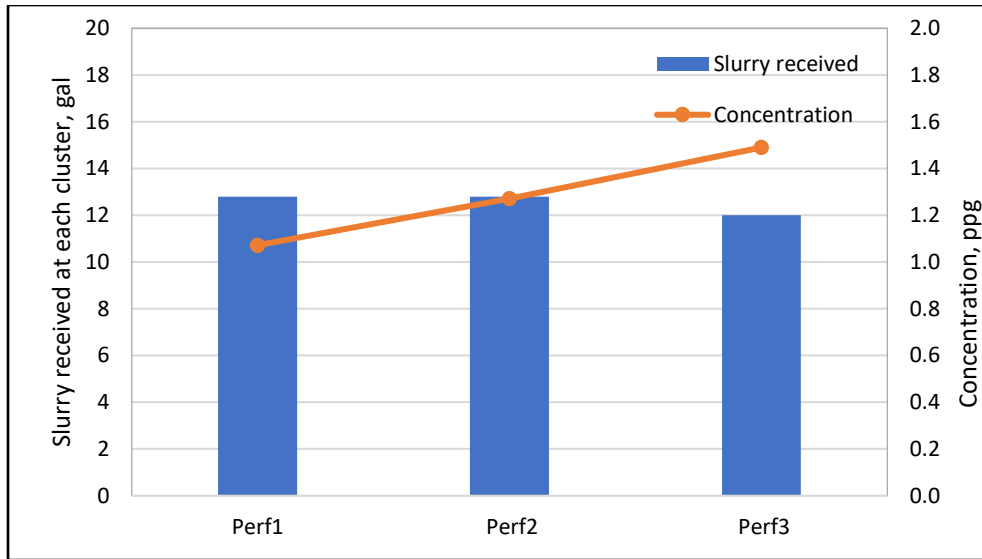


Figure 4.21: Proppant and slurry distribution between the perforation clusters at a slurry velocity of 11.0 ft/s and an injected proppant concentration of 1.2 ppg.

4.1.2.3 Flow Velocity of 13.7 ft/s

In this section, the fluid velocity was increased to 13.7 ft/. A total of three tests were conducted on 40/70 mesh white sand at different injected proppant concentrations. Figure 4.22 shows the proppant and slurry distribution between the perforation clusters at an injected proppant concentration of 0.20 ppg. Uneven proppant concentration was observed between the perforation clusters, even though the particle distribution across the vertical cross section in the horizontal wellbore was mostly uniform as can be seen in Figure 4.23.

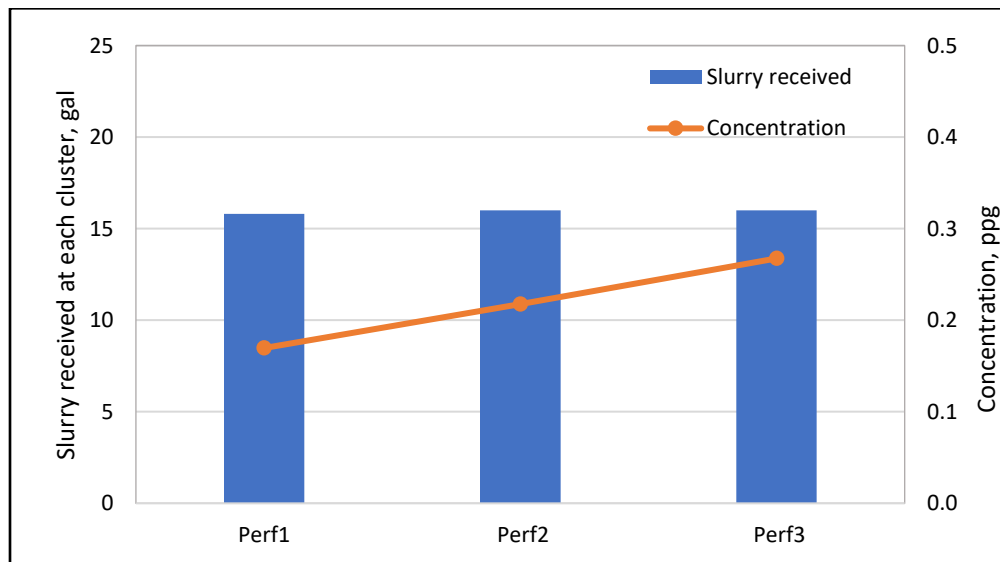


Figure 4.22: Proppant and slurry distribution between the perforation clusters at a slurry velocity of 11.0 ft/s and an injected proppant concentration of 0.20 ppg.

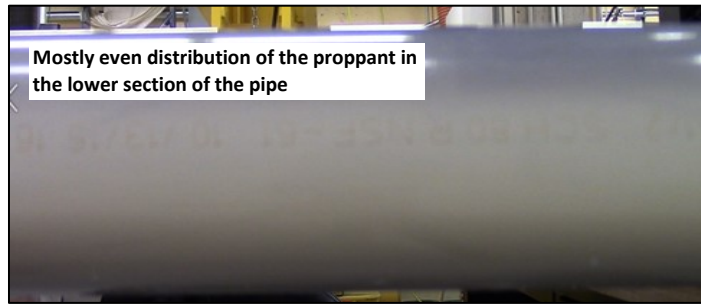


Figure 4.23: Proppant behavior and distribution for 40/70 mesh sand at a slurry velocity of 13.7 ft/s (example of heterogenous suspension).

When the injected proppant concentration was increased to 0.8 and then to 1.17 ppg, a similar trend was observed at these two injected proppant concentrations as can be seen in Figures 4.24 and 4.25, respectively. More proppant was received at the third cluster, whereas less proppant was received at the first and the second clusters. As mentioned previously, the momentum forces near the first and the second perforation clusters were higher than the gravity forces, and as a result, proppant particles were not able to turn into the perforations within these two clusters.

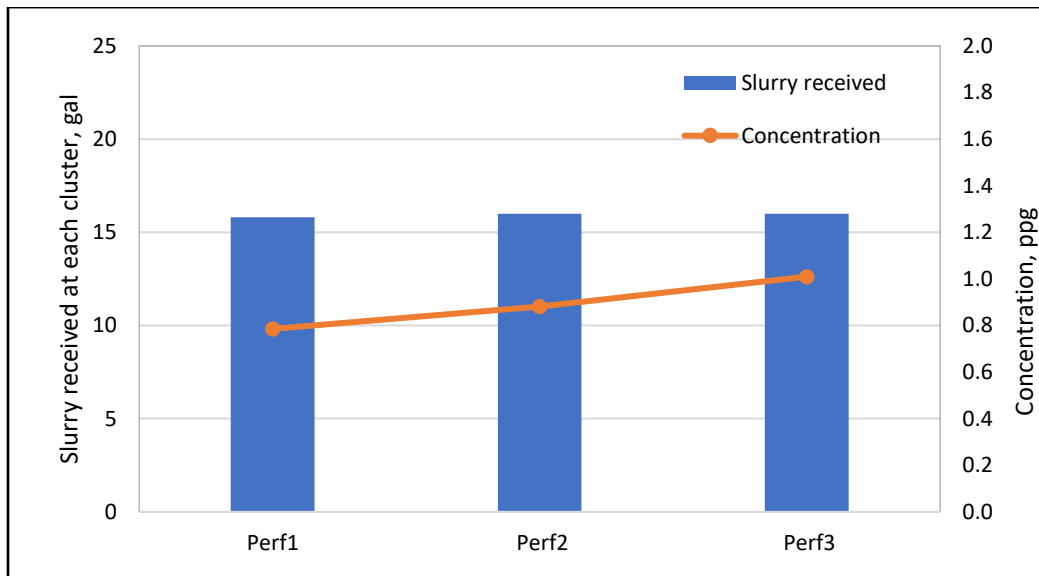


Figure 4.24: Proppant and slurry distribution between the perforation clusters at a slurry velocity of 13.7 ft/s and an injected proppant concentration of 0.8 ppg.

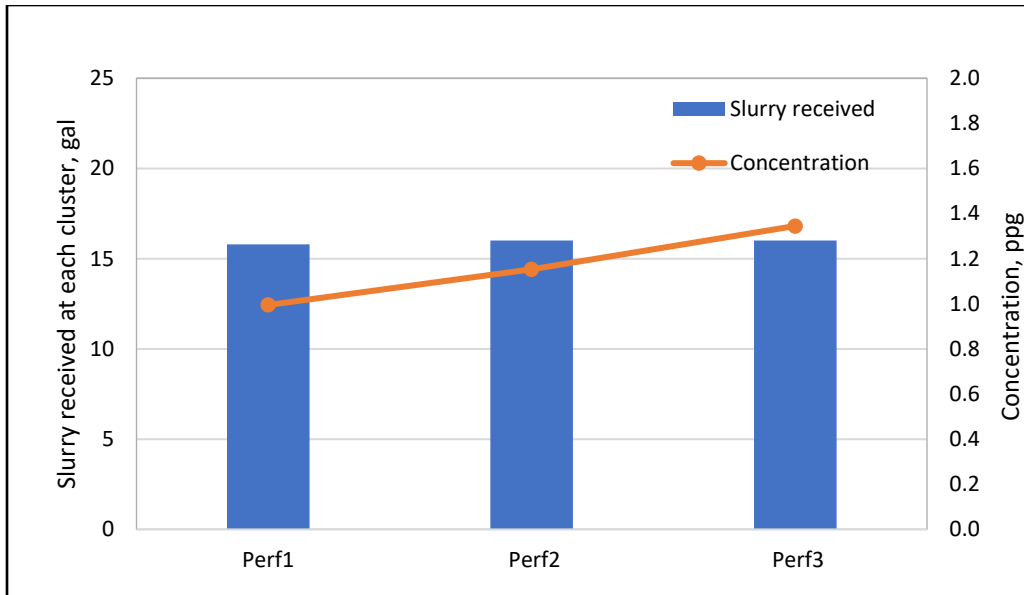


Figure 4.25: Proppant and slurry distribution between the perforation clusters at a slurry velocity of 13.7 ft/s and an injected proppant concentration of 1.17 ppb.

The particle distribution between the three perforation clusters at a flow velocity of 13.7 ft/s is shown in Figure 4.26. The size of the proppant particles was distributed fairly uniformly between the three clusters. The median diameter that was measured at the first cluster was 0.357 mm, whereas the median diameters that were measured at the second and the third perforation clusters were 0.362 and 0.364, respectively. As can be noted that the median diameter that was measured at the toe perforation cluster was higher than the median diameter that was measured at the first and second clusters. This can be explained that at high flow rates, the larger mass particles were not able to make a complete turn at the first and the second clusters where the momentum forces were more dominant over the gravitational forces. As mentioned in the Subsection of 4.1.1.3, according to the Newton's second law of motion, it is difficult to deviate larger mass particles from their preferred path of the motion in a straight line than smaller mass particles. Therefore, proppants with smaller particles such as 40/70 mesh could have a significant effect on proppant distribution in horizontal well treatments.

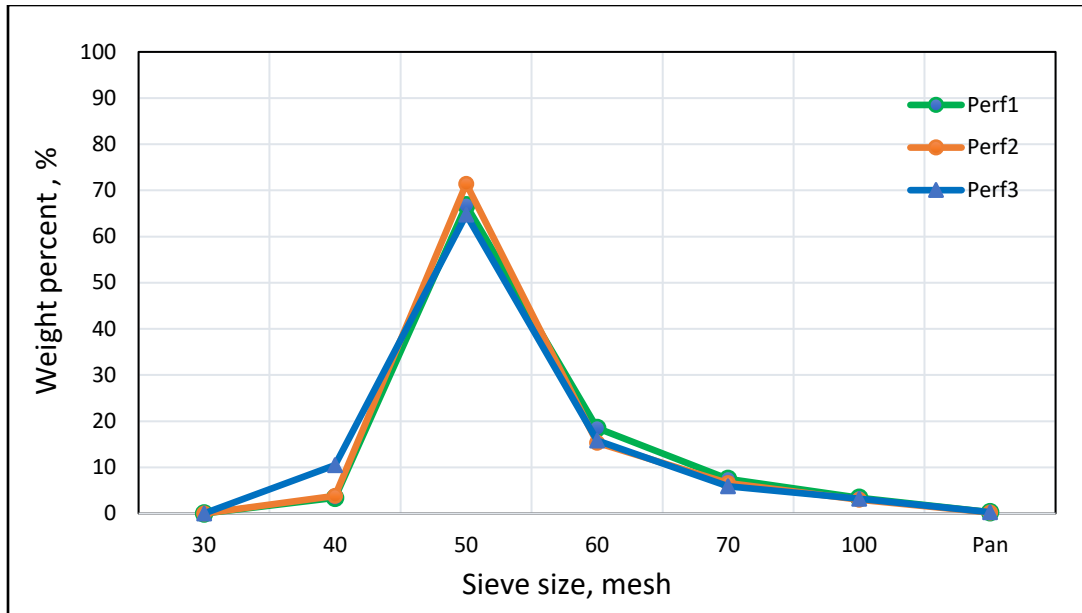


Figure 4.26: Particle distribution between the perforation clusters for the 40/70 mesh white sand at a slurry velocity of 13.7 ft/s.

4.1.3 20/40 Ultra-Light Weight Ceramic

The specific gravity of the tested 20/40 ULW ceramic is 2.0 which is 24.53% less than the specific gravity of the sand. This indicates that the momentum difference between the fluid and the proppant is relatively small. Three flow velocities were used to quantify the effect of slurry velocity on proppant distribution between the perforation clusters as shown in Table 4.3. As can be noted from Table 4.3, the three flow velocities achieved Reynolds numbers above 4000. Therefore, turbulent flow was observed for all the tests that were conducted on 20/40 ULW ceramic at different proppant concentrations.

Table 4.3: Reynolds number for 20/40 ULW ceramic at flow velocities of 6.4, 11.0 and 13.7 ft/s

Velocity, ft/s	Velocity, m/s	Fluid Density, kg/m ³	Fluid Viscosity, kg/m/s	Proppant Density, kg/m ³	Proppant Size, mm	Pipe Diameter, m	Re, unitless
6.4	1.948	1000	0.001	2000	0.650	0.038	74,017
11.0	3.339	1000	0.001	2000	0.650	0.038	126,886
13.7	4.174	1000	0.001	2000	0.650	0.038	158,608

4.1.3.1 Flow Velocity of 6.4 ft/s

Four experimental tests were conducted on 20/40 ULW ceramic at a flow velocity of 6.4 ft/s and at a range of injected proppant concentrations. Since the specific gravity is relatively low,

proppant particles tend to suspend without effort in the fluid column. Figures 4.27 and 4.28 show the proppant and slurry distribution between the perforation clusters at injected proppant concentrations of 0.3 and 0.72 ppg, respectively. As can be observed from Figures 4.27 and 4.28, even proppant distribution occurred between the first and the second clusters. The larger particles can create a change in the proppant concentration where more concentration occurs in the lower section of the horizontal pipe as can be seen in Figure 4.29.

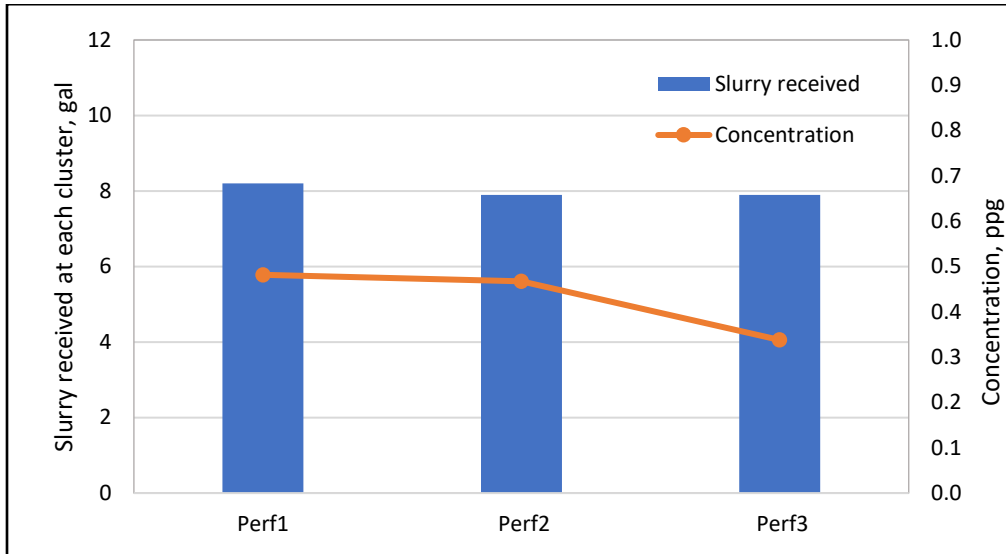


Figure 4.27: Proppant and slurry distribution between the perforation clusters at a slurry velocity of 6.4 ft/s and an injected proppant concentration of 0.3 ppg.

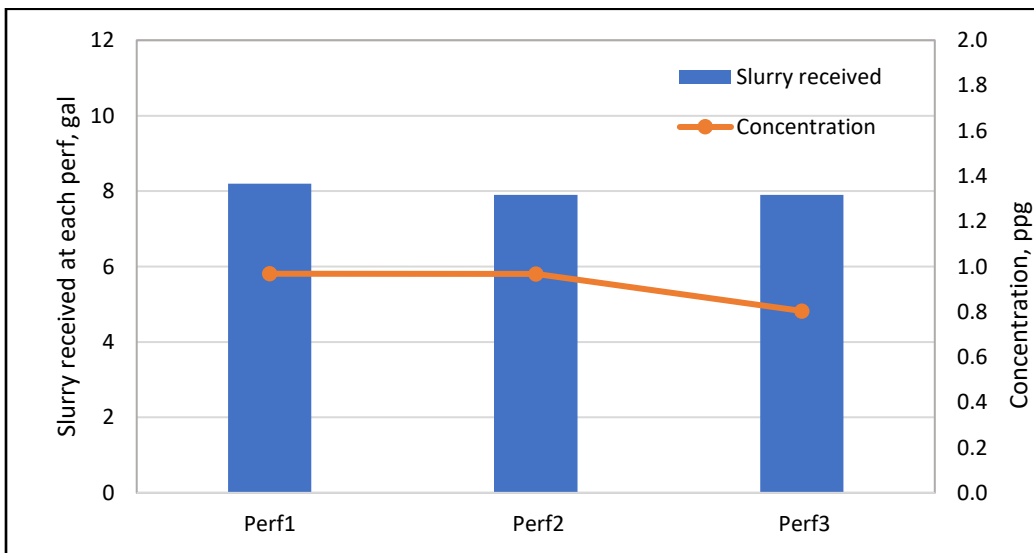


Figure 4.28: Proppant and slurry distribution between the perforation clusters at a slurry velocity of 6.4 ft/s and an injected proppant concentration of 0.72 ppg.

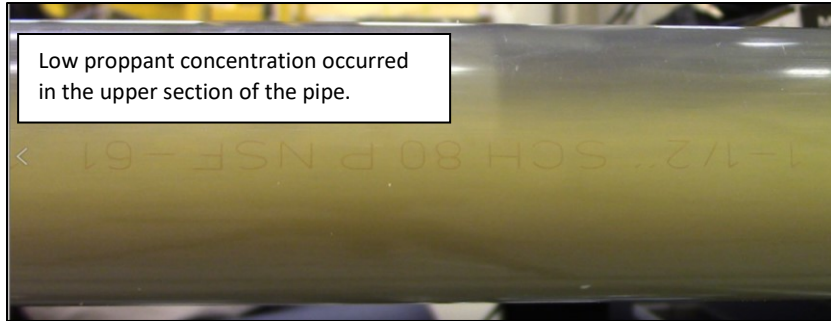


Figure 4.29: Proppant behavior and distribution of 20/40 ULW ceramic at a slurry velocity of 6.4 ft/s.

However, at injected proppant concentrations of 1.14 and 1.8 ppg as shown in Figures 4.30 and 4.31, respectively, the highest proppant concentration occurred at the second cluster followed by the third cluster. This implies that the flow velocity is sufficiently high enough to prevent the proppant particles settling to the bottom of the pipe. Larger proppant particles in the fluid can create a significant change in the proppant distribution under these conditions.

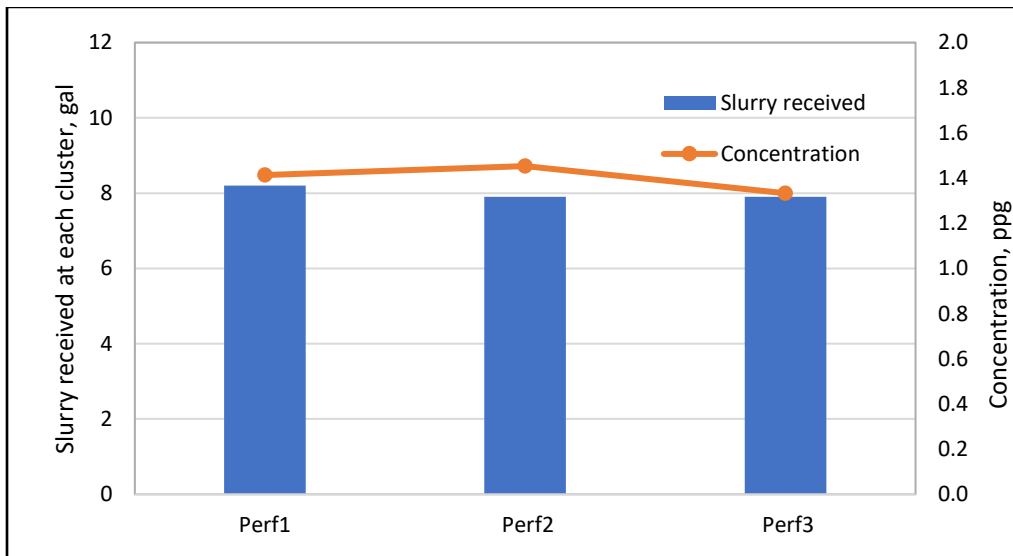


Figure 4.30: Proppant and slurry distribution between the perforation clusters at a slurry velocity of 6.4 ft/s and an injected proppant concentration of 1.14 ppg.

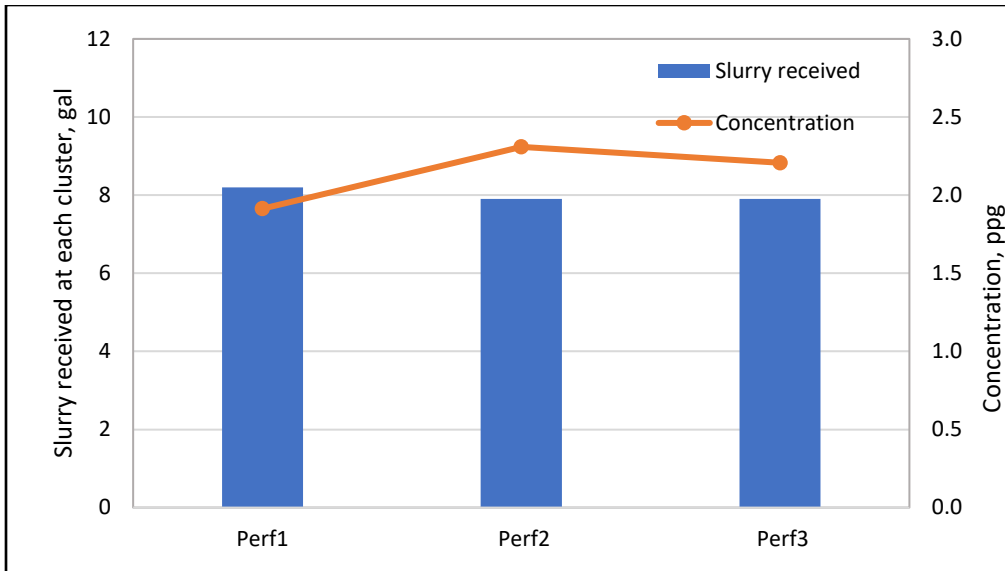


Figure 4.31: Proppant and slurry distribution between the perforation clusters at a slurry velocity of 6.4 ft/s and an injected proppant concentration of 1.8 ppg.

4.1.3.2 Flow Velocity of 11.0 ft/s

A total of three tests were conducted on 20/40 ULW ceramic at a slurry velocity of 11.0 ft/s and injected proppant concentrations of 0.7, 0.94 and 1.3 ppg. In this section, the fluid velocity was increased to 11.0 ft/s, at which the flow regime in the horizontal wellbore was turbulent ($Re = 126,886$).

Figures 4.32, 4.33 and 4.34 show the proppant and slurry distribution between the perforation clusters at injected proppant concentrations of 0.7, 0.94 and 1.3 ppg, respectively. As can be observed from the three graphs, the 20/40 ULW ceramic showed slightly uneven distribution with a higher proppant concentration towards the third cluster followed by a lesser amount of proppant at the second and the first clusters.

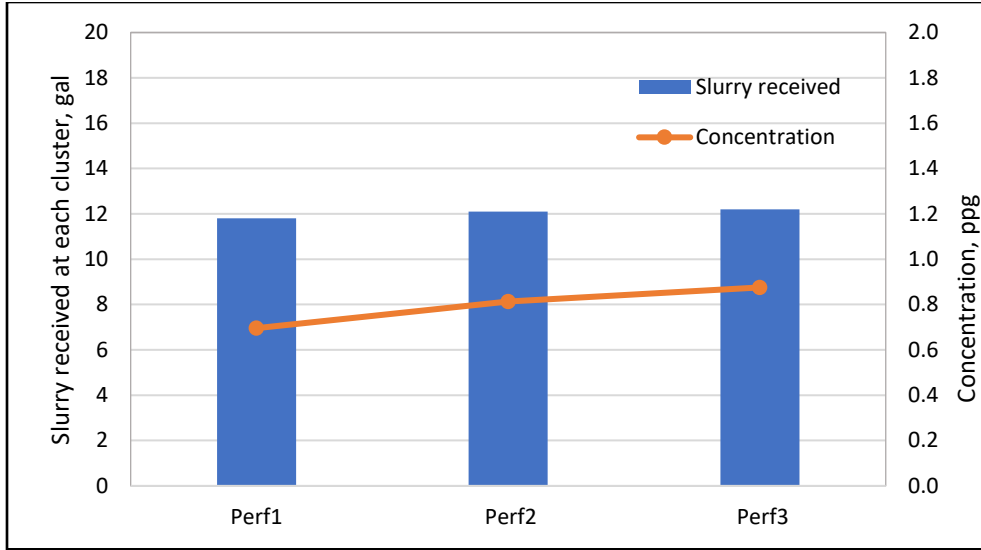


Figure 4.32: Proppant and slurry distribution between the perforation clusters at a slurry velocity of 11.0 ft/s and an injected proppant concentration of 0.7 ppg.

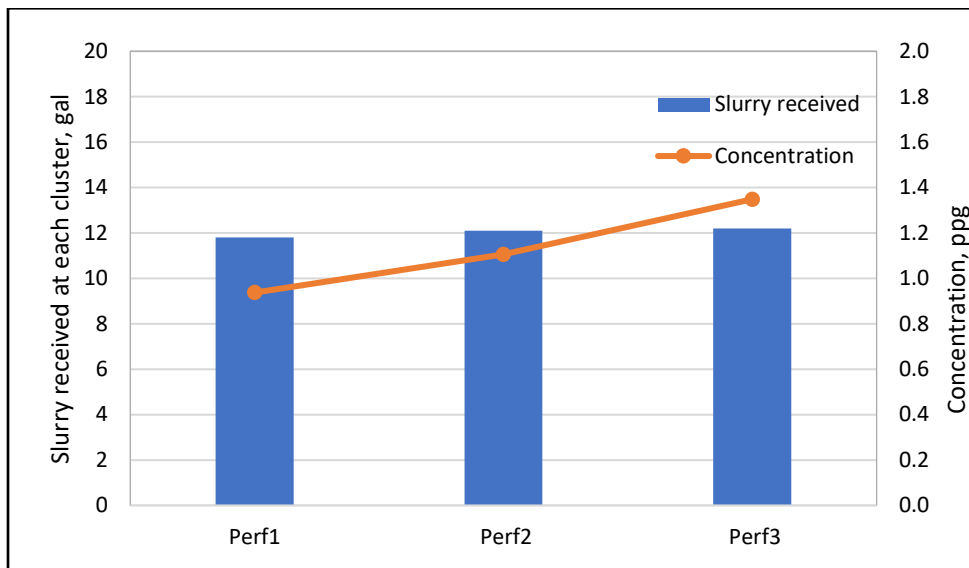


Figure 4.33: Proppant and slurry distribution between the perforation clusters at a slurry velocity of 11.0 ft/s and an injected proppant concentration of 0.94 ppg.

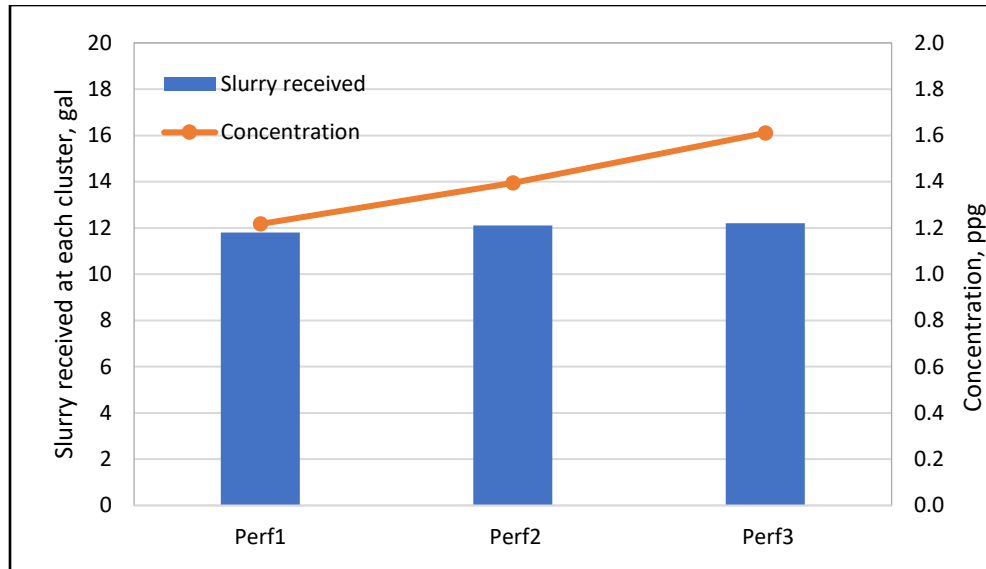


Figure 4.34: Proppant and slurry distribution between the perforation clusters at a slurry velocity of 11.0 ft/s and an injected proppant concentration of 1.3 ppg.

The particle distribution in the horizontal wellbore was mostly uniform, in other words the proppant particles were mostly distributed evenly in the fluid column as illustrated in Figure 4.35.

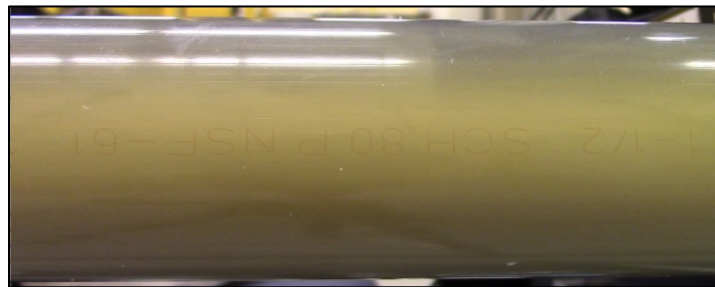


Figure 4.35: Proppant behavior and distribution of 20/40 ULW ceramic at a slurry velocity of 11.0 ft/s.

4.1.3.3 Flow Velocity of 13.7 ft/s

In this section, the fluid velocity was increased to 13.7 ft/s with the 20/40 ULW proppant. A total of four tests were conducted on 20/40 ULW ceramic at different injected proppant concentrations.

Figures, 4.36, 4.37, 4.38 and 4.39 shows the proppant and slurry distribution between the perforation clusters at a slurry velocity of 13.6 ft/s and injected proppant concentrations of 0.21, 0.55, 0.84, and 1.10 ppg, respectively. A review of Figures 4.36 through 4.39 through suggests that at a high flow rate, the proppant distribution is similar to the one that was obtained for 40/70

mesh white sand at the same flow velocity (13.7 ft/s). The proppant concentration at the third cluster was higher than the concentration at the first and the second clusters. The reason is attributed to the fact that proppant with larger grains moved with greater mass and momentum and this led to particles were not able to turn easily into the perforations placed within the first cluster. The amount of the fluid received at each perforation cluster was almost the same for all the tests. The suspension transport mechanisms can be described as pseudo-homogenous, where the proppant particles were distributed uniformly throughout the fluid column in the horizontal pipe.

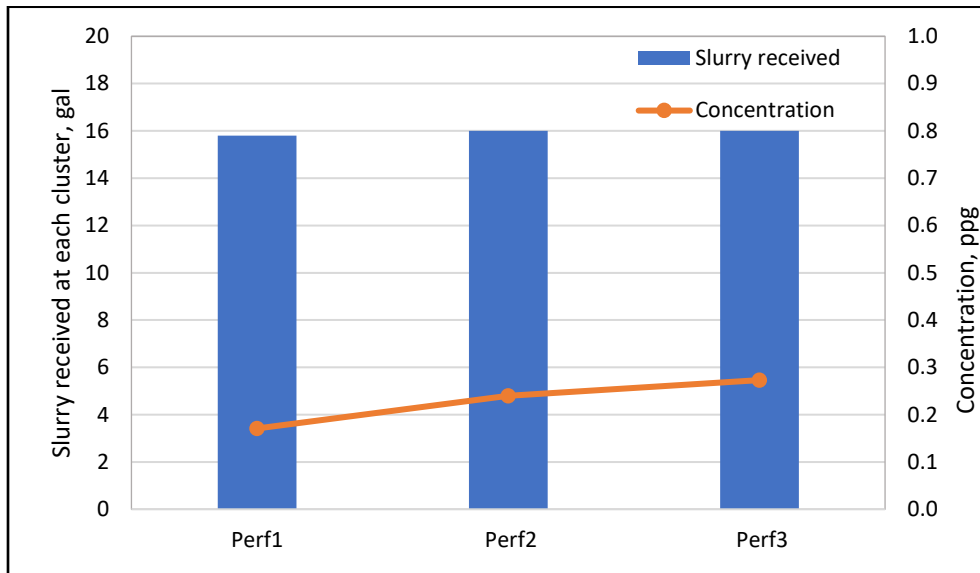


Figure 4.36: Proppant and slurry distribution between the perforation clusters at a slurry velocity of 13.7 ft/s and an injected proppant concentration of 0.21 ppg.

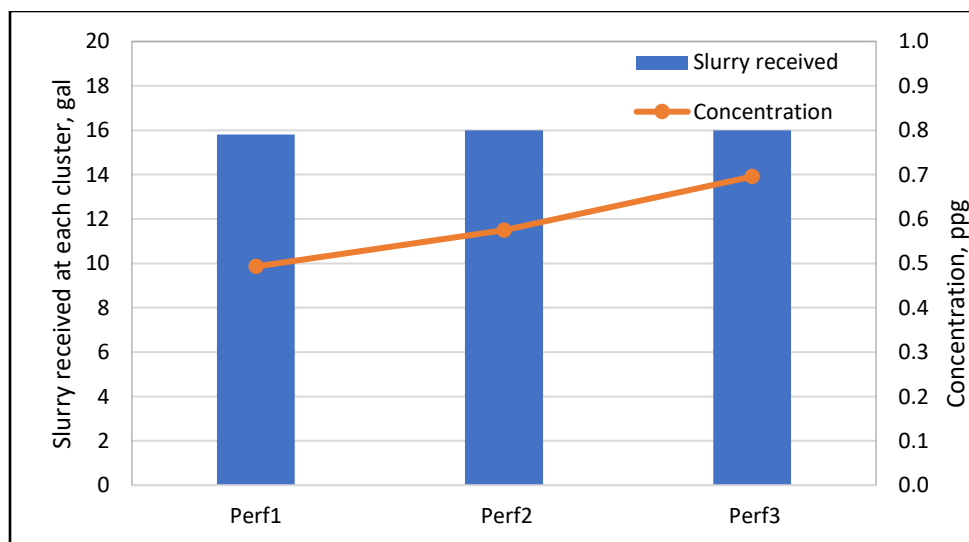


Figure 4.37: Proppant and slurry distribution between the perforation clusters at a slurry velocity of 13.7 ft/s and an injected proppant concentration of 0.55 ppg.

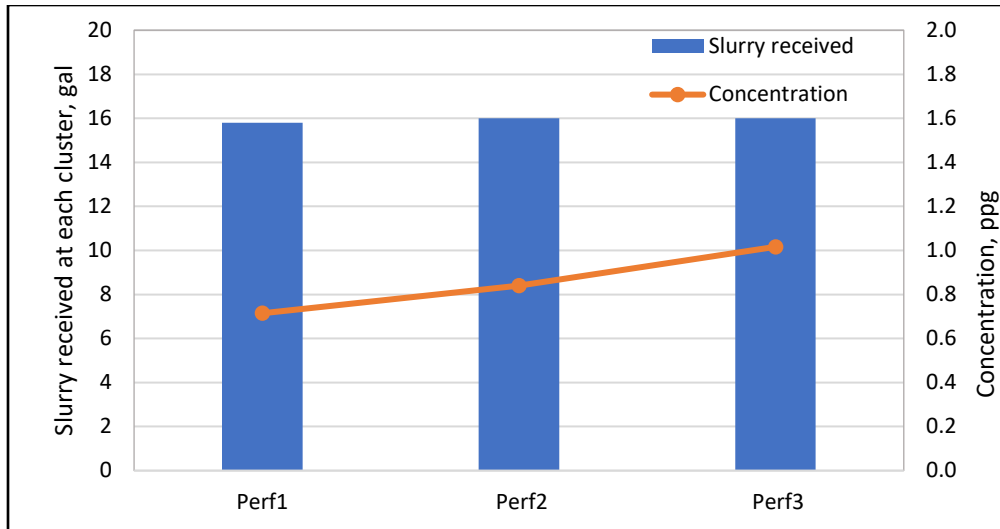


Figure 4.38: Proppant and slurry distribution between the perforation clusters at a slurry velocity of 13.7 ft/s and an injected proppant concentration of 0.85 ppg.

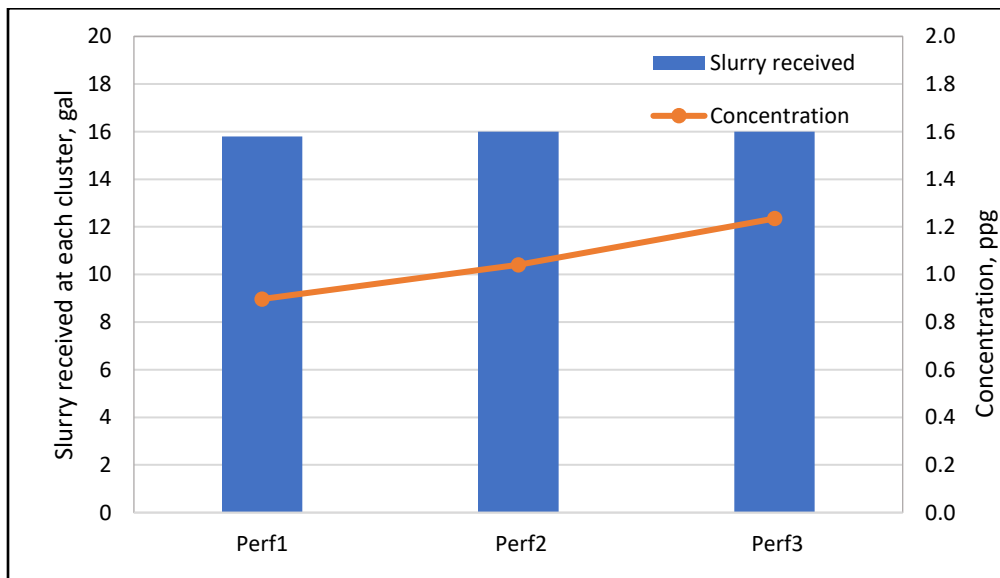


Figure 4.39: Proppant and slurry distribution between the perforation clusters at a slurry velocity of 13.7 ft/s and an injected proppant concentration of 1.10 ppg.

4.1.4 40/70 Ultra-Light Weight Ceramic

Sets of experimental runs were also conducted using 40/70 ultra-light weight (ULW) ceramic. The specific gravity of the 40/70 ULW ceramic is 2.0, which is 24.53% less than the specific gravity of sand at 2.65. In addition, the median diameter of the 40/70 mesh is 40% smaller than the median diameter of 20/40 mesh. The reduction in the particle size can result in a larger

spread of particles in the carrier fluid because smaller particles can be suspended and distributed easily by the turbulent eddies that are created in the fluid.

Three slurry velocities were used to quantify the effect of slurry velocity on proppant distribution between the three perforation clusters as shown in Table 4.4. Sections 4.1.4.1- 4.1.4.3 discuss the effect of slurry velocity and proppant concentration on distribution of 40/70 ULW ceramic in horizontal wellbores and between the perforation clusters.

Table 4.4: Reynolds number for 40/70 ULW ceramic at flow velocities of 6.4, 11.0 and 13.7 ft/s

Velocity, ft/s	Velocity, m/s	Fluid Density, kg/m ³	Fluid Viscosity, kg/m/s	Proppant Density, kg/m ³	Proppant Size, mm	Pipe Diameter, m	Re, unitless
6.4	1.948	1000	0.001	2000	0.350	0.038	74,017
11.0	3.339	1000	0.001	2000	0.350	0.038	126,886
13.7	4.174	1000	0.001	2000	0.350	0.038	158,608

4.1.4.1 Flow Velocity of 6.4 ft/s

Four experiments were carried out at a flow velocity of 6.4 ft/s. The proppant concentration at each cluster was measured at a range of injected proppant concentrations of 0.46, 1.08, 1.64 and 2.2 ppg.

Figures 4.40, 4.41, 4.42 and 4.43 show the proppant and slurry distribution between the perforation clusters at a slurry velocity of 6.4 ft/s and injected proppant concentrations of 0.46, 1.08, 1.64 and 2.2 ppg, respectively. The figures suggest that the reduction in the proppant size and in the specific gravity caused the proppant particles to distribute uniformly in the fluid column, and, as a result, the proppant distribution among the perforation clusters was mostly even. More specifically, at injected concentrations of 0.46 and 1.08 ppg, strong even proppant distribution was achieved between the three perforation clusters. However, at injected concentrations of 1.64 and 2.2 ppg, there was a slight increase in the proppant concentration towards the second cluster followed by the third cluster.

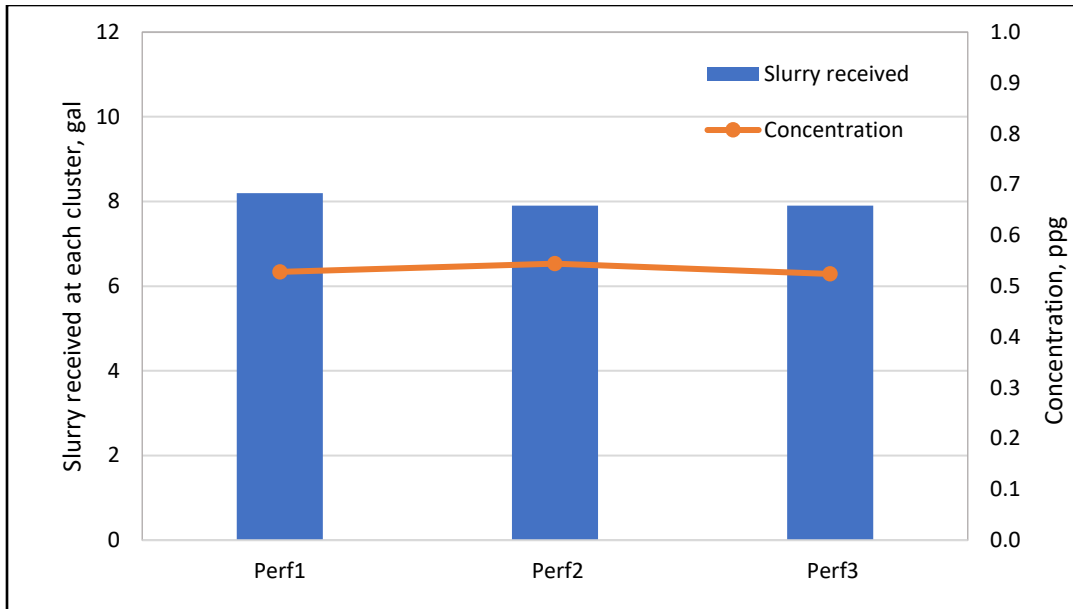


Figure 4.40: Proppant and slurry distribution between the perforation clusters at a slurry velocity of 6.4 ft/s and an injected proppant concentration of 0.46 ppg.

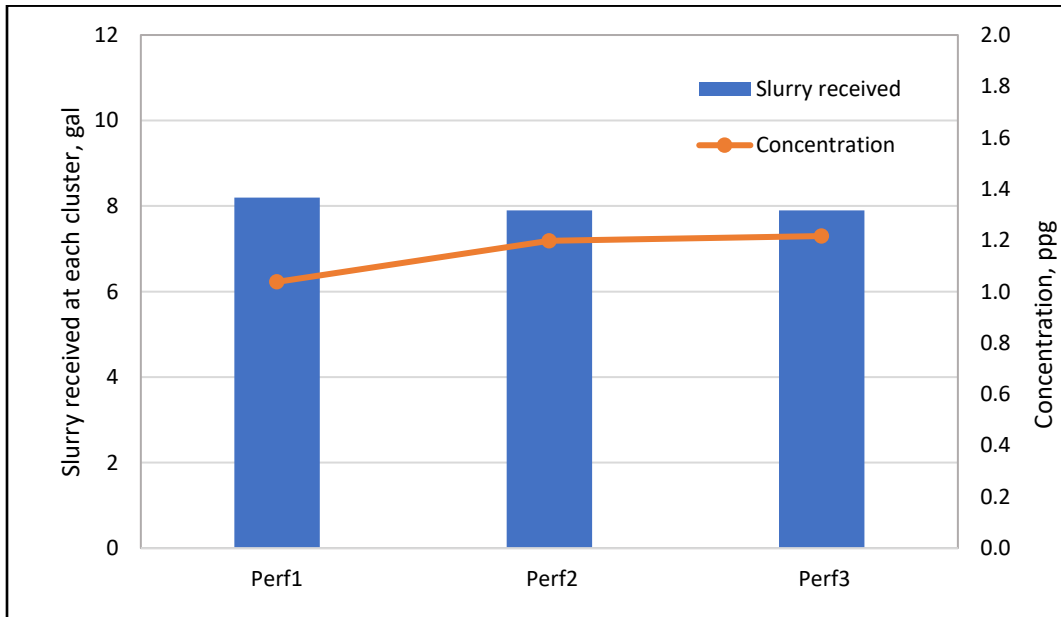


Figure 4.41: Proppant and slurry distribution between the perforation clusters at a slurry velocity of 6.4 ft/s and an injected proppant concentration of 1.08 ppg.

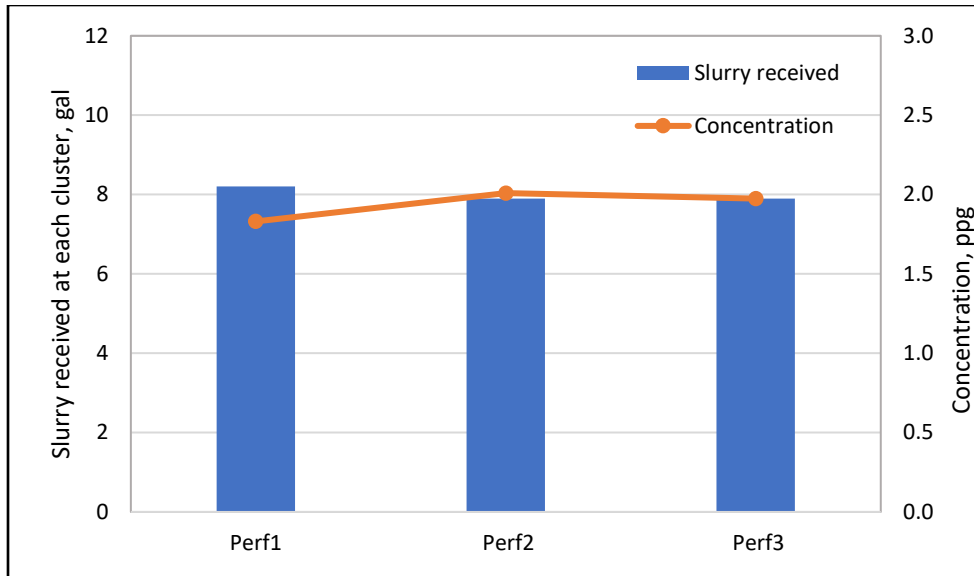


Figure 4.42: Proppant and slurry distribution between the perforation clusters at a slurry velocity of 6.4 ft/s and an injected proppant concentration of 1.64 ppg.

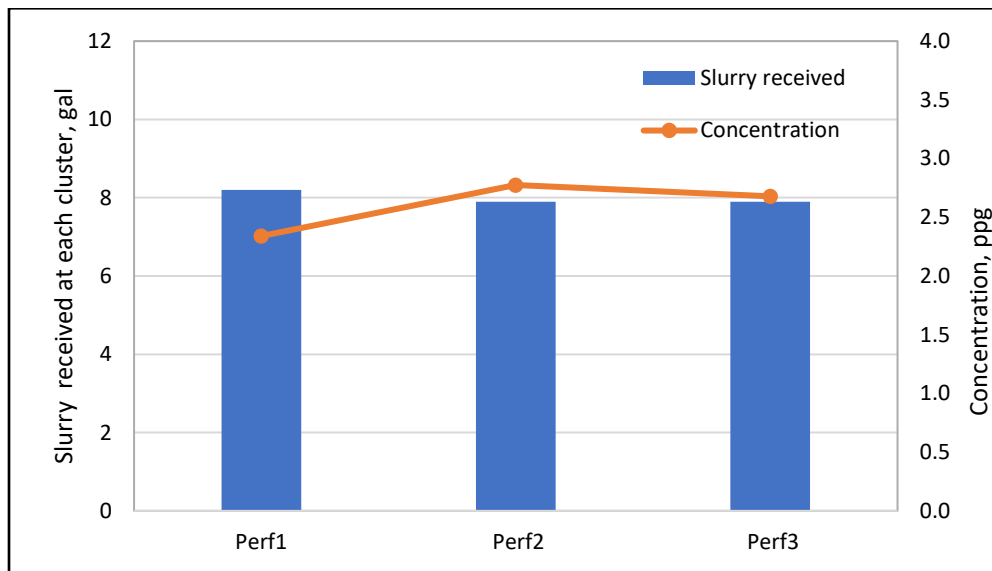


Figure 4.43: Proppant and slurry distribution between the perforation clusters at a slurry velocity of 6.4 ft/s and an injected proppant concentration of 2.2 ppg.

4.1.4.2 Flow Velocity of 11.0 ft/s

A total of four tests were conducted on 40/70 ULW ceramic at a slurry velocity of 11.0 ft/s and injected proppant concentrations of 0.39, 0.94, 1.25 and 2.1 ppg. Figures 4.44, 4.45 and 4.46 show the proppant and slurry distribution between the perforation clusters at injected proppant

concentrations of 0.39, 0.94 and 1.25 ppg, respectively. A fairly uniform distribution can be seen between the three clusters.

The lower density and smaller grain size associated with the 40/70 ULW ceramic led the proppant particles to be more fully suspended in the fluid. This also provides more even proppant distribution not only between the perforation clusters but also in the horizontal wellbore. According to the Biota and Medlin (1985), the particle distribution in the horizontal wellbore was mostly pseudo-homogenous, where the proppant particles were distributed uniformly in the fluid column as illustrated in Figure 4.47.

However, at the highest injected concentration of 2.1 ppg, the proppant concentration was not evenly distributed, with higher concentrations occurring towards the third cluster as shown in Figure 4.48.

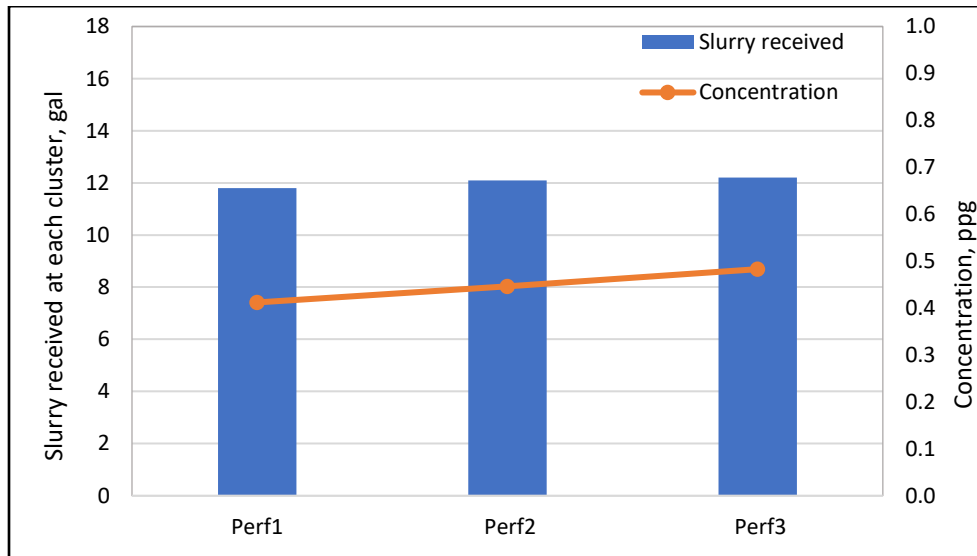


Figure 4.44: Proppant and slurry distribution between the perforation clusters at a slurry velocity of 11.0 ft/s and an injected proppant concentration of 0.39 ppg.

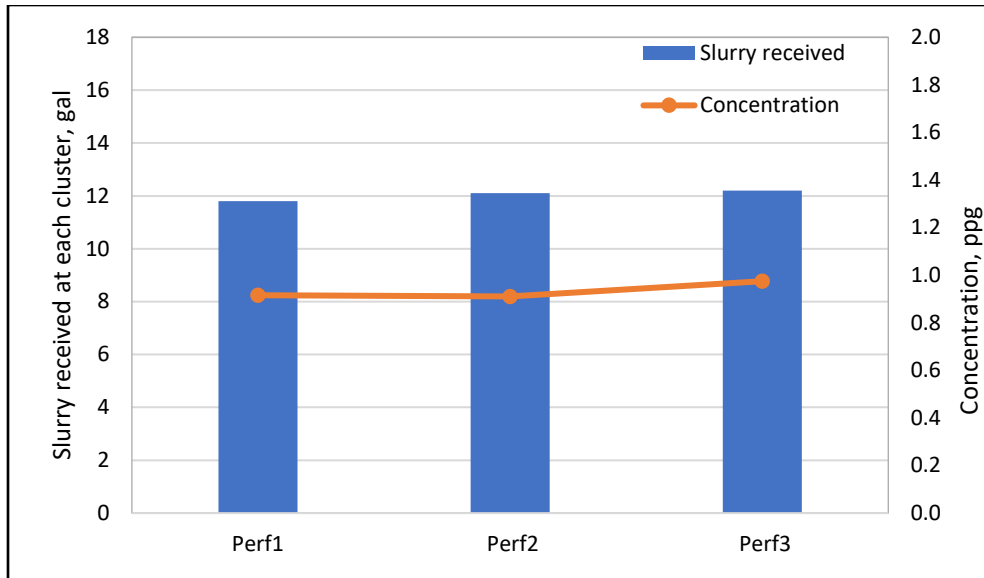


Figure 4.45: Proppant and slurry distribution between the perforation clusters at a slurry velocity of 11.0 ft/s and an injected proppant concentration of 0.94 ppg.

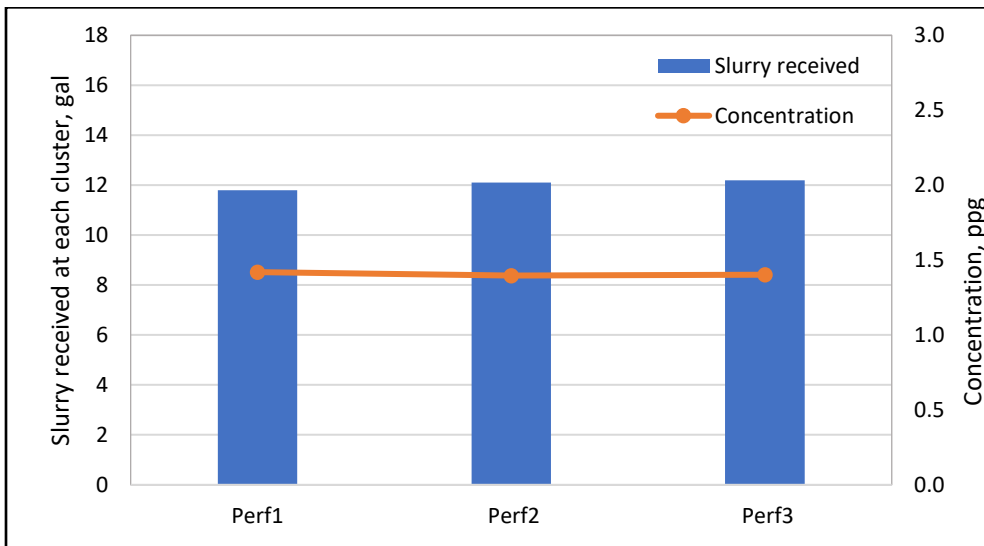


Figure 4.46: Proppant and slurry distribution between the perforation clusters at a slurry velocity of 11.0 ft/s and at an injected proppant concentration of 1.25 ppg.

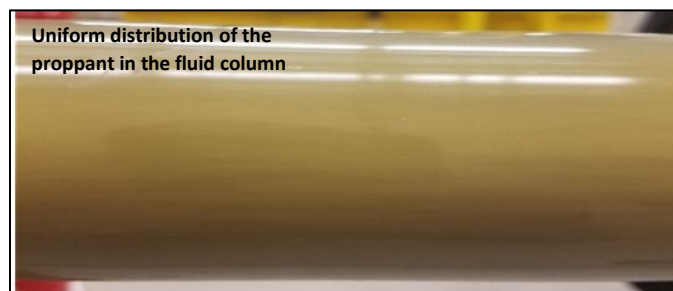


Figure 4.47: Proppant distribution of 40/70 ULW ceramic at a slurry velocity of 11.0 ft/s.

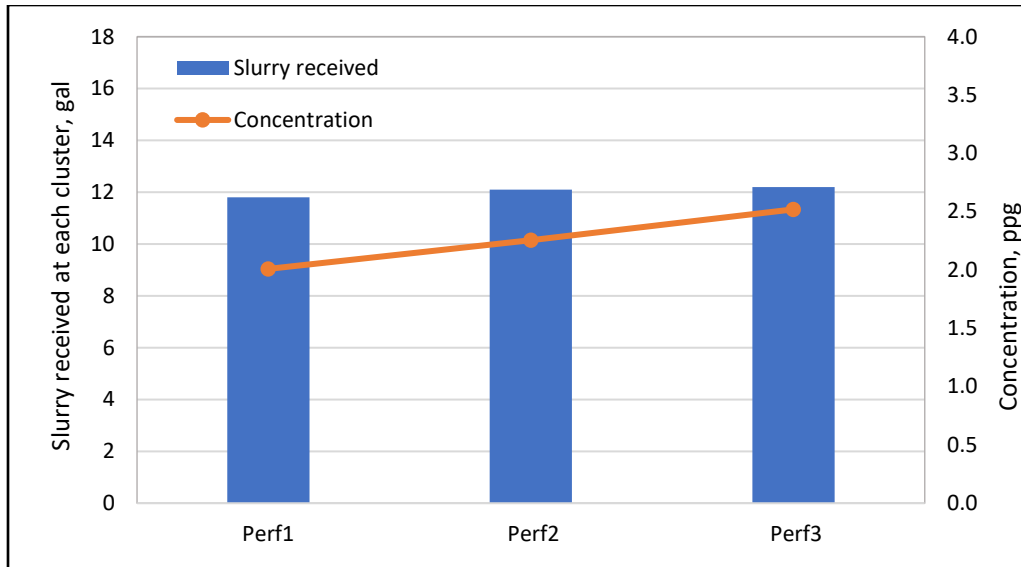


Figure 4.48: Proppant and slurry distribution between the perforation clusters at a slurry velocity of 11.0 ft/s and an injected proppant concentration of 2.1 ppg.

4.1.4.3 Flow Velocity of 13.7 ft/s

In this section, the fluid velocity was increased from 11.0 to 13.7 ft/s. A total of four tests were carried out on 40/70 ULW ceramic at injected proppant concentrations of 0.45, 1.02, 1.2 and 1.79 ppg.

Figures 4.49, 4.50, 4.51 and 4.52 show the proppant and slurry distribution between the perforation clusters at injected proppant concentrations of 0.45, 1.02, 1.2 and 1.79 ppg, respectively. For all tests, a slightly uneven proppant distribution was observed between the three perforation clusters with higher proppant concentration occurring towards the third cluster. Since the ULW ceramic proppants are light compared to sand, proppant particles can be entirely suspended in low viscosity fluids. In this case, proppant does not settle faster even under dynamic conditions. Also, the higher sphericity and roundness of these proppants appear to yield higher transport efficiency in slickwater fluids.

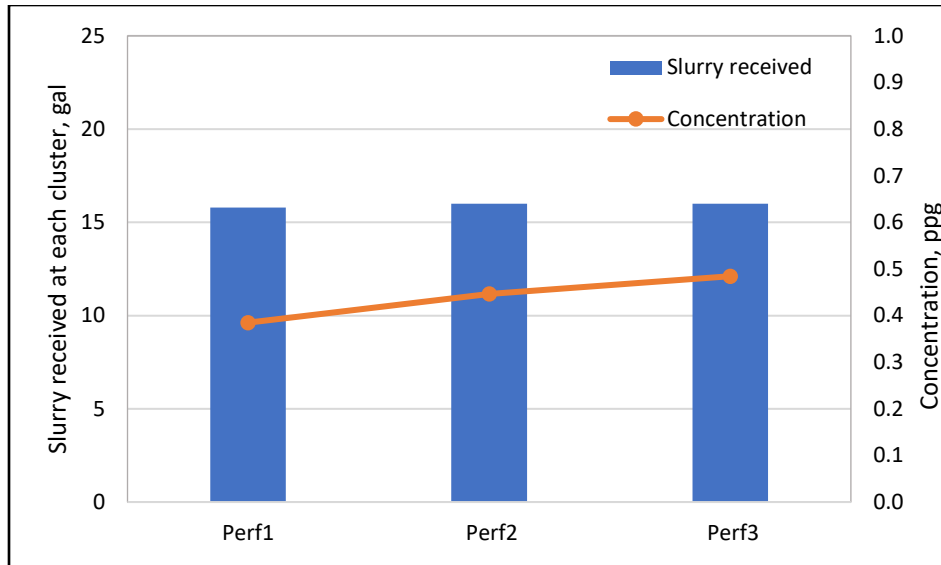


Figure 4.49: Proppant and slurry distribution between the perforation clusters at a slurry velocity of 13.7 ft/s and an injected proppant concentration of 0.45 ppg.

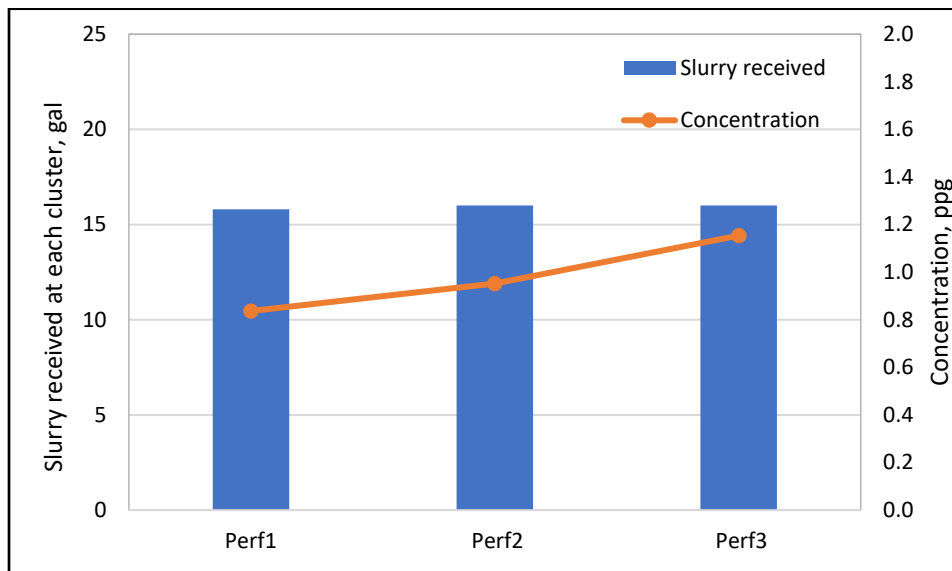


Figure 4.50: Proppant and slurry distribution between the perforation clusters at a slurry velocity of 13.7 ft/s and an injected proppant concentration of 1.02 ppg.

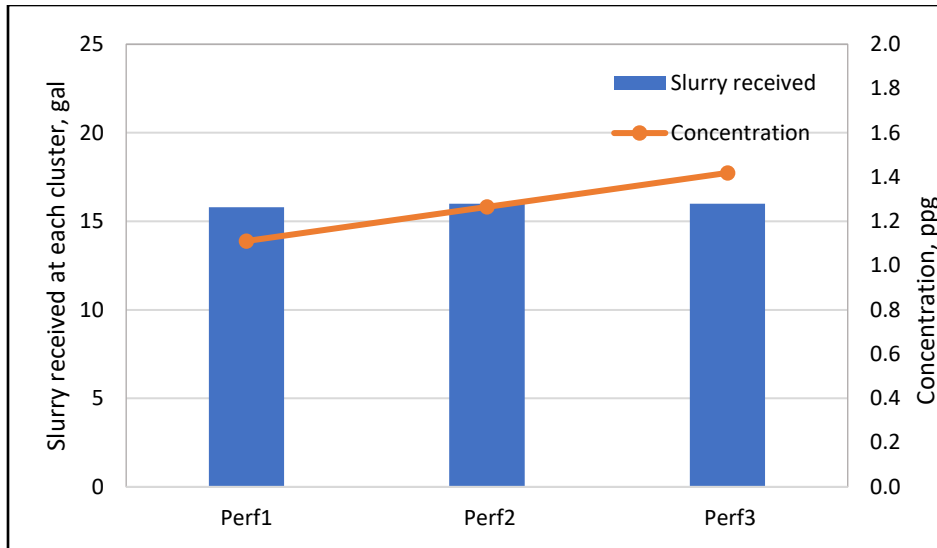


Figure 4.51: Proppant and slurry distribution between the perforation clusters at a slurry velocity of 13.7 ft/s and an injected proppant concentration of 1.2 ppg.



Figure 4.52: Proppant and slurry distribution between the perforation clusters at a slurry velocity of 13.7 ft/s and an injected proppant concentration of 1.79 ppg.

4.2 Proppant Settling in the Horizontal Wellbore

In this section, all the obtained results from proppant settling in the wellbore are presented. For each experimental test, the amount of proppant that was settled within 3 feet around each cluster, after the pumping was stopped, was taken out for quantification. Sections 4.2.1- 4.2.4 discuss and analyze the proppant that settled in the wellbore at flow velocities of 6.4, 11.0 and 13.7 ft/s.

4.2.1 20/40 Mesh White Sand

The amount of proppant that settled in the horizontal wellbore around each cluster was collected for twelve experimental tests after the pumping time for each test was completed. Figure 4.53 shows an image of 20/40 mesh sand that settled in the horizontal wellbore at a flow velocity of 6.4 ft/s and an injected proppant concentration of 0.31 ppg.

For a flow velocity of 6.4 ft/s and different injected proppant concentrations, a large amount of sand settled around the first perforation cluster whereas a small amount of sand settled around the third cluster as shown in Figure 4.54. When the fluid velocity was increased to 11.0 ft/s, a greater amount of proppant settled around the middle cluster and less proppant settled around the third cluster as illustrated in Figure 4.55. In contrast, at a fluid velocity of 13.7 ft/s, the amount of the proppant that settled in the horizontal wellbore around cluster three was higher than clusters one and two as shown in Figure 4.56. For all the tests, an increase in proppant concentration resulted in more proppant settling because the frictional effects, that resulted from interactions between proppant particles and between the proppant particles and the pipe wall, were large.

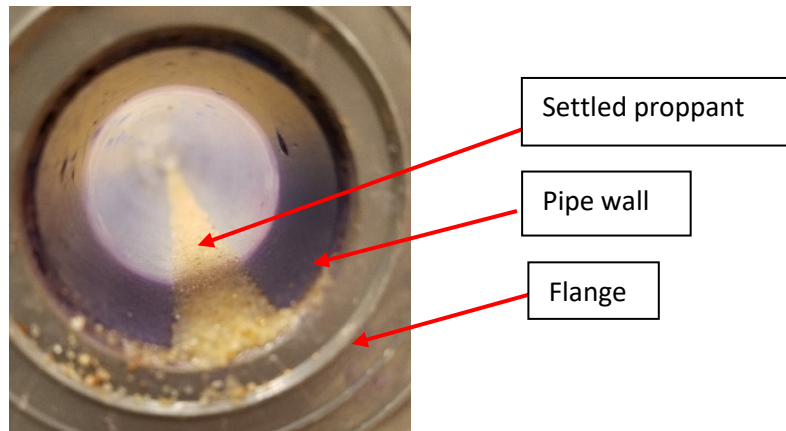


Figure 4.53: Picture of proppant settling in the horizontal wellbore for 20/40 mesh sand at a flow velocity of 6.4 ft/s and at an injected proppant concentration of 0.31 ppg.

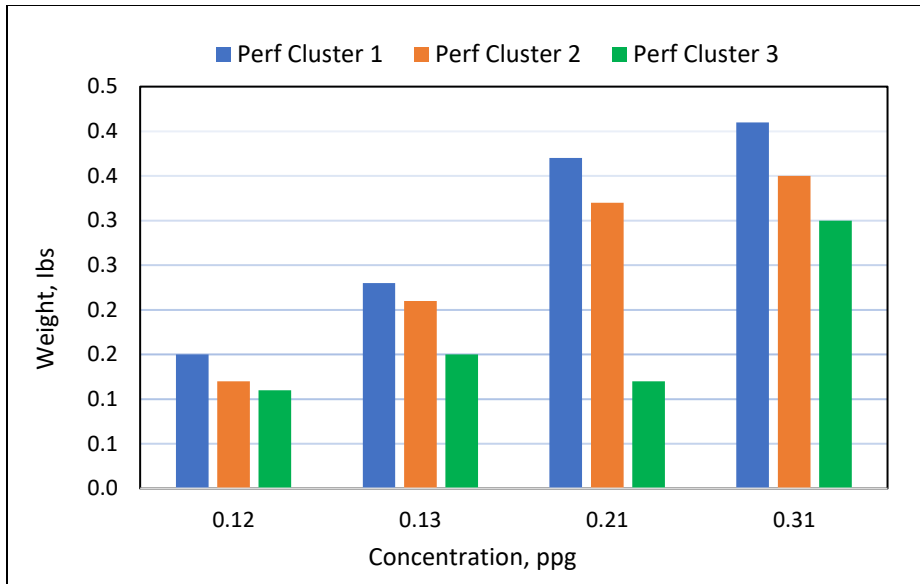


Figure 4.54: Amount of settled proppant in the horizontal wellbore for 20/40 mesh sand at a flow velocity of 6.4 ft/s and at different injected proppant concentrations.

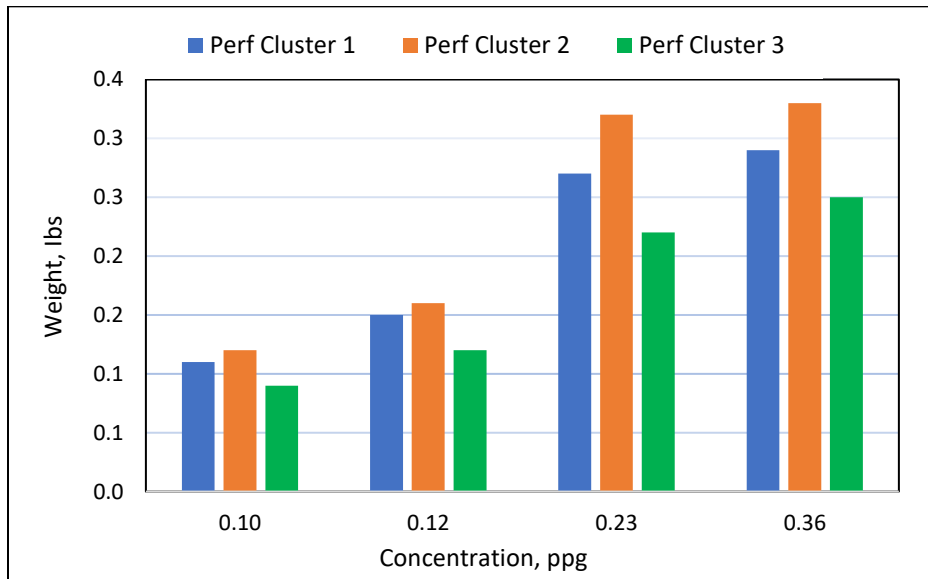


Figure 4.55: Amount of settled proppant in the horizontal wellbore for 20/40 mesh sand at a flow velocity of 11.0 ft/s and at different injected proppant concentrations.

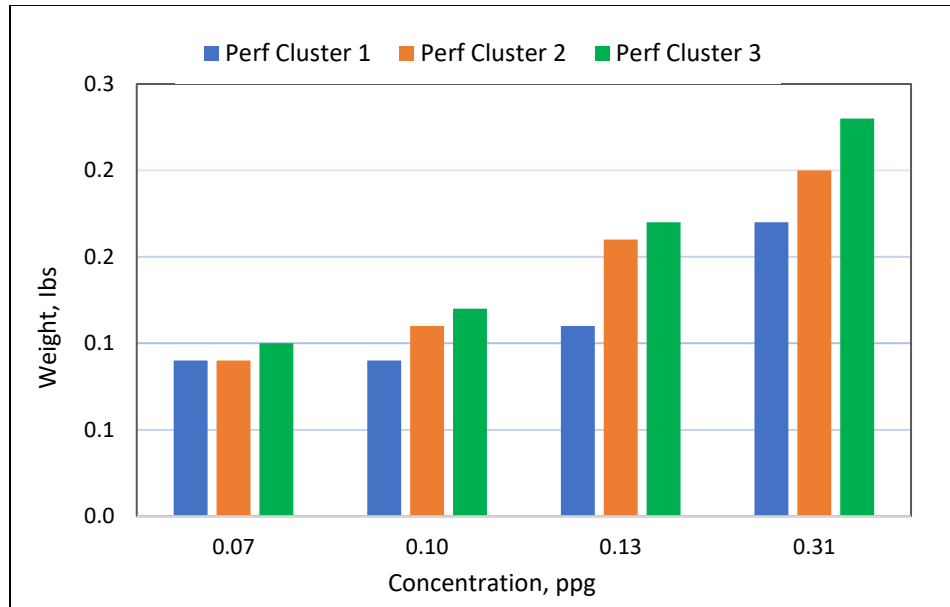


Figure 4.56: Amount of settled proppant in the horizontal wellbore for 20/40 mesh sand at a flow velocity of 13.7 ft/s and at different injected proppant concentrations.

4.2.2 40/70 Mesh White Sand

When observing the amount of proppant that settled in the wellbore for 40/70 mesh white sand, a similar trend was noticeable at a flow velocity of 6.4 ft/s, where the amount of proppant that settled at the first cluster was higher than proppant amounts that settled around the second and the third clusters as shown in Figure 4.57. For velocities of 11.0 and 13.7 ft/s, the proppant that settled in the horizontal wellbore showed a higher amount around the third perforation cluster and a lower amount around the first cluster, as can be shown in Figures 4.58 and 4.59, respectively.

The difference in the amount of proppant that settled between the perforation clusters in the horizontal wellbore was due to the change in the slurry velocity. One of the reasons attributed to the higher proppant concentration around the first cluster at low flow velocities is that the proppant particles were not suspended uniformly in the fluid column where a higher concentration occurred in the lower section. When the slurry reached the first cluster, proppant exited the first perforations within the cluster, and as the slurry passed the first cluster, the proppant concentration became lower; hence, the proppant that settled at the second cluster was not as high as the second cluster, and the same is true for the third cluster.

However, at a flow velocity of 13.7 ft/s, the proppant settled in the wellbore at the third cluster was higher than proppant settled at the first and the second clusters. One of the main reasons attributed to more proppant settling at the third cluster is that when the slurry reached the third

cluster, the slurry velocity dropped. As a result, proppant particles tended to settle down on the bottom of the pipe (due to their weight). In addition, the valve, which was placed at the end of the horizontal pipe, was not fully open; therefore, proppant particles were not able to get out of the wellbore and were forced to settle around the third perforation cluster.

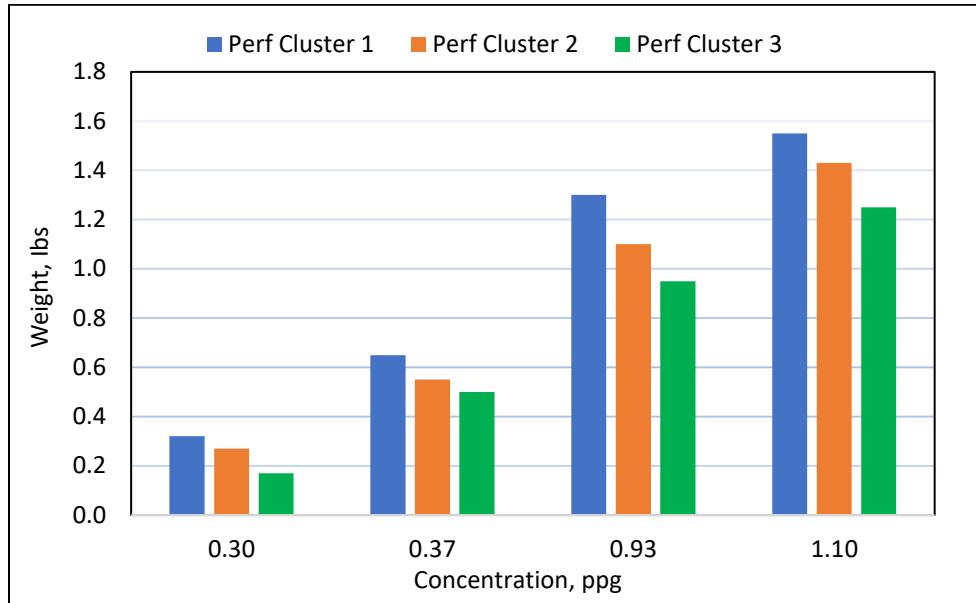


Figure 4.57: Amount of settled proppant in the horizontal wellbore for 40/70 mesh sand at a flow velocity of 6.4 ft/s and at different injected proppant concentrations.

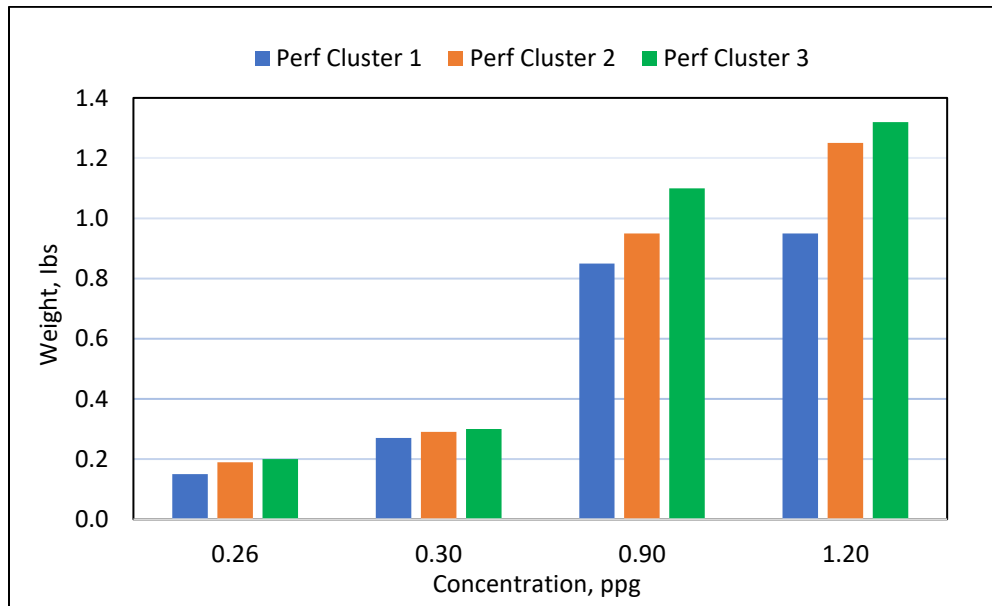


Figure 4.58: Amount of settled proppant in the horizontal wellbore for 40/70 mesh sand at a flow velocity of 11.0 ft/s and at different injected proppant concentrations.

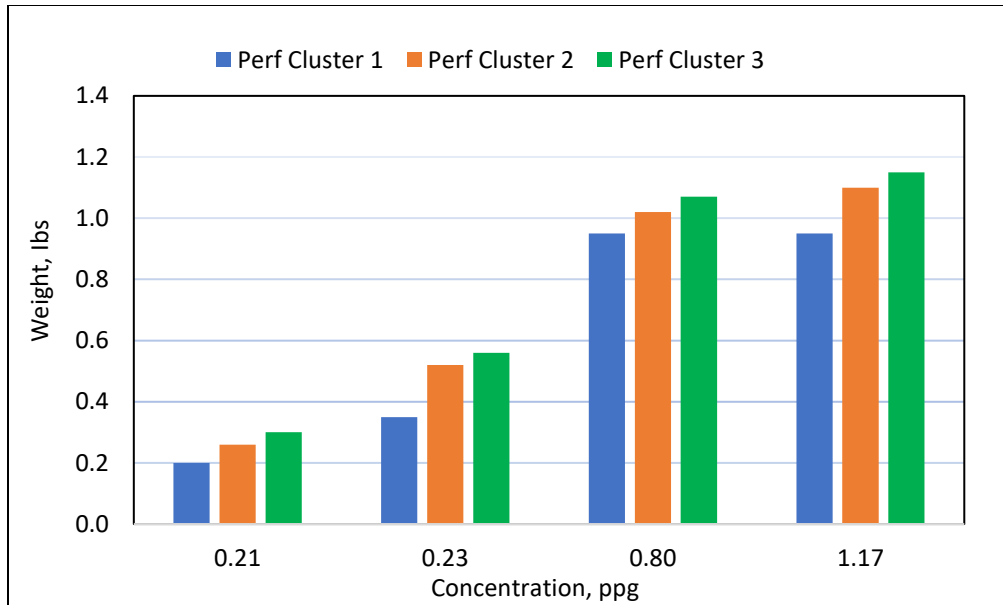


Figure 4.59: Amount of settled proppant in the horizontal wellbore for 40/70 mesh sand at a flow velocity of 13.7 ft/s and at different injected proppant concentrations.

4.2.3 20/40 ULW Ceramic

As mentioned in Section 4.1.3, the 20/40 ULW ceramic has a specific gravity of 2.0, which is 24.53% less than the specific gravity of sand. Thus, the momentum difference between the fluid and the proppant is relatively small. The small difference in the specific gravity between the proppant and the carrier fluid leads to more proppant suspension in the fluid column, and as a result, proppant particles tend to be distributed more uniformly in the horizontal wellbore.

For a flow velocity of 6.4 ft/s and injected proppant concentrations of 0.3, 0.7 and 1.14 ppg, a large amount of proppant settled around the first perforation cluster, whereas a lower amount of proppant settled around the second and the third perforation clusters as shown in Figure 4.60. However, a different trend was observed at an injected proppant concentration of 1.8 ppg, where more proppant settled around the second cluster (Figure 4.60).

In contrast, at fluid velocities of 11.0 and 13.7 ft/s, the amount of proppant that settled in the horizontal wellbore around the third perforation cluster was slightly higher than the proppant that settled at the second and the third clusters, as can be seen in Figures 4.61 and 4.62, respectively. As stated previously, when there was an increase in the injected proppant concentration, there was also more proppant settling in the horizontal wellbore.

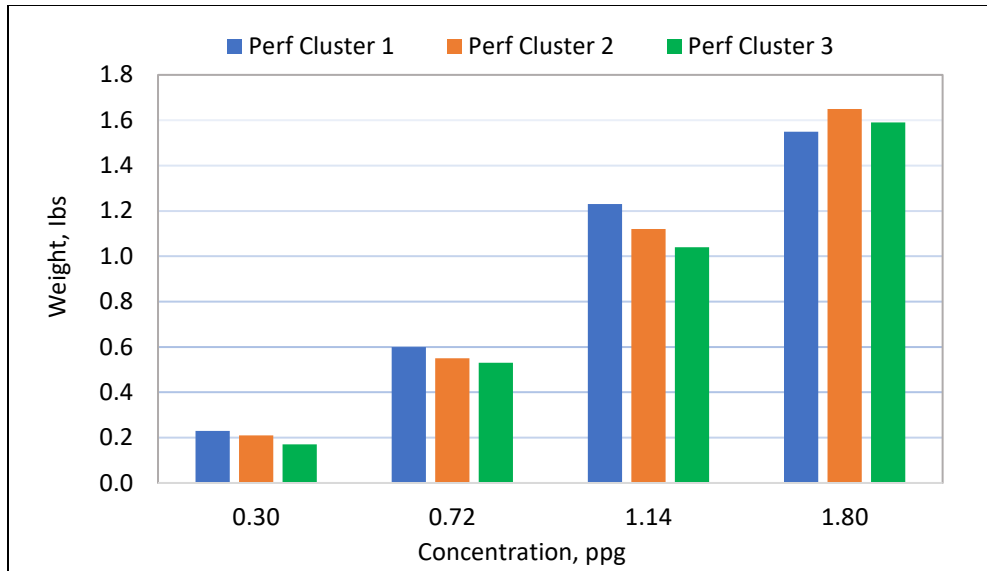


Figure 4.60: Amount of settled proppant in the horizontal wellbore for 20/40 ULW ceramic at a flow velocity of 6.4 ft/s and at different injected proppant concentrations.

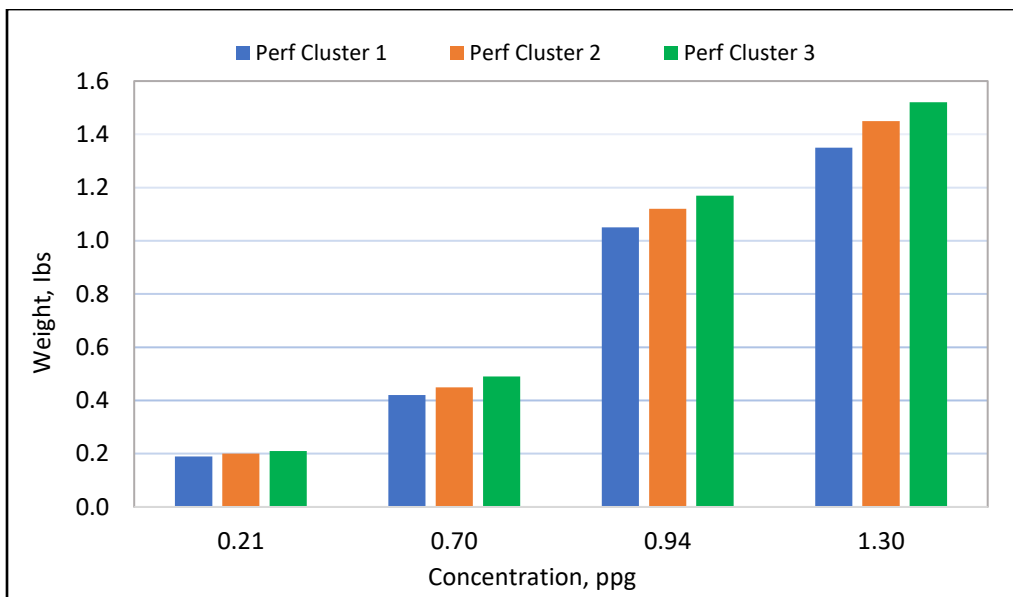


Figure 4.61: Amount of settled proppant in the horizontal wellbore for 20/40 ULW ceramic at a flow velocity of 11.0 ft/s and at different injected proppant concentrations.

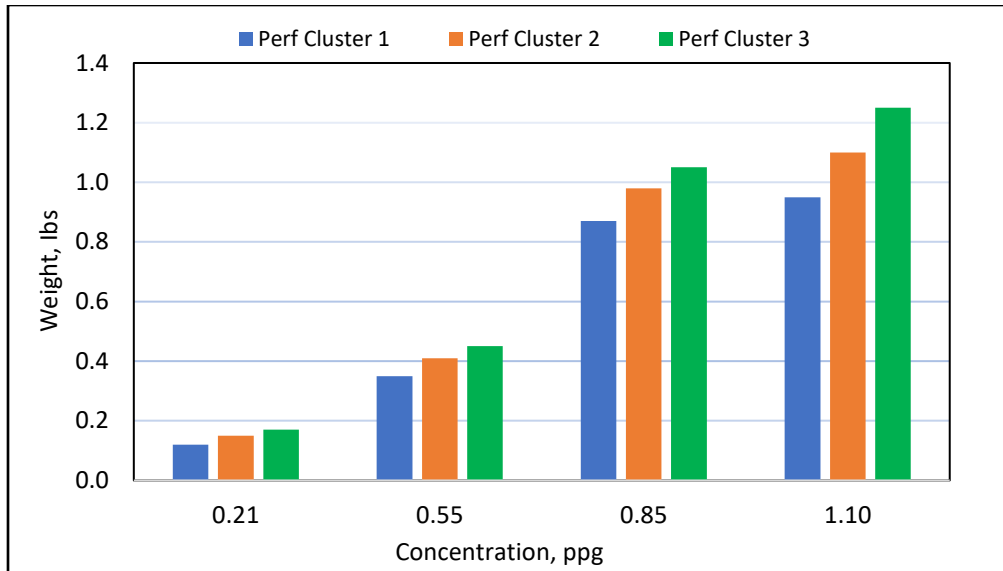


Figure 4.62: Amount of settled proppant in the horizontal wellbore for 20/40 ULW ceramic at a flow velocity of 11.0 ft/s and at different injected proppant concentrations.

4.2.4 40/70 ULW Ceramic

With lower density and smaller particle size, the 40/70 ULW ceramic tends to be more fully suspended in the fluid and provides more even proppant distribution, not only in the horizontal pipe, but also between the perforation clusters as concluded from the experimental results in Section 4.1.4.

The amount of proppant that settled in the horizontal wellbore was also collected for each test conducted on 40/70 ULW ceramic. Figure 4.63 shows an image of 40/70 ULW ceramic that settled in the horizontal wellbore and was not able to flow out of the perforations at a flow velocity of 6.4 ft/s and an injected proppant concentration of 2.2 ppg. At a flow velocity of 6.4 ft/s, proppant settling in the wellbore was observed to be evenly distributed through the entire horizontal section of the pipe, and as result, proppant settled evenly at the perforation clusters at different injected proppant concentrations as can be seen in Figure 4.64.

When the fluid velocity was increased to 11.0 ft/s, mostly even distribution occurred through the three perforation clusters at injected proppant concentrations of 0.39, 0.94 and 1.25 ppg as shown in Figure 4.65. However, at an injected proppant concentration of 2.1 ppg, the amount of proppant that settled at the third perforation cluster was slightly higher than the proppant that settled at the first and the second clusters (Figure 4.65). At a fluid velocity of 13.7 ft/s, the amount of proppant that settled in the horizontal wellbore at the third perforation cluster was a

slightly higher than the proppant that settled at the second and the third clusters as can be illustrated in Figure 4.66.

For all the tests that were conducted on 40/70 ULW ceramic, as the proppant concentration increased, more settling in the horizontal wellbore occurred. The first reason for this can be due to the interaction between the particles by which larger grains of the proppant will tend to settle on the bottom of the pipe. The second reason for this could be from the interaction between the particles and the pipe wall. This interaction can occur from the high turbulent velocity, which can force the particles to move away from the centerline of the pipe. This results in more friction loss and leads the particles to settle in the low velocity region near the pipe wall.

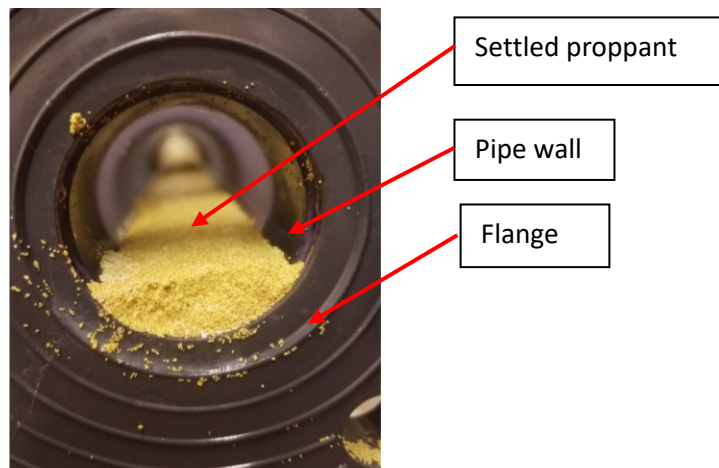


Figure 4.63: Picture of proppant settling in the horizontal wellbore for 40/70 ULW ceramic at a flow velocity of 6.4 ft/s and at an injected proppant concentration of 2.2 ppg.

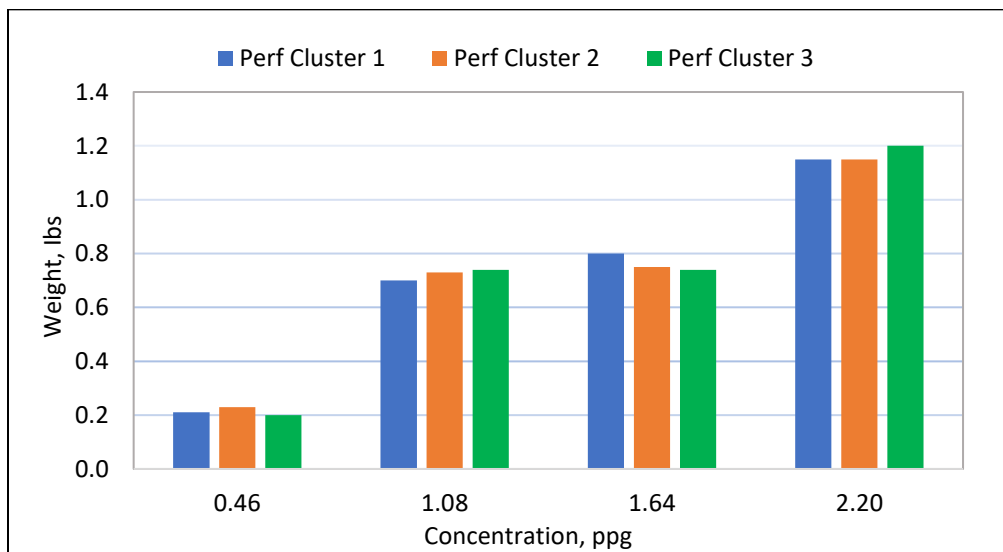


Figure 4.64: Amount of settled proppant in the horizontal wellbore for 40/70 ULW ceramic at a flow velocity of 6.4 ft/s and at different injected proppant concentrations.

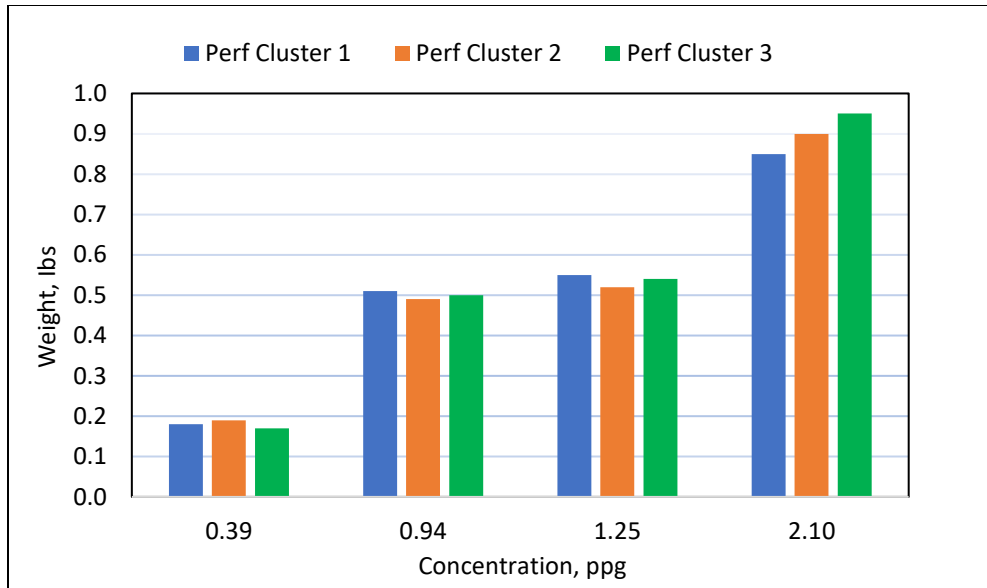


Figure 4.65: Amount of settled proppant in the horizontal wellbore for 40/70 ULW ceramic at a flow velocity of 11.0 ft/s and at different injected proppant concentrations.

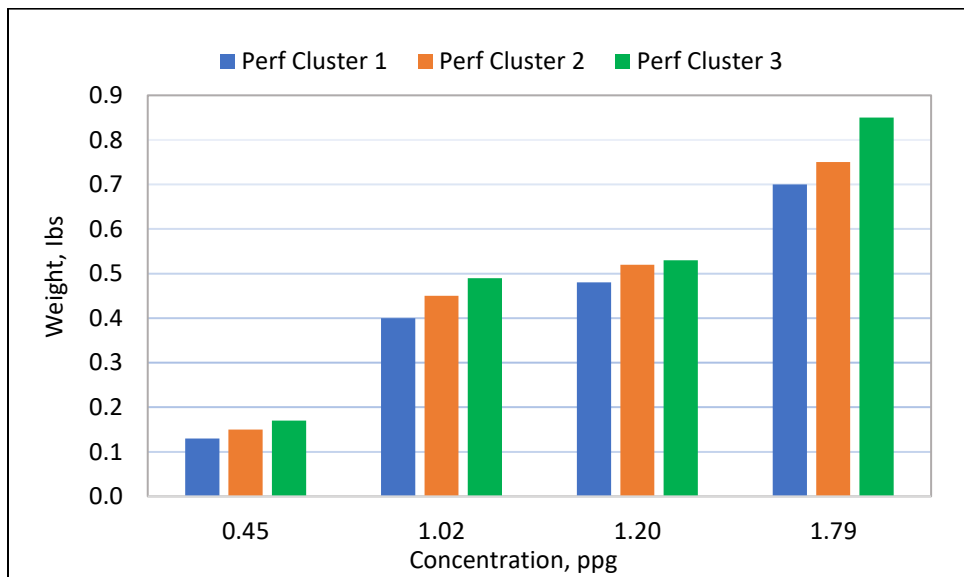


Figure 4.66: Amount of settled proppant in the horizontal wellbore for 40/70 ULW ceramic at a flow velocity of 13.7 ft/s and at different injected proppant concentrations.

CHAPTER 5

EXPERIMENTAL RESULTS USING FRICTION REDUCER IN WATER

This chapter presents the results of the laboratory tests that were conducted on proppant transport in horizontal wellbores using high loading friction reducer (HLFR) also known as high viscosity friction reducer (HVFR). The main reason for using a friction reducer is to increase the viscosity of the base fluid. These fluids are characterized by having high molecular weights. They are added to water at low concentrations to reduce the frictional energy that occurs in turbulent flow. A total of 24 tests were carried out to investigate the effect of the fluid viscosity and slurry velocity on distribution of proppant between the perforation clusters. There are two main sections in this chapter: the first section (Section 5.1) consists of the rheological properties of fracturing fluid, while the second section (Section 5.2) presents and discusses the experimental results that were obtained from the tests conducted on 20/40 and 40/70 mesh white sand.

5.1 Fluid Rheological Properties

Rheological properties on the HLFR fluids were performed to determine whether the fracturing fluid was a Newtonian or non-Newtonian fluid. Also, the viscosity and elasticity of the HLFR fluids were determined under a variety of HLFR concentrations and across a wide range of shear conditions. Samples of base HLFR were taken and their rheological measurements determined using a Model 3600 Fann viscometer as shown in Figure 5.1. Four concentrations of HLFR, 1, 2, 3, and 5 gpt, were selected to perform the rheological measurements. A number of experimental tests were conducted on the HLFR fluid using a M3600 Fann viscometer to determine the viscosity and shear stress for each concentration. Starting with 600 RPM and then successively reducing the RPM to 10, the properties at each RPM were measured and all the results for all the concentrations of HLFR are presented in Table 5.1.



Figure 5.1: Picture of a M3600 Fann Viscometer used to measure the rheological properties of fracturing fluid.

Table 5.1: The rheological properties of fracturing fluid at concentrations of 1, 2, 3, and 5 gpt of HLF

1 gpt of HLF								
RPM	600	300	200	100	60	30	20	10
Apparent Viscosity, cp	2.3	2.5	2.9	3.5	3.9	5.8	8.8	11.7
Shear Stress, dyne/cm ²	24	13	10	5	4	3	2.5	2
Apparent Viscosity, Ps.s	0.0023	0.0025	0.0029	0.0035	0.0039	0.0058	0.0088	0.0117
Shear Rate, s ⁻¹	1043	520	345	143	103	52	28	17
2 gpt of HLF								
RPM	600	300	200	100	60	30	20	10
Apparent Viscosity, cp	3.6	4.2	4.4	5.8	6.8	9.8	14.7	23.5
Shear Stress, dyne/cm ²	37	21	15	10	7	5	4.5	4
Apparent Viscosity, Ps.s	0.0036	0.0045	0.0044	0.0058	0.0068	0.0098	0.0147	0.0235
Shear Rate, s ⁻¹	1028	467	341	172	103	51	31	17
3 gpt of HLF								
RPM	600	300	200	100	60	30	20	10
Apparent Viscosity, cp	6.1	7.5	8.8	11.7	14.7	21.5	29.4	41.1
Shear Stress, dyne/cm ²	64	38	30	20	15	11	10	7
Apparent Viscosity, Ps.s	0.0061	0.0074	0.0088	0.0117	0.0147	0.0215	0.0294	0.0411
Shear Rate, s ⁻¹	1049	514	341	171	102	51	34	17
5 gpt of HLF								
RPM	600	300	200	100	60	30	20	10
Apparent Viscosity, cp	13.5	17	19.1	24.1	31.3	45	61.7	94.1
Shear Stress, dyne/cm ²	142	87	66	41	32	23	21	16
Apparent Viscosity, Ps.s	0.0135	0.017	0.0191	0.0241	0.0313	0.045	0.0617	0.0941
Shear Rate, s ⁻¹	1052	512	346	170	102	51	34	17

Typically, the shape of the flow curve, shear rate versus shear stress, can be used to characterize the rheological behavior of any fluid, Newtonian or non-Newtonian fluid. Thus, shear

stress was plotted against shear rate at concentrations of 1, 2, 3, and 5 gpt of HLFR, as shown in Figure 5.2.

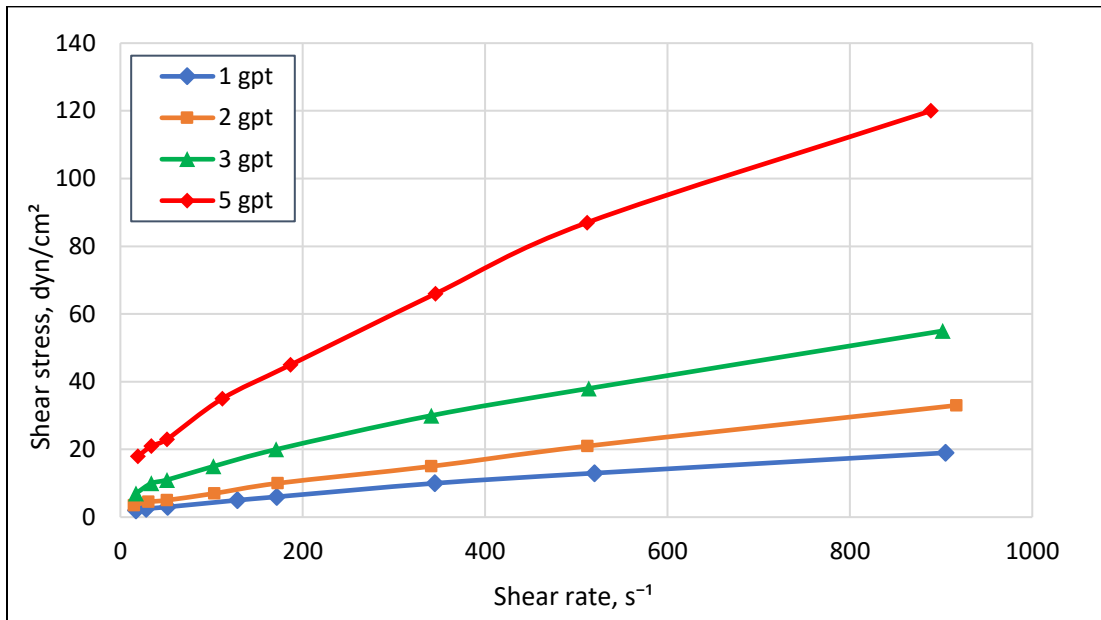


Figure 5.2: Shear stress versus shear rate for different concentrations of HLFR.

As can be observed from Figure 5.2, the relationship between the shear stress and the shear rate for all the HLFR concentrations is not linear. In other words, the shape of the flow curves between the shear stress and the shear rate is concave downwards. This indicates that the increase in the shear rate causes a decrease in the fluid viscosity. These fluids therefore can be described as Non-Newtonian /shear thinning fluids where the viscosity of the fluid decreases as shear rate increases.

One of the most important properties of Non-Newtonian fluids is that they have large viscosities which do not stay constant. As mentioned in Section 2.4, there are several mathematical models that can be used to describe the behavior of these fluids. Among them is the Power Law model, which has been used extensively to describe the behavior of fracturing fluids in hydraulic fracturing. The viscosity for Power Law fluids decreases when there is an increase in the shear rate. The Power Law model has two parameters, the flow behavior index, n , and the flow consistency index, K . In order to determine the n and K values for the Power Law equation (Equation 2.8), shear stress was plotted against shear rate for all the concentrations of HLFR on a logarithmic scale as shown in Figure 5.3.

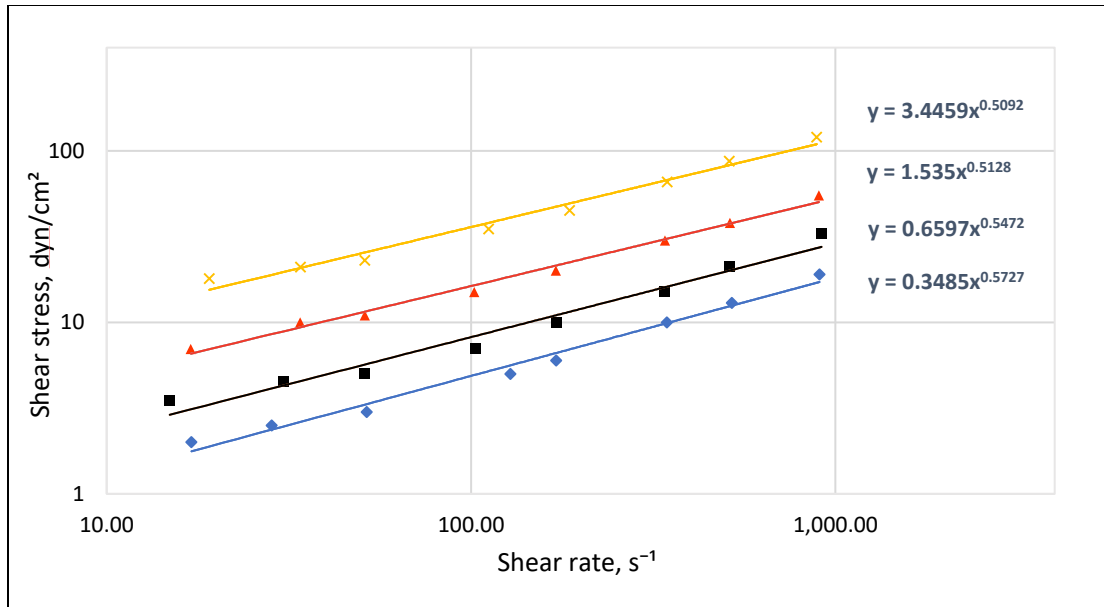


Figure 5.3: Shear stress versus shear rate at different concentrations of HLFBR on logarithmic coordinates showing Power Law behavior.

By fitting the power law trendlines in Figure 5.3 for each fluid concentration, the flow behavior index (n) and the consistency index (K) were determined. The resulting n and K values and the associated viscosity for each concentration of HLFBR are presented in Table 5.2.

Table 5.2: The flow behavior index (n) and the consistency index (K) and the associated viscosity at different loading of HLFBR

HLFR Concentration, gpt	n	K , dyn/cm ² . S ^{n}	Viscosity at RPM of 300, cp
1.0	0.57	0.348	2.5
2.0	0.54	0.660	4.2
3.0	0.51	1.535	7.5
5.0	0.50	3.446	17.0

The results in Table 5.2 show that the flow behavior index (n) is less than 1.0 for all the concentrations. This depicts the fluid behaving as shear thinning where the viscosity decreases with an increase of the shear rate. Also, it can be noted that as the flow behavior index (n) increases and reaches 1.0, the fluid becomes less viscous, and it behaves similarly to Newtonian fluids where the viscosity remains constant as shear rate increases or decreases. However, the resulting consistency index (K) in Table 5.2, demonstrates that when K increases, fluid viscosity increases and vice versa.

Once the flow behavior index (n) and the consistency index (K) were determined for each concentration of HLF_R, the Metzner and Reed (1955) equation (Equation 2.7) was used to calculate the Reynolds number in the horizontal pipe for three flow velocities of 4.5, 8.2 and 11.0 ft/s. Table 5.3 illustrates the flow regimes covered by the work discussed in this chapter. As can be seen in Table 5.3, three flow regimes, laminar, transition, and turbulent, were encountered at the three flow velocities used in the experimental tests. However, laminar flow conditions occurred more frequently not only at low flow velocities but also at relatively high flow velocities.

Table 5.3: Flow regimes for HLF_R concentrations at flow velocities of 4.5, 8.2 and 11.0 ft/s

HLF _R Concentration, gpt	Flow Velocity, ft/s	Re, unitless	Flow Regime Type
1.0	4.5	1751	Laminar
	8.2	4058	Turbulent
	11.0	6063	Turbulent
2.0	4.5	1088	Laminar
	8.2	2533	Transition
	11.0	3868	Transition
3.0	4.5	551	Laminar
	8.2	1300	Laminar
	11.0	2055	Transition
5.0	4.5	245	Laminar
	8.2	625	Laminar
	11.0	975	Laminar

5.2 Experimental Tests on Proppant Transport

Two proppants (20/40 and 40/70 mesh white sand) were used to conduct experimental tests on proppant transport in horizontal wellbores using HLF_R fluids. As mentioned previously, the main reason for using HLF_R was to investigate the effect of fluid viscosity on 20/40 and 40/70 mesh sand where previously using fresh water did not result in efficient transportation in horizontal wellbores. For each test, the amount of proppant and fluid that exited each of the perforation clusters was collected for quantification. In addition, the proppant behavior in the horizontal wellbore was observed and analyzed at different flow velocities. The phenomena of even and uneven proppant distribution between the perforation clusters are presented and analyzed.

5.2.1 20/40 Mesh White Sand

A total of 12 tests were conducted on 20/40 mesh white sand at three flow velocities and four different concentration (1, 2, 3 and 5 gpt) of HLFRR. Sections 5.2.1.1 through 5.2.1.4 present and analyze the obtained results from proppant transport in horizontal wellbores using different loading of HLFRR.

5.2.1.1 Concentration of 1 gpt of HLFRR

Three experiments were conducted on 20/40 mesh sand at 1.0 gpt of HLFRR and flow velocities of 4.5, 8.2 and 11.0 ft/s. The fluid viscosity for the fracturing fluid was measured at 2.5 cp. Figure 5.4 shows the proppant concentration and the fluid distribution at each of the three perforation clusters at a flow velocity of 4.5 ft/s and an injected proppant concentration of 1.0 ppg. As can be seen in Figure 5.4, the proppant distribution is highly uneven between the three clusters. A proppant concentration of 1.78 ppg was received at the first cluster, whereas the proppant concentrations that were received at the second and the third clusters were 0.91 and 0.32 ppg, respectively. The slurry was distributed fairly evenly between the three perforation clusters as shown in same graph. At this flow velocity, the gravity forces were more significant than the momentum and the viscous forces; therefore, particles of the proppant were concentrated in the lower section of the horizontal pipe. In this case, the suspension mechanism can be described as heterogeneous suspension where a higher proppant concentration occurred in the bottom of the pipe. This can be illustrated that when the slurry reached the first cluster, the perforation which has a downward orientation within the first cluster received more proppant. As the slurry traveled in the horizontal wellbore and reached the middle cluster, the fluid was less concentrated; and hence, the second cluster received less proppant than the first cluster. The same is true for the third cluster.

When the flow velocity was increased to 8.2 ft/s, a similar trend was observed. The first cluster received more proppant than the second and the third perforation clusters, even though the fluid distribution at the third cluster was slightly higher than fluid received at the first and second clusters as shown in Figure 5.5. However, at the flow velocity of 11.0 ft/s and an injected proppant concentration of 1.0 ppg, the proppant distribution was also uneven. A higher proppant concentration occurred at the second cluster at 1.26 ppg followed by the first cluster at 0.97 ppg and the third cluster at 0.69 ppg as shown in Figure 5.6. This can be explained as the flow rate

near the first cluster being fairly high and preventing the proppant particles from turning completely into the perforations within the first cluster. When fluid passed the first cluster and as soon as it reached the second cluster, the fluid velocity dropped, and the gravity forces became dominant over the momentum forces. Thus, the proppant particles were able to turn easily into the perforations within the second cluster. As a result, the second cluster received more proppant concentration. After the second cluster, the fluid traveled in the horizontal wellbore with less proppant concentration; and hence, lower proppant concentration occurred at the third perforation cluster.

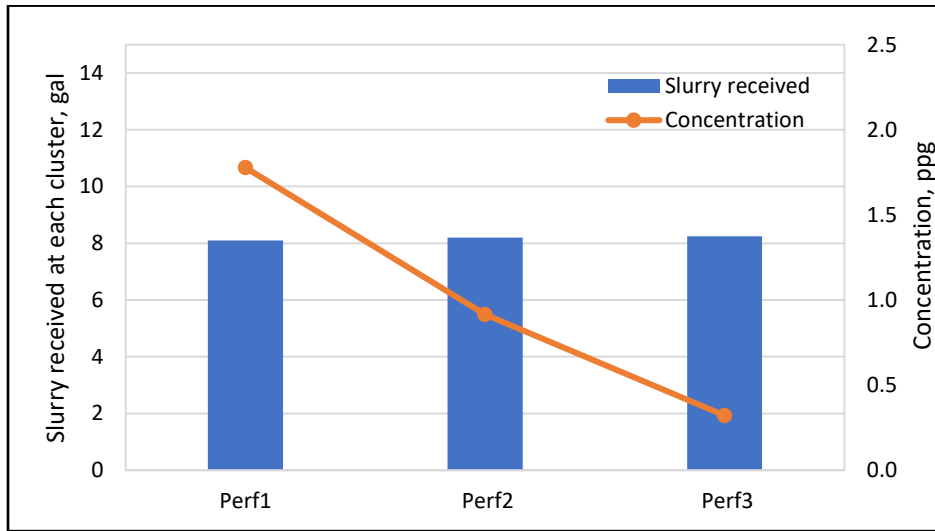


Figure 5.4: Proppant and slurry distribution between the perforation clusters at a flow velocity of 4.5 ft/s and an injected proppant concentration of 1.0 ppg.

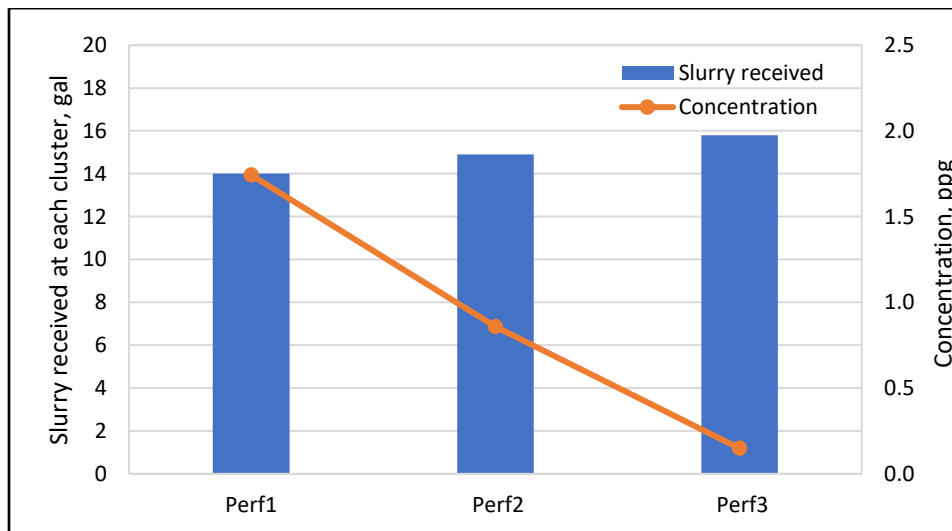


Figure 5.5: Proppant and slurry distribution between the perforation clusters at a flow velocity of 8.2 ft/s and an injected proppant concentration of 1.0 ppg.

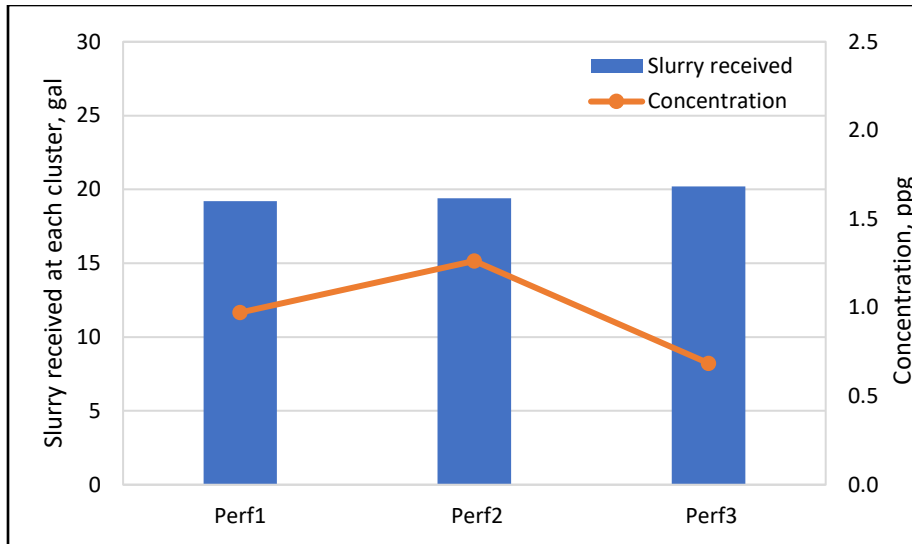


Figure 5.6: Proppant and slurry distribution between the perforation clusters at a flow velocity of 11.0 ft/s and an injected proppant concentration of 1.0 ppg.

5.2.1.2 Concentration of 2 gpt of HLFRR

In this phase of the experiments, the fluid viscosity was increased from 2.5 to 4.2 cp. Figures 5.7, 5.8 and 5.9 show the proppant and the fluid distribution between the three perforation clusters at flow velocities of 4.5, 8.2 and 11.0 ft/s, respectively. As can be observed from the three graphs, uneven proppant distribution was also observed between the perforation clusters at a fluid viscosity of 4.2 cp. At flow velocities of 4.5 and 8.2 ft/s, higher proppant concentration occurred at the first cluster and lower concentration occurred at the third cluster. However, the fluid that was received at the third cluster was slightly higher than the fluid received at the first cluster as shown in Figures 5.7 and 5.8, respectively.

At a flow velocity of 4.5 ft/s, the viscous forces were not able to suspend the proppant particles in the fluid column. Gravity forces were still dominant over the viscous forces and because of this, particles of proppant were concentrated in the lower section of the fluid column. Once again, the suspension mechanism can be described as heterogenous suspension where particles of the proppant were concentrated in the bottom of the horizontal pipe.

In contrast, at a higher flow velocity of 11.0 ft/s, the proppant concentration that was received by the third perforation cluster was higher than the proppant concentration that was received by the first and the second clusters as shown in Figure 5.9. This can be explained by the momentum forces near the first cluster being dominant over the viscous and the gravity forces,

and as a result, a small portion of proppant particles were able to turn into the first perforation cluster.

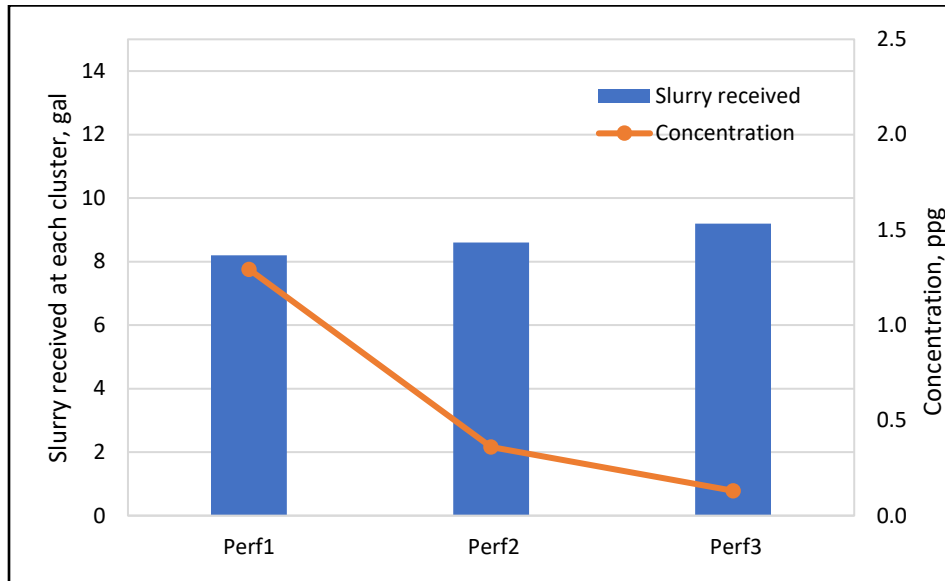


Figure 5.7: Proppant and slurry distribution between the perforation clusters at a flow velocity of 4.5 ft/s and an injected proppant concentration of 0.5 ppg.

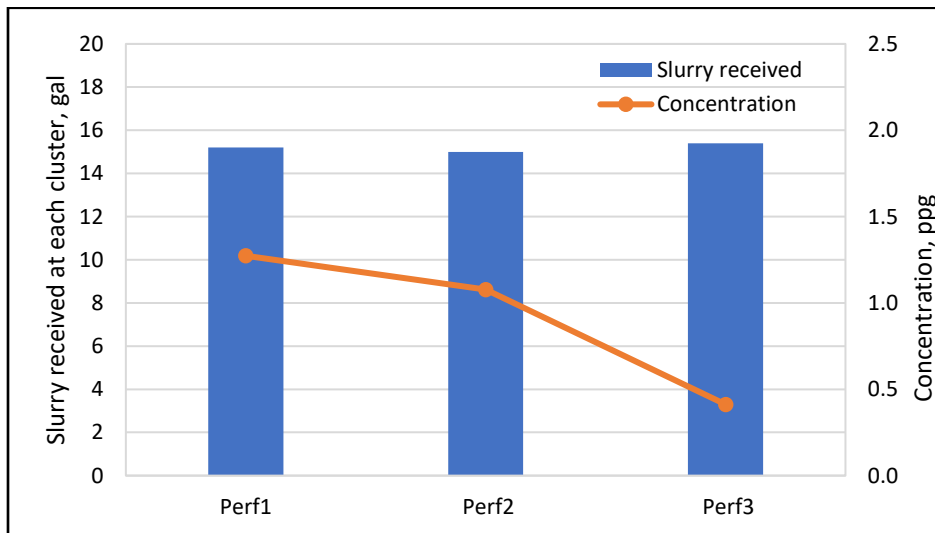


Figure 5.8: Proppant and slurry distribution between the perforation clusters at a flow velocity of 8.2 ft/s and an injected proppant concentration of 1.0 ppg.



Figure 5.9: Proppant and slurry distribution between the perforation clusters at a flow velocity of 11.0 ft/s and an injected proppant concentration of 1.25 ppg.

5.2.1.3 Concentration of 3 gpt of HLFR

Three experiments were performed using the same flow velocities of 4.5, 8.2 and 11.0 ft/s at 3 gpt of HLFR (an apparent viscosity of 7.5 cp). At a flow velocity of 4.5 ft/s, the same behavior was observed at the fluid viscosity of 7.5 cp as at the viscosities of 2.5 and 4.2 cp. Highly uneven proppant distribution was observed between the three perforation clusters as shown in Figure 5.10. More proppant was received at the first cluster, whereas less proppant was received at the third cluster. This indicates that at a low flow velocity and a viscosity of 7.5 cp, the viscous forces were still not dominant over the gravity forces upon the particles.

However, at a flow velocity of 45 gpm and an injected proppant concentration of 0.9 ppg, the proppant distribution was also uneven with more proppant concentration occurring at the middle cluster at 1.22 ppg followed by the first cluster at 0.92 ppg as shown in Figure 5.11. This can be clarified by the high flow rate (at the first cluster being fairly high) and preventing the proppant particles from exiting the perforations placed around the cluster. When the slurry passed the first cluster, the fluid velocity decreased. The reduction in the fluid velocity led the particles to concentrate in the bottom of the pipe. At this point, the particles were able to turn into the second perforations within the second cluster; hence the second cluster received higher particle concentration than the other two clusters. After the second cluster, the fluid traveled in the horizontal wellbore with less proppant concentration, and as a result, lower proppant concentration was received by the third cluster.

At a flow velocity of 11.0 ft/s and an injected proppant concentration of 1.0 ppg, uneven proppant distribution was also observed between the perforation clusters, as can be seen in Figure 5.12. Around 1.2 ppg of proppant concentration was received at the third cluster, followed by the second and the first perforation clusters at concentrations of 1.08 and 0.81 ppg, respectively. All the obtained results show that when the fluid viscosity increased to 7.5 cp, the 20/40 particles were not able to be suspended uniformly in the horizontal wellbore.

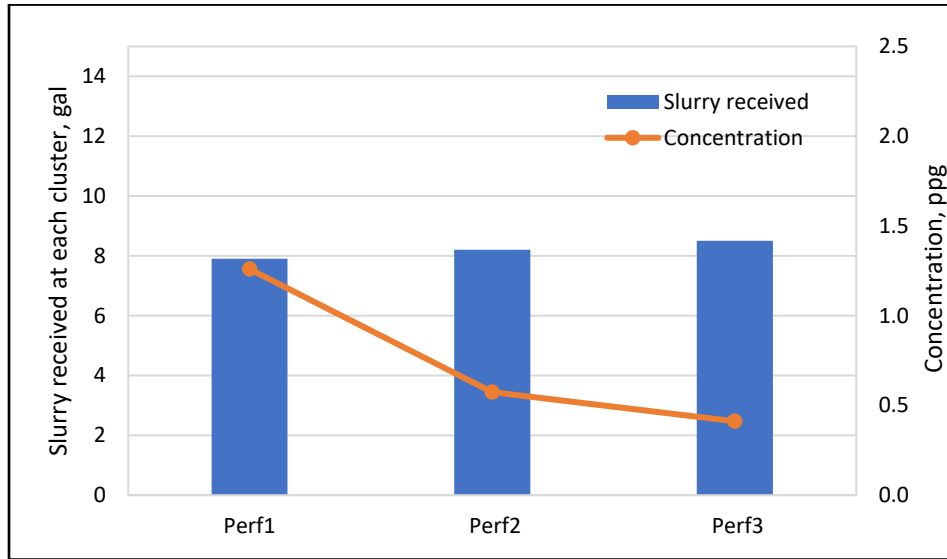


Figure 5.10: Proppant and slurry distribution between the perforation clusters at a flow velocity of 4.5 ft/s and an injected proppant concentration of 0.75 ppg.

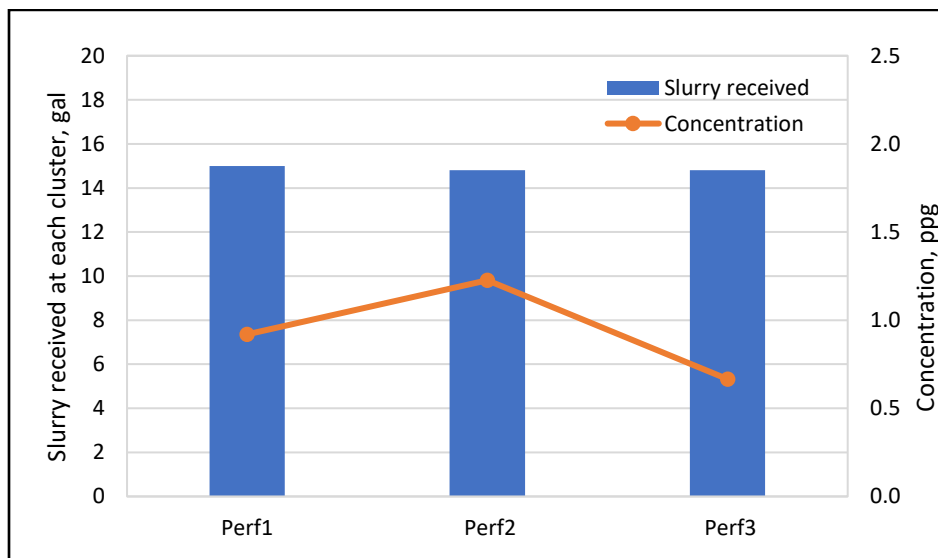


Figure 5.11: Proppant and slurry distribution between the perforation clusters at a flow velocity of 8.2 ft/s and an injected proppant concentration of 0.9 ppg.

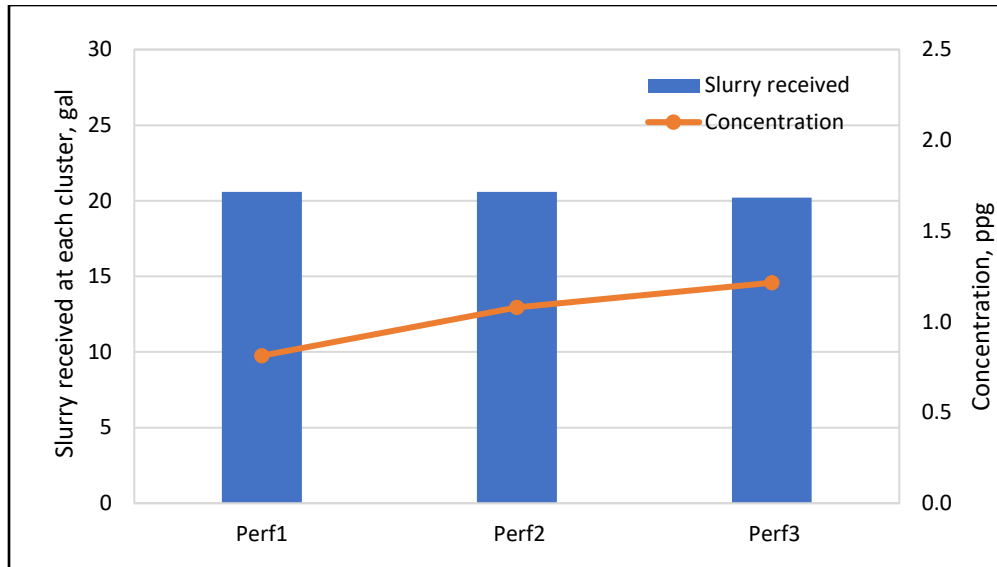


Figure 5.12: Proppant and slurry distribution between the perforation clusters at a flow velocity of 11.0 ft/s and an injected proppant concentration of 1.0 ppg.

5.2.1.3 Concentration of 5 gpt of HLFR

A total of three experiments were conducted on 20/40 mesh sand at a loading of 5 gpt of HLFR (apparent viscosity of 17 cp). For a flow velocity of 4.5 ft/s, highly uneven proppant distribution was observed between the three perforation clusters as shown in Figure 5.13. The graph shows more proppant was received at the first cluster although the fluid that was received by the third cluster was higher than the fluid that was received by the first cluster. At this flow velocity, the gravity forces were still dominant over the viscous and the momentum forces, and this led the particles of the 20/40 mesh sand to settle down in the bottom of the horizontal pipe.

A similar trend to a fluid viscosity of 7.5 cp was observed using a fluid viscosity of 17 cp for a flow velocity of 8.2 ft/s as shown in Figure 5.14. High proppant concentration occurred at the second cluster than followed by less concentration at the third cluster. This can be explained that the momentum forces near the first perforation were dominant over gravity forces cluster. In this case, particles were not able to turn completely into the perforations. As fluid reached the middle cluster, velocity decreased, and due to the decrease in the fluid velocity near the second cluster, gravity became more significant; hence, high proppant concentration occurred at the second perforation cluster.

In contrast, at a flow rate of 11.0 ft/s and an injected proppant concentration of 1.5 ppg, as shown in Figure 5.15, the same behavior was observed. High proppant concentration occurred at

the third cluster and low proppant concentration was measured at the first cluster. However, there was a minor increase in the viscous forces over the gravitational forces. It can be noticed that a slightly even proppant distribution was observed between the perforation clusters.

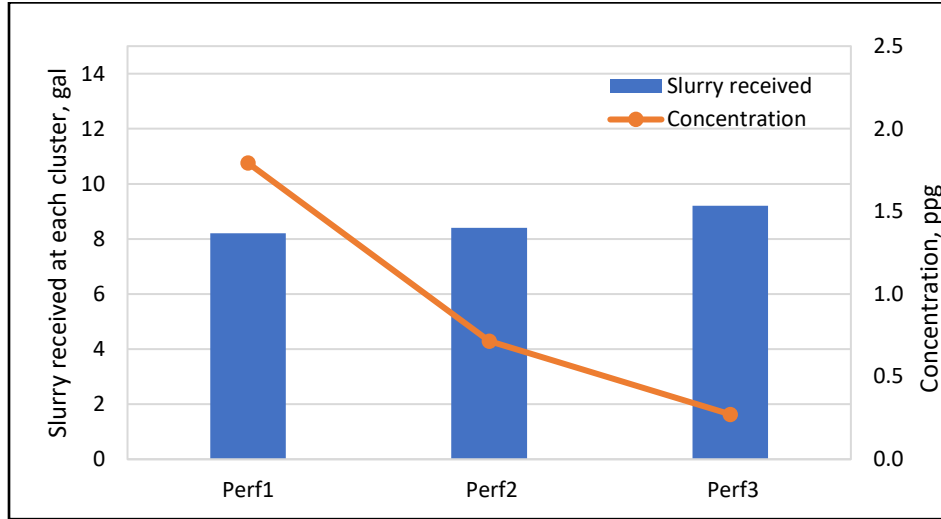


Figure 5.13: Proppant and slurry distribution between the perforation clusters at a flow velocity of 4.5 ft/s and an injected proppant concentration of 1.0 ppg.

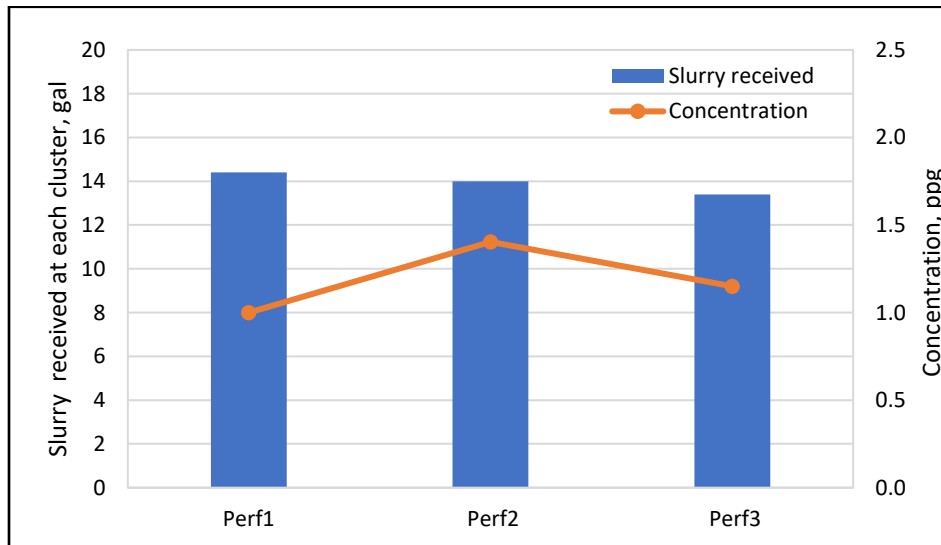


Figure 5.14: Proppant and slurry distribution between the perforation clusters at a flow velocity of 8.2 ft/s and an injected proppant concentration of 1.25 ppg.

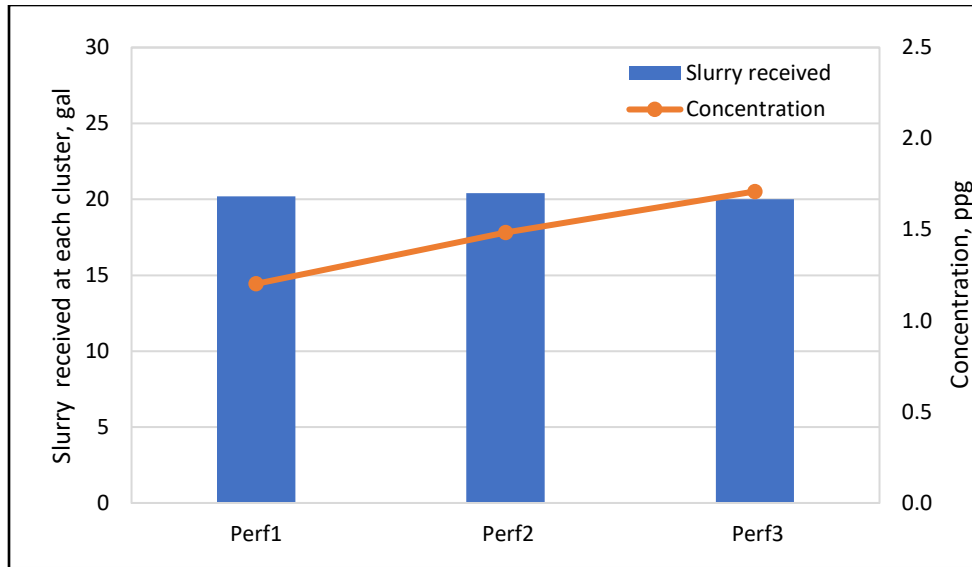


Figure 5.15: Proppant and slurry distribution between the perforation clusters at a flow velocity of 11.0 ft/s and an injected proppant concentration of 1.5 ppg.

5.2.2 40/70 Mesh Sand

A total of 12 tests were conducted on 40/70 mesh white sand at three flow velocities and four different concentrations (1, 2, 3 and 5 gpt) of HLFR. Sections 5.2.2.1-5.2.2.4 present and discuss the obtained results from proppant transport in horizontal wellbores using different loading of HLFR.

5.2.2.1 Concentration of 1 gpt of HLFR

The tested 40/70 mesh sand has a median diameter of 0.014 inch (almost half of the median particle diameter of the 20/40 mesh sand). The earlier findings in Chapter 4 indicated that the 40/70 mesh sand was transported in horizontal wellbores better than 20/40 mesh in freshwater fluids. In other words, the distribution of 40/70 particles in the horizontal wellbore was more uniform than 20/40 mesh sand. Three tests were conducted on 40/70 mesh sand at three different flow velocities of 4.5, 8.2 and 11.0 ft/s.

At a flow velocity of 4.5 ft/s and an injected concentration of 0.75 ppg, as shown in Figure 5.16, extremely uneven proppant distribution occurred with higher proppant concentration towards the first perforation cluster. The proppant concentration that was measured at the first cluster was 1.21 ppg, which is six times greater than the concentration that was received by the third cluster at 0.21 ppg. At this flow velocity, the proppant particles tended to settle down due to the gravitational forces, as the viscous forces were negligible.

When the fluid velocity was increased to 8.2 ft/s, the proppant concentration at the middle cluster was a slightly higher than the concentration measured at the first and third cluster as can be seen in Figure 5.17. The fluid distribution was almost the same across the three clusters, though. However, at a flow velocity of 11.0 ft/s, proppant concentrations of 0.96 and 0.94 ppg occurred at the second and the third perforation clusters, respectively, as illustrated in Figure 5.18. At this flow velocity, the momentum and the viscous forces were more dominant over the gravitational forces. In this case, the proppant particles of 40/70 sand were able to be suspended in the fluid column, which was the opposite condition for the 20/40 sand particles.

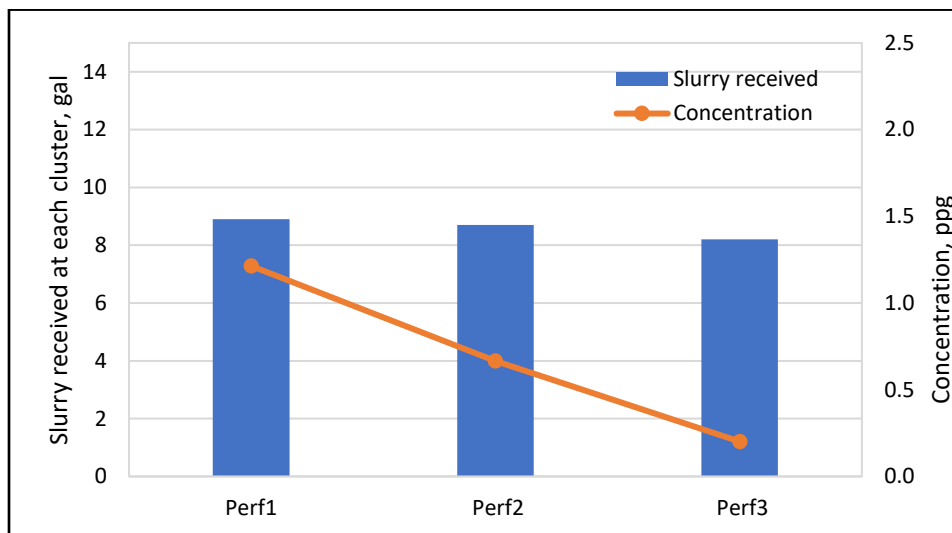


Figure 5.16: Proppant and slurry distribution between the perforation clusters at a flow velocity of 4.5 ft/s and an injected proppant concentration of 0.75 ppg.

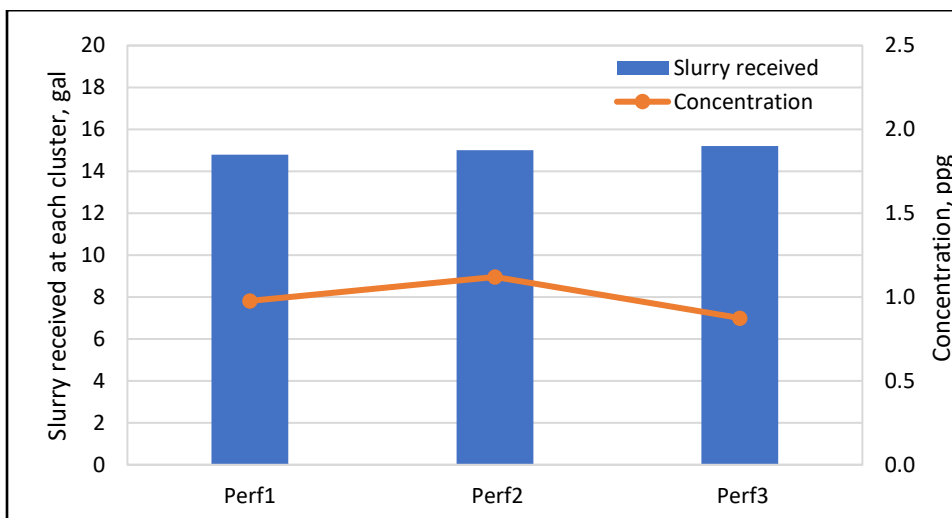


Figure 5.17: Proppant and slurry distribution between the perforation clusters at a flow velocity of 8.2 ft/s and an injected proppant concentration of 1.0 ppg.

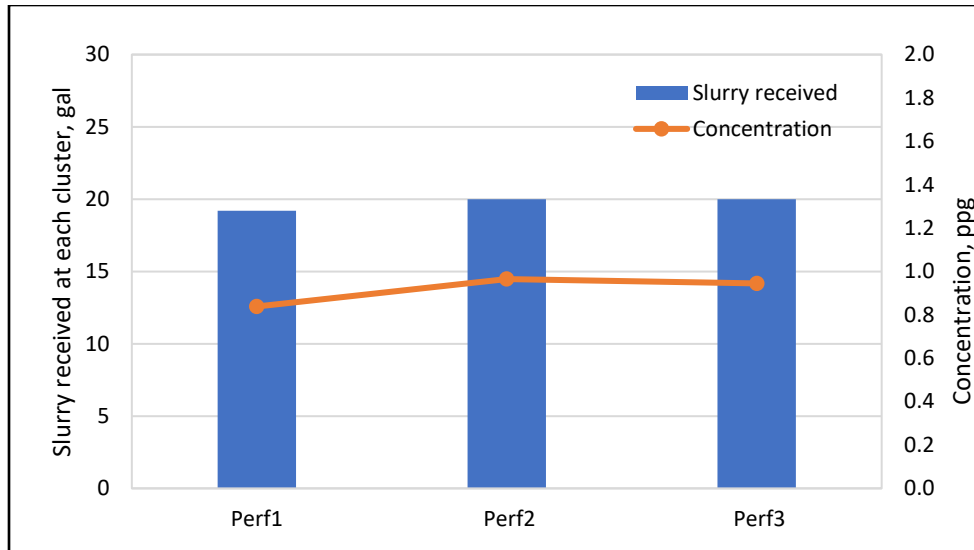


Figure 5.18: Proppant and slurry distribution between the perforation clusters at a flow velocity of 11.0 ft/s and an injected proppant concentration of 0.9 ppg.

5.2.2.2 Concentration of 2 gpt of HLFRR

In this phase of the experiments, three tests were performed on 40/70 mesh sand at 2 gpt of HLFRR with an apparent viscosity of 4.2. At a flow velocity of 4.5 ft/s and an injected proppant concentration of 0.75 ppg, the same behavior as with 0.75 gpt of HLFRR was observed at 2 gpt of HLFRR as shown in Figure 5.19. Even though, the fluid viscosity was increased to 4.2 cp, uneven proppant distribution occurred between the perforation clusters. Around 1.26 ppg of proppant concentration was measured at the first cluster, whereas proppant concentrations of 0.74 and 0.26 ppg were measured at the middle and the last clusters, respectively. The proppant concentration received at the first cluster was five times greater than the proppant concentration measured at the third cluster, although the amount of fluid at the third cluster was higher. This can be explained because at the low flow velocity of 4.5 ft/s, the gravity forces were still dominant over the viscous forces, and as a result, proppant particles were concentrated in the lower section of the horizontal pipe making the distribution of particles uneven. As there were four perforations on each cluster at 90-degree phasing, the perforation which was placed on the bottom of pipe within the first cluster received more proppant particles. After the first cluster, the slurry was less concentrated in the horizontal pipe, hence the proppant that was measured at the second cluster was less than proppant that was measured at the first cluster. The same is true for the third cluster.

Alternatively, at flow velocities of 8.2 and 11.0 ft/s, uniform proppant distribution was observed between the perforation clusters, as can be seen in Figures 5.20 and 5.21, respectively.

At these two flow velocities, the 40/70 sand particles were distributed uniformly in the fluid. According to Biot and Medlin (1985), this particle distribution can be described as pseudo-homogeneous distribution. Also, it can be noted that the gravity forces did not have a significant effect upon the fluid. In other words, the momentum and the viscous forces were dominant over the gravitational forces and were considered to be the most significant drivers for achieving uniform proppant distribution between the three perforation clusters.

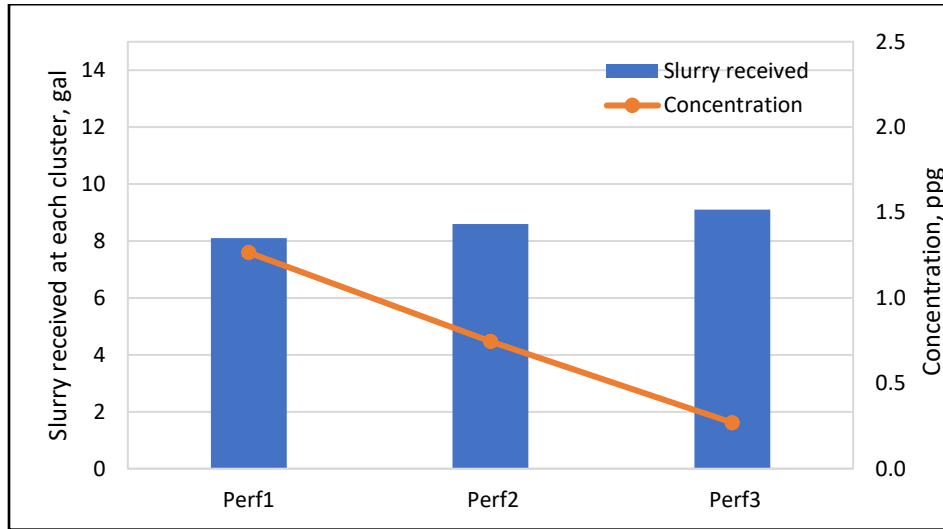


Figure 5.19: Proppant and slurry distribution between the perforation clusters at a flow velocity of 4.5 ft/s and an injected proppant concentration of 0.75 ppg.

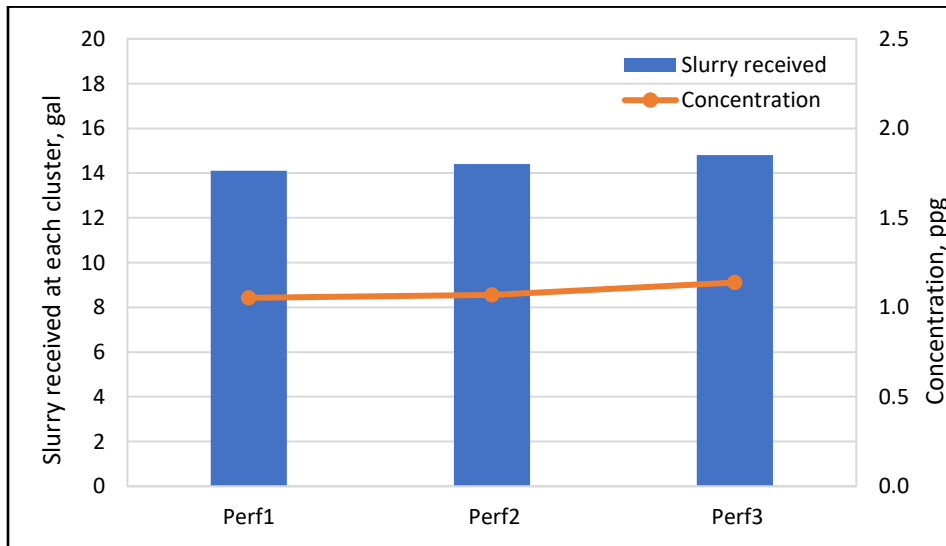


Figure 5.20: Proppant and slurry distribution between the perforation clusters at a flow velocity of 8.2 ft/s and an injected proppant concentration of 1.0 ppg.

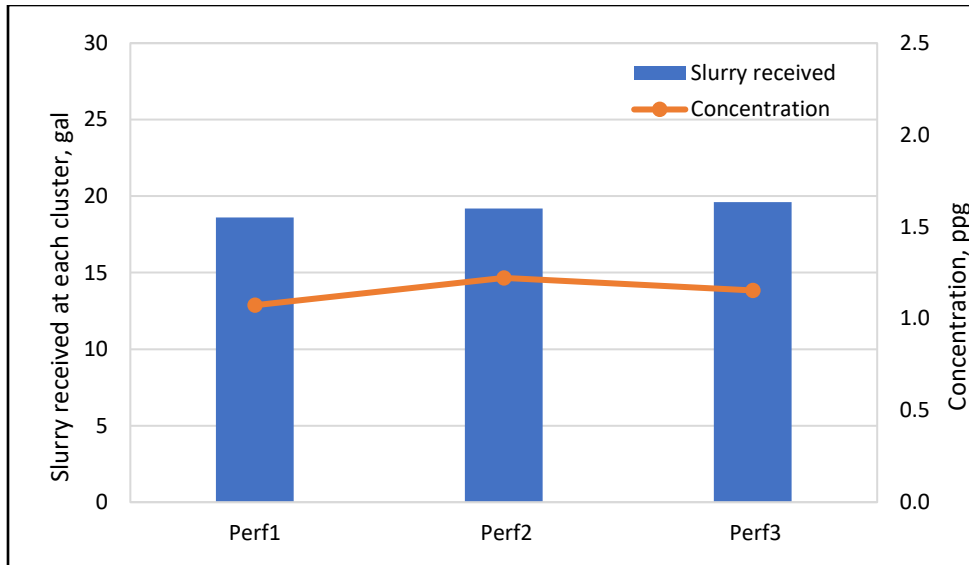


Figure 5.21: Proppant and slurry distribution between the perforation clusters at a flow velocity of 11.0 ft/s and an injected proppant concentration of 1.15 ppg.

5.2.2.3 Concentration of 3 gpt of HLFRR

In this section of the experimental tests, the viscosity of the carrier fluid was increased from 4.2 to 7.5 cp. Three experiments were performed on 40/70 mesh sand using the same fluid velocities of 4.5, 8.2 and 11.0 ft/s.

Figure 5.22 shows proppant and fluid distribution at each of the three perforation clusters at a flow velocity of 4.5 ft/s and an injected proppant concentration of 1.0 ppg. As can be observed from the graph, the proppant concentrations that were received by the first and second cluster were 1.2 and 1.11 ppg, respectively, even though the injected proppant concentration was 1.0 ppg. At this low flow velocity, the viscous forces were dominant over the momentum forces, and the proppant particles were able to be suspended in the horizontal pipe. Hence, improved proppant distribution was observed between the first and the second perforation clusters. After the first cluster, the proppant particles were still suspended in the fluid but with less concentration. Therefore, lower proppant concentration occurred at the third cluster.

However, at flow velocities of 8.2 and 11.0 ft/s, uniform proppant distribution was achieved between the three perforation clusters as shown in Figures 5.23 and 5.24, respectively. The two graphs demonstrate that the effect of the viscosity forces was more significant than the momentum forces on distribution of the 40/70 sand particles in the horizontal wellbore. This was the most

important driver for achieving uniform proppant distribution between the three perforation clusters.

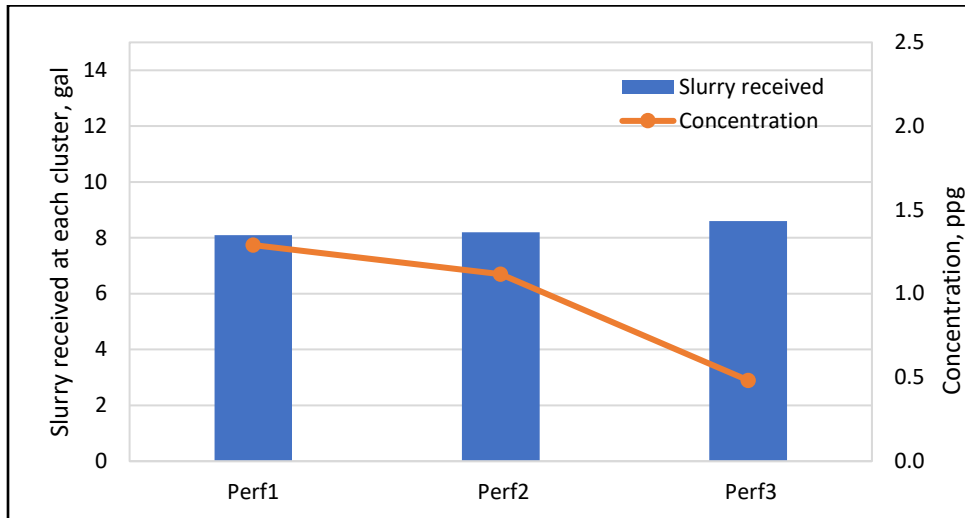


Figure 5.22: Proppant and slurry distribution between the perforation clusters at a flow velocity of 4.5 ft/s and an injected proppant concentration of 1.0 ppg.

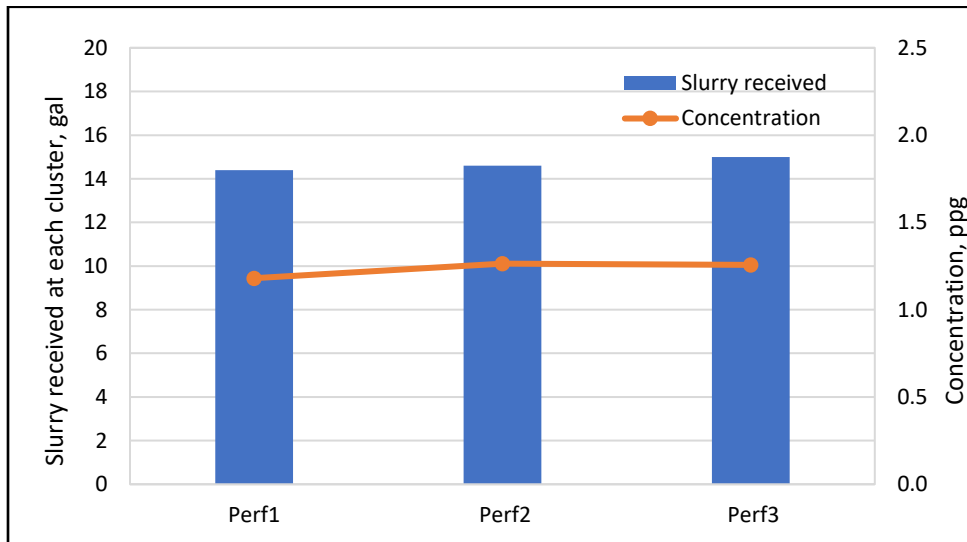


Figure 5.23: Proppant and slurry distribution between the perforation clusters at a flow velocity of 8.2 ft/s and an injected proppant concentration of 1.25 ppg.

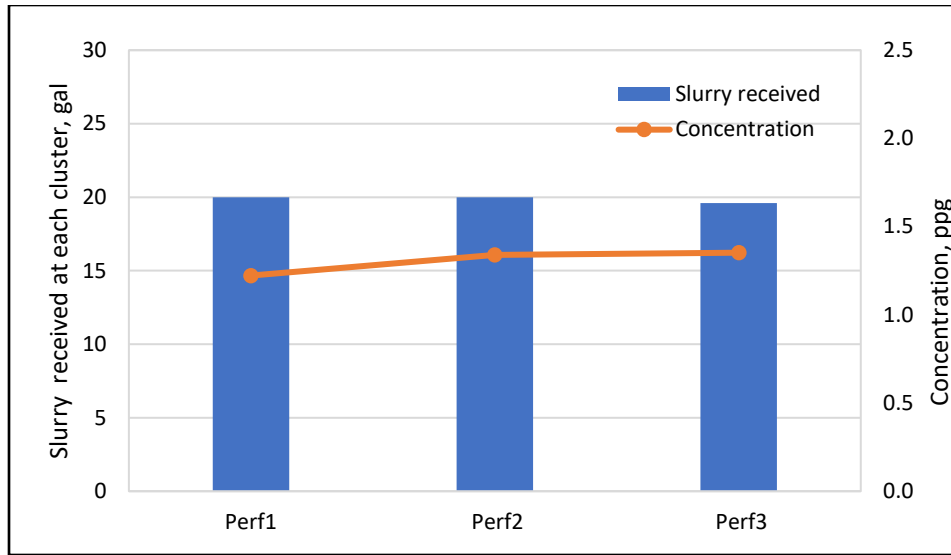


Figure 5.24: Proppant and slurry distribution between the perforation clusters at a flow velocity of 11.0 ft/s and an injected proppant concentration of 1.3 ppg.

5.2.2.4 Concentration of 5 gpt of HLFRR

The final phase of the experimental tests was performed using a fluid viscosity of 17 cp (5 gpt of HLFRR). Figures 5.25, 5.26 and 5.27 show the proppant concentration and the fluid distribution between the perforation clusters at flow velocities of 4.5, 8.2 and 11.0, respectively. As can be noted from the three graphs, even proppant distribution occurred between the three perforation clusters. For the first time, at the flow velocity of 4.5 ft/s, the gravity became insignificant, even though the fluid velocity was low. It can be illustrated that the particles of 40/70 sand were able to be fully suspended in the horizontal wellbore by the viscous forces at the fluid viscosity of 17 cp. Similarly, at the flow velocities of 8.2 and 11.0 ft/s, the viscosity forces were dominant over the momentum forces and led the particles of 40/70 sand to distribute uniformly in the horizontal wellbore; hence, uniform proppant distribution was achieved between the perforation clusters.

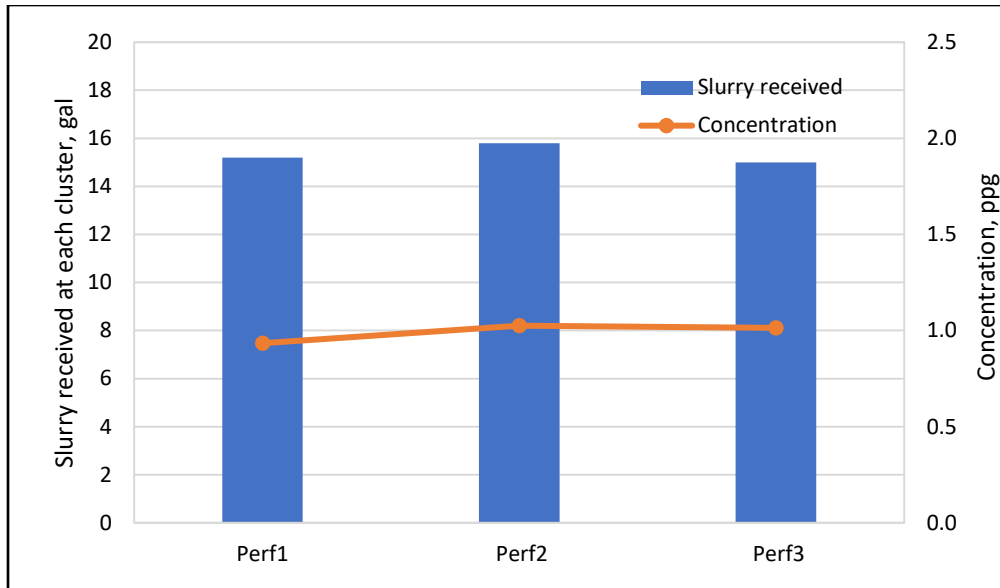


Figure 5.25: Proppant and slurry distribution between the perforation clusters at a flow velocity of 4.5 ft/s and an injected proppant concentration of 1.0 ppg.

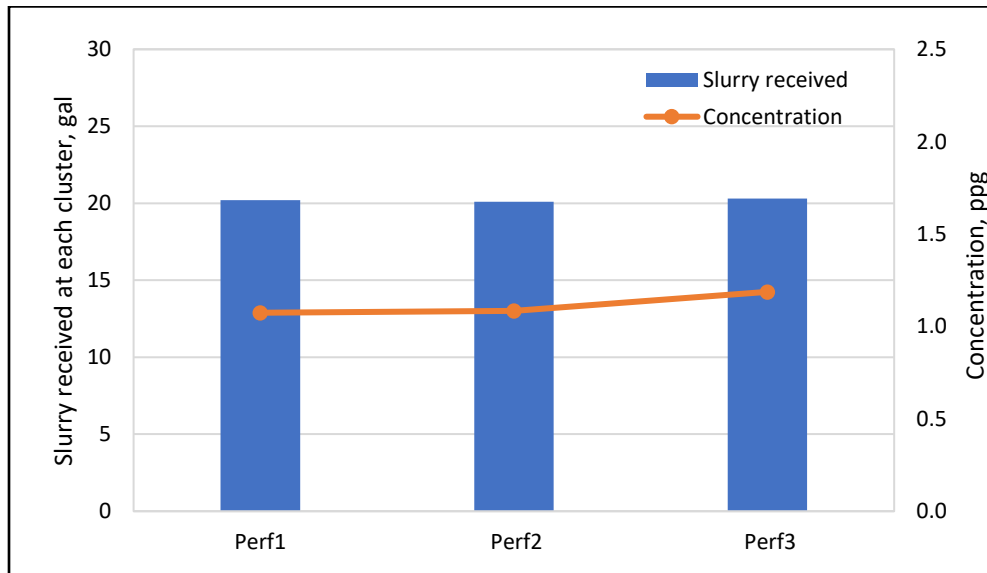


Figure 5.26: Proppant and slurry distribution between the perforation clusters at a flow velocity of 8.2 ft/s and an injected proppant concentration of 1.0 ppg.

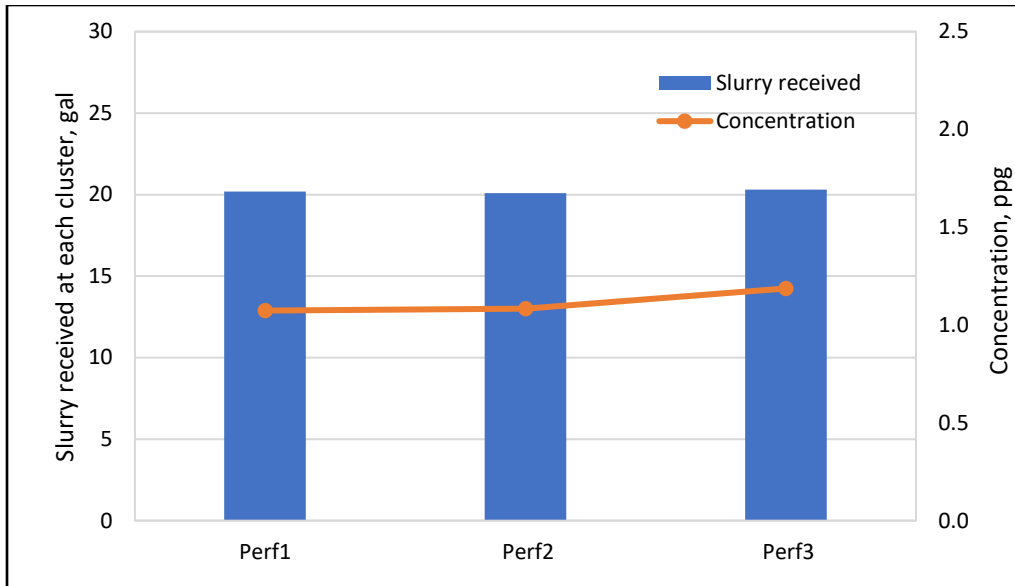


Figure 5.27: Proppant and slurry distribution between the perforation clusters at a flow velocity of 11.0 ft/s and an injected proppant concentration of 1.1 ppg.

CHAPTER 6

EXPERIMENTAL CORRELATIONS

This chapter presents the correlation development based on the experimental results obtained from proppant transport in the horizontal wellbore apparatus. No published studies on correlations for proppant distribution prediction between perforation clusters have been found. The developed correlations, that are presented in this chapter, are the first of their kind to be based on experimental data. These correlations can be used to predict the proppant distribution (sand and ULW ceramic) between multiple clusters in hydraulic fracturing treatments.

The correlation of experimental data was mostly achieved by utilizing dimensional analysis which requires appropriate experimental data to be obtained. Experimental tests were conducted on 20/40 and 40/70 for white sand and ultra-light weight ceramic over a wide range of slurry velocities and proppant concentrations. Such correlations help to determine the optimum flow rate that is required to attain an even distribution of the proppant and provide more insight about the anticipated proppant distribution into and out of the perforations. Also, these correlations can be extrapolated to field scale for optimizing the design of hydraulic fracturing treatments.

Typically, there are two important approaches to dimensional analysis by which correlations between the experimental physical quantities can be developed. These methods are the Rayleigh's method and the Buckingham's pi-theorem. In the Rayleigh's approach, the relationship of the physical parameters is expressed in the form of an exponential equation which must be dimensionally homogeneous. This method is simple and time effective for a small number of variables, but it's considered to be lengthy when more variables are involved. Therefore, in order to overcome this, Buckingham's method was utilized in this study and is considered to be very effective when more variables are involved. In this method, the independent and dependent variables are related to a dimensional homogeneous equation as shown in Equation 6.1.

$$\Pi_1 = \text{function} (\Pi_2, \Pi_3, \dots, \Pi_{n-k}) \quad (6.1)$$

Where; Π_1 is the dependent variable, and, $\Pi_2, \Pi_3, \dots, \Pi_{n-k}$ are the independent variables.

In the experimental tests, there are two main variables, the dependent and the independent. The dependent variables are the proppant and fluid distribution between the perforation clusters. The independent variables include flow rate or slurry velocity, fluid density, particle density, median particle diameter, fluid viscosity, proppant concentration, and the pipe diameter. The

independent variables such as fluid velocity, proppant density, median particle diameter, and proppant concentration were changed or controlled in the experimental runs to test the effects on the dependent variable (proppant distribution). As the independent variables are changed, the effect on the proppant distribution is observed and recorded.

The first step of the correlation development was to determine the proppant distribution (PD) between the perforation clusters utilizing different proppant types, sizes, and concentrations based on slurry velocity. In order to determine the proppant distribution, the percentage increase/decrease at each run was calculated. The percentage increase/decrease represents the difference between the proppant concentration received at the perforation clusters and the injected/actual proppant concentration, divided by the injected/actual proppant concentration. If the average value of the percentage is equal to zero, then the proppant distribution between the perforation clusters will be 100 %. Table 6.1. shows the proppant distribution status for each value of the percentage increase/decrease.

Table 6.1: Proppant distribution status for each value of percentage increase/decrease

Percentage Increase/Decrease, %	Proppant Distribution (PD), %	Proppant Distribution Status
0	100	Strongly even distribution
10	90	Slightly uneven distribution
20	80	Moderately even distribution
40	60	Partially even distribution
60	40	Uneven distribution
80	20	Highly uneven distribution
90	10 and less	Very highly uneven distribution

Then the proppant distribution for all the experimental tests, that were conducted on 20/40 and 40/70 white sand and ultra-light weight ceramic, was used to develop a multivariable correlation. Then, the developed correlation can be generalized to account for different proppant characteristics distribution between the perforation clusters.

As stated previously, the Buckingham Pi theorem as illustrated in Munson et al. (2012) was used to build dimensionless terms which can be used to develop the experimental correlations. Based on the Buckingham Pi theorem, all the variables that are involved in the experimental tests must be determined. Therefore, the independent variables such as slurry velocity, proppant density and median proppant diameter, proppant concentration and fluid velocity were all determined for each test. In addition, the dependent variable, which is the proppant distribution between the

perforation clusters, was also determined for each experimental run. Then, all the variables were expressed in terms of basic dimensions as illustrated in Table 6.2.

Table 6.2: Basic dimensions for all the variables involved in the experimental tests

Quantity	SI Unit	Dimension
Flow rate (q)	m ³ /s	L ³ /T
Fluid density (ρ _f)	Kg/m ³	M/L ³
Particle density (ρ _p)	Kg/m ³	M/L ³
Proppant size (P _d)	m	L
Fluid viscosity (μ _f)	Kg/m.s	M/LT
Proppant concentration (C _p)	Kg/m ³	M/L ³
Pipe diameter (D)	m	L

The seven variables stated in Table 6.2 have three basic units: M, L, and T, which represent the mass, length, and time, respectively. Then, the total number of pi terms was determined by subtracting the reference dimensions (3 dimensions) from the total number of variables (8 variables), and as result, five pi terms were determined. The next step was to determine the number of repeating variables, where the number required is equal to the number of reference dimensions. Therefore, the variables such as flow rate (q), fluid density (ρ_f), and pipe diameter (D) were selected to represent the repeating variables. Finally, the pi terms were developed by multiplying the product of the repeating variables by one of the nonrepeating variables and each term was raised to an exponent to make the combination dimensionless.

Starting with the dependent variable which is the proppant distribution (PD), and combining it with the repeating variables forms the first pi term as follows:

$$\pi_1 = PD * D * \rho_f * q \quad (6.2)$$

The combination on the right side of Equation 62 must be dimensionless and it follows that

$$(M^0L^0T^0)(L)^a(ML^{-3})^b(L^3T^{-1})^c = M^0L^0T^0 \quad (6.3)$$

The exponents, a, b, and c are determined and the resulting exponent for each of the basic dimensions M, L, and T is equal to zero (so that the resulting combination is dimensionless).

Therefore:

$$a - 3b + 3c = 0 \quad \text{for (L)} \quad (6.4)$$

$$b = 0 \quad \text{for (M)} \quad (6.5)$$

$$-c = 0 \quad \text{for (T)} \quad (6.6)$$

The system of the linear algebraic equations is solved and the resulting values for a, b and c is 0. Therefore, the first pi term is formed as shown in Equation 6.7.

$$\pi_1 = PD \quad (6.7)$$

The previous step is repeated for another nonrepeating variable. In this case, the variable of the proppant density, ρ_p , is chosen.

$$\pi_2 = \rho_p * D * \rho_f * q \quad (6.8)$$

$$(ML^{-3})(L)^a(ML^{-3})^b(L^3T^{-1})^c = M^0L^0T^0 \quad (6.9)$$

Therefore:

$$1 + b = 0 \quad \text{for (M)} \quad (6.10)$$

$$-3 + a - 3b + 3c = 0 \quad \text{for (L)} \quad (6.11)$$

$$-c = 0 \quad \text{for (T)} \quad (6.12)$$

The same steps are also repeated for solving the algebraic equations to obtain the values of a, b, and c. Therefore, the anticipated values for a, b and c are 0, -1, and 0, respectively. As a result, the second pi term is determined as shown in Equation 6.13.

$$\pi_2 = \frac{\rho_p}{\rho_f} \quad (6.13)$$

The third nonrepeating variable is the fluid viscosity, μ_f , as illustrated below:

$$\pi_3 = \mu_f * D * \rho_f * q \quad (6.14)$$

$$(ML^{-1}T^{-1})(L)^a(ML^{-3})^b(L^3T^{-1})^c = M^0L^0T^0 \quad (6.15)$$

Therefore:

$$1 + b = 0 \quad \text{for (M)} \quad (6.16)$$

$$-1 + a - 3b + 3c = 0 \quad \text{for (L)} \quad (6.17)$$

$$-1 - c = 0 \quad \text{for (T)} \quad (6.18)$$

The solution of these equations gives values for a = 1, b = -1, and c = -1. Therefore, the third pi term for the fluid viscosity is formed as shown in Equation 6.19.

$$\pi_3 = \frac{\mu_f D}{\rho_f q} \quad (6.19)$$

The proppant concentration, C_p , is also chosen as a nonrepeating variable as shown below.

$$\pi_4 = C_p * D * \rho_f * q \quad (6.20)$$

$$(ML^{-3})(L)^a(ML^{-3})^b(L^3T^{-1})^c = M^0L^0T^0 \quad (6.21)$$

Therefore:

$$1 + b = 0 \quad \text{for (M)} \quad (6.22)$$

$$-3 + a - 3b + 3c = 0 \quad \text{for (L)} \quad (6.22)$$

$$-c = 0 \quad \text{for (T)} \quad (6.24)$$

Similarly, the solution of these equations gives the values for $a = 0$, $b = -1$, and $c = 0$, therefore,

$$\pi_4 = \frac{C_p}{\rho_f} \quad (6.25)$$

The last nonrepeating variable is the median particle diameter, P_d .

$$\pi_5 = P_d * D * \rho_f * q \quad (6.26)$$

$$(L)(L)^a(ML^{-3})^b(L^3T^{-1})^c = M^0L^0T^0 \quad (6.27)$$

Therefore:

$$1 + a - 3b + 3c = 0 \quad \text{for (L)} \quad (6.28)$$

$$b = 0 \quad \text{for (M)} \quad (6.29)$$

$$-c = 0 \quad \text{for (T)} \quad (6.30)$$

Solving these equations simultaneously gives the values for $a = -1$, $b = 0$, and $c = 0$, therefore

$$\pi_5 = \frac{P_d}{D} \quad (6.31)$$

The five required pi terms are determined and must be checked to ensure that they are dimensionless. Thus, as shown in Equations 6.32-6.36:

$$\pi_1 = PD = M^0L^0T^0 \quad (6.32)$$

$$\pi_2 = \frac{\rho_p}{\rho_f} = \frac{ML^{-3}}{ML^{-3}} = M^0L^0T^0 \quad (6.33)$$

$$\pi_3 = \frac{\mu_f D}{\rho_f q} = \frac{(ML^{-1}T^{-1})(L)}{(ML^{-3})(L^3T^{-1})} = M^0L^0T^0 \quad (6.34)$$

$$\pi_4 = \frac{C_p}{\rho_f} = \frac{ML^{-3}}{ML^{-3}} = M^0L^0T^0 \quad (6.35)$$

$$\pi_5 = \frac{P_d}{D} = \frac{L}{L} = M^0L^0T^0 \quad (6.36)$$

Finally, the results of the dimensional analysis can be expressed in the form of pi terms as shown in Equation 6.37.

$$\text{Proppant distribution, (PD)} = f\left(\frac{\rho_P}{\rho_f}, \frac{\mu_f D}{\rho_f q}, \frac{C_p}{\rho_f}, \frac{P_d}{D}\right) \quad (6.37)$$

Where;

PD = Proppant distribution, dimensionless

ρ_P = Proppant density, kg/m³

ρ_f = Fluid density, kg/m³

μ_f = Fluid viscosity, kg/m/s

q = Flow rate, m³/s

C_p = Proppant concentration, kg/m³

P_d = Median particle diameter, m

D = Pipe diameter, m

This form of dimensionless analysis (Equation 6.37) indicates that variables that have a significant effect on the proppant distribution between the perforation clusters can be studied in terms of these five pi terms, rather than the original eight variables. Therefore, all the variables in the dimensionless pi terms must be obtained for all the experimental tests.

6.1 20/40 Mesh White Sand

Sets of experimental tests were conducted on 20/40 mesh white sand with a median diameter of 0.675 mm and a specific gravity of 2.65 g/cm³. Three velocities were used to evaluate the effect of velocity on proppant distribution between the perforation clusters as illustrated in Table 6.3. As can be seen in Table 6.3, the three flow rates achieved Reynolds numbers above 4000. In other words, turbulent flow was observed for all the tests at different proppant concentrations.

Table 6.3: Fluid and the proppant properties for 20/40 mesh white sand at slurry velocities of 6.4, 11.0 and 13.7 ft/s

Velocity, ft/s	Velocity, m/s	Fluid Density, kg/m ³	Fluid Viscosity, kg/m/s	Proppant Density, kg/m ³	Proppant Size, mm	Pipe Diameter, m	Re, unitless
6.4	1.948	1000	0.001	2650	0.675	0.038	74,016
11.0	3.339	1000	0.001	2650	0.675	0.038	126,886
13.7	4.174	1000	0.001	2650	0.675	0.038	158,607

6.1.1 Proppant Distribution Determination

As stated previously, in order to determine the proppant distribution (PD), the percentage increase/decrease at each experimental test was calculated. The percentage increase/decrease represents the difference between the proppant concentration received at the perforation clusters and the injected/actual proppant concentration, divided by the injected/actual proppant concentration.

6.1.1.1 Flow Velocity of 6.4 ft/s

The proppant concentration at each cluster was calculated at the injected proppant concentrations of 0.12, 0.13, 0.21 and 0.31 ppg as illustrated in Figure 6.1. The highest proppant concentration was received at the first cluster followed by the second cluster, etc. Therefore, highly uneven proppant distribution was observed between the perforation clusters at the four injected proppant concentrations.

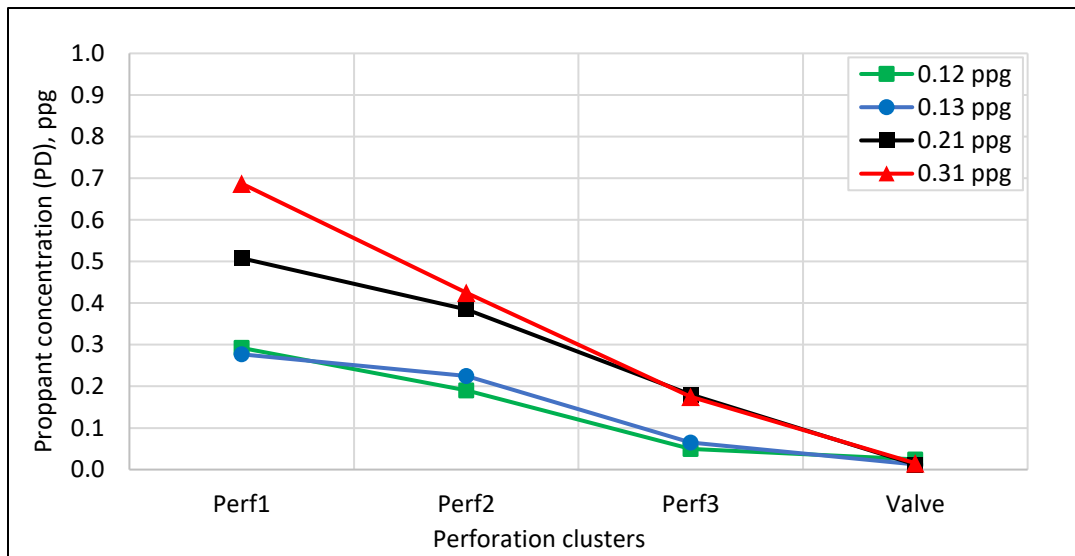


Figure 6.1: Proppant distribution between the perforation clusters for 20/40 mesh sand at a slurry velocity of 6.4 ft/s and injected proppant concentrations of 0.12, 0.13, 0.21 and 0.31 ppg.

The following step was to determine the percentage increase/decrease at each of the perforation clusters as well as at the valve. As stated previously, the percentage was determined by obtaining the difference between the injected proppant concentration and the concentration received at the perforation cluster divided by the injected concentration. The average of the percentage was also determined for each test. Then, the proppant distribution (PD) was calculated from the average of the percentage increase/decrease for each test (100 - percentage

increase/decrease). Table 6.4 shows the proppant distribution associated with the percentage increase/decrease at each proppant concentration.

Table 6.4: Proppant distribution and the percentage increase/decrease for 20/40 mesh sand at a slurry velocity of 6.4 ft/s and injected proppant concentrations of 0.12, 0.13, 0.21 and 0.31 ppg

Concentration, ppg	Percentage Increase/Decrease, %				Absolute Value of Percentage, %			
	0.13	0.12	0.21	0.31	0.13	0.12	0.21	0.31
Perf1	119.629	137.985	139.527	121.438	119.629	137.985	139.527	121.438
Perf2	78.448	54.690	81.641	36.953	78.448	54.690	81.641	36.953
Perf3	-48.448	-59.292	-64.615	-43.608	48.448	59.292	64.615	43.608
Valve	-90.239	-79.959	-94.193	-95.042	90.239	79.959	94.193	95.042
Average of Percentage, %					84.191	82.982	94.994	74.260
Proppant Distribution (PD), %					15.809	17.018	5.006	25.740

As can be noted from Table 6.4, the highest proppant distribution (PD) across the perforation clusters at the flow velocity of 6.4 ft/s was 25.74 % at an injected concentration of 0.31 ppg. This indicates that highly uneven proppant distribution was observed between the perforation clusters at this injected concentration. As discussed in Section 4.1.1.1, the gravity forces associated with the proppant particles were the main forces acting upon the fluid flow in the horizontal wellbore. These forces were able to settle the larger particles of the proppant on the bottom of the pipe. Therefore, more proppant concentration was received at the first perforation cluster.

6.1.1.2 Flow Velocity of 11.0 ft/s

A total of four tests were conducted on 20/40 mesh sand at a slurry velocity of 11.0 ft/s at concentrations of 0.1, 0.12, 0.23 and 0.36 ppg as shown in Figure 6.2. The fluid velocity was increased from 6.4 to 11.0 ft/s, at which the Reynolds number was 126,866. From Figure 6.2, the proppant concentration received at the second cluster was higher than the concentration received at the first and the third clusters. Therefore, the proppant distribution between the perforation clusters was uneven for the four different concentrations.

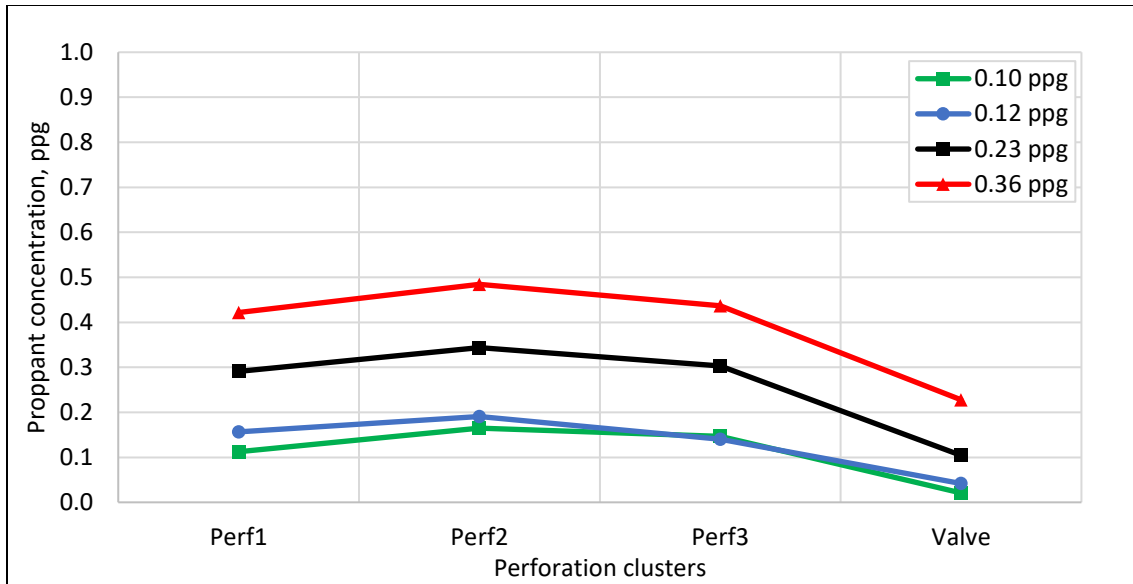


Figure 6.2: Proppant distribution between the perforation clusters for 20/40 mesh sand at a slurry velocity of 11.0 ft/s and injected proppant concentrations of 0.1, 0.12, 0.23 and 0.36 ppg.

The percentage increase/decrease was also calculated at each of the perforation clusters as well as at the valve. Once again, the proppant distribution (PD) was calculated from the average of percentage increase/decrease for each test. Table 6.5 shows the proppant distribution and the percentage increase/decrease at each proppant concentration.

Table 6.5: Proppant distribution and the percentage increase/decrease for 20/40 mesh sand at a slurry velocity of 11.0 ft/s and injected proppant concentrations of 0.1, 0.12, 0.23 and 0.36 ppg

Concentration, ppg	Percentage Increase/Decrease, %				Absolute Value of Percentage, %			
	0.1	0.12	0.23	0.36	0.1	0.12	0.23	0.36
Perf1	33.739	17.746	24.378	15.786	33.739	17.746	24.378	15.786
Perf2	63.162	72.531	47.113	32.940	63.162	72.531	47.113	32.940
Perf3	19.831	53.506	29.816	19.846	19.831	53.506	29.816	19.846
Valve	-64.274	-78.157	-55.343	-37.472	64.274	78.157	55.343	37.472
	Average of Percentage, %				45.252	55.485	39.163	26.511
	Proppant Distribution (PD), %				54.748	44.515	60.837	73.489

From Table 6.5, the highest proppant distribution across the perforation clusters at a flow velocity of 11.0 ft/s was 73.49 % at an injected concentration of 0.36 ppg. This specifies that uneven proppant distribution was observed between the perforation clusters. However, the PD that obtained from the four tests at this slurry velocity was higher than the PD for a velocity of 6.4 ft/s. This indicates that the change in the slurry velocity has an impact on the proppant distribution.

6.1.1.3 Flow Velocity of 13.7 ft/s

In this section, the fluid velocity was increased to 13.7 ft/s. As before, the proppant concentration at each cluster was determined from the total fluid and proppant that exited each cluster. Figure 6.3 shows the proppant concentration at each perforation cluster for injected concentrations of 0.07, 0.1, 0.13 and 0.3 ppg. The highest proppant concentration was received at the third cluster followed by the second cluster. As before, uneven proppant concentration was observed between the perforation clusters.

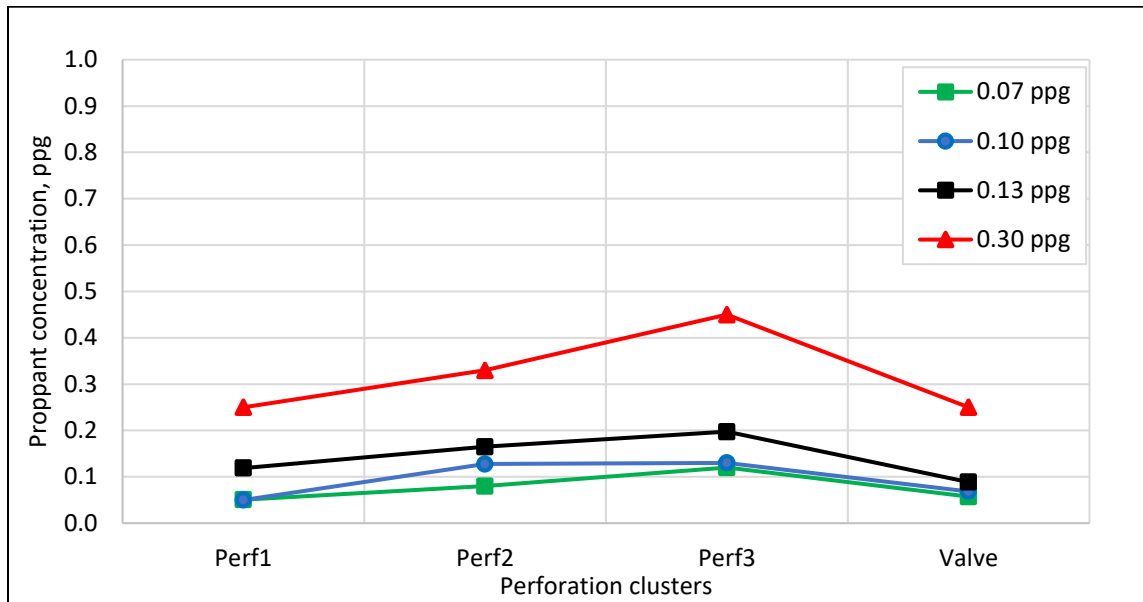


Figure 6.3: Proppant distribution between the perforation clusters for 20/40 mesh sand at a slurry velocity of 13.7 ft/s and injected proppant concentrations of 0.07, 0.1, 0.13 and 0.3 ppg.

Table 6.6 presents the proppant distribution associated with the percentage increase/decrease at each injected proppant concentration for this sets of runs.

Table 6.6: Proppant distribution and the percentage increase/decrease for 20/40 mesh sand at a slurry velocity of 13.7 ft/s and injected proppant concentrations of 0.07, 0.1, 0.13 and 0.31 ppg

Concentration, ppg	Percentage Increase/Decrease, %				Absolute Value of Percentage, %			
	0.10	0.07	0.13	0.31	0.10	0.07	0.13	0.31
Perf1	0.471	-31.465	-11.228	-14.566	0.471	31.465	11.228	14.566
Perf2	26.499	8.286	23.100	16.004	26.499	8.286	23.100	16.004
Perf3	28.979	62.429	47.347	53.320	28.979	62.429	47.347	53.320
Valve	-31.967	-22.653	-33.920	-31.394	31.967	22.653	33.920	31.394
	Average of Percentage, %				21.979	31.208	28.899	28.821
	Proppant Distribution (PD), %				78.021	68.792	71.101	71.179

From Table 6.6, the proppant distribution for all tests was higher than 68%, indicating that partial even distribution was achieved between the perforation clusters. As discussed in Section 4.1.1.3, the momentum forces associated with the proppant particles were the main forces acting upon the fluid flow in the horizontal wellbore in this situation. However, the proppant distribution for the four tests that were conducted at this flow rate was higher than the PD obtained at velocities of 6.4 and 11.0 ft/s.

6.1.2 Correlation Development for 20/40 Mesh Sand

The resulting data from the experimental tests was used to develop a correlation that predicts the proppant distribution between the perforation clusters based on the change in the slurry velocity (V), proppant concentration (C_p), specific gravity of the particles (ρ_p) and median proppant diameter (P_d). The relationship between the dependent variable (PD) and the seven independent variables (ρ_p , ρ_f , μ_f , D , q , C_p and P_d) was first studied to describe the correlation type that best fits the experimental data. In this section, the correlation of experimental data was developed by utilizing the dimensionless correlation stated in Equation 6.37

The left-hand side of Equation 6.37 represents the proppant distribution, which was determined for each individual test, whereas the right side of the equation represents the independent variables. Table 6.7 shows the values of the proppant distribution as well as the values of the dimensionless terms for each run.

Table 6.7: Proppant distribution and the associated dimensionless terms for each test for 20/40 mesh white sand

Velocity, ft/s	Concentration, ppg	PD	$\frac{\rho_p}{\rho_f}$	$\frac{\mu_f D}{\rho_f q}$	$\frac{C_p}{\rho_f}$	$\frac{P_d}{D}$
6.40	0.13	0.158	2.650	0.000017	0.016	0.017
	0.12	0.170	2.650	0.000017	0.014	0.017
	0.21	0.174	2.650	0.000017	0.025	0.017
	0.31	0.257	2.650	0.000017	0.037	0.017
11.00	0.11	0.547	2.650	0.000010	0.013	0.017
	0.10	0.445	2.650	0.000010	0.012	0.017
	0.23	0.608	2.650	0.000010	0.028	0.017
	0.36	0.735	2.650	0.000010	0.043	0.017
13.70	0.10	0.780	2.650	0.000008	0.012	0.017
	0.07	0.688	2.650	0.000008	0.008	0.017
	0.13	0.711	2.650	0.000008	0.016	0.017
	0.31	0.712	2.650	0.000008	0.037	0.017

For the three slurry velocity values, the proppant distribution (PD) was plotted against the proppant concentration per fluid density for velocities of 6.4, 11.0 and 13.7 ft/s as shown in Figure 6.4. The resulting power law trends with fitted equations and R^2 values for the three stated velocities indicate that proppant distribution is considerably affected by proppant concentration. The PD can be improved by an increase in the proppant concentrations at higher slurry velocities.

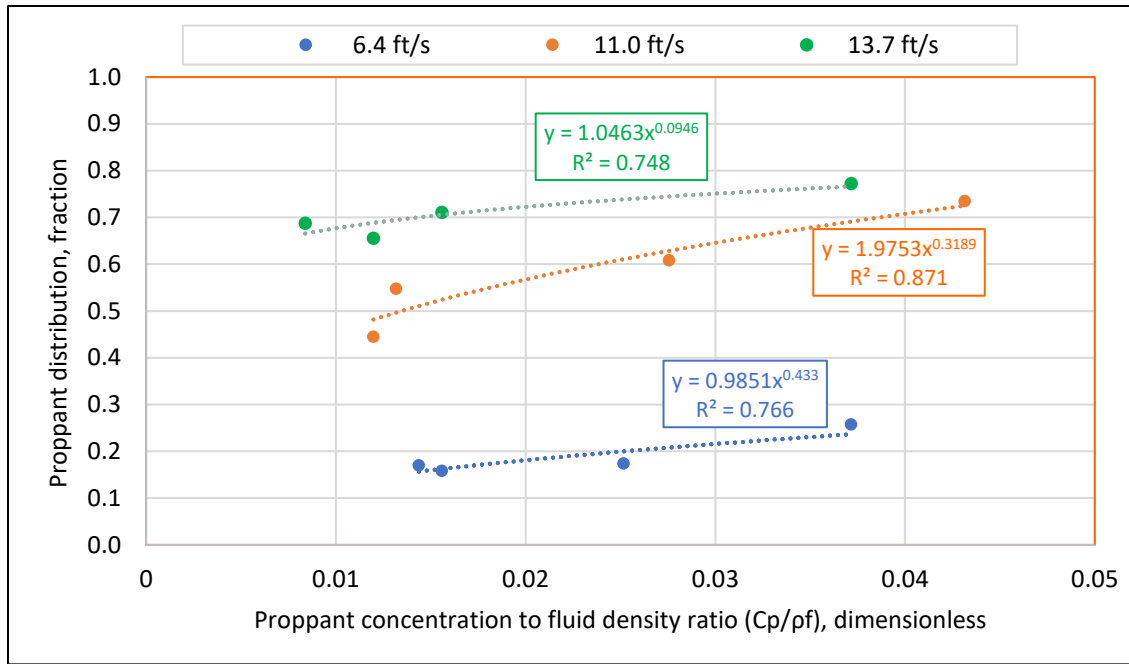


Figure 6.4: Proppant distribution as function of proppant concentration to fluid density ratio for slurry velocities of 6.4, 11.0 and 13.7ft/s.

The resulting equations and R^2 values that are shown in Table 6.8 can be used for any proppant concentration for 20/40 mesh sand. As the slope of these fitted equations increases, the effect of the proppant concentration on the PD increases. Also, the power law equations have the proppant concentration variable in the numerator depicting its effect on the proppant distribution between the perforation clusters.

Table 6.8: Power law equations and R^2 values for different slurry velocities for 20/40 mesh sand

Slurry Velocity, ft/s	Developed Correlations	R^2
6.4	$PD = 0.9851(C_p/\rho_f)^{0.4332}$	0.77
11.0	$PD = 1.9753(C_p/\rho_f)^{0.3189}$	0.87
13.7	$PD = 1.0463(C_p/\rho_f)^{0.0946}$	0.75

When the dimensionless values for the three velocity values were combined in developing the experimental correlation for 20/40 mesh white sand, a multivariable linear regression was used to develop Equation 6.38 with R² value of 0.97.

$$PD = - 57789.191 \left(\frac{\mu_f D}{\rho_f q} \right) + 5.238 \left(\frac{C_p}{\rho_f} \right) + 1.059 \quad (6.38)$$

The multivariable linear regression was done through a Microsoft Excel Solver to find the values of the Equation 6.38 constants. The developed correlation has the slurry velocity variable in the denominator and proppant concentration in the numerator depicting their impacts on proppant distribution. The resulting correlation (Equation 6.38) can be used for any proppant concentration as well as for any slurry velocity for 20/40 mesh white sand.

6.2 40/70 Mesh White Sand

A number of experimental tests were also conducted using 40/70 mesh white sand with a median diameter of 0.360 mm. The median diameter of the 40/70 is 43% smaller than the median diameter of the 20/40 at 0.675 mm. Three flow rates were also used to study the effect of slurry velocity on the proppant distribution between the perforation clusters as shown in Table 6.9.

Table 6.9: Fluid and the proppant properties for 40/70 mesh white sand at slurry velocities of 6.4, 11.0 and 13.7 ft/s

Velocity, ft/s	Velocity, m/s	Fluid Density, kg/m ³	Fluid Viscosity, kg/m/s	Proppant Density, kg/m ³	Proppant Size, mm	Pipe Diameter, m	Re, unitless
6.4	1.948	1000	0.001	2650	0.360	0.038	74,017
11.0	3.339	1000	0.001	2650	0.360	0.038	126,886
13.7	4.174	1000	0.001	2650	0.360	0.038	158,608

6.2.1 Proppant distribution determination

In order to determine the proppant distribution (PD), the percentage increase/decrease at each experimental test was calculated. The percentage increase/decrease represents the difference between the proppant concentration received at the perforation clusters and the injected/actual proppant concentration, divided by the injected/actual proppant concentration.

6.2.1.1 Flow Velocity of 6.4 ft/s

The proppant concentration at each cluster was also measured for a wide range of proppant concentrations of 0.3, 0.37, 0.93 and 1.1 ppg as shown in Figure 6.5. Similar to 20/40 mesh sand, at the flow velocity of 6.4 ft/s, the proppant concentration that was received at the first cluster was higher than the concentration received at the second and the third clusters. Additionally, uneven proppant concentration was observed between the perforation clusters. As stated previously, the gravity forces were dominant over the viscous and the momentum forces. In this case, the bigger particles of the proppant settled on the bottom of the pipe and led to more proppant concentration received at the first perforation within the first cluster which has a downward orientation.

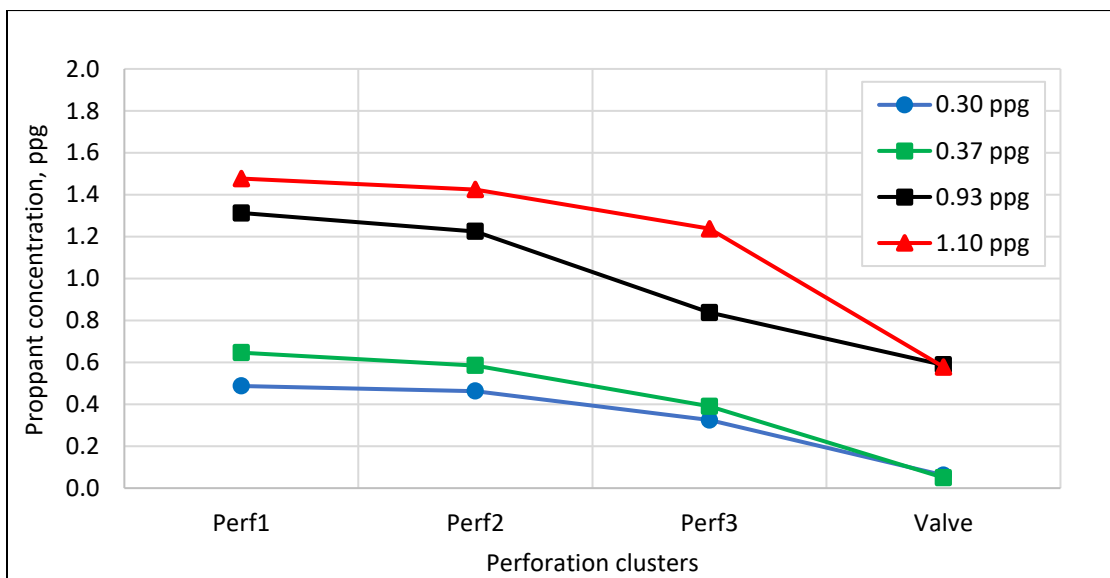


Figure 6.5: Proppant distribution between the perforation clusters for 40/70 mesh sand at a slurry velocity of 6.4 ft/s and injected proppant concentrations of 0.3, 0.37, 0.93 and 1.1 ppg.

The percentage increase/decrease and the proppant distribution between the perforation clusters were determined for each experiment run. Table 6.10 shows the proppant distribution associated with the percentage increase/decrease at a range of proppant concentrations for 40/70 mesh white sand at a velocity of 6.4 ft/s.

Table 6.10: Proppant distribution and the percentage increase/decrease for 40/70 mesh sand at a slurry velocity of 6.4 ft/s and injected proppant concentrations of 0.3, 0.37, 0.93 and 0.31 ppg

Concentration, ppg	Percentage Increase/Decrease, %				Absolute Value of Percentage, %			
	0.3	0.37	0.93	1.1	0.3	0.37	0.93	1.1
Perf1	64.479	76.267	40.523	34.732	64.479	76.267	40.523	34.732
Perf2	56.147	59.585	31.123	29.995	56.147	59.585	31.123	29.995
Perf3	9.725	6.390	-10.355	12.890	9.725	6.390	10.355	12.890
Valve	-79.224	-86.360	-37.094	-47.230	79.224	86.360	37.094	47.230
	Average of Percentage, %				52.394	57.151	29.774	31.212
	Proppant Distribution (PD), %				47.606	42.849	70.226	68.788

As can be observed from Table 6.10, the proppant distribution across the perforation clusters at a flow velocity of 6.4 ft/s ranged between 47.61% and 70.27%. The higher PD was observed at the higher proppant concentration. There are some reasons that might be involved for explaining this phenomenon. The first reason can be the interaction between the particles by which larger grains of the proppant will tend to settle down and exit the perforation holes that are placed on the bottom of the pipe. The second reason could be from the interaction between the particles and the pipe wall. This interaction can occur from the high turbulent velocity which can force the particles to move away from the centerline of the pipe. This results in more friction loss and leads the particles to settle in the low velocity region near the pipe wall.

6.2.1.2 Flow Velocity of 11.0 ft/s

Sets of experiments were also conducted with 40/70 mesh white sand at a velocity of 11.0 ft/s. The proppant concentration at each cluster was also measured for a range of injected proppant concentrations of 0.26, 0.3, 0.9 and 1.2 ppg as shown in Figure 6.6. As can be noted from the graph, the proppant concentration received at the third cluster was higher than the concentration received at the first and the second clusters for all four injected concentrations. The proppant distribution between the perforation clusters and the valve was highly uneven for concentrations of 0.26 and 0.3 ppg. On the other hand, there was moderate even proppant distribution between the perforation clusters and the valve for concentrations of 0.9 and 1.2 ppg.

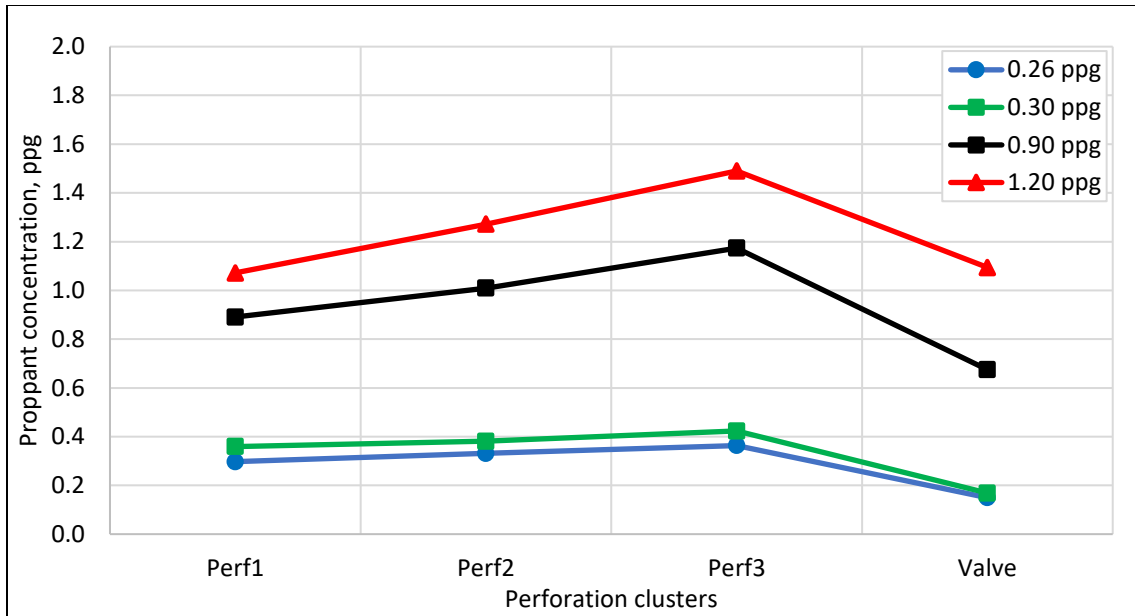


Figure 6.6: Proppant distribution between the perforation clusters for 40/70 mesh sand at a slurry velocity of 11.0 ft/s and injected proppant concentrations of 0.26, 0.3, 0.9 and 1.2 ppg.

Table 6.11 shows the proppant distribution associated with the percentage increase/decrease at each proppant concentration. The consequence of increasing the fluid velocity by 42% from 6.4 to 11.0 ft/s is shown to have a significant effect on the PD. The average PD was increased from 57.37% at a flow velocity of 6.4 ft/s to 76.98% at a flow velocity of 11.0 ft/s. The higher PD outcome by the 40/70 slurry is attributed to its relatively small grain size, making it easier on transport in a slurry.

Table 6.11: Proppant distribution and the percentage increase/decrease for 40/70 mesh sand at slurry velocity of 11.0 ft/s and injected proppant concentrations of 0.26, 0.3, 0.89 and 1.2 ppg

Concentration, ppg	Percentage Increase/decrease, %				Absolute Value of Percentage, %			
	0.26	0.3	0.89	1.2	0.26	0.3	0.89	1.2
Perf1	13.577	18.103	0.096	-11.068	13.577	18.103	0.096	11.068
Perf2	26.728	25.291	13.442	5.525	26.728	25.291	13.442	5.525
Perf3	39.003	39.121	31.869	23.623	39.003	39.121	31.869	23.623
Valve	-42.780	-44.561	-24.162	-9.240	42.780	44.561	24.162	9.240
Average of Percentage, %					30.522	31.769	17.393	12.364
Proppant Distribution (PD), %					69.478	68.231	82.607	87.636

6.2.1.3 Flow Velocity of 13.7 ft/s

Four experimental runs were also conducted at a flow velocity of 13.7 ft/s and the resulting concentrations for each test are shown in Figure 6.7. The four plotted concentrations in the figure

confirm earlier findings with a velocity of 11.0 ft/s for 40/70 mesh white sand. These results showed more concentration at the toe cluster, whereas less concentration occurred at the first cluster.

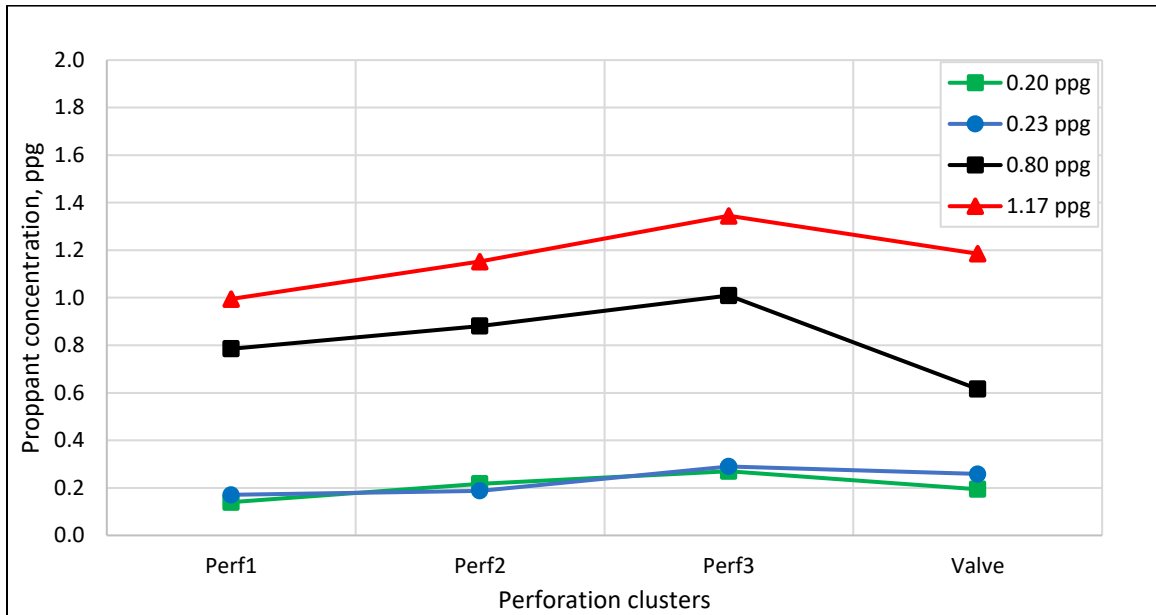


Figure 6.7: Proppant distribution between the perforation clusters for 40/70 mesh sand at a slurry velocity of 13.7 ft/s and injected proppant concentrations of 0.2, 0.23, 0.8 and 1.17 ppg.

The percentage increase/decrease and the PD for each test were calculated and the results are shown in Table 6.12. From the table, the increase in proppant concentration proportionally affects the PD. In addition, the significance of increasing the fluid velocity from 11.0 to 13.7 ft/s is shown to an impact on the PD where the average PD was increased by 7.04%. The resulting PD by the 40/70 slurry is attributed to its relatively small grain size, making it easier on the slurry to transport.

Table 6.12: Proppant distribution and the percentage increase/decrease for 40/70 mesh sand at a slurry velocity of 13.7 ft/s and injected proppant concentrations of 0.21, 0.23, 0.8 and 1.17 ppg

Concentration, ppg	Percentage Increase/Decrease, %				Absolute Value of Percentage, %			
	0.21	0.23	0.8	1.17	0.21	0.23	0.8	1.17
Perf1	-33.174	-26.319	-0.623	-15.148	33.174	26.319	0.623	15.148
Perf2	3.819	-19.155	11.498	-1.711	3.819	19.155	11.498	1.711
Perf3	28.879	25.040	27.709	14.706	28.879	25.040	27.709	14.706
Valve	-7.262	11.489	-22.053	1.122	7.262	11.489	22.053	1.122
Average of Percentage, %					18.283	20.501	15.471	8.172
Proppant distribution (PD), %					81.717	79.499	84.529	91.828

6.2.2 Correlation Development for 40/70 Mesh Sand

In order to develop the experimental correlation for 40/70 mesh white sand, the dimensionless terms in Equation 6.37 were determined for each run. Table 6.13 shows the proppant distribution as well as the dimensionless terms for each experimental test at flow velocities of 6.4, 11.0 and 13.7 ft/s.

Table 6.13: Proppant distribution and the associated dimensionless terms for each test for 40/70 mesh white sand

Velocity, ft/s	Concentration, ppg	PD	$\frac{\rho_P}{\rho_f}$	$\frac{\mu_f D}{\rho_f \nu}$	$\frac{C_P}{\rho_f}$	$\frac{P_d}{D}$
6.4	0.30	0.476	2.65	0.000017	0.0360	0.0100
	0.37	0.428	2.65	0.000017	0.0443	0.0100
	0.93	0.702	2.65	0.000017	0.1114	0.0100
	1.10	0.688	2.65	0.000017	0.1318	0.0100
11.0	0.26	0.695	2.65	0.000010	0.0312	0.0100
	0.30	0.682	2.65	0.000010	0.0360	0.0100
	0.89	0.826	2.65	0.000010	0.1067	0.0100
	1.20	0.876	2.65	0.000010	0.1438	0.0100
13.7	0.23	0.795	2.65	0.000008	0.0276	0.0100
	0.21	0.817	2.65	0.000008	0.0252	0.0100
	0.80	0.845	2.65	0.000008	0.0959	0.0100
	1.17	0.918	2.65	0.000008	0.1402	0.0100

The proppant distribution (PD) for each test was plotted against the proppant concentration to fluid density ratio for velocities of 6.4, 11.0 and 13.7 ft/s as shown in Figure 6.8. The plotted PDs in Figure 6.8 confirm previous findings by the 20/40 mesh sand. Also, the power law trends are comparable to the ones obtained at 20/40 mesh white sand and show that the proppant concentration has a significant effect on the PD. In addition, the slope value of the power law equations can reflect the magnitude of change in the dependent variable (PD) based on the change of the independent variable (proppant concentration). In other words, the if the power law equation slope is high, the effect of the proppant concentration on proppant distribution will be higher and vice versa.

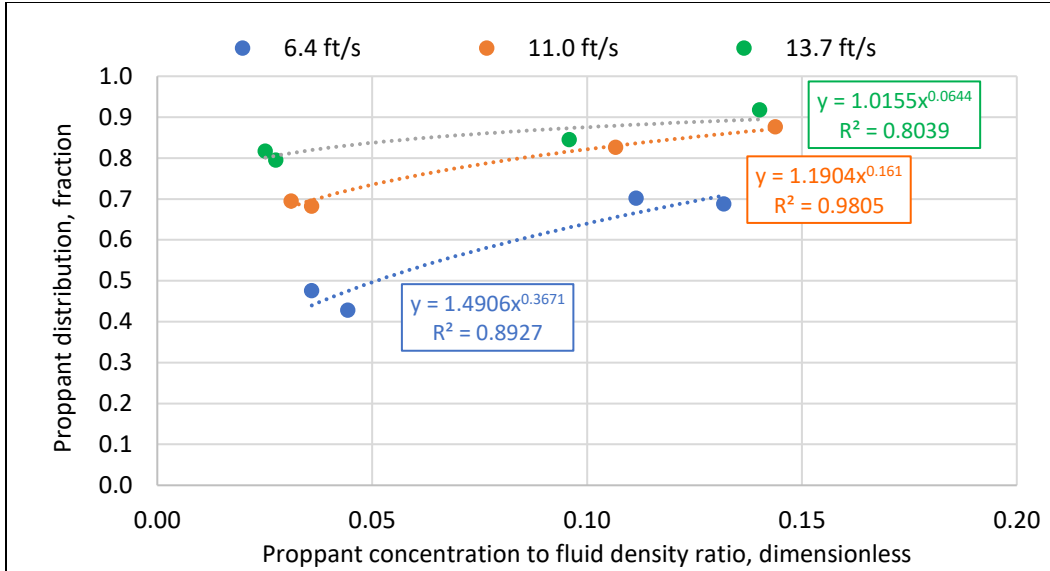


Figure 6.8: Proppant distribution as function of proppant concentration to fluid density ratio for slurry velocities of 6.4, 11.0 and 13.7ft/s.

The resulting power law equations and the R^2 values that are shown in Table 6.14 can be utilized for any proppant concentration for 40/70 mesh sand. These equations have the proppant concentration variable in the numerator showing its effect on the proppant distribution between the perforation clusters.

Table 6.14: Power law equations and R^2 values for different slurry velocities for 40/70 mesh white sand

Slurry Velocity, ft/s	Developed Correlations	R^2
6.4	$PD = 1.4906(C_p/\rho_f)^{0.3671}$	0.89
11.0	$PD = 1.1904(C_p/\rho_f)^{0.161}$	0.98
13.7	$PD = 1.0155(C_p/\rho_f)^{0.0644}$	0.80

When the three values of the velocity were involved in developing the experimental correlations for 40/70 mesh sand, a multivariable linear regression was used to develop Equation 6.9 with R^2 value of 0.91. This correlation was developed in Excel Solver using the multivariable linear regression to find the values of the constants. The developed correlation has the flow rate in the denominator term also with a negative constant value which implies that the increase in the slurry velocity of the proppant leads to increase in the PD. Also, the correlation has the proppant concentration as a numerator term, which indicates as the proppant concentration increases, the PD between the perforation clusters also increases. The resulting correlation (Equation 6.39) can be used for any proppant concentration at any slurry velocity for 40/70 mesh white sand.

$$PD = 0.951 - 30178.073 \left(\frac{\mu_f D}{\rho_f q} \right) + 1.713 \left(\frac{C_p}{\rho_f} \right) \quad (6.39)$$

6.3 Correlation Development for 20/40 and 40/70 Mesh Sand

In this section, all the results for the dimensionless terms for 20/40 and 40/70 mesh sand were combined to form Equation 6.40. The values of the constants in the equation, as well as the R^2 value, were established by utilizing multivariable linear regression. The R^2 of the regression is 0.90 which is relatively high. This implies that 90% of the variability of the dependent variables have been considered for determining the generated equation. The correlation that is stated in Equation 6.40 can be used to predict the proppant distribution between the perforation clusters for 20/40 and 40/70 mesh sand at any flow rate and proppant concentration.

$$PD = 1.280 - 43495.800 \left(\frac{\mu_f D}{\rho_f q} \right) + 1.949 \left(\frac{C_p}{\rho_f} \right) - 18.998 \left(\frac{P_d}{D} \right) \quad (6.40)$$

The developed correlation for the PD that is shown in Equation 6.40, was tested against the PD measured for 20/40 and 40/70 mesh sand as illustrated in Figure 6.9. An acceptable match is observed between the predicted PD from the model and the measured PD for all the three velocities. This implies that the model is valid for predicting the PD between the perforation clusters for any proppant concentration, slurry velocity, and any mesh size.

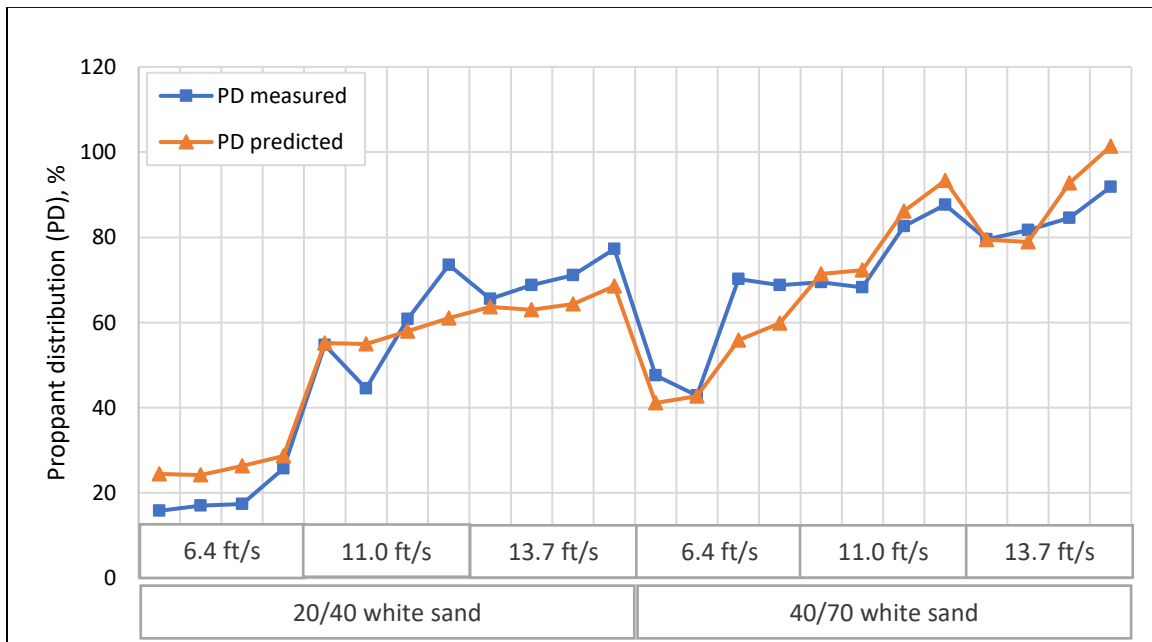


Figure 6.9: The predicted and the measured PD for 20/40 and 40/70 mesh white sand.

6.4 20/40 Ultra-Light Weight Ceramic

Several experimental tests were also conducted using 20/40 ultra-light weight (ULW) ceramic. The specific gravity of the 20/40 ULW ceramic is 2.0 which is 24.53% less than the specific gravity of the sand at 2.65. Three flow rates were also used to quantify the effect of slurry velocity on proppant distribution between the perforation clusters as shown in Table 6.15.

Table 6.15: Fluid and the proppant properties for 20/40 ULW ceramic at slurry velocities of 6.4, 11.0 and 13.7 ft/s

Velocity, ft/s	Velocit, m/s	Fluid Density, kg/m ³	Fluid Viscosity, kg/m/s	Proppant Density, kg/m ³	Proppant Size, mm	Pipe Diameter, m	Re, unitless
6.4	1.948	1000	0.001	2000	0.650	0.038	74,017
11.0	3.339	1000	0.001	2000	0.650	0.038	126,886
13.7	4.174	1000	0.001	2000	0.650	0.038	158,608

6.4.1 Proppant Distribution Determination

As stated previously, in order to determine the proppant distribution (PD), the percentage increase/decrease at each experimental test was calculated. The percentage increase/decrease represents the difference between the proppant concentration received at the perforation clusters and the injected/actual proppant concentration, divided by the injected/actual proppant concentration.

6.4.1.1 Flow Velocity of 6.4 ft/s

Four experimental tests were conducted on 20/40 ULW ceramic at a velocity of 6.4 ft/s and at injected proppant concentrations of 0.3, 0.72, 1.14 and 1.8 ppg as illustrated in Figure 6.10. Since the specific gravity is relatively low, proppant particles tend to suspend without difficulty in the fluid column, causing the proppant distribution to be mostly uniform. At concentrations of 0.3, 0.72 and 1.14, there was even distribution of proppant between the first and second clusters. At an injected concentration of 1.8, the highest proppant concentration was received at the second cluster followed by the third cluster. This implies that the bigger particles in the fluid can create a significant change in the proppant distribution where more concentration occurs lower in the pipe bottom. Therefore, highly uneven proppant distribution was observed between the perforation clusters.

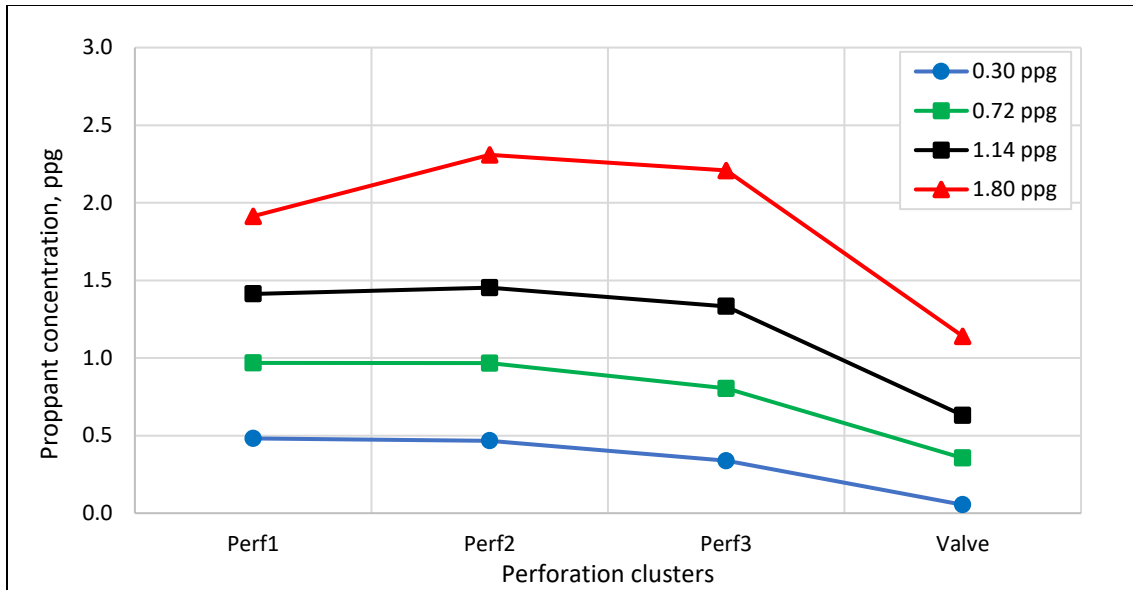


Figure 6.10: Proppant distribution between the perforation clusters for 20/40 ULW ceramic at slurry velocity of 6.4 ft/s and injected proppant concentrations of 0.3, 0.72, 1.14 and 1.80 ppg.

The proppant distribution (PD) across each of the perforation clusters was also determined, and the results are shown in Table 6.16. As can be noted from Table 6.16, the highest proppant distribution (PD) across the perforation clusters at the flow velocity of 6.4 ft/s is 76.8% at a concentration of 1.18 ppg, whereas the lowest PD is 48.78% at a concentration of 0.3 ppg. This indicates that proppant concentration has an effect on the PD, and if the proppant concentration increases, the PD between the perforation clusters increases and vice versa.

Table 6.16: Proppant distribution and the percentage increase/decrease for 20/40 ULW ceramic at a slurry velocity of 6.4 ft/s and injected proppant concentrations of 0.3, 0.72, 1.14 and 1.8 ppg

Concentration, ppg	Percentage Increase/Decrease, %				Absolute Value of Percentage, %			
	0.30	0.72	1.14	1.80	0.30	0.72	1.14	1.80
Perf1	58.225	33.099	23.622	5.892	58.225	33.099	23.622	5.892
Perf2	53.423	32.933	27.099	27.777	53.423	32.933	27.099	27.777
Perf3	11.014	10.488	16.581	22.173	11.014	10.488	16.581	22.173
Valve	-82.208	-51.203	-44.898	-36.910	82.208	51.203	44.898	36.910
	Average of Percentage, %				51.217	31.931	28.050	23.188
	Proppant Distribution (PD), %				48.783	68.069	71.950	76.812

6.4.1.2 Flow Velocity of 11.0 ft/s

Four injected proppant concentrations were used to study the effect of proppant concentration on the PD. The proppant distribution was determined at each perforation cluster for each test. Figure 6.11 shows the proppant distribution between the perforation clusters at a slurry

velocity of 11.0 ft/s and proppant concentrations of 0.21, 0.7, 0.94 and 1.3 ppg. From the four plotted concentrations, the proppant concentration received at the third cluster was higher than the proppant concentration received at the first and the second clusters.

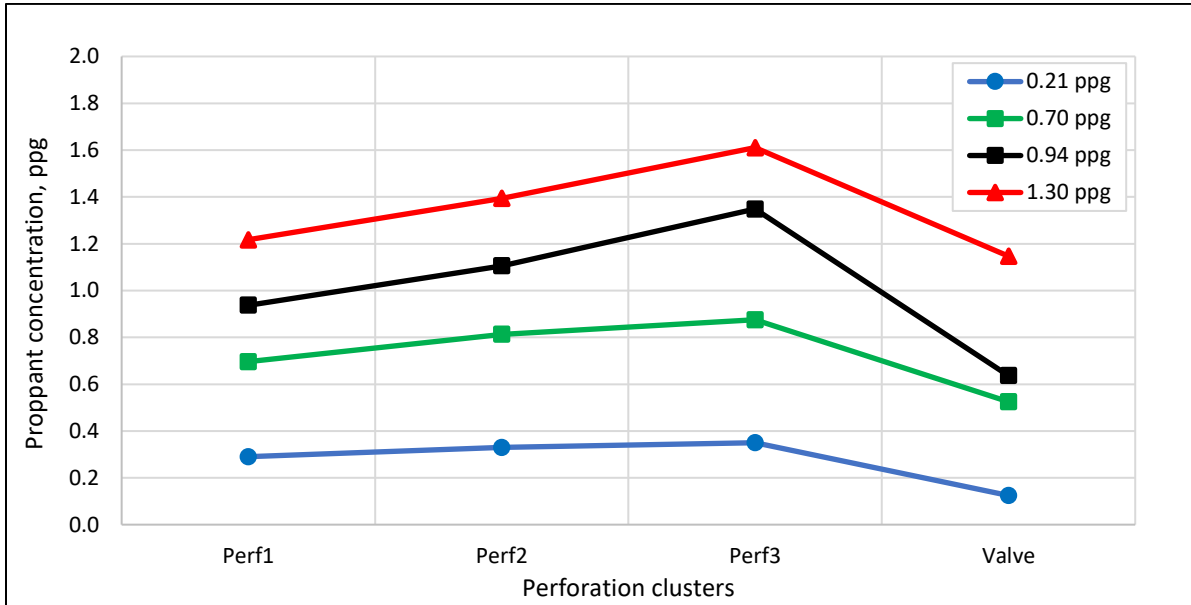


Figure 6.11: Proppant distribution between the perforation clusters for 20/40 ULW ceramic sand at a slurry velocity of 11.0 ft/s and proppant concentrations of 0.21, 0.7, 0.94 and 1.3 ppg.

The percentage increase/decrease and the PD for the slurry velocity of 11.0 ft/s at each experimental run were calculated, and the results are shown in Table 6.17. The PD at a concentration of 0.21 was determined to be 62.61%, whereas the PD at a concentration of 1.3 was calculated to be 87.76%. The increase in concentration proportionally affects the proppant distribution between the perforation clusters. Also, the significance of increasing the fluid velocity from 6.4 to 11.0 ft/s is shown to have a significant effect on the PD. The resulting PD by the 20/40 ULW ceramic slurry is attributed to its relatively light weight, making it easier for the fluid to transport it.

Table 6.17: Proppant distribution and the percentage increase/decrease for 20/40 ULW ceramic at slurry velocity of 11.0 ft/s and injected proppant concentrations of 0.21, 0.7, 0.94 and 1.3 ppg

Concentration, ppg	Percentage Increase/Decrease, %				Absolute Value of Percentage, %			
	0.21	0.70	0.94	1.30	0.21	0.70	0.94	1.30
Perf1	36.681	0.357	-0.790	-7.102	36.681	0.357	0.790	7.102
Perf2	55.508	17.300	17.045	6.430	55.508	17.300	17.045	6.430
Perf3	-16.119	26.269	42.721	22.952	16.119	26.269	42.721	22.952
Valve	-41.265	-24.274	-32.642	-12.455	41.265	24.274	32.642	12.455
	Average of Percentage, %				37.393	17.050	23.300	12.235
	Proppant Distribution (PD), %				62.607	82.950	76.700	87.765

6.4.1.3 Flow Velocity of 13.7 ft/s

Sets of experimental tests were also performed at wide range of proppant concentrations at the slurry velocity of 13.7 ft/s as presented in Figure 6.12. Similar results were seen at velocity of 13.7 ft/s, where more proppant particles were received at the third cluster. In this case, the flow rate was typically high, therefore, particles were not able to turn easily into the first and second clusters. However, when the slurry passed the second cluster, the fluid velocity decreased. The reduction in the velocity caused the particles to settle down on the bottom of the horizontal pipe, hence the concentration at the toe cluster was higher than the concentration at the first and the second clusters.

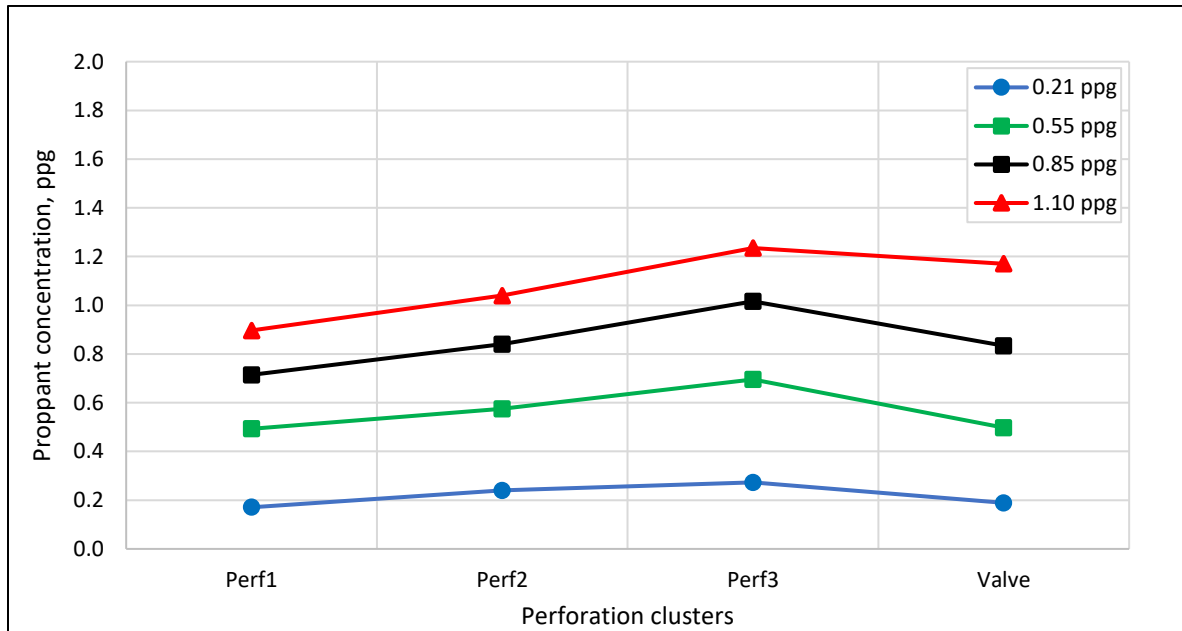


Figure 6.12: Proppant distribution between the perforation clusters for 20/40 ULW ceramic at a slurry velocity of 13.7 ft/s and injected proppant concentrations of 0.21, 0.55, 0.85 and 1.1 ppg.

A comparison of PD levels for different proppant concentrations at the slurry velocity of 13.7 ft/s is presented in Table 6.18. It can be seen the PD levels are higher for the four proppant concentrations when compared to flow velocities of 6.4 ft/s and 11.0 ft/s. The average PD level increased by 20.87% when compared to the velocity of 6.4 ft/s and by 9.76% when compared to the velocity of 11.0 ft/s. This indicates that the increase in the slurry velocity leads to higher PD levels between the perforation clusters.

Table 6.18: Proppant distribution and the percentage increase/decrease for 20/40 ULW ceramic at a slurry velocity of 11 ft/s and proppant concentrations of 0.21, 0.55, 0.85 and 1.1 ppg

Concentration, ppg	Percentage Increase/Decrease, %				Absolute Value of Percentage, %			
	0.21	0.55	0.85	1.10	0.21	0.55	0.85	1.10
Perf1	-19.547	-10.662	-15.748	-18.710	19.547	10.662	15.748	18.710
Perf2	12.991	4.189	-0.884	-5.734	12.991	4.189	0.884	5.734
Perf3	28.586	26.046	19.824	11.941	28.586	26.046	19.824	11.941
Valve	-11.137	-9.854	-1.694	6.134	11.137	9.854	1.694	6.134
	Average of Percentage, %				18.066	12.688	9.538	10.630
	Proppant Distribution (PD), %				81.934	87.312	90.462	89.370

6.4.2 Correlation Development for 20/40 ULW Ceramic

An experimental correlation for 20/40 ULW ceramic was also developed by determining all the dimensionless terms in Equation 6.37. Table 6.19 shows the proppant distribution as well as the dimensionless terms for each experimental test at flow velocities of 6.4, 11.0 and 13.7 ft/s.

Table 6.19: Proppant distribution and the associated dimensionless terms for each test for 20/40 ULW ceramic

Velocity, ft/s	Concentration, ppg	PD	$\frac{\rho_p}{\rho_f}$	$\frac{\mu_f D}{\rho_f \eta}$	$\frac{C_p}{\rho_f}$	$\frac{P_d}{D}$
6.4	0.30	0.488	2.0	1.72107E-05	0.03595	0.016711
	0.73	0.681	2.0	1.72107E-05	0.08747	0.016711
	1.14	0.719	2.0	1.72107E-05	0.13660	0.016711
	1.81	0.768	2.0	1.72107E-05	0.21689	0.016711
11.0	0.21	0.626	2.0	1.00396E-05	0.02516	0.016711
	0.69	0.830	2.0	1.00396E-05	0.08268	0.016711
	0.94	0.767	2.0	1.00396E-05	0.11264	0.016711
	1.31	0.878	2.0	1.00396E-05	0.15697	0.016711
13.7	0.21	0.819	2.0	8.03168E-06	0.02516	0.016711
	0.55	0.873	2.0	8.03168E-06	0.06590	0.016711
	0.85	0.905	2.0	8.03168E-06	0.10185	0.016711
	1.10	0.894	2.0	8.03168E-06	0.13181	0.016711

In order to determine the experimental correlations for 20/40 ULW ceramic, the results presented in Table 6.19 were investigated in two ways. First, the PD was plotted against the dimensionless term (C_p/ρ_f) to develop an experimental correlation for each flow velocity, and second, the three velocity values were involved in developing the experimental correlation for 20/40 ULW ceramic.

Figure 6.13 shows the proppant distribution versus the dimensionless term (C_p/ρ_f) for velocities of 6.4, 11.0, and 13.7 ft/s. The power law trends for 20/40 ULW ceramic are also comparable to the ones obtained for 20/40 and 40/70 mesh sand and they show that proppant concentration has a significant effect on the PD. Also, the slope value of the power law equations can reflect the magnitude of change in the dependent variable (PD) based on the change of the independent variable (proppant concentration). If the slope of the power law equation is high, the effect of the concentration on the proppant distribution is substantial.

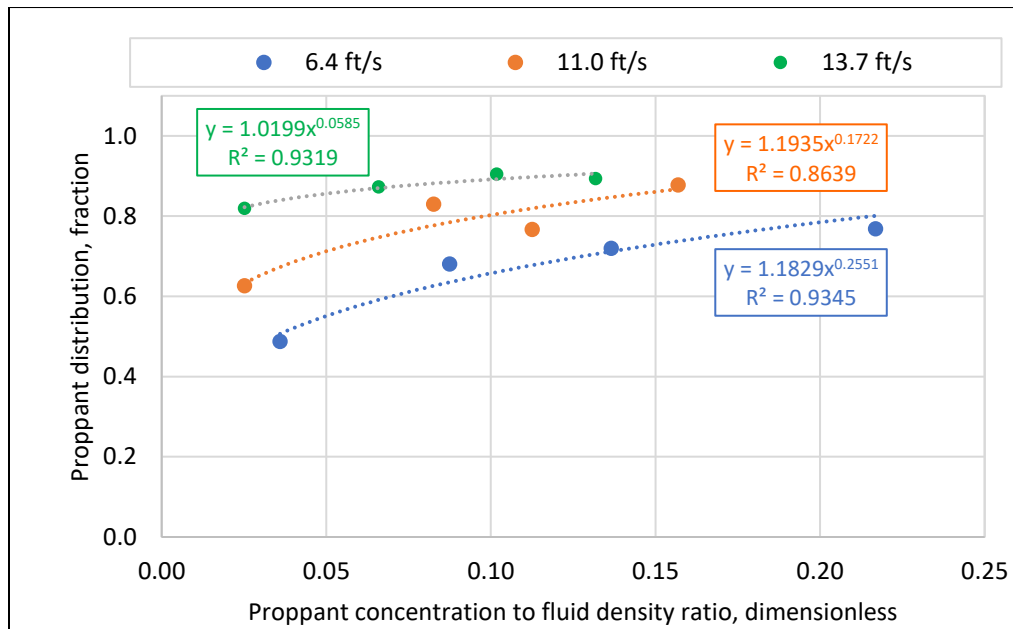


Figure 6.13: Proppant distribution as function of proppant concentration to fluid density ratio for 20/40 ULW ceramic at flow velocities of 6.4, 11.0 and 13.7 ft/s.

The resulting power law equations associated with the R^2 values that are presented in Table 6.20 can be used for any proppant concentration for 20/40 ULW ceramic. As mentioned in previous sections, the equations have the proppant concentration variable in the numerator depicting its effect on the proppant distribution between the perforation clusters.

Table 6.20: Power law equations and R² values at different slurry velocities for 20/40 ULW ceramic

Flow Velocity, ft/s	Developed Correlations	R ²
4.6	PD = 1.1829(C _p /ρ _f) ^{0.2551}	0.93
11.0	PD = 1.1935(C _p /ρ _f) ^{0.1722}	0.86
13.7	PD = 1.0199(C _p /ρ _f) ^{0.0585}	0.93

The second way of determining the experimental correlation was to involve the three values of the tested velocities. Therefore, a multivariable linear regression in Excel solver was also used to develop Equation 6.41 with an R² value of 0.91. The developed correlation has the proppant concentration in the numerator and the slurry velocity variable in the denominator and illustrate their effects on proppant distribution. Therefore, the resulting correlation (Equation 6.41) can be utilized for any proppant concentrations and any slurry velocity for 20/40 ULW ceramic.

$$PD = 0.946 - 26194.505 \left(\frac{\mu_f D}{\rho_f q} \right) + 1.358 \left(\frac{C_p}{\rho_f} \right) \quad (6.41)$$

6.5 40/70 Ultra-Light Weight Ceramic

Sets of experimental runs were also conducted using 40/70 ultra-light weight (ULW) ceramic. The specific gravity of the 40/70 ULW ceramic is 2.0 which is 24.53% less than the specific gravity of the sand of 2.65. In addition, the median diameter of the 40/70 mesh of 0.350 mm which is 40% smaller than the median diameter of the 20/40 mesh. One more time, three slurry velocities were used to evaluate the effect of slurry velocity on proppant distribution between the perforation clusters as shown in Table 6.21.

Table 6.21: Fluid and the proppant properties for 40/70 ULW ceramic at slurry velocities of 6.4, 11.0 and 13.7 ft/s

Velocity, ft/s	Velocity, m/s	Fluid Density, kg/m ³	Fluid Viscosity, kg/m/s	Proppant Density, kg/m ³	Proppant Size, mm	Pipe Diameter, m	Re, unitless
6.4	1.948	1000	0.001	2000	0.350	0.038	74,017
11.0	3.339	1000	0.001	2000	0.350	0.038	126,886
13.7	4.174	1000	0.001	2000	0.350	0.038	158,608

6.5.1 Proppant Distribution Determination

The proppant distribution (PD) was determined by calculating the percentage increase/decrease at each experimental. The percentage increase/decrease represents the difference between the proppant concentration received at the perforation clusters and the injected/actual proppant concentration, divided by the injected/actual proppant concentration.

6.5.1.1 Flow Velocity of 6.4 ft/s

A total of four experimental tests were conducted on 40/70 ULW ceramic at a velocity of 6.4 ft/s using four different proppant concentrations. The proppant concentration at each cluster was determined at injected proppant concentrations of 0.46, 1.08, 1.64 and 2.2 ppg as demonstrated in Figure 6.14. Since the proppant size and the specific gravity are relatively low, particles tend to distribute uniformly in the fluid column, and as a result, the proppant distribution among the perforation clusters was mostly even. More specifically, at concentrations of 0.46 and 1.08 ppg, strong even proppant distribution was achieved between the perforation clusters. At concentrations of 1.64 and 2.2 ppg, there was a slight increase in the proppant concentration towards the second cluster followed by the third cluster.

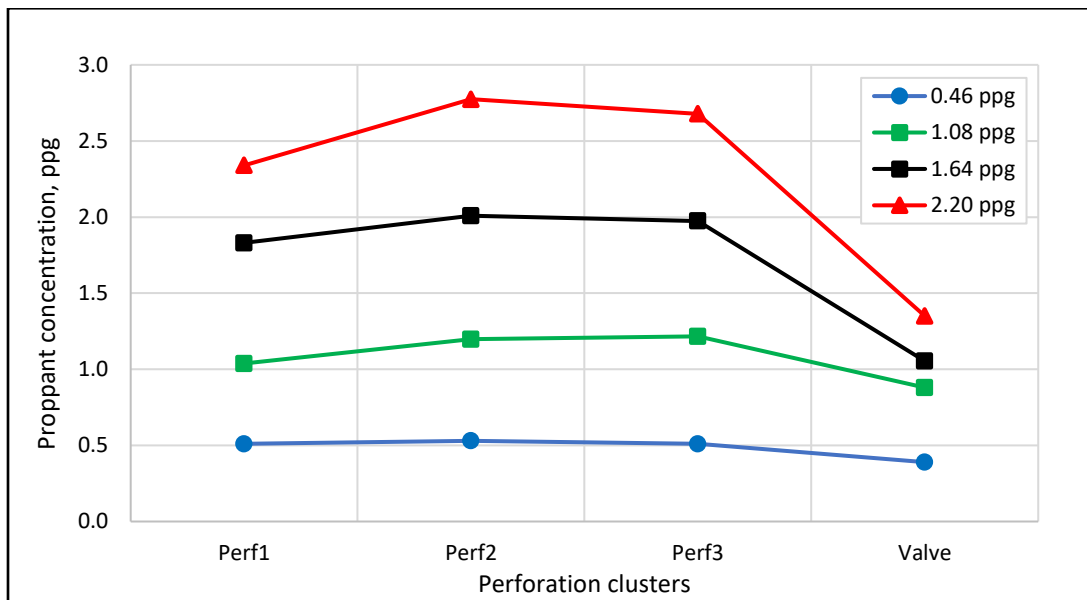


Figure 6.14: Proppant distribution between the perforation clusters for 40/70 ULW ceramic at a slurry velocity of 6.4 ft/s and injected proppant concentrations of 0.46, 1.08, 1.64 and 2.2 ppg.

Table 6.22 shows the proppant distribution (PD) and the percentage increase/decrease at each proppant concentration at a slurry velocity of 6.4 ft/s. It can be noted from Table 6.22, the highest PD was recorded at a concentration of 1.08 ppg, whereas the lowest PD level was determined at a concentration of 2.2 ppg. This implies that at a low slurry velocity, the increase in the proppant concentration may not have a significant impact on the proppant distribution between the perforation clusters.

Table 6.22: Proppant distribution and the percentage increase/decrease for 40/70 ULW ceramic at a slurry velocity of 6.4 ft/s and injected proppant concentrations of 0.46, 1.08, 1.64 and 2.2 ppg

Concentration, ppg	Percentage Increase/Decrease, %				Absolute Value of Percentage, %			
	0.46	1.08	1.64	2.20	0.46	1.08	1.64	2.20
Perf1	10.072	-4.153	11.445	6.147	10.072	4.153	11.445	6.147
Perf2	14.388	10.592	22.305	25.852	14.388	10.592	22.305	25.852
Perf3	10.072	12.346	20.224	21.488	10.072	12.346	20.224	21.488
Valve	-24.460	-12.263	-35.819	-38.768	24.460	12.263	35.819	38.768
Average of Percentage, %					14.748	9.839	22.448	23.064
Proppant Distribution (PD), %					85.252	90.161	77.552	76.936

6.5.1.2 Flow Velocity of 11.0 ft/s

In this section, four injected proppant concentrations were also used to evaluate the effect of the concentration on the PD. The proppant concentration was determined at each perforation cluster for each test. Figure 6.15 shows the proppant distribution between the perforation clusters at a slurry velocity of 11.0 ft/s and injected proppant concentrations of 0.39, 0.94, 1.25 and 2.1 ppg. At the fluid velocity of 11.0 ft/s, the proppant distribution was mostly even between the perforation clusters at injected concentrations of 0.39, 0.94 and 1.25 ppg. However, there was a slightly uneven distribution at the concentration of 2.1 ppg, where more proppant was measured at the third cluster.

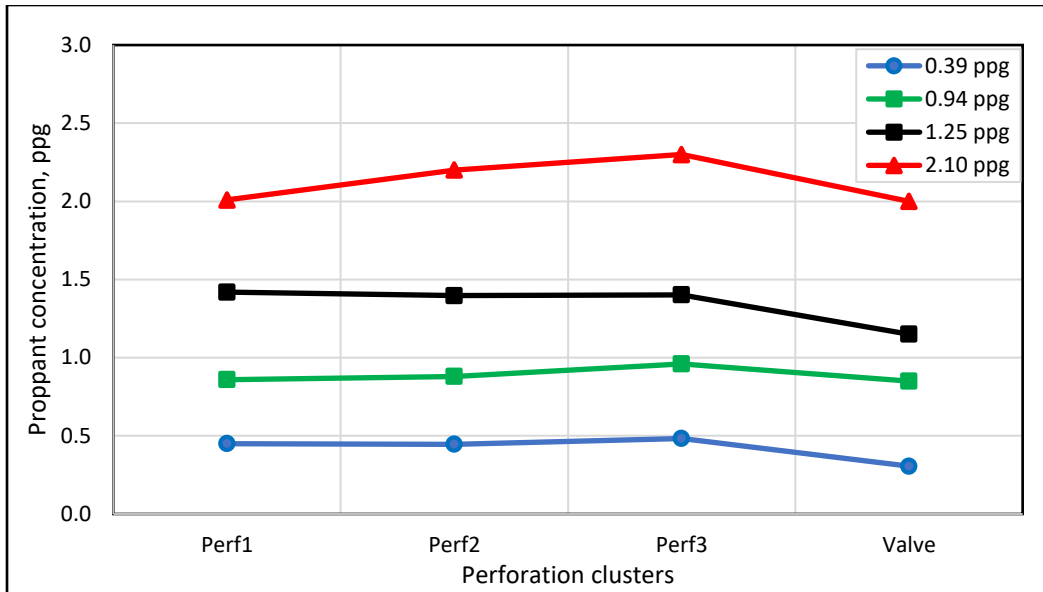


Figure 6.15: Proppant distribution between the perforation clusters for 40/70 ULW ceramic at a slurry velocity of 11.0 ft/s and injected proppant concentrations of 0.39, 0.94, 1.25 and 2.1 ppg.

The PD was also determined from the percentage increase/decrease as described in previous sections. Table 6.23 shows the proppant distribution and the percentage increase/decrease for 40/70 ULW ceramic at a slurry velocity of 11.0 ft/s and proppant concentrations of 0.39, 0.94, 1.25 and 2.1 ppg. It can be noted from the table, that when the slurry velocity increased from 6.4 to 11 ft/s, the average PD level was increased by 7.03%. The resulting PDs verify previous findings that when the slurry velocity increases, the PD between the perforation clusters also increases.

Table 6.23: Proppant distribution and the percentage increase/decrease for 40/70 ULW ceramic at a slurry velocity of 11.0 ft/s and injected proppant concentrations of 0.39, 0.94, 1.25 and 2.1 ppg

Concentration, ppg	Percentage Increase/Decrease, %				Absolute Value of Percentage, %			
	0.39	0.94	1.25	2.10	0.39	0.94	1.25	2.10
Perf1	14.270	-8.771	13.364	-4.398	14.270	8.771	13.364	4.398
Perf2	13.326	-6.650	11.544	4.666	13.326	6.650	11.544	4.666
Perf3	22.596	1.837	11.938	9.423	22.596	1.837	11.938	9.423
Valve	-22.319	-9.832	-8.158	-4.849	22.319	9.832	8.158	4.849
	Average of percentage, %				18.128	6.772	11.251	5.834
	Proppant Distribution (PD), %				81.872	93.228	88.749	94.166

6.5.1.3 Flow Velocity of 13.7 ft/s

Four experimental runs were also conducted at a flow velocity of 13.7 ft/s, and the resulting proppant concentrations for each test was plotted as shown in Figure 6.16. The four plotted concentrations in the figure confirm earlier findings at a velocity of 11.0 ft/s for 40/70 ULW ceramic. The proppant distribution among the perforations was mostly even for the four conducted tests. However, there was a little increase of proppant at the third cluster. The reduction in the density and the particle size appear to play a significant role in transporting the proppant into the induced fractures.

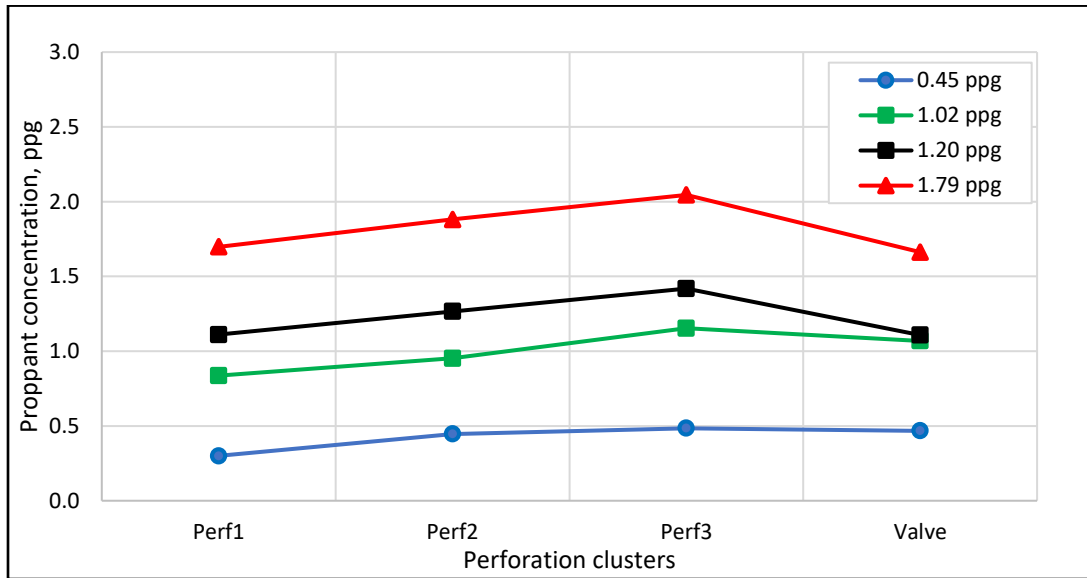


Figure 6.16: Proppant distribution between the perforation clusters for 40/70 ULW ceramic at a slurry velocity of 13.7 ft/s and injected proppant concentrations of 0.45, 1.02, 1.2 and 1.8 ppg.

The percentage increase/decrease and the PD for each test were also determined, and the resulting data are shown in Table 6.24. The same PD behavior was also observed at a velocity of 13.7 ft/s, but the PD was increased slightly when there was an increase in the proppant concentration. For example, the PD at the proppant concentration of 0.45 ppg was determined to be 88.58%, and at the proppant concentration of 1.8 ppg was determined to be 92.1%. This indicates that the increase in the proppant concentration has mostly a negligible effect on the PD for 40/70 ULW ceramic.

Table 6.24: Proppant distribution and percentages increase/decrease for 40/70 ULW ceramic at a slurry velocity of 13.7 ft/s and injected proppant concentrations of 0.45, 1.02, 1.2 and 1.80 ppg

Concentration, ppg	Percentage Increase/Decrease, %				Absolute Value of Percentage, %			
	0.45	1.02	1.20	1.80	0.45	1.02	1.20	1.80
Perf1	-33.342	-17.680	-7.620	-5.139	33.342	17.680	7.620	5.139
Perf2	-0.916	-6.350	5.260	5.092	0.916	6.350	5.260	5.092
Perf3	7.549	13.512	17.995	14.239	7.549	13.512	17.995	14.239
Valve	3.872	5.149	-7.865	-7.128	3.872	5.149	7.865	7.128
Average of Percentage, %					11.420	10.673	9.685	7.900
Proppant Distribution (PD), %					88.580	89.327	90.315	92.100

6.5.2 Correlation Development for 40/70 ULW ceramic

For the purpose of developing the experimental correlation for 40/70 ULW ceramic, the dimensionless terms in Equation 6.37 were determined for each flow velocity and proppant concentration. Table 6.25 shows the proppant distribution and the dimensionless terms for each experimental test at velocities of 6.4, 11.0 and 13.7 ft/s.

Table 6.25: Proppant distribution and the associated dimensionless terms for each test for 40/70 ULW ceramic

Velocity, ft/s	Concentration, ppg	PD	$\frac{\rho_p}{\rho_f}$	$\frac{\mu_f D}{\rho_f Q}$	$\frac{C_p}{\rho_f}$	$\frac{P_d}{D}$
6.4	0.46	0.853	2.0	1.72107E-05	0.05512	0.01002632
	1.08	0.902	2.0	1.72107E-05	0.12941	0.01002632
	1.64	0.776	2.0	1.72107E-05	0.19652	0.01002632
	2.20	0.769	2.0	1.72107E-05	0.26362	0.01002632
11.0	0.39	0.819	2.0	1.00396E-05	0.04673	0.01002632
	0.94	0.932	2.0	1.00396E-05	0.11264	0.01002632
	1.25	0.887	2.0	1.00396E-05	0.14978	0.01002632
	2.10	0.942	2.0	1.00396E-05	0.25164	0.01002632
13.7	0.45	0.886	2.0	8.03168E-06	0.05392	0.01002632
	1.02	0.893	2.0	8.03168E-06	0.12222	0.01002632
	1.20	0.903	2.0	8.03168E-06	0.14379	0.01002632
	1.79	0.921	2.0	8.03168E-06	0.21449	0.01002632

Figure 6.17 shows the proppant distribution versus the dimensionless term (C_p/ρ_f) for velocities of 6.4, 11.0, and 13.7 ft/s. The slope of the fitted power law equation at a flow velocity of 6.4 ft/s is negative which indicates that there is a certain proppant concentration where beyond it, increasing proppant concentration has an almost negative effect on proppant distribution. In

contrast, the slope of the fitted power law equations is positive for velocities of 11.0 and 13.7 ft/s. The resulting trends for both velocities indicate that proppant distribution is considerably affected by proppant concentration. In other words, the PD can be improved by an increase in the proppant concentration at higher slurry velocities.

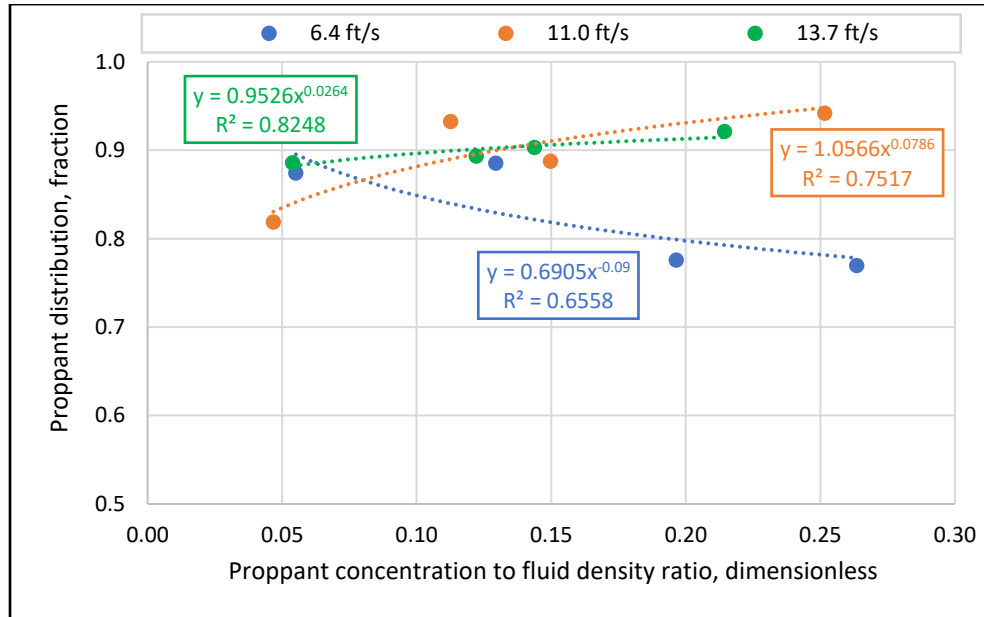


Figure 6.17: Proppant distribution as function of proppant concentration to fluid density ratio for 40/70 ULW ceramic at flow velocities of 6.4, 11.0 and 13.7 ft/s.

The resulting power law correlations for all conducted tests for 40/70 ULW ceramic showed R^2 values ranging from 0.66 to 0.82 as shown in Table 6.26. The developed correlations in this section predict the PD as a function of proppant concentration. The proppant concentration variable is in the numerator, illustrating its effect on the proppant distribution between the perforation clusters. Therefore, the use of these correlations is restricted to a certain slurry condition that has to match the fluid velocities that have been used in this study.

Table 6.26: Power law equations and R^2 values for different slurry velocities for 40/70 ULW ceramic

Flow Velocity, ft/s	Developed correlations	R^2
6.4	$PD = 0.6905(C_p/\rho_f)^{-0.09}$	0.66
11.0	$PD = 1.0566(C_p/\rho_f)^{0.0786}$	0.75
13.7	$PD = 0.9526(C_p/\rho_f)^{0.0264}$	0.82

The second step for determining the experimental correlation was to involve the three velocity values so that the final correlation for 40/70 ULW ceramic can be developed. Multivariable linear regression was used in a Microsoft Excel Solver to develop Equation 6.12. Therefore, the resulting correlation (Equation 6.42) with an R^2 value of 0.77 can be used to predict the proppant distribution between the perforation clusters at any proppant concentration and slurry velocity for 40/70 ULW ceramic.

$$PD = 1.050 - 23339.950 \left(\frac{\mu_f D}{\rho_f q} \right) + 0.495 \left(\frac{C_p}{\rho_f} \right) \quad (6.42)$$

6.6 Correlation Development for 20/40 and 40/70 ULW Ceramic

In this section, all the results for the dimensionless terms for 20/40 and 40/70 ULW ceramic were combined to form Equation 6.43. The values of the constants in the equation and the R^2 value were also established by utilizing the multivariable linear regression. The R^2 of the regression is 0.61, which is not relatively high. The resulting correlation has the flow rate term in the denominator with a negative constant value. This indicates that when the fluid velocity increases, the PD between the perforation clusters also increases. In addition, the concentration term is placed as a numerator term, which implies as proppant concentration increases, the PD between the perforation clusters also increases.

$$PD = 1.119 - 16312.818 \left(\frac{\mu_f D}{\rho_f q} \right) + 0.473 \left(\frac{C_p}{\rho_f} \right) - 12.161 \left(\frac{P_d}{D} \right) \quad (6.43)$$

The developed correlation for the PD shown in Equation 6.43 was tested against the actual PD as illustrated in Figure 6.18. Although the R^2 value is 0.61, a good match is observed between the predicted PD from the model and the actual PD in the lab at velocities of 11.0 and 13.7 ft/s. However, at a velocity of 6.4 ft/s, there is divergence between the predicted and the actual PD for both 20/40 and 40/70 ULW ceramic. This implies that this model (Equation 6.13) can be valid for predicting the PD between the perforation clusters at relatively high fluid velocities and a wide range of proppant concentrations, but likely not as beneficial at lower velocities.

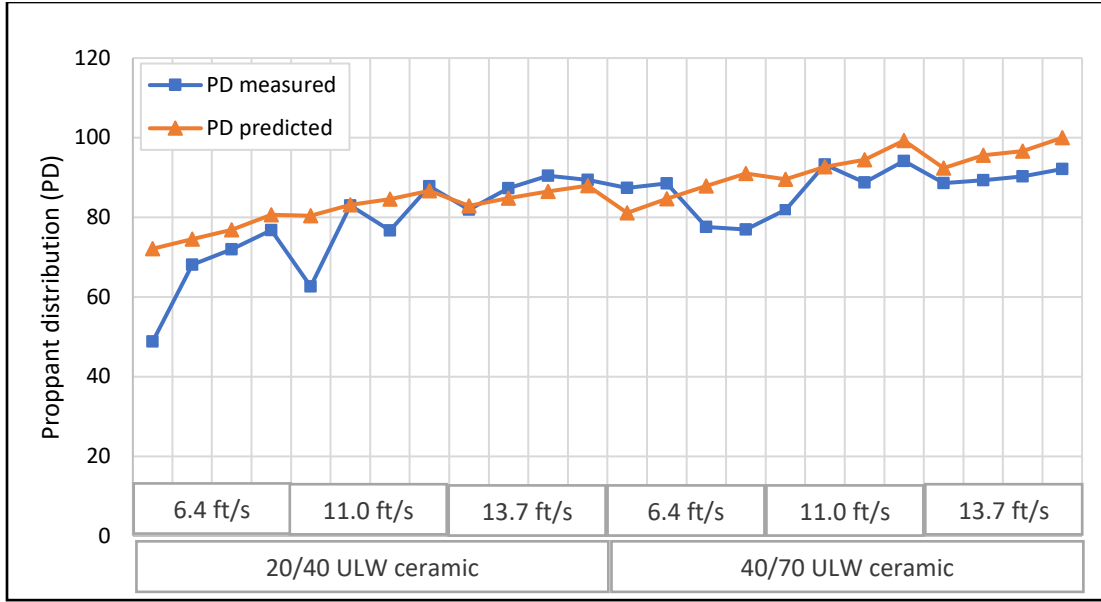


Figure 6.18: The predicted and the measured PD for 20/40 and 40/70 ULW ceramic.

6.7 Correlation Development for Sand and Ultra-light Weight Ceramic

In this section, all the obtained results for the dimensionless terms in Equation 6.37 for 20/40 and 40/70 white sand and ULW ceramic were combined to form Equation 6.44. As mentioned previously, the values of the constants in the equation as well as the R^2 value were developed by utilizing the multivariable linear regression in Excel Solver. The R^2 value of the regression is 0.79, which is reliable, and indicates that 79% of the variability of the dependent variables has been considered for determining the developed correlation. Therefore, the correlation that is shown in Equation 6.44 can be used to predict the proppant distribution between the perforation clusters for any flow rate and proppant concentration.

$$PD = 1.746 - 0.220 \left(\frac{\rho_p}{\rho_f} \right) - 30453 \left(\frac{\mu_f D}{\rho_f q} \right) + 0.948 \left(\frac{C_p}{\rho_f} \right) - 18.094 \left(\frac{P_d}{D} \right) \quad (6.44)$$

Where,

μ_f = Fluid viscosity, kg/m/s

D = Pipe diameter, m

ρ_f = Fluid density, kg/m³

ρ_p = Particle density, kg/m³

q = Flow rate, m³/s

C_p = Proppant concentration, kg/m³

P_d = Median particle diameter, m

The variables that can be changed in the final correlation (Equation 6.44) are: proppant density, flow rate, proppant concentration, and proppant median diameter. The proppant density variable as a numerator term with a negative constant value, which indicates that the increase in the specific gravity of the proppant leads to a reduction in the PD. The flow rate in the denominator term has a negative constant value which implies that the increase in the slurry velocity of the proppant leads to an increase in the PD. Also, the correlation has the proppant concentration as a numerator term, which indicates as the proppant concentration increases, the PD between the perforation clusters also increases. In addition, the median proppant diameter term is shown in the equation as a numerator term with a negative constant value, which indicates as the median proppant diameter increases, the PD between the perforation clusters decreases.

6.8 Correlation Analysis

In this section, the accuracy of the developed PD correlation was assessed and compared with the actual PD. The first step for the accuracy analysis was to plot the predicted PD from the model with the actual PD for all the tests and observe if there was a good match between the two values. The second step was to calculate the error of the predicted values relative to the actual PD values using Equation 6.45. The correlation percent error can be defined as the absolute value of the difference between the predicted and actual PD divided by the actual PD and multiplied by 100.

$$\text{Percent error} = \left(\left| \frac{PD_{\text{Lab}} - PD_{\text{Pred.}}}{PD_{\text{Lab}}} \right| \right) \times 100 \quad (6.45)$$

Where,

PD_{Lab} = Lab measured PD, %

$PD_{\text{Pred.}}$ = Correlation predicted PD, %

6.8.1 20/40 Mesh White Sand

The predicted PD from the model was plotted with the actual PD at different injected proppant concentrations as shown in Figure 6.19. Also, the percent error was calculated for each velocity over a wide range of proppant concentrations. Equation 6.45 was used to calculate the error of the predicted values of the correlation. Table 6.27 shows the predicted PD values and their calculated errors for the 20/40 mesh white sand. As can be observed from Figure 6.19, the

predicted PD was higher than the actual PD at a velocity of 6.4 ft/s, with an average error value of 95.64%. Whereas at the velocities of 11.0 and 13.7 ft/s, a good match was observed between the predicted PD and the actual PD. The average calculated error values were 13.6% and 9.95%, respectively. The low error values at higher fluid velocities show high reliability of the developed correlation in predicting the proppant concentration (PD) between the perforation clusters under these conditions.

Table 6.27: The predicted PD values and their calculated error values for 20/40 mesh white sand

Velocity, ft/s	Concentration, ppg	PD, %		Error, %	
		Actual	Predicted	Value	Average
6.4	0.120	17.018	35.151	106.555	95.64
	0.130	15.810	35.265	123.056	
	0.210	17.391	36.173	108.005	
	0.310	25.740	37.310	44.948	
11.0	0.100	44.515	56.762	27.513	13.60
	0.110	54.748	56.876	3.886	
	0.230	60.837	58.239	4.271	
	0.360	73.489	59.716	18.742	
13.7	0.070	68.792	62.537	9.093	9.95
	0.100	65.541	62.877	4.064	
	0.130	71.101	63.218	11.087	
	0.310	77.286	65.263	15.557	

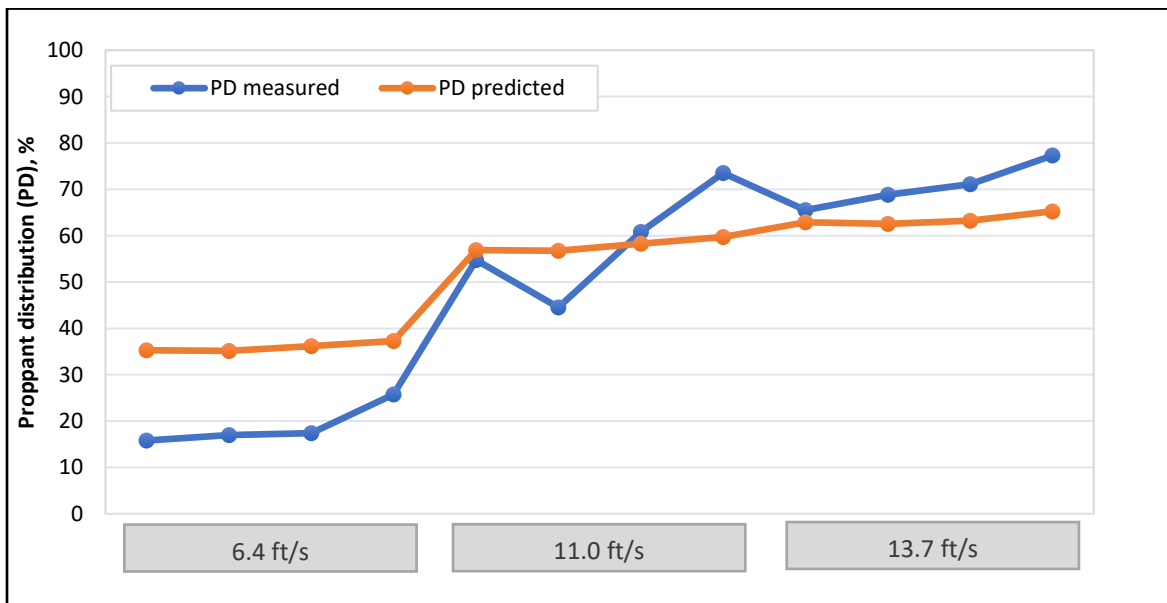


Figure 6.19: The predicted PD from the developed correlation and the measured PD for 20/40 mesh white sand.

6.8.2 40/70 Mesh White Sand

The same error analysis was conducted on the 40/70 mesh sand. Table 6.28 shows the predicted PD values and their calculated errors for three fluid velocities at different proppant concentrations. The predicted PD from the model was also plotted with the actual PD at different injected proppant concentrations as shown in Figure 6.20. The 40/70 mesh white sand at a velocity of 6.4 ft/s shows relatively lower average error value than the 20/40 mesh sand at the same velocity. However, at velocities of 11.0 and 13.7, the 40/70 mesh white sand shows even lower error values than the velocity of 6.4 ft/s. The calculated error values are 4.73% and 4.39%, respectively. The low error values indicate high reliability of the developed correlations in predicting the PD between the perforation clusters and good precision relative to the measured PD.

Table 6.28: The predicted PD values and their calculated error values for 40/70 mesh white sand

Velocity, ft/s	Concentration, ppg	PD, %		Error, %	
		Actual	Predicted	Value	Average
6.4	0.300	47.606	49.290	3.537	13.79
	0.370	42.849	50.086	16.888	
	0.930	70.226	56.445	19.624	
	1.100	68.788	58.376	15.137	
11.0	0.260	69.478	70.674	1.721	4.73
	0.300	68.231	71.129	4.247	
	0.890	82.607	77.829	5.784	
	1.200	87.636	81.349	7.173	
13.7	0.230	79.499	76.448	3.838	4.39
	0.210	81.717	76.221	6.725	
	0.800	84.529	82.922	1.902	
	1.170	91.828	87.124	5.123	

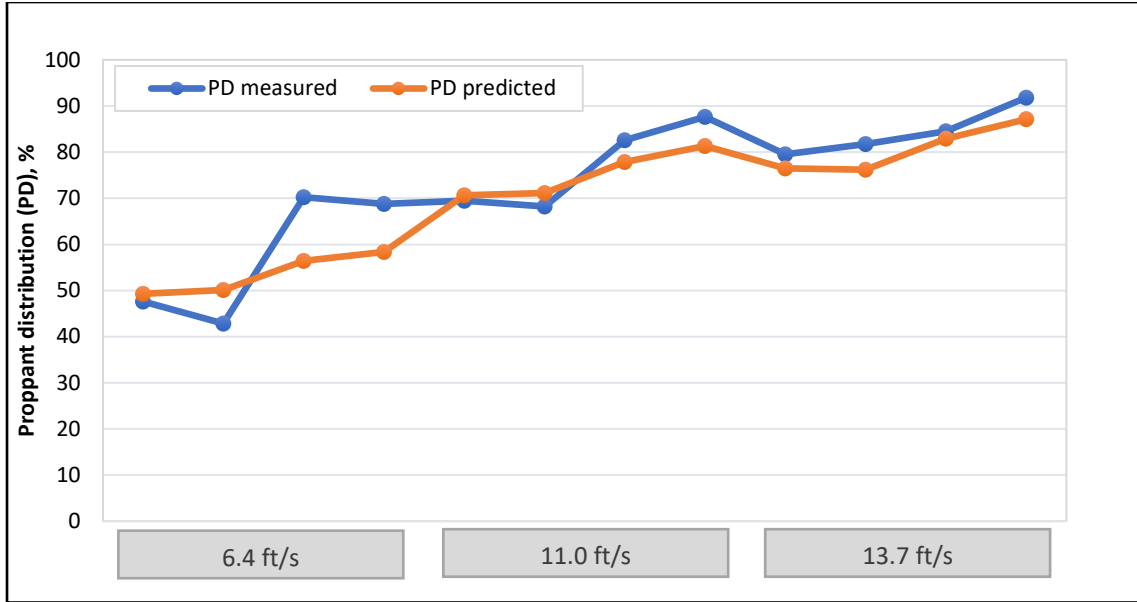


Figure 6.20: The predicted PD from the developed correlation and the actual PD for 40/70 mesh white sand.

6.8.3 20/40 ULW Ceramic

The first step for the accuracy analysis was to plot the predicted PD from the model with the actual PD at different injected proppant concentrations as shown in Figure 6.21. The actual PD is mostly high for all the tests that were conducted on the 20/40 ULW ceramic at the three velocities. Therefore, a good match is observed between the predicted and the actual PD as shown in Figure 6.21. Only at a velocity of 6.4 ft/s, the measured PD is a little higher than the actual PD for concentrations of 0.73, 1.14 and 1.7 ppg. The second step for determining the accuracy of the developed correlation was to calculate the error of the predicted values of the correlation using Equation 6.45. Table 6.29 shows the predicted PD values and their calculated errors for the 20/40 ULW Ceramic. The average calculated error value at a velocity of 6.4 ft/s is 12.15%, whereas at velocities of 11 and 13.7 ft/s is 7.55% and 4.09%, respectively. As mentioned previously, the low error values at the fluid velocities show high reliability of the developed correlations in predicting the proppant concentration (PD) between the perforation clusters for 20/40 ULW ceramic.

Table 6.29: The predicted PD values and their calculated error values for 20/40 ULW ceramic

Velocity, ft/s	Concentration, ppg	PD, %		Error, %	
		Actual	Predicted	Value	Average
6.4	0.30	48.783	51.465	5.499	12.15
	0.73	68.069	56.348	17.220	
	1.14	71.950	61.004	15.213	
	1.80	76.812	68.614	10.673	
11.0	0.21	62.607	72.281	15.453	7.55
	0.70	82.950	77.732	6.290	
	0.94	76.700	80.572	5.048	
	1.31	87.765	84.773	3.409	
13.7	0.21	81.934	78.396	4.319	4.09
	0.55	87.312	82.257	5.790	
	0.85	90.462	85.664	5.304	
	1.10	89.370	88.503	0.970	

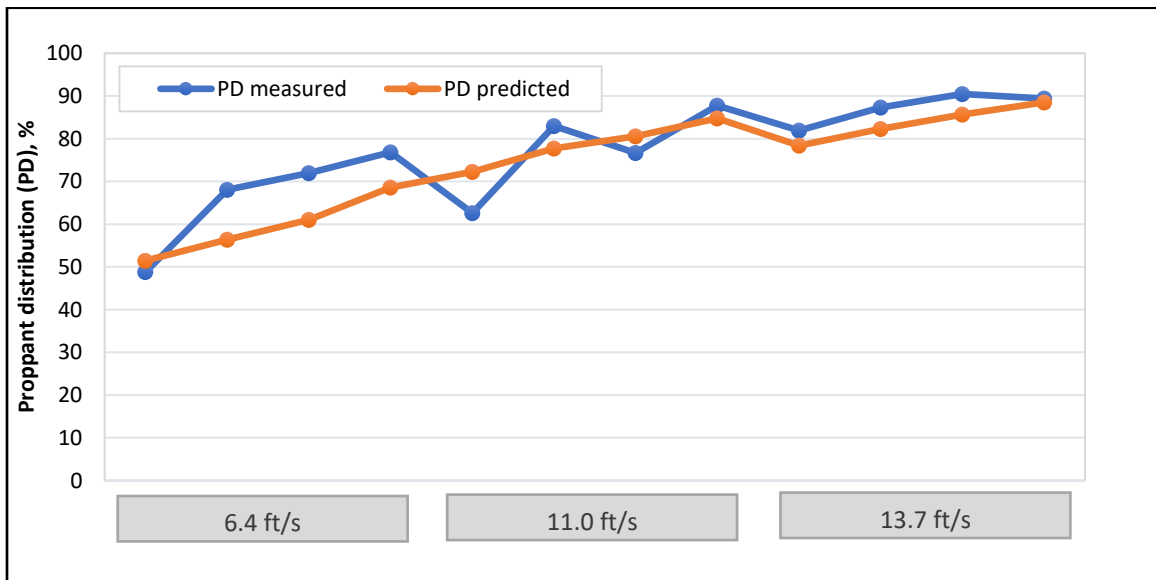


Figure 6.21: The predicted PD from the developed correlation and the measured PD for 20/40 ULW ceramic.

6.8.4 40/70 ULW Ceramic

The 40/70 ULW ceramic has a specific gravity value less than 20/40 mesh white sand. Also, the median diameter of 40/70 ULW ceramic is 0.35 mm which is 40% smaller than the median diameter of 20/40 mesh size proppant of 0.65 mm. Therefore, higher PD values were also expected at the three tested velocities as discussed in Section 6.5. For the correlation analysis purpose, the predicted PD from was plotted with the actual PD at different injected proppant

concentrations as shown in Figure 6.22. The predicted PD values at velocities of 11.0 and 13.7 ft/s are a little higher than the actual PD values. In addition, at these two velocities, the 40/70 ULW ceramic shows a relatively lower average error value than at a velocity of 6.4 ft/s. Again, the low error values for this proppant indicate high reliability of the developed correlations in predicting the PD between the perforation clusters.

Table 6.30: The predicted PD values and their calculated error values for 40/70 ULW ceramic

Velocity, ft/s	Concentration, ppg	PD, %		Error, %	
		Actual	Predicted	Value	Average
6.4	0.46	87.410	65.377	25.207	13.91
	1.08	88.545	72.418	18.214	
	1.64	77.552	78.778	1.582	
	2.20	76.936	85.138	10.660	
11.0	0.39	81.872	86.420	5.555	6.73
	0.94	93.228	92.667	0.602	
	1.25	88.749	96.187	8.381	
	2.10	94.166	105.840	12.398	
13.7	0.45	88.580	93.216	5.233	11.80
	1.01	89.327	99.689	11.600	
	1.20	90.315	101.734	12.643	
	1.79	92.100	108.434	17.735	

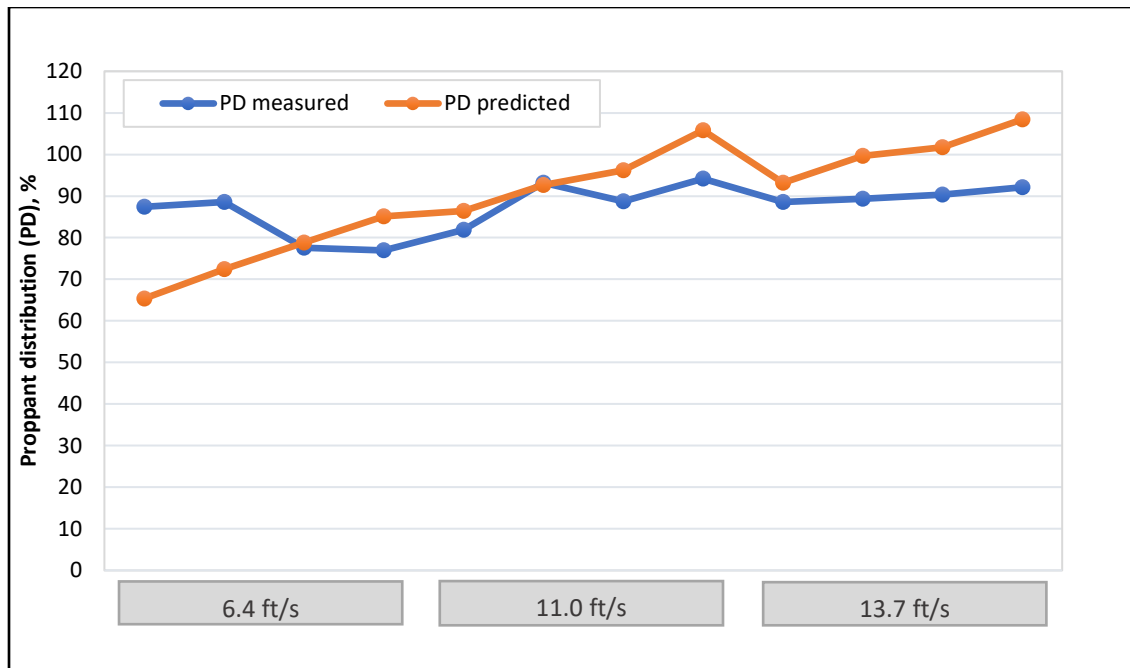


Figure 6.22: The predicted PD from the correlation and the measured PD for 40/70 ULW ceramic.

CHAPTER 7

DISCUSSION OF THE RESULTS

Hydraulic fracturing has become a widely applied technology for stimulating low permeability reservoirs. The reason for stimulating tight formations is to increase recoverable reserves and to accelerate production. This can be established by placing hydraulic fractures in the targeted formations to allow the flow of oil and/or gas from the reservoir to the wellbore. These fractures are created by pumping a fracturing fluid at a high flow rate and then introducing proppant with the fluid to keep the fractures open after the pumping is stopped.

One of the most significant concerns in hydraulic fracturing is the proppant transport and distribution between multiple perforation clusters in multi-stage horizontal wells. Uniform proppant distribution between multiple clusters/fractures can play a significant role in achieving successful hydraulic fracturing treatments. In the past, it was frequently assumed that all the proppant that is injected into a wellbore is distributed evenly between the perforation clusters. Even though the hydraulic fracturing technology has made substantial progress over the last several years, proppant transport and distribution in multiple hydraulic fracture completions is not well understood.

Therefore, it is crucial to ensure that proppant is sufficiently transported both in the wellbore and into the induced fractures. The aim of this research is to investigate the parameters that have a large influence on proppant transport and settling in the horizontal wellbore, as well as distribution of the proppant among multiple perforation clusters. These parameters include, but are not limited to, proppant concentration, injection rate, fluid viscosity, and proppant types and sizes.

This experimental research was divided into three focus areas: (1) proppant transport using fresh water as described in Chapter 4, (2) proppant transport using HLFRR fluids as described in Chapter 5, and (3) experimental correlations development to predict the proppant distribution through perforation clusters as presented and discussed in Chapter 6.

7.1 Discussion of the Results Using Freshwater Fluids

As mentioned in Chapter 4, the main reason for using freshwater fluids without additives was to simulate slickwater fluids. Experiments were carried out on 20/40 and 40/70 mesh sand and ultra-light weight (ULW) ceramic across a wide range of proppant concentrations. Three flow

velocities were used to quantify the proppant distribution and particle concentrations in the wellbore and through multiple perforation clusters.

Before conducting experimental tests using freshwater at the three flow velocities, the minimum/critical transport velocity for each proppant was calculated using Wasp's Modified Durand Equation (Equation 2.3) (Wasp et al. 1970). The results of critical velocity calculations conducted on 20/40 and 40/70 mesh sand and ULW ceramic indicate that the specific gravity of proppant can play a significant role in the settling of the particles in horizontal wellbores. If the specific gravity of the proppant is high, the minimum transport velocity is high and vice versa. Also, the findings indicate that proppant size and proppant concentration can also have a significant effect on the proppant settling. If there is an increase in the particle size or in the proppant concentration, there is also a significant increase in the critical transport velocity. Therefore, for all the tests, the injection rate for the slurry which was pumped into the wellbore was above the critical rate to ensure that no proppant settling would occur during each test.

Higher-density proppant has different transport behavior in horizontal wellbores than lower-density proppant. The higher-density proppant always tends to settle down and concentrate in the lower section of the pipe even at relatively high flow rates. Experiments which were conducted on proppant using fresh water as a carrier fluid indicate that both the 20/40 and 40/70 mesh sand (sp. gr. of 2.65) at a flow velocity of 6.4 ft/s were distributed unevenly in the horizontal wellbore. The gravity forces acting on the fluid (due to particles' weight) were stronger on larger particles than momentum forces, and greater turbulence energy was required to suspend larger particles against gravity. Therefore, highly uneven proppant distribution was observed through the perforation clusters with higher concentration occurring at the first cluster, and lower concentration occurring at the third cluster. According to Biot and Medlin (1985), the transport mechanisms can be described as heterogenous suspension. In addition, there is always a viscous sublayer that exists at the pipe wall. This layer is very thin, and it may hinder the fluid's ability to transport proppant particles that deposited in the bottom of the pipe. However, the particles that are trapped in the viscous sublayer can cause an increase in the density of the carrying fluid, that in turn, increases the viscous shear stress towards the pipe wall. Hence, the particles in this sublayer cannot be transported at low flow velocities.

When the velocity was increased to 11.0 ft/s, the 20/40 mesh sand also showed uneven proppant concentration. The interpretation of the results suggests that the momentum forces near

the first perforation cluster were stronger than the gravity forces and were the main reason for preventing some of proppant particles from turning into the perforations within the first cluster. As fluid traveled in the wellbore and reached the second cluster, the slurry velocity dropped. This reduction in the slurry velocity near the second cluster resulted in an increase in the gravity forces by which larger particles tended to concentrate on the bottom of the pipe. Therefore, particles of proppant were able to turn into the perforation tunnels within the second cluster. As a result, a high proppant concentration was received at the second perforation cluster. After the second cluster, slurry traveled down the wellbore with less proppant concentration; hence, the proppant concentration at the third cluster was less than the proppant concentration at the second cluster.

At the highest flow velocity of 13.7 ft/s, the 20/40 and 40/70 mesh sand showed uneven proppant distribution where high proppant concentration occurred at the third perforation cluster, even though the fluid distribution at each cluster was uniform. This indicates that the momentum forces that act upon the proppant particles with higher-density proppant prevent them from turning into the first and the second perforation clusters. However, in all the high flow rate runs, the eddy currents which were created by the high turbulent flow, were the main reason to transport the proppant particles that were locked in the viscous/laminar sublayers in the horizontal wellbore. Therefore, high flow rates associated with high turbulent flow values are more effective than low flow rates for proppant transport because the diffusive forces on proppant particles are more significant than drag alone to re-suspend the proppant.

The results from the experimental runs conducted on 20/40 and 40/70 ULW ceramic with a specific gravity of 2.0 using fresh water showed fairly uniform proppant distribution across each of the perforation clusters. Since the momentum difference between the fluid and the proppant is relatively small, minimal settling in the horizontal wellbore was observed for all the runs. Even at a much lower flow velocity (the total momentum (mV) is relatively low), the 40/70 ULW ceramic achieved a fairly uniform proppant distribution. This demonstrates that proppant associated with low specific gravity can be transported more effectively than those with high specific gravity in slickwater fluids.

The findings obtained from tests conducted on sand proppant demonstrate that the low viscosity associated with freshwater fluids is not able to suspend proppant efficiently, and as a result, proppant placement across multiple clusters/fractures cannot be achieved. In contrast, results of using the low-density proppant in low viscosity fluids has successfully achieved a fairly

even proppant distribution, not only in the horizontal wellbore but also between the perforation clusters, making proppant transport and the potential for stimulation treatments very effective.

7.2 Discussion of the Results Using Friction Reducer

The main reason for using high loading friction reduced (HLFR) fluids is to increase the viscosity of the fracturing fluid. These fluids are characterized by having high molecular weights. They are added to water at low concentrations to reduce the frictional energy that dissipates in turbulent flow. Runs were carried out on 20/40 and 40/70 mesh sand at four different apparent fluid viscosities: 2.5, 4.2, 7.5 and 17.0 cp. Three flow velocities 4.5, 8.2 and 11.0 ft/s were used to quantify the proppant distribution and particle concentrations in the wellbore and through the three perforation clusters.

The results of the rheological property measurements of the HLFR fluids reveal that these fluids are shear thinning non-Newtonian fluids in which the viscosity behaves differently than Newtonian fluids (fresh water). In other words, the viscosity of these fluids increases as shear rate decreases. When these fluids are not moving or at static conditions, the viscosity is high because the shear forces are very low. However, during the injection process when fluid is pumped from the mixing tank through the pumping unit, and then through the vertical and horizontal wellbore, a reduction in the fluid viscosity occurs because the shear forces that are applied to the fluids are relatively high. Also, the results of the Reynolds number calculations on these fluids indicate that three flow regimes, laminar, transition, and turbulent, were encountered at the three flow velocities used in the experimental tests. However, laminar flow conditions occurred more frequently not only at low flow velocities but also at relatively high flow velocities, which typically are encountered under field conditions.

The results of tests conducted on 20/40 mesh sand at the lowest flow velocity of 4.5 ft/s (laminar flow) using four loadings (1, 2, 3 and 5 gpt) of HLFR showed highly uneven proppant distribution through the perforation clusters. Similar to fresh water, at all of the fluid viscosities, 2.5, 4.2, 7.5 and 17.0 cp, the 20/40 mesh sand particles were not able to distribute uniformly in the fluid column; hence, higher proppant concentration occurred through the first cluster. The explanation for this phenomenon is that the gravity forces on the fluid were stronger than the viscous and the momentum forces. In this case, particles of proppant tended to concentrate in the lower section of the horizontal pipe and form a bed load transport particularly after the first cluster

as the fluid velocity reduced further. The overall velocity of the bed load transport is less than the average fluid velocity; as a result, the particle distribution was highly uneven not only in the horizontal pipe, but also through the perforation clusters.

When the flow velocity was increased to 8.2 ft/s, the same scenario for 20/40 mesh sand was also observed at concentrations 1.0 and 2.0 gpt of HLFRR where high proppant concentration occurred at the first cluster. Similar to the obtained results using freshwater fluids, the gravity forces were able to settle proppant particles in the bottom of the pipe and; therefore, uneven proppant distribution was observed. At fluid viscosities of 7.5 and 17.0 cp, more proppant was measured at the second cluster. This can be described as the flow rate near the first cluster being fairly high and preventing the proppant particles from turning completely into the perforations within the first cluster. As fluid exited the first cluster and reached the second cluster, the fluid velocity dropped, and the gravity forces became dominant over the momentum forces. Thus, the proppant particles were able to turn more easily into the perforations within the second cluster resulting in more proppant concentration occurring at the second cluster. After the second cluster, the fluid traveled in the horizontal wellbore with less proppant concentration; hence, lower proppant concentration occurred at the third perforation cluster.

However, at the flow velocity of 11.0 ft/s, high proppant concentration occurred at the third cluster and low proppant concentration was measured at the first cluster for all the concentrations of HLFRR. In these situations, there was a minor increase in the viscous forces over the gravitational forces. It was observed that a slightly even proppant distribution was observed between the perforation clusters.

The results for 40/70 mesh sand at the low flow velocity of 4.5 ft/s and fluid viscosities of 2.5, 4.2 and 7.5 cp showed uneven proppant distribution between the perforation clusters. Even though the median particle size for 40/70 is almost half of the median particle size of 20/40, the fluid viscosities were not able to suspend the proppant particles in the fluid. In addition, at this flow velocity, the gravitational forces were significant over the viscous forces on the particles. This caused the first cluster to receive more proppant concentration than the other two clusters. However, when the fluid viscosity was increased to 17.0 cp, the viscous forces were stronger than the gravity forces, and as a result of this, fairly uniform proppant distribution was achieved among the three perforation clusters. On the other hand, at flow velocities of 8.2 and 11.0 ft/s and at all fluid viscosities, the proppant particles of 40/70 mesh sand were reasonably suspended in the

horizontal wellbore, and, as a result, uniform proppant distribution occurred between the three clusters. The results demonstrate that the viscosity forces became dominant over the gravitational forces in such situations.

The results from all the runs that were performed using HLFR fluids demonstrate that the 20/40 mesh sand cannot be transported efficiently in the horizontal wellbore even at higher fluid viscosities. The viscous forces were not strong enough to suspend large proppant particles in the horizontal wellbore. The gravitational and the momentum forces were dominant over the viscous forces in the fluid flow. This results in uneven proppant distribution between the perforation clusters. Conversely, the 40/70 mesh sand, which has an average particle diameter of 0.015 inches, was able to be distributed uniformly in the fluid column resulting in highly uniform proppant distribution among the perforation clusters. These results show that a reduction in the particle diameter can have a large impact, not only on the proppant suspension in the fluid but also on the distribution of the proppant between the perforation clusters.

7.3 Discussion of the Results for the Experimental Correlations

Correlations were developed based on the experimental results obtained from proppant transport in the horizontal wellbore apparatus. No published studies on correlations for proppant distribution predictions between perforation clusters have been found. The developed correlations presented in Chapter 6 are the first of their kind to be based on experimental data.

The correlation of experimental data was achieved by utilizing dimensional analysis (Buckingham's pi-theorem), which requires appropriate experimental data to be obtained. Therefore, results of the experimental tests, which were conducted on 20/40 and 40/70 mesh sand and ultra-light weight ceramic were collected at three flow velocities and over a wide range of proppant concentrations. Such correlations help to determine the optimum flow rate that is required to attain an even distribution of the proppant and provide more insight about the anticipated proppant distribution into and out of the perforations. Also, these correlations can be extrapolated to field scale for optimizing the design of hydraulic fracturing treatments.

Four types of experimental correlations were developed for 20/40 and 40/70 mesh sand and ULW ceramic proppant to predict the proppant distribution between the perforation clusters. The first correlation type is based on the proppant concentration that can be used at flow velocities of 6.4, 11.0 and 13.7 ft/s, and different proppant concentrations for the tested proppants. The

second correlation is a velocity-concentration type which can be also used to predict the proppant distribution for a specific proppant size. The third correlation type combines the particle diameter as part of the dependent variables along with slurry velocity and proppant concentration. This correlation can be used to predict the proppant distribution for a specific proppant type. The fourth and final developed correlation includes the proppant density along with the proppant median diameter, flow velocity and proppant concentration as parts of the dependent variables.

The resulting power law trends with fitted equations and R^2 values for the three velocities indicate that that proppant distribution is considerably affected by proppant concentration. In other words, the proppant distribution between clusters can be improved greatly with increasing proppant concentrations at higher velocities. However, the power law trend for 40/70 ULW ceramic at a flow velocity of 6.4 ft/s, suggests that there is a certain proppant concentration where beyond it, increasing proppant concentration has a negative effect on proppant distribution.

The increase in the proppant concentration with an increase in the proppant distribution (PD) is attributed to two reasons. The first reason could be the interaction between the particles by which larger grains of the proppant will tend to settle down and exit the perforation holes that are placed on the bottom of the pipe. The second reason could be from the interaction between the particles and the pipe wall. This interaction can occur from the high turbulent velocity which can force the particles to move away from the centerline of the pipe. This results in more friction loss and encourages the particles to settle in the low velocity region near the pipe wall.

The analysis of the final developed correlation for 20/40 and 40/70 mesh sand and ULW ceramic shows that an increase in the specific gravity of proppant leads to a reduction in the PD, and an increase in the slurry velocity leads to an increase in the PD. Also, the correlation has the proppant concentration as a numerator term, which indicates as the proppant concentration increases, the PD between the perforation clusters also increases. In addition, the median proppant diameter term has a negative impact on the PD; in other words, if the median proppant diameter increases, the PD between the perforation clusters decreases.

Analysis of the developed correlation shows lower average error values for all the tested proppants except 20/40 mesh white sand at a flow velocity of 6.4 ft/s, which was relatively high. The reason for obtaining a higher percent error for 20/40 mesh sand is that the gravitational forces that were acting on the proppant grains were significantly high and led the proppant particles to settle, resulting in highly uneven proppant distribution (PD is very low) among the perforation

clusters. However, the low error values indicate high reliability of the developed correlation in predicting the PD between the perforation clusters in all other situations.

7.4 Comparison of the Experimental Results with Published Data

As mentioned previously, proppant distribution through multiple clusters/fractures has a significant impact on the effectiveness of hydraulic fracturing treatments. Fracture conductivity, which is not easily determined compared with other hydraulic fracturing properties, is strongly controlled by proppant concentration and distribution in the induced fractures. Uniform proppant distribution between multiple clusters/fractures can play a significant role in achieving effective hydraulic fracturing treatments. During the last 15 years, there have been many efforts for achieving even proppant distribution by optimizing proppant design in tight gas formations (Yu et al. 2015, Woodworth and Miskimins 2007; Warpinsk 2010; Cipolla et al. 2008).

Yu et al. (2015) investigated proppant distribution using four perforation clusters in three different scenarios for one stage as shown in Figure 7.1. The three different scenarios are 1) the proppant is evenly distributed with high proppant concentration throughout the fracture; 2) the proppant distribution is uneven between the four perforations with proppant concentration ratio of 1:1.5:2.5:4, which is similar to these findings and might also be the real case under the field conditions; and 3) the proppant is distributed uniformly between the four clusters, but with low proppant concentration. For all three cases, the proppant distribution in each perforation cluster is considered to be uniform in both directions, lateral and vertical. Then, the reservoir model was built for each scenario by averaging the reservoir properties values, which were based on available data from the Marcellus Shale. The model was run for the three scenarios to determine the cumulative gas production for 30 years as shown in Figure 7.2. As can be noted from the plot, the smallest gas production was observed at scenario 3, whereas the largest gas production was achieved at scenario 1. The difference in cumulative gas production between scenarios 1 and 2 is 11%, and between scenarios 1 and 3 is around 24%. These findings suggest that proppant distribution between multiples clusters has a large impact on the gas production, which should be considered when designing hydraulic fracturing treatments.

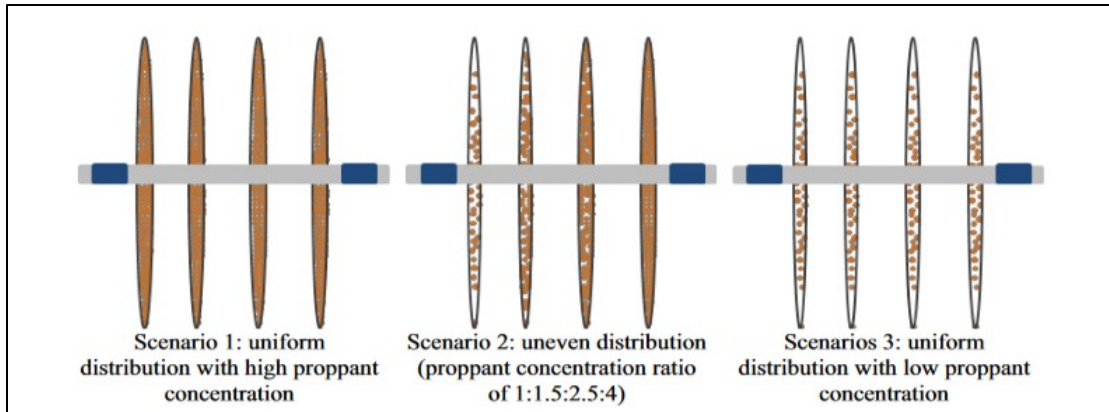


Figure 7.1: Proppant distribution in four perforation clusters within one fracturing stage (from Yu et al. 2015).

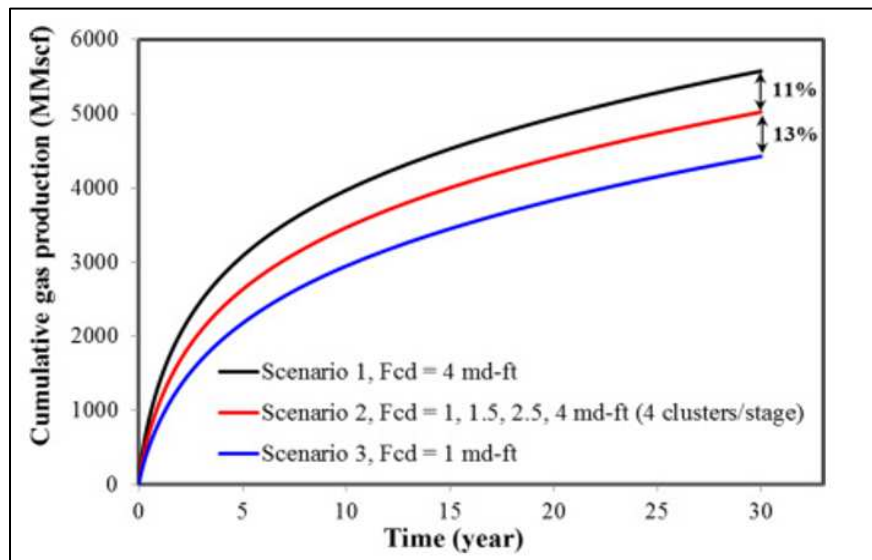


Figure 7.2: Comparison of cumulative gas production in a 30-year period between three scenarios (from Yu et al. 2015).

The results from the experimental tests performed in this research show comparable trends with a numerical simulation study conducted by Daneshy (2011). The objective of his work was to investigate the proppant distribution within four perforation clusters in one fracturing stage utilizing the plug-and-perf technique. His results demonstrate that uneven proppant distribution was observed between the four perforation clusters as shown in Figure 7.3. Several factors were involved in his study including pumping rate, fluid viscosity, and proppant size and density. For all the cases, highly uneven proppant distribution was observed among the perforation clusters with high proppant concentration towards the fourth cluster. The proppant concentration that was

received by the toe/fourth cluster was four times greater than the amount of proppant received by the first cluster.

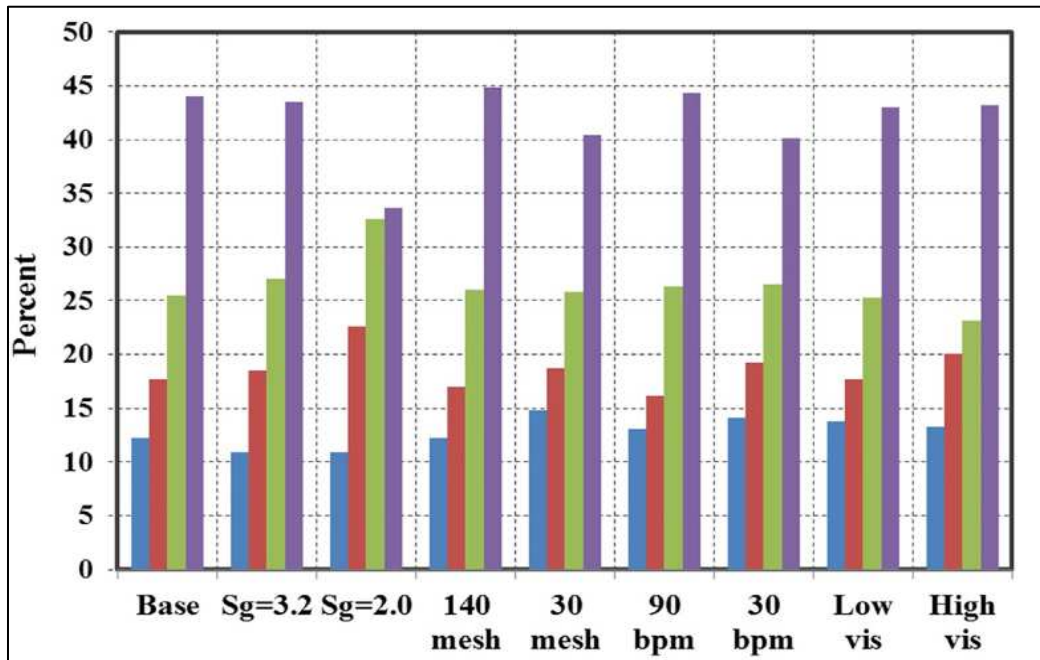


Figure 7.3: Proppant distribution between four perforation clusters in one fracturing stage (from Daneshy 2011).

The results of this research were also compared with other experimental and simulation studies on proppant transport such as those conducted by Crespo et al. (2013) and Bokane et al. (2013) and a more recent study by Ngameni et al. (2017).

The experimental study carried out by Crespo et al. (2013) was conducted on a large scale using a 63-foot stage and three 0.42-inch simulated perforations with zero phasing. The flow rates in their tests ranged from 8 bbl/min to 12 bbl/min. Their work demonstrates that proppant does not distribute evenly across perforations, but the work was also limited to a single perforation scheme. Their results indicate that at a low flow rate of 8 bbl/min, the 20/40 mesh sand showed highly uneven distribution, with higher concentration towards the first perforation, which is similar to the findings presented here on 20/40 mesh sand at a low flow velocity of 6.4 ft/s (Section 4.1.1.1). Also, the results from all the experimental runs performed in this research indicate that fluid was distributed uniformly through the perforation clusters, which is very similar to their findings. In addition, their results using CFD modeling indicate that even at high flow rates, the proppant particle settling still occurs (due to gravity). This is comparable to observations in this work on

high density proppant (sand) where the gravity forces, which were acting on the proppant particles, were significant enough to settle the particles on the bottom of the pipe, resulting in highly uneven proppant distribution through the perforation clusters.

A simulation study conducted by Bokane et al. (2013) was intended to investigate proppant transport in multiple perforation clusters by using computational fluid dynamics (CFD) software. They investigated parameters that have significant effects on proppant transport such as slurry flow rate, proppant and fluid specific gravity, fluid viscosity, and proppant size. Their results using linear gels with fluid viscosities of 17 and 19 cp show that proppant with higher density tends to settle down resulting in uneven proppant distribution with more proppant towards the first cluster. These are comparable to this study's results that were obtained from runs conducted on 20/40 mesh sand using a fluid viscosity of 17 cp. This study's results demonstrate that the 20/40 mesh sand cannot be suspended efficiently in the horizontal wellbore even at relatively higher fluid viscosities (up to 17 cp in the subject tests). The viscous forces were not strong enough to suspend large proppant particles in the horizontal wellbore. The gravitational and the momentum forces were dominant over the viscous forces in the fluid flow. This results in uneven proppant distribution between the perforation clusters.

The most recent study on proppant transport in horizontal wellbores was conducted by Ngameni et al. (2017). They utilized a 2.5-inch horizontal wellbore with three perforation clusters at 6 SPF at a 60-degree phasing using freshwater. Their findings suggest that uneven distribution of proppant was observed between each of the clusters when using 40/70 and 20/40 mesh sand. This is similar to this study's results on proppant distribution within perforation clusters as presented in Sections 4.1.1.1 and 4.1.1.2. When they used low ultra-light weight (ULW) proppant (specific gravity of 1.06), their results showed that even proppant distribution was observed among the perforation clusters. This is also similar to this study's findings on 40/70 ULW ceramic with a specific gravity of 2.0, where uniform proppant distribution occurred within the perforation clusters. The reason for obtaining even proppant distribution was that the momentum difference between the fluid and the proppant is relatively low.

7.5 Applications to the Field

In any typical fluid flow situation, the flow is mainly dependent on the density and viscosity of the fluid. In contrast, the results of this research show that in fracturing fluid flow, the flow is

not only dependent on the physical properties of the carrying fluid itself, but also on other parameters such as: proppant size, proppant density, particle distribution in the slurry, and the mixture ratio between the particles and the carrying fluid. These should be considered when designing an optimal hydraulic fracturing treatment.

Another important aspect of the application is the proppant settling in horizontal wellbores. Proppant settling depends mainly on the flow regimes of the slurry, which in turn depend on the slurry velocity and the hydrodynamic interactions between the proppant particles and between the particles and the pipe wall. Therefore, when a flow rate is low, the clusters toward the heel encounter more proppant settling around them in the wellbore than the other clusters, whereas at high flow rates, the clusters close to the toe encounter more proppant settling in the horizontal wellbore than the other clusters. This situation is believed to be occurring in the field when performing a plug and perf technique. By predicting how much proppant settles in the wellbore at the end of each hydraulic fracturing stage, it can help to optimize the over-flush volumes (excess volume to the volume of pipe displacement) that are needed to clean the proppant in the wellbore. A study was conducted by Al-Tailji et al. (2014) to minimize over-flush volumes at the end of hydraulic fracturing treatment for one stage in a plug and perf technique for Eagle Ford Shale formation. The study indicates that over-flush volumes of 20 bbl or greater can disturb the near-wellbore conductivity by harming the continuity of the fracture with the wellbore.

In addition, the settling velocity calculation is another important factor that should be considered not only in the wellbore but also in the induced fractures. The specific gravity of proppant can play a significant role in settling proppant particles in horizontal wellbores and in the fractures. If the specific gravity of proppant is high, the settling velocity is high and vice versa. A study was conducted by Kong et al. (2015) to study the settling velocity effect on proppant distribution and conductivity of fractures in the Marcellus Shale formation. Their study showed that ignoring proppant settling velocity can result in more than an 18% overestimation in the dimensionless productivity index.

From a flow standpoint using the laboratory shear rates that are equivalent to the field conditions, the flow velocities used in this work, i.e. 4.2, 6.4, 8.2, 11.0 and 13.7 ft/s, combined with a horizontal pipe of 1.5 inches, can mimic the field conditions for flow rates of 19, 27, 35, 46, and 58 bpm, respectively, with a horizontal pipe of 4.778 inches. Based on the obtained results from these flow velocities, it should be considered that in plug-and-perf completion techniques at

high flow rates, the bigger particle proppant such as 20/40 mesh cannot be distributed uniformly among the perforation clusters. The slurry concentration received by the clusters toward the toe could be several times greater than the slurry concentration received by the clusters toward the heel. On the other hand, at low flow rates, the amount of proppant at the clusters toward the heel is greater than the amount of proppant at the toe clusters. Additionally, the results for tests conducted at low flow rates can be applied to other horizontal transport conditions such as wellbore cleaning after the plug-and-perf technique in a cemented casing. This method of well completions requires low flow rates to initiate the flow.

The HLFGR fluids have proved to be more effective transport systems for smaller particle proppant (40/70 mesh) than other fluids such as slickwater or freshwater fluids. The HLFGR fluids can typically overcome the settling of the proppant not only in the horizontal wellbore but also in the fractures resulting in uniform proppant distribution. The HLFGR fluids may also have caused less formation damage than other fluids such as crosslinked guar and linear fluids.

Understanding proppant transport in the horizontal wellbore is a critical consideration for effectively placing proppant uniformly into the fractures. This in turn impacts fracture conductivity, and ultimately achieves success of a hydraulic fracturing treatment.

7.6 Experimental Limitations

It is important to mention that there are some limitations from an experimental design standpoint. For all the tests that were conducted using fresh water as a carrier fluid, high flow rates were not able to be achieved when the valve, which was placed at the end of the horizontal wellbore, was closed. This is because the back pressure acting upon the pump was greater than the maximum operating pressure for the pump (maximum working pressure is 125 psi). Another thing that should be noted is that the high-density proppant (sand) tended to settle and concentrate at the bottom of the mixing tanks. Therefore, particle settling of the tested sand proppant was observed even at higher RPMs of the mixer. As a result, higher injection proppant concentrations were not able to be achieved, particularly for 20/40 mesh sand. For all the tests that were conducted on proppant using HLFGR fluids, the proppant flow behavior in the horizontal wellbore was not able to be seen/captured because it was cloudy, even at low concentrations of the friction reducer.

CHAPTER 8

CONCLUSIONS AND RECOMMENDATIONS

This PhD research study experimentally investigated proppant transport in horizontal wellbores with three main research areas. The first area was to evaluate proppant transport in horizontal wellbores using fresh water to mimic slickwater fluids. The second area of research was to study and quantify proppant transport in horizontal wellbores using high loading friction reducer (HLFR) fluids. The third focus area was to develop experimental correlations to predict proppant distribution within perforation clusters using the data obtained from the laboratory experiments. Even though the work conducted during these trials focused on proppant transport into the wellbore during hydraulic fracturing treatments, the experimental results of proppant transport behavior can be applied to other lateral transport conditions such as proppant flowback and wellbore cleaning in plug-and-perf completions.

The conclusions of the thesis are summarized in Section 8.1, while the recommendations for future work are provided in Section 8.2.

8.1 Conclusions

Sections 8.1.1- 8.1.3 present the major conclusions that have been drawn from results that were obtained from the laboratory experiments.

8.1.1 Proppant Transport Using Freshwater Fluids

Based on the obtained results from the experimental tests on proppant transport using fresh water as a carrier fluid and on the proppant transport theories discussed in this thesis, the following conclusions are drawn:

- Uneven proppant distribution among the perforation clusters was mostly seen in cases where the proppant density and proppant size were relatively high.
- The 20/40 and 40/70 mesh sand at low flow rates showed highly uneven proppant distribution among the perforation clusters. The gravitational forces were dominant over the momentum forces resulting in more proppant received by the first cluster.
- At low flow rates, the distribution of the sand particles in the horizontal wellbore was uneven and more proppant concentration occurred on the bottom of the horizontal pipe.

- At high flow rates, the amount of proppant received at the toe cluster was higher than the amount of proppant received at the first and the second clusters for both 20/40 and 40/70 mesh sand proppants. The total momentum forces near the first and second clusters were relatively higher than the gravity forces. This resulted in some of the proppant particles not being to make a complete turn into perforations within the first and the second clusters.
- Even at high flow rates, 20/40 and 40/70 mesh sand particle settling still occurs in the bottom of the pipe (gravity effect).
- The ultra-light weight ceramic (20/40 mesh) showed improved proppant distribution between the perforation clusters due to the difference in the momentum between the proppant and the carrier fluid being relatively low if compared with sand.
- The 40/70 ULW ceramic proppant showed the most uniform proppant distribution between the perforation clusters. The small difference in the momentum between the proppant and the carrier fluid and the smaller particle size led the particles to distribute more uniformly in the fluid and resulted in even distribution between the clusters.
- Proppant settling behaviors in the horizontal wellbore are different for each proppant type and size.
- Minimum transport velocity calculations for the tested proppant indicate that proppant density, proppant median diameter, and proppant concentration play a significant role in the settling of the proppant particles in horizontal wellbores.
- If the specific gravity of the proppant is high, more proppant settling will occur. Also, if there is an increase either in the particle size or in the proppant concentration, there is also a significant increase in the proppant settling in the wellbore.
- At low flow rates for 20/40 and 40/70 mesh sand, more proppant settling occurred in the wellbore around the third perforation cluster, whereas at low flow rates, more proppant settling occurred in the wellbore around the first cluster.
- The results proved that the low viscosity freshwater fluids are ineffective transport systems for larger particles with relatively higher density, particularly for 20/40 mesh sand.
- In a plug-and-plug completion technique, it is inappropriate to assume that proppant is distributed uniformly among the perforation clusters.

8.1.2 Proppant Transport Using HLFRR Fluids

The conclusions on proppant transport using 20/40 and 40/70 mesh sand in the horizontal wellbore utilizing HLFRR fluids are as follows:

- The results of the rheological property measurements for HLFRR fluids showed that as the shear rate increases for these fluids, the fluid viscosity decreases. This was evidence that the HLFRR fluids used in this study follow non-Newtonian fluid behavior.
- At low flow rates and low loadings of HLFRR, both 20/40 and 40/70 mesh sand showed a similar result as in freshwater fluids. The first cluster received more proppant than the other two clusters.
- For 20/40 mesh sand, the viscous forces were not strong enough to suspend large proppant particles in the horizontal wellbore. The gravitational and the momentum forces were dominant over the viscous forces in the fluid flow.
- At high flow rates, the proppant concentration at the toe cluster was higher than the injected proppant concentration for 20/40. This occurs because the high momentum near the first cluster prevents the proppant from turning into the perforation holes.
- The results demonstrate that the 20/40 mesh sand cannot be suspended efficiently in the horizontal wellbore even at relatively higher fluid viscosities (up to 17 cp in the subject tests).
- The 40/70 mesh sand showed the most uniform distribution between the perforation clusters at relatively higher fluid viscosity, where the viscous forces were stronger on the fluid flow.
- The 40/70 mesh sand in the HLFRR fluids showed much better transportation in the horizontal wellbore than 20/40 mesh sand.
- The HLFRR fluids are proved to be very effective transport systems for smaller particle proppant. This is true when compared to low viscosity fluids, such as slickwater and freshwater fluids.

8.1.3 Experimental Correlations

Based on the obtained results from the experimental correlations on distribution of 20/40 and 40/70 mesh sand and ULW ceramic between multiple clusters, the following conclusions are drawn:

- The correlation of experimental data was achieved by utilizing dimensional analysis (Buckingham's pi-theorem), which proved to be very effective.
- Four types of experimental correlations were developed for 20/40 and 40/70 mesh sand and ULW ceramic proppant to predict the proppant distribution between the perforation clusters as follows:
 - The first correlation type is based on the proppant concentration that can be used at a specific velocity (tested velocities) and different concentrations for a specific proppant type.
 - The second correlation is a velocity-concentration type which can be also used to predict the proppant distribution for a specific proppant size.
 - The third correlation type combines the particle diameter as part of the independent variables along with slurry velocity and proppant concentration. This correlation can be used to predict the proppant distribution for a specific proppant type.
 - The fourth and final developed correlation includes the proppant density along with the proppant median diameter, flow velocity and proppant concentration as parts of the independent variables.
- The resulting power law trends with fitted equations and R^2 values at the three flow velocities for the tested proppant indicate that proppant distribution is considerably affected by proppant concentration; as injected proppant concentration increases, the PD increases.
- However, the power law trend for 40/70 ULW ceramic proppant at a flow velocity of 6.4 ft/s, suggests that there is a certain proppant concentration where increasing proppant concentration beyond it has a negative effect on proppant distribution.
- The proppant distribution can be improved greatly with increasing proppant concentrations at high flow velocities.
- The results of correlation analysis on the final developed correlation show that the ULW ceramic showed low error values compared to sand. The low error values indicate high reliability of the developed correlation in predicting the PD between the perforation clusters.

8.2 Recommendations for Future Work

The results of this experimental work have provided better insights into proppant transport behavior in horizontal wellbores and distribution of proppant between perforation clusters. However, additional work is recommended in order to further expand this understanding of proppant transport in horizontal wellbores. With all the information and knowledge gained during this research, the recommendations for future work are listed below:

- Use 100 mesh sand to evaluate its transport efficiency in freshwater fluids and compare it with 20/40 and 40/70 mesh sand used in this study. The reason for recommending 100 mesh sand is that most of frac jobs start with 100 mesh to seal off microfractures so that leakoff can be eliminated. This will also help to gain more knowledge how such a reduction in proppant size can affect the proppant transport and distribution between multiple clusters.
- Use other proppant types such as light-weight ceramic with specific gravities of 2.7 and compare the results with sand 2.65 (the most common proppant used in the oil industry). This will give more insight about if the sphericity and roundness have a significant effect on the distribution of the proppant between perforation clusters.
- Use higher fluid viscosities to evaluate their effects on suspension of high-density proppant particularly 20/40 sand which was not transported efficiently using a fluid viscosity up to 17 cp.
- A significant effort is to change the wellbore configuration to evaluate proppant transport and distribution between perforation clusters and compare the results with the results obtained from the configuration that was used in this study. The wellbore configuration might be as following:
 - Change the perforation density from four shots per foot (4 SPF) to 6 SPF,
 - Change the perforation phasing from 90 degree (used in this study) to 60° or 30° or even 0-degree phasing, and;
 - Change the ID of the pipe from 1.5 inch used in this study to 2.5- or 3-inch pipe.
- Make sure the proppant can be also collected from each perforation hole instead of from the entire cluster. This can be performed by placing a tube with a valve at each perforation hole. This can also help to control/limit the fluid and proppant that exit the wellbore.

- Include an inclination angle to the wellbore (for example 10°), to evaluate also the effect of an inclination angle (gravity effect) on proppant transport, because the lateral section in hydraulic fracturing may not be entirely horizontal.
- Use a combination of different proppant sizes, for example mixing 20/40 with 40/70 mesh sand or 40/70 with 100 mesh sand to gain more knowledge about how it may affect the proppant behavior and distribution in horizontal wellbores, particularly when pumping 40/70 mesh sand followed by 20/40 mesh sand or pumping 100 mesh sand followed by 40/70 mesh, which is typically done in hydraulic fracturing treatments.
- Develop experimental correlations to predict the proppant distribution between multiple clusters by including other variables such as a pipe diameter. Then, combine the obtained results with the results in this research to develop a new correlation that takes into the account the change in the pipe diameter.

NOMENCLATURE

a	= Exponent, dimensionless
b	= Exponent, dimensionless
c	= Exponent, dimensionless
C_p	= Proppant concentration, ML^{-3} , kg/m^3
D	= Pipe inner diameter, L, m
dp	= Average particle diameter, L, m
f_{Darcy}	= Darcy friction factor, dimensionless
F_L	= Modified Froude number, dimensionless
g	= Gravitational velocity, LT^{-2} , m/s^2
K	= Flow consistency index ($dyn/cm^2 \cdot s^n$ or $Pa \cdot s^n$)
l_e	= Entrance length, L, m
Lp/l	= Pressure drop in the pipe, ML^{-3} , Pa/m
n	= Flow behavior index, dimensionless
PD	= Proppant distribution, Fraction or %
P_d	= Median particle diameter, L, m
PD_{Lab}	= Lab measured PD, %
$PD_{Pred.}$	= Correlation predicted PD, %
q	= Flow rate, L^3T^{-1} , m^3/s
Re	= Reynolds number, dimensionless
Re_{gen}	= Generalized Reynolds number, dimensionless
SG_F	= Fluid specific gravity, dimensionless
SG_P	= Particle specific gravity, dimensionless
u	= Average fluid velocity, LT^{-1} , m/s
u_s	= Shear velocity at pipe wall, LT^{-1} , m/s
V_c	= Minimum/critical transport velocity, LT^{-1} , m/s
V_t	= Terminal/vertical settling velocity, LT^{-1} , m/s
V_t/u	= Proppant settling velocity to horizontal fluid flow velocity ratio, dimensionless

γ	= Shear rate, T^{-1} , s^{-1}
ν	= Kinematic viscosity of fluid, L^2T^{-1} , m^2/s
ρ_f	= Density of the fluid carrier, ML^{-3} , Kg/m^3
ρ_p	= Density of the particle, ML^{-3} , Kg/m^3
Φ_{16}	= Sieve size at 16% of the sample weight, L, mm
Φ_{50}	= Sieve size at 50% of the sample weight, L, mm
Φ_{84}	= Sieve size at 84% of the sample weight, L, mm
τ_w	= Shear stress at the pipe wall, ML^{-2} , Pa
μ_f	= Fluid dynamic viscosity, $ML^{-1}T^{-1}$, $kg/m/s$
τ	= Shear stress, Pa

ABBREVIATIONS

ASTM	= The American Standard Test Sieve Series
bpm	= Barrel per minute
CFD	= Computational fluid dynamics
CT	= Coiled tubing
GPM	= Gallons per minute
GPT	= Gallon per thousand
HDC	= High density ceramic
HHP	= Hydraulic horsepower
HLFR	= High loading friction reducer
HVFR	= High viscosity friction reducer
ISO	= International Organization for Standardization
ID	= Internal diameter
IDC	= Intermediate density ceramic
mV	= Total momentum
Perf1	= Perforation cluster #1
Perf2	= Perforation cluster #2
Perf3	= Perforation cluster #3
PnP	= Plug-and-perf completion method
PPG	= Pound per gallon
R ²	= Coefficient of determination
RPM	= Revolutions per minute
SPF	= Shot per foot
SRV	= Stimulated reservoir volume
ULWC	= Ultra-light weight ceramic
VFD	= Variable frequency drive

REFERENCES

- Algadi, O. A., Castro, L., and Mittal, R. 2015. Comparison of Single-Entry Coiled Tubing-Activated Frac Sleeves vs. Multi-Cluster Plug-and-Perf Completion in the Permian and Anadarko Basin: A Case Study. Presented at the SPE Annual Technical Conference and Exhibition, 28-30 September, Houston, Texas. SPE-174943-MS. <https://doi.org/10.2118/174943-MS>.
- Almond, W., Penny, S., and Conway, W. 1995. Factors Affecting Proppant Flowback with Resin Coated Proppants. Presented at European Formation Damage Conference, The Hague, Netherlands, 15-16 May. SPE 30096-MS. <https://doi.org/10.2118/30096-MS>.
- Al-Tailji, W. H., Northington, N., Conway, M. et al. 2014. Minimizing Over-Flush Volumes at the End of Fracture-Stimulation Stages - An Eagle Ford Case Study. Presented at the SPE Annual Technical Conference and Exhibition, Amsterdam, The Netherlands, 27-29 October. SPE-170743-MS. <https://doi.org/10.2118/170743-MS>.
- Anadarko. 2015. Facts on Hydraulic Fracturing - Exploring Chemicals, https://www.anadarko.com/content/documents/apc/news/Fact_Sheets/FAQChemical_Usage_Final_Web.pdf (accessed 12 August 2018).
- API RP 19C. 2006. Measurements of Properties of Proppants used in Hydraulic Fracturing and Gravel Packing Operations, (ISO 13503-6:2006, Identical). Washington, DC: API.
- Bagci, S., Castro, L., and Flores, J. 2017. Optimization of Hydraulic Fracturing and Production Enhancement: Case Studies for US Shale Plays and Tight Sand Reservoirs. Presented at the SPE Europec featured at 79th EAGE Conference and Exhibition, Paris, France, 12-15 June. SPE-185773-MS. <https://doi.org/10.2118/185773-MS>.
- Biot, M.A., and Medlin, W.L. 1985. Theory of Sand Transport in Thin Fluids. Presented at the SPE Annual Technical Conference and Exhibition, Las Vegas, NV, 22-25 September. SPE-14468-MS. <https://doi.org/10.2118/14468-MS>.
- Bokane, A. B., Jain, S., Deshpande, Y. K. et al. 2013. Transport and Distribution of Proppant in Multistage Fractured Horizontal Wells: A CFD Simulation Approach. Presented at the SPE Annual Technical Conference and Exhibition, New Orleans, Louisiana, USA, 30 September-2 October. SPE-166096-MS. <https://doi.org/10.2118/166096-MS>.
- CARBO Ceramics Inc. 2017. 2017 ANNUAL REPORT, <https://www.carboceramics.com/investors/financial-reports-and-information/annual-reports> (accessed 02 August 2018).
- Chhabra, R. P., and Richardson, J. F. 2008. *Non-Newtonian Flow and Applied Rheology*, second edition. Oxford: Butterworth-Heinemann.

- Cipolla, C. L., Warpinski, N. R., Mayerhofer, M. J., et al. 2008. The Relationship between Fracture Complexity, Reservoir Properties, and Fracture Treatment Design. Presented at SPE Annual Technical Conference and Exhibition, Denver, CO. 21–24 September. SPE-115769-MS. <https://doi.org/10.2118/115769-MS>.
- Clark, P.E. 2006. Transport of proppant in hydraulic fractures. Presented at the SPE Annual Technical Conference and Exhibition, San Antonio, Texas, 24-27 September. SEP-103167-MS. <http://dx.doi.org/10.2118/103167-MS>.
- Cleary, M. and Fonseca, A. 1992. Proppant Convection and Encapsulated in Hydraulic Fracturing: Practical Implications of Computer and Laboratory Stimulations. Presented at the SPE Annual Technical Conference and Exhibition, Washington, D.C., USA, 4-7 October. SPE-24825-MS. <http://dx.doi.org/10.2118/24825-MS>.
- COMSOL 2017, Which Turbulence Model Should I Choose for My CFD Application? <https://www.comsol.com/blogs/which-turbulence-model-should-choose-cfd-application/> (accessed 20 March 2019).
- Coulter, A. W., Crowe, C. W., Barrett, N. D. et al. 1976. Alternate Stages of Pad Fluid and Acid Provide Improved Leak off Control for Fracture Acidizing. Presented at the SPE Annual Fall Technical Conference and Exhibition, New Orleans, Louisiana, 3-6 October. SPE-6124-MS. <https://doi.org/10.2118/6124-MS>.
- Crespo, F., Aven, N.K., Cortez, J. et al. 2013. Proppant Distribution in Multistage Hydraulic Fractured Wells: A Large-Scale Inside-Casing Investigation. Presented at the SPE Hydraulic Fracturing Technology Conference held in The Woodlands, Texas, 4-6 February. SPE-163856-MS. <https://doi.org/10.2118/163856-MS>.
- Daneshy A. 1978. Numerical solution of sand transport in hydraulic fracturing. *J Pet Technol* 30 (01): 132-140. SPE-5636-PA. <http://dx.doi.org/5636-PA>.
- Daneshy, A., 2011. Uneven distribution of proppants in perf clusters. *World Oil*, 232(4).
- Durand, R. 1953. Basic relationships of the transportation of solids in pipes experimental research. Proc. Minn. Int. Hyd. Conv., Univ. of Minnesota: 89-103.
- Durand, R. and Condolios, E. 1952. Experimental Investigation of the Transport of Solids in Pipes. Deuxieme Journé e de L'Hydraulique, Societé Hydrotechnique de France, 29–55.
- Fisher, K. 2012. Trends Take Fracturing Back to the Future. *American Oil and Gas Reporter*, 55(8): 86–97.

- Fisher, M. K., Heinze, J. R., Harris, C. D., et al. 2004. Optimizing Horizontal Completion Techniques in the Barnett Shale Using Microseismic Fracture Mapping. Presented at the SPE Annual Technical Conference and Exhibition, Houston, Texas, 26-29 September. SPE-90051-MS. <https://doi.org/10.2118/90051-MS>.
- Folk, R. and Ward, W. 1957. Brazos River bar: A study in the significance of grain size parameters. *Journal of Sedimentary Petrology*, 27: 3-26.
- Goel, N. and Shah, S. 2001. A Rheological Criterion for Fracturing Fluids to Transport Proppant during a Stimulation Treatment. Presented at Annual Technical Conference and Exhibition, New Orleans, Louisiana, USA, 30 September-3 October. SPE-71663-MS. <http://dx.doi.org/10.2118/71663-MS>.
- Gruesbeck, C., and Collins, R. E. 1982. Particle Transport Through Perforations. *SPE J* 22 (06): 857 – 865. SPE-7006-PA. <https://doi.org/10.2118/7006-PA>.
- Hareland, G., Rampersad, P., Dharaphop, J. et al. 1993. Hydraulic Fracturing Design Optimization. Presented at the SPE Eastern Regional Meeting, Pittsburgh, Pennsylvania. 2-4 November. SPE-26950-MS. <https://doi.org/10.2118/26950-MS>.
- Harris, P. C., Morgan, G., and Heath, J. 2005. Measurement of Proppant Transport of Fracturing Fluids. Presented at the SPE Annual Technical Conference and Exhibition, Dallas, Texas, 9-12 October. SPE-95287-MS. <https://doi.org/10.2118/95287-MS>.
- Ibrahim, A. F., Nasr-El-Din, H. A., Rabie, A. et al. 2018. A New Friction-Reducing Agent for Slickwater Fracturing Treatments. *SPE Prod & Oper* 33 (03): 583 – 595. SPE-180245-PA. <https://doi.org/10.2118/180245-PA>.
- ISO13503-2:2006/Amd.1:2009(E): 2006, Petroleum and Natural Gas Industries- Completion Fluids and Materials- Part 5: Procedures for Measuring the Long-Term Conductivity, First Edition. 2006. Geneva, Switzerland: ISO.
- King, G.E. 2010. Thirty Years of Gas Shale Fracturing: What Have We Learned? Presented at the SPE Annual Technical Conference and Exhibition, Florence, Italy, 19–22 September. SPE-133456-MS. <http://dx.doi.org/10.2118/133456-MS>.
- Kong, B., Fathi, E., Ameri, S. 2015. Coupled 3-D numerical simulation of proppant distribution and hydraulic fracturing performance optimization in Marcellus shale reservoirs. *Int. J. Coal Geol.* 147–148, 35–45.
- Kostenuk, N. and Browne, D.J. 2010. Improved Proppant Transport System for Slickwater Shale Fracturing. Presented at the Canadian Unconventional Resources and International Petroleum Conference, Calgary, 19–21 October. SPE-137818-MS. <http://dx.doi.org/10.2118/137818-MS>.

- Liang, F., Sayed, M., Al-Muntasheri, G. A. et al. 2016. A comprehensive review on proppant technologies. *Petroleum*, 2 (1): 26–39. <http://doi.org/10.1016/j.petlm.2015.11.001>.
- Mali, T., Khudabadi, V., Vijay, A. et al. 2014. Slurry-Flow Pressure Drop in Pipes with Modified Wasp Method. Presented at SME Annual Meeting/Exhibit, Salt Lake City, UT. 24-26 February. <https://www.onemine.org/document/document.cfm?docid=218341&docorgid=10>.
- Metzner, A.B., and J.C. Reed. 1955. Flow of non-Newtonian Fluids - correlation of the laminar, transition and turbulent-flow regions. *AIChE J.* 1(4):434-40.
- Miller, C. K., Waters, G. A., and Rylander, E. I. 2011. Evaluation of Production Log Data from Horizontal Wells Drilled in Organic Shales. Presented at the North American Unconventional Gas Conference and Exhibition, The Woodlands, Texas, 14-16 June. SPE-144326-MS. <https://doi.org/10.2118/144326-MS>.
- Miskimins, J. L. 2016. Well Completion and Stimulation Course. Lecture Notes. Colorado School of Mines, Golden, Colorado (Fall 2016).
- Montgomery, C. 2013. Fracturing Fluids. International Society for Rock Mechanics and Rock Engineering. ISRM-ICHF-2013-035. <http://dx.doi.org/10.5772/56192>.
- Montgomery, C. T., and Smith, M. B. 2010. Hydraulic Fracturing: History of an Enduring Technology. *SPE J* 62 (12): 26 – 40. SPE-1210-0026-JPT. <https://doi.org/10.2118/1210-0026-JPT>.
- Munson, B., Okiishi, T., Huebsch, W. et al. 2012. Fundamental of Fluid Mechanics, seventh edition, New York: Wiley.
- Murtaza, M., Al Naeim, S., and Waleed, A. 2013. Design and Evaluation of Hydraulic Fracturing in Tight Gas Reservoirs. Presented at SPE Saudi Arabia Section Technical Symposium and Exhibition, Al-Khobar, Saudi Arabia, 19-22 May. SPE-168100-MS. <https://doi.org/10.2118/168100-MS>.
- Ngameni, L., Miskimins, J., and J., Abass, H. et al. 2017. Experimental Study of Proppant Transport in Horizontal Wellbore Using Fresh Water. Presented at the SPE Hydraulic Fracturing Technology Conference and Exhibition held in The Woodlands, Texas, USA, 24-26 January. SPE-184841-MS. <https://doi.org/10.2118/184841-MS>.
- Nixon, T., Tomszak, J., Lawrence, S. et al. 2014. Environmentally Friendly Fracturing Fluid as Utilized in a Western Canada Sedimentary Basin Case Study. Presented at the SPE Annual Technical Conference and Exhibition, Amsterdam, The Netherlands, 27-29 October. SPE-170737-MS. <https://doi.org/10.2118/170737-MS>.

- Norton Rose Fulbright. 2015. Shale Gas Handbook. A quick-reference guide for companies involved in the exploitation of unconventional gas resources. Second edition. <http://oilproduction.net/files/shale-gas-handbook.pdf> (accessed 10 August 2019).
- Palisch, T. T., Vincent, M., and Handren, P. J. 2010. Slickwater Fracturing: Food for Thought. *SPE J* 25 (03): 327-344. SPE-115766-PA. <https://doi.org/10.2118/115766-PA>.
- Palisch, T., Wilson, B., and Duenckel, B. 2014. New Technology Yields Ultra High-Strength Proppant. Presented at the SPE Hydraulic Fracturing Technology Conference, The Woodlands, Texas, USA, 4-6 February. SPE-168631-MS. <http://10.2118/168631-MS>.
- Parshall, J. 2008. Barnett Shale Showcases Tight-Gas Development. *SPE J* 60 (09): 48-55. SPE-0908-0048-JPT. <https://doi.org/10.2118/0908-0048-JPT>
- Penny, G. S., Zelenev, A. S., Long, W. et al. 2012. Laboratory and Field Evaluation of Proppants and Surfactants used in Fracturing of Hydrocarbon Rich Gas Reservoirs. Presented at the SPE Annual Technical Conference and Exhibition, San Antonio, Texas, 8-10 October. SPE-159692-MS. <https://doi.org/10.2118/159692-MS>.
- Petrowiki, 2016. Fracturing fluids and additives, https://petrowiki.org/Fracturing_fluids_and_additives (accessed 27 March 2018).
- Roodhart, L. P. 1985. Proppant Settling in Non-Newtonian Fracturing Fluids. Society of Petroleum Engineers. Presented at the SPE/DOE Low Permeability Gas Reservoirs Symposium, Denver, Colorado, 19-22 March. SPE-13905-MS. <https://doi.org/10.2118/13905-MS>.
- Schein, G. 2005. The Application and Technology of Slickwater Fracturing. Paper SPE 108807 presented as a Distinguished Lecture during the 2004–05 season.
- Shah, S. N., and Lord, D. L. 1990. Hydraulic Fracturing Slurry Transport in Horizontal Pipes. *SPE Drill Eng* 5 (03): 225 – 232. SPE-18994-PA. <https://doi.org/10.2118/18994-PA>.
- Shah, S. N. 1993. Rheological Characterization of Hydraulic Fracturing Slurries. *SPE J* 08 (02): 123-130. SPE-22839-PA. <https://doi.org/10.2118/22839-PA>.
- Sinclair, A. R., Graham, J. W., and Sinclair, C. P. 1983. Improved Well Stimulation with Resin-Coated Proppants. Presented at SPE Production Operations Symposium, Oklahoma City, Oklahoma, 27 February-1 March. SPE-11579-MS. <https://doi.org/10.2118/11579-MS>.
- Speight, J. G. 2016. *Handbook of Hydraulic Fracturing*, third edition., Hoboken, New Jersey: Wiley.

- Stephenson, C. J., Rickards, A. R., and Brannon, H. D. 2003. Is Ottawa Still Evolving? API Specifications and Conductivity in 2003. Presented at the Annual Technical Conference and Exhibition, Denver, Colorado, USA, 5-8 October. SPE-84304-MS. <http://dx.doi.org/10.2118/84304-MS>.
- U.S. Department of Energy Office of Fossil Energy and National Energy Technology Laboratory. 2009. Modern Shale Gas Development in the United States: A Primer, https://www.energy.gov/sites/prod/files/2013/03/f0/ShaleGasPrimer_Online_4-2009.pdf (accessed 29 November 2019).
- U.S. Energy Information Administration (EIA). 2011. Review of Emerging Resources: U.S. Shale Gas and Shale Oil Plays, <https://www.eia.gov/analysis/studies/usshalegas/pdf/usshaleplays.pdf> (accessed 20 August 2019).
- U.S. Energy Information Administration (EIA). 2018. Annual Energy Outlook 2018. Oil and Natural Gas Resources and Technology, <https://www.eia.gov/outlooks/aeo/grt.php> (accessed 22 August 2019).
- U.S. Energy Information Administration (EIA). 2019a. Natural gas explained Where our natural gas comes from, <https://www.eia.gov/energyexplained/natural-gas/where-our-natural-gas-comes-from.php> (accessed 25 August 2019).
- U.S. Energy Information Administration (EIA). 2019b. The U.S. leads global petroleum and natural gas production with record growth in 2018, <https://www.eia.gov/todayinenergy/detail.php?id=40973> (accessed 25 August 2019).
- Underdown, D. R., Day, J. C. and Sparlin, D. D. 1980. A Plastic Pre-Coated Gravel for Controlling Formation Sand. Presented at Formation Damage Control Symposium, Bakers-Field, CA, 28-29 January. SPE-880-MS. <http://dx.doi.org/10.2118/8801-MS>.
- Van Domelen, M., Cutrer, W., Collins, S., et al. 2017. Applications of Viscosity-Building Friction Reducers as Fracturing Fluids. Presented at the SPE Oklahoma City Oil and Gas Symposium. Oklahoma City, OK. 27-30 March. SPE-185084-MS. <https://doi.org/10.2118/185084-MS>.
- Vincent, M. 2011. Restimulation of Unconventional Reservoirs: When Are Refracs Beneficial? *J Can Pet Technol* 50 (05): 36-52. SPE-136757-PA. <https://doi.org/10.2118/136757-PA>.
- Vincent, M. C. 2002. Proving It - A Review of 80 Published Field Studies Demonstrating the Importance of Increased Fracture Conductivity. Presented at the SPE Annual Technical Conference and Exhibition, San Antonio, Texas, 29 September-2 October. SPE-77675-MS. <https://doi.org/10.2118/77675-MS>.

- Warpinski, N. R. 2010. Stress Amplification and Arch Dimensions in Proppant Beds Deposited by Waterfracs. *SPE Prod & Oper* 25 (04): 461 – 471. SPE-19350-PA. <https://doi.org/10.2118/119350-PA>.
- Warpinski, N.R., Mayerhofer, M.J., Vincent, M.C. et al. 2009. Stimulating Unconventional Reservoirs: Maximizing Network Growth While Optimizing Fracture Conductivity. Presented at the SPE Unconventional Reservoirs Conference, Keystone, Colorado, 10-12 February. SPE-114173-MS. <http://dx.doi.org/10.2118/114173-MS>.
- Wasp, E.J., Aude, T.C., Kenny, J.P., Seiter, R.H., and Jacques, R.B. 1970. Deposition velocities, transition velocities and spatial distributions of solids in slurry pipelines. Proc. Hydrotransport 1 Conf. BHRA, Paper H4: 53-76.
- Woodworth, T.R. and Miskimins, J.L. 2007. Extrapolation of laboratory proppant placement behavior to the field in slickwater fracturing applications. Presented at the 2007 SPE Hydraulic Fracturing Technology Conference, College Station, Texas, 29-31 January. SPE-106089-MS. <http://dx.doi.org/10.2118/106089-MS>.
- Wutherich, K.D and Walker, K.J., 2012. Designing Completions in Horizontal Shale Gas Wells Perforation Strategies. Presented at the Americas Unconventional Resources Conference held in Pittsburgh, Pennsylvania. 5-7 June. SPE-155485-MS. <https://doi.org/10.2118/155485-MS>.
- Yu, W., Zhang, T., Du, S., Sepehrnoori, K., 2015. Numerical study of the effect of uneven proppant distribution between multiple fractures on shale gas well performance. *Fuel* 142, 189–198.
- Zandi, I. 1971. *Advances in solid-liquid flow in pipes and its application*, first edition. Oxford: Pergamon Press/ Elsevier.

APPENDIX A

SIEVE ANALYSIS

This appendix consists of several sieve analysis tests that were performed on white sand and ULW ceramics for two sieve sizes 20/40 and 40/70.

A.1 20/40 Mesh White Sand

Table A.1.1: Results of a sieve analysis test for 20/40 mesh white sand (sample weight = 1235.88 g)

Sieve Size, mesh	Sieve weight, g	Sieve opening, mm	Full sieve weight, g	Net proppant weight, g	Weight percent, %	Cumulative weight percent, %	Median, mm
16	413.13	1.190	413.23	0.10	0.008	0.008	0.671
20	387.43	0.841	439.24	51.81	4.192	4.200	
25	385.34	0.707	848.15	462.81	37.448	41.648	
30	373.28	0.595	768.23	394.95	31.957	73.605	
35	353.61	0.500	582.47	228.86	18.518	92.123	
40	358.18	0.420	429.33	71.15	5.757	97.880	
50	348.32	0.297	368.27	19.95	1.614	99.494	
Pan	369.45	-	375.70	6.25	0.506	100.000	

Table A.1.2: Results of a sieve analysis test for 20/40 mesh white sand (sample weight = 1079.36 g)

Sieve Size, mesh	Sieve weight, g	Sieve opening, mm	Full sieve weight, g	Net proppant weight, g	Weight percent, %	Cumulative weight percent, %	Median, mm
16	413.13	1.190	413.19	0.06	0.006	0.006	0.707
20	387.43	0.841	422.58	35.15	3.257	3.262	
25	385.34	0.707	707.23	321.89	29.822	33.084	
30	373.28	0.595	730.98	357.70	33.140	66.224	
35	353.61	0.500	612.38	258.77	23.974	90.199	
40	358.18	0.420	433.96	75.78	7.021	97.220	
50	348.32	0.297	371.23	22.91	2.123	99.342	
Pan	369.45	-	377.61	8.16	0.756	100.098	

Table A.1.3: Results of a sieve analysis test for 20/40 mesh white sand (sample weight = 1071.11 g)

Sieve Size, mesh	Sieve weight, g	Sieve opening, mm	Full sieve weight, g	Net proppant weight, g	Weight percent, %	cumulative weight percent, %	Median, mm
16	413.11	1.19	413.66	0.55	0.051	0.051	0.689
20	388.33	0.841	466.18	77.85	7.268	7.320	
25	385.29	0.774	799.78	414.49	38.697	46.017	
30	373.62	0.595	735.91	362.29	33.824	79.841	
35	353.74	0.500	496.32	142.58	13.311	93.152	
40	357.92	0.420	404.96	47.04	4.392	97.544	
50	348.34	0.297	369.25	20.91	1.952	99.496	
Pan	369.45	-	375.32	5.87	0.548	100.044	

Table A.1.4: Results of a sieve analysis test for 20/40 mesh white sand (sample weight = 1341.91 g)

Sieve Size, mesh	Sieve weight, g	Sieve opening, mm	Full sieve weight, g	Net proppant weight, g	Weight percent, %	cumulative weight percent, %	Median, mm
16	413.12	1.19	413.32	0.2	0.015	0.015	0.676
20	387.32	0.841	460.73	73.41	5.471	5.485	
25	385.17	0.707	890.36	505.19	37.647	43.132	
30	373.28	0.595	810.2	436.92	32.559	75.692	
35	353.2	0.5	560.11	206.91	15.419	91.110	
40	357.6	0.42	435.4	77.8	5.798	96.908	
50	348.22	0.297	379.89	31.67	2.360	99.268	
Pan	369.4		379.22	9.82	0.732	100.000	

A.2 40/70 Mesh White Sand

Table A.2.1: Results of a sieve analysis test for 40/70 mesh white sand (sample weight = 1046.88 g)

Sieve Size, mesh	Sieve Weight, g	Sieve Opening, mm	Full Sieve Weight, g	Net Weight, g	Weight percent, %	cumulative weight percent, %	Median Diameter, mm
30	358.47	0.595	358.5	0.03	0.003	0.003	0.361
40	349.89	0.420	417.92	68.03	6.498	6.501	
50	346.13	0.297	1088.07	741.94	70.872	77.373	
60	337.3	0.250	487.27	149.97	14.325	91.698	
70	325.63	0.210	384.64	59.01	5.637	97.335	
100	319.16	0.149	345.64	26.48	2.529	99.864	
Pan	357.65	-	359.02	1.37	0.131	99.995	

Table A.2.2: Results of a sieve analysis test for 40/70 mesh white sand (sample weight = 1006.01 g)

Sieve Size, mesh	Sieve Weight, g	Sieve Opening, mm	Full Sieve Weight, g	Net Weight, g	Weight percent, %	cumulative weight percent, %	Median Diameter, mm
30	358.47	0.595	358.47	0.00	0.000	0.000	0.369
40	349.89	0.420	459.04	109.15	10.850	10.850	
50	346.13	0.297	1032.74	686.61	68.251	79.101	
60	337.3	0.250	462.49	125.19	12.444	91.545	
70	325.63	0.210	382.24	56.61	5.627	97.172	
100	319.16	0.149	346.38	27.22	2.706	99.878	
Pan	357.65	-	359.31	1.66	0.165	100.043	

Table A.2.3: Results of a sieve analysis test for 40/70 mesh white sand (sample weight = 1084.33 g)

Sieve Size, mesh	Sieve Weight, g	Sieve Opening, mm	Full Sieve Weight, g	Net Weight, g	Weight percent, %	cumulative weight percent, %	Median Diameter, mm
30	358.47	0.595	358.5	0.03	0.003	0.003	0.359
40	349.89	0.420	518.48	168.59	15.548	15.551	
50	346.13	0.297	1056.93	710.80	65.552	81.103	
60	337.3	0.250	465.45	128.15	11.818	92.921	
70	325.63	0.210	371.51	45.88	4.231	97.152	
100	319.16	0.149	347.89	28.73	2.650	99.802	
Pan	357.65	-	359.88	2.23	0.206	100.007	

Table A.2.4: Results of a sieve analysis test for 40/70 mesh white sand (sample weight = 1141.96 g)

Sieve Size, mesh	Sieve Weight, g	Sieve Opening, mm	Full Sieve Weight, g	Net Weight, g	Weight percent, %	cumulative weight percent, %	Median Diameter, mm
30	373.29	0.595	373.35	0.06	0.005	0.005	0.355
40	357.63	0.420	429.51	71.88	6.294	6.300	
50	348.23	0.297	1052.97	704.74	61.713	68.013	
60	341.38	0.250	528.16	186.78	16.356	84.369	
70	332.30	0.210	490.27	157.97	13.833	98.202	
100	334.22	0.149	352.56	18.34	1.606	99.808	
Pan	369.36	-	371.55	2.19	0.192	100.000	

A.3 20/40 ULW Ceramic

Table A.3.1: Results of a sieve analysis test for 20/40 ULW ceramic (sample weight = 1117.15 g)

Sieve Size, mesh	Sieve weight, g	Sieve opening, mm	Full sieve weight, g	Net proppant weight, g	Weight percent, %	cumulative weight percent, %	Median Diameter, mm
16	413.12	1.190	413.1200	0.00	0.000	0.000	0.651
20	387.32	0.841	390.5200	3.20	0.286	0.286	
25	385.17	0.707	399.5500	14.38	1.287	1.574	
30	373.28	0.595	798.8500	425.57	38.094	39.668	
35	353.20	0.500	922.2500	569.05	50.938	90.606	
40	357.60	0.420	462.5500	104.95	9.394	100.000	
50	348.22	0.297	348.2200	0.00	0.000	100.000	
Pan	369.40	-	369.4000	0.00	0.000	100.000	

Table A.3.2: Results of a sieve analysis test for 20/40 ULW ceramic (sample weight = 1137.18 g)

Sieve Size, mesh	Sieve weight, g	Sieve opening, mm	Full sieve weight, g	Net proppant weight, g	Weight percent, %	cumulative weight percent, %	Median Diameter, mm
16	413.12	1.190	413.1200	0.00	0.000	0.000	0.685
20	387.32	0.841	388.9400	1.62	0.142	0.142	
25	385.17	0.707	401.4800	16.31	1.433	1.576	
30	373.28	0.595	720.7300	347.45	30.537	32.113	
35	353.20	0.500	996.3000	643.10	56.521	88.633	
40	357.60	0.420	486.9300	129.33	11.367	100.000	
50	348.22	0.297	348.2200	0.00	0.000	100.000	
Pan	369.40	-	369.4000	0.00	0.000	100.000	

A.4 40/70 ULW Ceramics

Table A.4.1: Results of a sieve analysis test for 20/40 ULW ceramic (sample weight = 1006.55 g)

Sieve Size, mesh	Sieve weight, g	Sieve opening, mm	Full sieve weight, g	Net proppant weight, g	Weight percent, %	cumulative weight percent, %	Median diameter, mm
30	358.48	0.595	358.53	0.05	0.005	0.005	0.345
40	349.85	0.420	355.23	5.38	0.534	0.539	
50	346.07	0.297	1243.65	897.58	89.174	89.713	
60	337.21	0.250	399.82	62.61	6.220	95.934	
70	325.85	0.210	354.88	29.03	2.884	98.818	
100	319.14	0.149	330.55	11.41	1.134	99.951	
Pan	357.76		358.25	0.49	0.049	100.000	

Table A.4.2: Results of a sieve analysis test for 20/40 ULW ceramic (sample weight = 944.50 g)

Sieve Size, mesh	Sieve weight, g	Sieve opening, mm	Full sieve weight, g	Net proppant weight, g	Weight percent, %	cumulative weight percent, %	Median diameter, mm
30	358.48	0.595	358.59	0.11	0.012	0.012	0.359
40	349.85	0.420	359.36	9.51	1.006	1.018	
50	346.07	0.297	1198.22	852.15	90.184	91.202	
60	337.21	0.250	389.47	52.26	5.531	96.733	
70	325.85	0.210	345.11	19.26	2.038	98.771	
100	319.14	0.149	329.22	10.08	1.067	99.838	
Pan	357.76		359.29	1.53	0.162	100.000	